High-Order Weak Galerkin Finite Element Methods for Maxwell's Equations

by

RAMAN KUMAR

DEPARTMENT OF MATHEMATICS

INDIAN INSTITUTE OF TECHNOLOGY GUWAHATI

GUWAHATI-781039, INDIA

June, 2023

High-Order Weak Galerkin Finite Element Methods for Maxwell's Equations

A thesis submitted

in partial fulfillment of the requirements

for the degree of

DOCTOR OF PHILOSOPHY

by

RAMAN KUMAR

(Roll No. 186123013)

Under the supervision of
Prof. Bhupen Deka

Department of Mathematics

INDIAN INSTITUTE OF TECHNOLOGY GUWAHATI

June, 2023

This thesis

is dedicated

to
my family

CERTIFICATE

It is certified that the work contained in this thesis entitled **"High-Order Weak Galerkin Finite Element Methods for Maxwell's Equations"** by **Raman Kumar**, a student of Department of Mathematics, Indian Institute of Technology Guwahati, for the award of the degree of Doctor of Philosophy has been carried out under my supervision and that this work has not been submitted elsewhere for a degree.

June, 2023

Prof. Bhupen Deka
Professor
Department of Mathematics
Indian Institute of Technology Guwahati

ACKNOWLEDGEMENT

I would like to acknowledge and give my warmest thanks to my supervisor Prof. Bhupen Deka, Department of Mathematics who made this work possible. His guidance and advice carried me through all the stages of writing my thesis. I would also like to thank my doctoral committee members: Prof. R. K. Sinha, Prof. S.N. Bora, and Dr. Sweta Tiwari, Department of Mathematics for letting my research work be an enjoyable moment, and for your brilliant comments and suggestions, thanks to you.

I would also like to thank all of the faculty members in the Department of Mathematics for their assistance and support throughout my research and teaching practices. I am also thankful to all of the department's technical and nontechnical staff members for their assistance and cooperation over the course of my research.

I am also grateful to my entire family and friends for their unwavering support and understanding while I was conducting research and writing my thesis. Your kind wishes for me have kept me going this far.

Finally, I would like to thank God, for letting me through all the difficulties. I have experienced your guidance day by day. You are the one who let me finish my thesis work. I will keep on trusting you for my future.

June, 2023

Raman kumar

Department of Mathematics

Indian Institute of Technology Guwahati

ABSTRACT

The main objective of this thesis is to develop high-order numerical schemes for the various simplified models that approximate Maxwell's equations involving the curl and divergence operators. In these problems, one has to deal with vector-valued function spaces $\mathbf{H}(div)$ *and* $\mathbf{H}(curl)$*, which offers many consequences for the numerical techniques as a whole. The collection of the existing literature has suggested that finite element methods (FEMs) are one of the most accurate, efficient, and reliable approximation schemes in scientific computing due to their significant applications for real-world physical phenomena. Besides these advantages, the limited choices for the approximating spaces, underlying finite element partitions, low global regularity of the exact solutions, and interfaces having geometric singularities compromise the consistency of classical FEMs. So, there is still a scope to design cost-efficient higher order methods for* $\mathbf{H}(div)$ *and* $\mathbf{H}(curl)$ *problems for the general polygonal/polyhedral meshes. In an implementation, the finite partition which allows arbitrary shape elements provides additional flexibility in numerical methods and mesh generations such as general hybrid meshes, polygonal/polyhedral meshes, and meshes with hanging nodes. In recent years, newly developed weak Galerkin finite element methods (WG-FEMs) and least-squares weak Galerkin finite element methods (LSWG-FEMs) are much more appreciated in computational fields to solve different kinds of partial differential equations (PDEs). In this thesis, high-order accurate weak Galerkin finite element schemes to the PDEs having curl and divergence operators on the general polygonal/polyhedral domains have been designed and further, the convergence analysis is also extended for grad-div and curl curl-grad div interface problems with non-homogenous jump conditions. An additional attempt has been made to improve the order of convergence for the WG-FEMs. For this purpose, the least-squares weak Galerkin finite element approximations have been performed on a system of equations. The theoretical analysis of high-order convergence for the system of equations with polygonal/polyhedral meshes and meshes with hanging nodes adds more challenges than one could imagine. The first problem in this thesis deals with high-order WG-FEMs for* $\mathbf{H}(div)$*-elliptic problems with variable physical parameters. The key feature of this approach is that the usual divergence operator is approximated*

by its weak form as distributions for generalized functions. The optimal order error estimates in discrete H^1 and L^2 norms are established with weak Galerkin approximation space $\Big(\big[\mathcal{P}_k(T)\big]^d,\ \big[\mathcal{P}_k(\partial T)\big]^d,\ \mathcal{P}_{k-1}(T)\Big)$, where $d = 2, 3$, $k \geq 1$ is an integer and T is an arbitrary shape polygonal/polygonal domain. The next problem considers the WG algorithm for the $\mathbf{H}(curl)$-elliptic problems with variable physical coefficients in the general polygonal/polyhedral domain. The proposed algorithm is based on the discrete weak curl operator with appropriately defined stabilizations that enforce a weak continuity of the approximating functions. The optimal order error bounds for discrete energy and L^2 norms are holds for the weak Galerkin space $\Big(\big[\mathcal{P}_k(T)\big]^d,\ \big[\mathcal{P}_k(\partial T)\big]^d,\ [\mathcal{P}_{k-1}(T)]^{2d-3}\Big)$. The third problem concerns the weak Galerkin finite element methods for the $\mathbf{H}(curl, div)$-elliptic problems. In most of the existing literature, the well-posedness of div-curl models has been established with the help of two or more additional penalty terms, but this study justifies the uniqueness of the WG algorithm with one extra stabilizer term, which reduces the computational cost significantly and simplifies the weak formulation. The optimal order convergence for both H^1 and L^2 norms have been discussed with WG space $\Big(\big[\mathcal{P}_k(T)\big]^d,\ \big[\mathcal{P}_k(\partial T)\big]^d,\ [\mathcal{P}_{k-1}(T)]^{2d-3},\ \mathcal{P}_{k-1}(T)\Big)$. Next, the focus has been shifted to study some interface problems due to their more practical relevance in various physical phenomena. The WG algorithm requires special treatment near the interface because of discontinuities in the exact solution and corresponding flux variables. In the fourth problem, the high-order weak Galerkin finite element methods for the $\mathbf{H}(div)$-elliptic interface problems with non-homogenous jump conditions have been studied. Then attention has been paid to discuss the WG algorithm for the $\mathbf{H}(curl, div)$-elliptic interface problem with non-homogeneous jump conditions. The optimal order error estimates with respect to discrete energy and L^2 norms for the both aforementioned interface problems are derived with suitable weak Galerkin spaces. Further, from the previously existing work one can predict that super-convergence error bounds can be derived from the least-square techniques. In the sixth problem, the development of least-squares weak Galerkin finite element methods is discussed for time-harmonic Maxwell's equations. The super-convergence of order one is achieved for the discrete energy norm. Finally, LSWG-FEMs have been studied for Maxwell's equations. For the discrete energy norm, the

super-convergence of order one has been derived for the proposed algorithm.

Several numerical experiments have been performed to justify the accuracy, efficiency, flexibility, and robustness of each proposed algorithm. All the mesh generations and computations are carried out by using MATLAB software.

Contents

List of Figures

List of Tables

1 Introduction

Electromagnetic phenomena are very pivotal in most modern technologies. The design and analysis of numerical schemes for electromagnetic field models are major concerns in numerical mathematics and scientific computing. In electromagnetism, the governing spatial partial differential operators are mainly the curl and divergence operators. As a mathematical foundation of electromagnetism, the well-known Maxwell's equation is the set of partial differential equations in terms of these two operators [31]. The numerical solution of the full system of Maxwell's equations can be extremely expensive in terms of computer time. In some cases, however, it is possible to use a simplified model which approximates Maxwell's equations in some sense and which can be solved in a more economical way. The main purpose of this thesis is to develop and inspect the high-order weak Galerkin finite element methods (WG-FEMs) for various Maxwell's equations in polygonal/polyhedral meshes. Several numerical experiments in two-dimensional (2D)/three-dimensional (3D) have been described and analyzed to establish the efficiency of WG-FEMs in scientific computing. Our numerical results broadly cover the scope of various applied problems under one umbrella, including discontinuous coefficients, variable coefficients, and meshes with hanging nodes, aiming to fill the gap in the existing literature.

1.1 Modeling Framework

Maxwell's model equations are one of the most important phenomena in modern physics. Maxwell's equations were first introduced in 1861, which leads to the theoretical existence of the electromagnetic (EM) wave, especially after the first ever experimental observation of the EM wave in 1886 by Hertz. The construction of these equations is the fundamentals of light communication, photonics, wireless communication, fluid-structure interactions, and so on. Further, it is discovered that Maxwell's equations

are also very useful to understand the theory of optic sciences and the power output of nano-generators. The theory of EM waves is a direct result of Maxwell's equations, which is our general understanding of their practical implications. One of the greatest creative ideas by Maxwell in 1861 was the introduction of displacement current, $\frac{\partial D}{\partial t}$ in Ampere's law, in order to satisfy the conservation law of charges, which resulted in the unification of electricity and magnetism, where D is called the electric displacement vector, based on which Maxwell proves the equivalence of electricity and magnetism.

In mathematical formulation, the fundamental governing equations of electromagnetism are Maxwell's equations, which are encountered in the form of coupled magnetic and electric equations given by

$$\begin{cases} \text{Faraday's law:} & \nabla \times \mathbf{E} = -i\omega \mathbf{b} \text{ in } \Omega, \\ \text{Ampère's law:} & \nabla \times \mathbf{H} = i\omega \mathbf{d} + \mathbf{j} \text{ in } \Omega, \end{cases} \tag{1.1.1}$$

with the constitutive relations:

$$\mathbf{d} = \epsilon \mathbf{E}, \;\; \mathbf{j} = \sigma \mathbf{E} + \mathbf{j}_e \;\text{ and }\; \mathbf{b} = \mu \mathbf{H}, \tag{1.1.2}$$

where $\Omega \subset \mathbb{R}^d (d = 2, 3)$ is a bounded polyhedral domain with a Lipschitz continuous boundary $\partial\Omega$. Here, $\mathbf{E}$ is the electric field intensity, $\mathbf{b}$ is the magnetic flux density, $\mathbf{H}$ is the magnetic field intensity, $\mathbf{d}$ is the electric displacement flux density, $\mathbf{j}$ is the electric current density, $\mu = \{\mu_{ij}(\mathbf{x})\}_{d\times d}$ is called permeability, $\mathbf{j}_e$ is the external current density, σ is real-valued and is known as the electric conductivity, and $\epsilon = \{\epsilon_{ij}(\mathbf{x})\}_{d\times d}$ is the material parameter which is called permittivity.

Combining the above three equations, we get

$$\begin{cases} \nabla \times \mathbf{E} &= -i\omega\mu\mathbf{H} & \text{in } \Omega, \\ \nabla \times \mathbf{H} &= i\omega\epsilon\mathbf{E} + \sigma\mathbf{E} + \mathbf{j}_e & \text{in } \Omega, \end{cases} \tag{1.1.3}$$

where ω is a constant in the domain Ω.

For the electric field intensity $\mathbf{E}$, we first apply the differential operator $\nabla \times \mu^{-1}$ to the first equation in (1.1.3), and then use second equation to obtain

$$\nabla \times (\mu^{-1} \nabla \times \mathbf{E}) = (\omega^2 \epsilon - i\omega\sigma)\mathbf{E} - i\omega \mathbf{j}_e \;\text{ in }\; \Omega. \tag{1.1.4}$$

For the magnetic field intensity $\mathbf{H}$, we apply $\nabla \times (i\omega\epsilon + \sigma)^{-1}$ to second equation in (1.1.3), and then use first equation to obtain

$$\nabla \times ((i\omega\epsilon + \sigma)^{-1} \nabla \times \mathbf{H}) = -i\omega\mu\mathbf{H} + \nabla \times (i\omega\epsilon + \sigma)^{-1} \mathbf{j}_e \;\text{ in }\; \Omega. \tag{1.1.5}$$

Above equations (1.1.4)-(1.1.5), involving curl-curl operator, are known time-harmonic Maxwell equations for **E** and **H**, respectively.

In electromagnetism, the governing spatial partial differential operators are mainly the curl operator and the divergence operator. The models related to these operators are **H**(div)-elliptic, **H**(curl)-elliptic and **H**(curl, div)-elliptic problems.

1.1.1 Problem Description

In this subsection, we introduce various Maxwell problems that are to be studied in this thesis. It also contains a brief overview of the occurrence of these problems and their applications in the fields of science and engineering.

H(div)-**Elliptic Problem:** In this thesis, we consider a **H**(div)-elliptic problem of the form

$$-\nabla(\alpha\nabla\cdot\mathbf{p})+\gamma\mathbf{p} = \mathbf{f} \text{ in } \Omega, \tag{1.1.6}$$

$$\mathbf{p}\cdot\boldsymbol{\eta} = 0 \text{ on } \partial\Omega, \tag{1.1.7}$$

where $\Omega \subset \mathbb{R}^d$ $(d = 2, 3)$ is a bounded polygonal/polyhedral domain with Lipschitz continuous boundary $\partial\Omega$ and $\boldsymbol{\eta}$ stands for outward unit normal vector to the boundary $\partial\Omega$. Further, we assume that α and γ are uniformly positive coefficients in $L^\infty(\Omega)$, and $\mathbf{f} : \Omega \subset \mathbb{R}^d \to [L^2(\Omega)]^d$ is the given source function.

H(div)-elliptic problems are ubiquitous in solid as well as fluid mechanics (cf. [8, 10, 65, 107]). **H**(div; Ω)-elliptic problems like (1.1.6)-(1.1.7) arise from, e.g., the first-order system least-squares formulation of second-order elliptic problems [25], the stabilized formulations of the Stokes equations [21], preconditioning for the mixed methods using a gradient formulation of the Dirichlet problem [4], or the implementation of the sequential regularization method for the nonstationary incompressible Navier-Stokes system [95].

H(curl)-**Elliptic Problem:** Let $\Omega \subset \mathbb{R}^d$ $(d = 2, 3)$ be a bounded polygonal/polyhedral domain with Lipschitz continuous boundary $\partial\Omega$. The **H**(curl)-elliptic problem reads as

$$\nabla\times(\beta\nabla\times\mathbf{p})+\gamma\mathbf{p}=\mathbf{f} \text{ in } \Omega \tag{1.1.8}$$

with Dirichlet boundary condition

$$\mathbf{p}\times\boldsymbol{\eta}=0 \text{ on } \partial\Omega. \tag{1.1.9}$$

Here, $\mathbf{f} \in \left[L^2(\Omega)\right]^d$, γ is a $d \times d$ positive constant matrix, and β is a $(2d-3)\times(2d-3)$ symmetric matrix with the assumption that there exist two positive constants $\underline{\lambda}$, $\bar{\lambda} > 0$ such that $\underline{\lambda}\zeta^t\zeta \le \zeta^t\beta\zeta \le \bar{\lambda}\zeta^t\zeta$ for all $\zeta \in \mathbb{R}^{2d-3}$. Further, $\boldsymbol{\eta}$ is the unit outward normal vector to $\partial\Omega$.

When $\gamma > 0$, the semi-discretizations of the electric fields in time-dependent Maxwell problems are closely related to (1.1.8)-(1.1.9). Specifically, problems such as (1.1.8)-(1.1.9) must be solved at each time step for the eddy current model, which arises from Maxwell's equations as a magneto-quasi-static approximation by dropping the displacement current (see, e.g., [14, 22, 48]). β denotes magnetic susceptibility in this context, while γ relates to conductivity. The boundary condition (1.1.9) represents walls that conduct electricity properly. For $\gamma \leq 0$, model problem (1.1.8)-(1.1.9) is associated with the time-harmonic Maxwell equations (see, e.g., [17, 19]).

Time-Harmonic Maxwell's equation: In this study, we consider the classical time-harmonic Maxwell's equation with a perfectly conducting boundary, which seeks the unknown electric field function $\mathbf{p}$ that satisfies

$$\nabla \times (\mu_r^{-1} \nabla \times \mathbf{p}) - \gamma^2 \epsilon_r \mathbf{p} = \mathbf{g} \text{ in } \Omega, \tag{1.1.10}$$

$$\mathbf{p} \times \boldsymbol{\eta} = 0 \text{ on } \partial\Omega, \tag{1.1.11}$$

where $\Omega \subset \mathbb{R}^d$ $(d = 2, 3)$ is bounded polygonal/polyhedral domain with Lipschitz continuous boundary $\partial\Omega$. Here, the relative magnetic permeability and electric permittivity are considered in the vacuum, i.e., $(\mu_r^{-1} = \epsilon_r = 1)$. The source term $\mathbf{g} \in [L^2(\Omega)]^d$. In order to establish the well-posedness of the aforementioned problem, we assume that wave number $\gamma > 0$ which should not be the eigenvalue of Maxwell's system (more precisely, γ is not an eigenvalue of the differential operator $\mathcal{L} : \nabla \times (\nabla \times \mathbf{p})$).

The time-harmonic Maxwell's problems are often encountered in several engineering, electromagnetic, telecommunications, medicine, biology, and defence phenomena such as frequency single, antenna designs, radar, satellite modeling, nano-photonic devices, the detection of hidden targets, micromodel design, and medical imaging. For an extensive discussion on the applications for time-harmonic Maxwell's equations, please see [17, 19, 68, 99].

H(curl, div)-**Elliptic Problem:** The **H**(curl, div)-elliptic problem is given by

$$\nabla \times (\beta \nabla \times \mathbf{p}) - \alpha \nabla (\nabla \cdot \alpha \mathbf{p}) + \gamma \mathbf{p} = \mathbf{f} \text{ in } \Omega, \tag{1.1.12}$$

$$\mathbf{p} \times \boldsymbol{\eta} = 0, \quad \nabla \cdot \alpha \mathbf{p} = 0 \text{ on } \partial\Omega, \tag{1.1.13}$$

where $\Omega \subset \mathbb{R}^d$ $(d = 2, 3)$ is a bounded polygonal/polyhedral domain with Lipschitz continuous boundary $\partial\Omega$. Let $\mathbf{f} \in \left[L^2(\Omega)\right]^d$, γ is a $d \times d$ positive constant matrix, α is a $d \times d$ symmetric matrix with the assumption that there exist two positive constants $\underline{\lambda}$, $\bar{\lambda} > 0$ such that $\underline{\lambda} \zeta^t \zeta \leq \zeta^t \alpha \zeta \leq \bar{\lambda} \zeta^t \zeta$ for all $\zeta \in \mathbb{R}^d$ and β is a $(2d-3) \times (2d-3)$ symmetric matrix with the restriction that there exist two positive constants $\underline{\theta}$, $\bar{\theta} > 0$

such that $\underline{\theta}\zeta^t\zeta \leq \zeta^t\beta\zeta \leq \bar{\theta}\zeta^t\zeta$ for all $\zeta \in \mathbb{R}^{2d-3}$. Further, $\boldsymbol{\eta}$ is the unit outward normal vector to $\partial\Omega$.

Equation (1.1.12) is highly generic, as it applies to a vast array of models in numerous physical phenomena involving div and curl operators. The physical problem referenced by (1.1.12) encompasses several model problems in the fields of electromagnetism and fluid-structure mechanics in heterogeneous/homogeneous media (cf. [15, 31, 43, 100, 102, 109, 110, 112]).

Maxwell's Equations with Lagrange Multiplier: We can relate (1.1.12) with vector potential Maxwell model problem as given below (cf. [50])

$$\nabla \times (\beta\nabla \times \mathbf{p}) + \gamma\mathbf{p} = \mathbf{f} \;\; \& \;\; \nabla \cdot (\alpha\mathbf{p}) = 0 \text{ in } \Omega. \tag{1.1.14}$$

To relax the divergence condition, as usual, we introduce a Lagrangian multiplier q; hence, we consider the following general system (cf. [37])

$$\begin{cases} \nabla \times (\beta\nabla \times \mathbf{p}) + \gamma\mathbf{p} - \alpha\nabla q = \mathbf{f} \;\; \& \;\; \nabla \cdot (\alpha\mathbf{p}) = g \;\; \text{in } \Omega, \\ \mathbf{p} \times \boldsymbol{\eta} = \mathbf{0} \;\; \text{and} \;\; q = 0 \;\; \text{on } \partial\Omega. \end{cases} \tag{1.1.15}$$

H(div)-**Elliptic Interface Problem:** Given a polygonal/polyhedral domain $\Omega \subset \mathbb{R}^d$ $(d = 2, 3)$ with a Lipschitz continuous boundary $\partial\Omega$ and a closed smooth interface Γ which separates Ω into two non-intersecting open sub-domains Ω_1 and Ω_2 (see, Fig. 1.1.1 for an illustration) having different physical properties. In this thesis, we consider following **H**(div)-elliptic interface problem:

$$-\nabla(\alpha\nabla \cdot \mathbf{p}) + \gamma\mathbf{p} = \mathbf{f} \;\; \text{in } \Omega, \tag{1.1.16}$$

$$\mathbf{p} \cdot \boldsymbol{\eta} = 0 \;\; \text{on } \partial\Omega, \tag{1.1.17}$$

with non-homogeneous interface jump conditions

$$\begin{cases} [\alpha\nabla \cdot \mathbf{p}] &= \psi \;\; \text{on} \;\; \Gamma, \\ [\mathbf{p} \cdot \boldsymbol{\eta}] &= \phi \;\; \text{on} \;\; \Gamma. \end{cases} \tag{1.1.18}$$

Here, notation $\boldsymbol{\eta}$ stands for the unit outward normal vector to Γ or the unit outward normal vector to $\partial\Omega$. For vector-valued function $\mathbf{v}$, we denote $[\mathbf{v} \cdot \boldsymbol{\eta}] := \mathbf{v} \cdot \boldsymbol{\eta}|_{\Omega_1} - \mathbf{v} \cdot \boldsymbol{\eta}|_{\Omega_2}$ and for scalar function v, we denote, $[v] := v|_{\Omega_1} - v|_{\Omega_2}$. Further, $\mathbf{f} \in \left[L^2(\Omega)\right]^d$ and

$$\alpha \;\; = \;\; \begin{cases} \alpha_1 \;\; \text{in} \;\; \Omega_1, \\ \alpha_2 \;\; \text{in} \;\; \Omega_2, \end{cases} \tag{1.1.19}$$

is a discontinuous function with assumption that there exist two constants $\underline{\alpha}$, $\bar{\alpha}$ with $0 < \underline{\alpha} \leq \bar{\alpha}$ such that $\underline{\alpha} \leq \alpha \leq \bar{\alpha}$ a.e. in Ω. Along with this, we consider γ to be piecewise positive constant, i.e.,

$$\gamma = \begin{cases} \gamma_1 \text{ in } \Omega_1, \\ \gamma_2 \text{ in } \Omega_2 \end{cases} \tag{1.1.20}$$

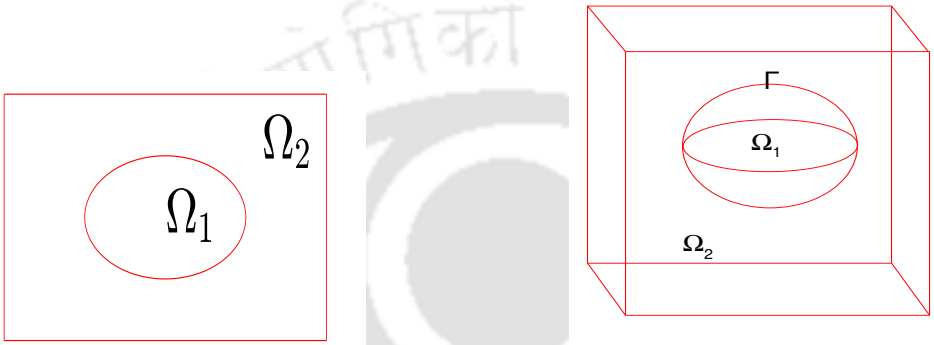

Figure 1.1.1: Domain Ω and its subdomains Ω_1, Ω_2 with interface Γ in $\mathbb{R}^2$ (left) and $\mathbb{R}^3$ (right).

Interface problems occur in various fields of applied sciences such as electromagnetic spectrum field, bio-medical models, and coupled thermoelastic theory. Most of the phenomenon arises in fluid dynamics and hydrodynamic fields are governed by partial differential equations with discontinuity in the physical coefficients along the interface. $\mathbf{H}$(div)-elliptic interface model (1.1.16)-(1.1.18) can be obtained from the least-square formulation of the system of the elliptic interface models [24], gradient formulation of saddle point elliptic interface problems by using mixed finite element methods [72, 115] and regularization technique for the non-stationary Navier-stokes models [60, 94].

$\mathbf{H}$(curl, div)-Elliptic Interface Problem: We consider a $\mathbf{H}(\text{curl}, \text{div})$-elliptic interface problem in $\Omega = \Omega_1 \cup \Omega_2 \in \mathbb{R}^d$ $(d = 2, 3)$ filled with different anisotropic non-homogenous physical properties i.e., permeability and permittivity of the materials in the case of electromagnetism are discontinuous along the interface $\Gamma = \Omega_1 \cap \Omega_2$ (cf. Fig. 1.1.1). The second order $\mathbf{H}(\text{curl}, \text{div})$-elliptic interface system is read as follows:

$$\begin{cases} \nabla \times (\beta \nabla \times \mathbf{p}) - \nabla(\alpha \nabla \cdot \mathbf{p}) + \gamma \mathbf{p} = \mathbf{f} \text{ in } \Omega, \\ \nabla \cdot \mathbf{p} = 0, \quad \mathbf{p} \times \boldsymbol{\eta} = 0 \text{ on } \partial\Omega, \\ [\mathbf{p} \times \boldsymbol{\eta}] = \boldsymbol{\rho}, \quad [(\beta \nabla \times \mathbf{p}) \times \boldsymbol{\eta}] = \boldsymbol{\chi} \text{ on } \Gamma, \\ [\mathbf{p} \cdot \boldsymbol{\eta}] = \phi, \quad [\alpha \nabla \cdot \mathbf{p}] = \psi \text{ on } \Gamma, \end{cases} \tag{1.1.21}$$

where the symbols $[\mathbf{v}\cdot\boldsymbol{\eta}]$, $[v]$ and $\boldsymbol{\eta}$ are defined as in the model problem (1.1.16)-(1.1.18). In addition, jump $[\mathbf{v}\times\boldsymbol{\eta}]$ is defined as $[\mathbf{v}\times\boldsymbol{\eta}] := \mathbf{v}\times\boldsymbol{\eta}|_{\Omega_1} - \mathbf{v}\times\boldsymbol{\eta}|_{\Omega_2}$. Setting $\zeta \in \{\alpha, \beta, \gamma\}$, we assume that

$$\zeta \;=\; \begin{cases} \zeta_1 \;\text{ in }\; \Omega_1, \\ \zeta_2 \;\text{ in }\; \Omega_2, \end{cases} \tag{1.1.22}$$

is a discontinuous function with the assumption that there exist two constants $p_1,\ p_2$ with $0 < p_1 \le p_2$ such that $p_1 \le \zeta \le p_2$ a.e. in Ω and $\mathbf{f} \in \left[L^2(\Omega)\right]^d$. For the detailed discussions, we refer to [50].

1.2 Notations and Preliminaries

This section concerns some standard notations and preliminary materials, which are crucial for the construction of this thesis. All the scalar and vector functions used in this thesis are real-valued. Let Ω be a convex polygonal/polyhedral bounded domain in $\mathbb{R}^d$ $(d = 2, 3)$ with boundary $\partial\Omega$. Let $x = (x_1, \cdots, x_d) \in \Omega$ and $dx = dx_1 \cdots dx_d$. Further, let $\theta = (\theta_1, \cdots, \theta_2)$ be a non negative integer with d-components and the order of θ is defined as $|\theta| = \theta_1 + \cdots + \theta_2$. Then, the θ-th derivative of v is denoted by $D^\theta v$ given as follows

$$D^\theta v = \frac{\partial^\theta v}{\partial {v_1}^{\theta_1} \cdots \partial {v_d}^{\theta_d}}.$$

Next, we recall some basic functional spaces. For any domain $\mathcal{K} \subseteq \Omega$ with $1 \le p < \infty$, $L^p(\mathcal{K})$ be the normed linear space of equivalence classes of measurable functions v in $\mathcal{K}$ with $\|v\|_{L^p(\mathcal{K})} < \infty$.

$$\begin{aligned} \|v\|_{L^p(\mathcal{K})} &:= \left(\int_{\mathcal{K}} |v(x)|^p dx\right)^{\frac{1}{p}},\ 1 \le p < \infty, \\ \|v\|_{L^p(\mathcal{K})} &= \operatorname*{ess\,sup}_{x\in\mathcal{K}} |v| < \infty. \end{aligned}$$

For simplicity, we write the norm $\|\cdot\|_{L^p(\mathcal{K})}$ on $L^p(\mathcal{K})$ by $\|\cdot\|_{\mathcal{K}}$ and when $\mathcal{K} = \Omega$, then we omit the subscript $\mathcal{K}$.

In particular, for $p = 2$, $L^2(\mathcal{K})$ is a Hilbert space with the norm induced from the inner product given as follows

$$(v_1, v_2)_{\mathcal{K}} = \int_{\mathcal{K}} v_1 v_2 dx \;\;\forall\;\; v_1, v_2 \in L^2(\mathcal{K}).$$

The support of a function v is denoted by $\operatorname{supp}(v)$ defined as the closure of a set of all points x such that $v(x) \neq 0$.

For any integer $m \geq 0$, $C^m(\bar{\Omega})$ is a space of all functions with continuous derivatives up to and including order m in $\bar{\Omega}$. $C^m(\bar{\Omega}) \subset C_0^m(\bar{\Omega})$ is a subspace consisting of all the functions with compact support in Ω and $C_0^\infty(\bar{\Omega})$ is a space of all infinitely differentiable functions with compact support in Ω. For any integer $k \geq 0$ and $1 \leq p \leq \infty$, the standard Sobolev space denoted by $W^{k,p}(\mathcal{K})$ is a space of all functions whose distributional derivatives of order upto k are in $L^p(\mathcal{K})$. More precisely,

$$W^{k,p}(\mathcal{K}) = \{\upsilon \in L^p(\mathcal{K}) : D^\theta \upsilon \in L^p(\mathcal{K}) \text{ for } 0 \leq |\theta| \leq k\}.$$

The norm associated to $W^{k,p}(\mathcal{K})$ is given as follows

$$\begin{aligned} \|\upsilon\|_{k,p,\mathcal{K}} &= \left(\sum_{0 \leq \theta \leq k} \|D^\theta \upsilon\|^p_{L^p(\mathcal{K})} \right)^{\frac{1}{p}}, \ 1 \leq |\theta| < \infty. \\ \|\upsilon\|_{k,\infty,\mathcal{K}} &= \max_{0 \leq \theta \leq k} \|D^\theta \upsilon\|_{L^\infty(\mathcal{K})}, \ p = \infty, \end{aligned}$$

and the semi-norm on $W^{k,p}(\mathcal{K})$ is defined as

$$|\upsilon|_{k,p,\mathcal{K}} = \sum_{\theta = k} \|D^\alpha \upsilon\|_{L^p(\mathcal{K})}.$$

In particular, for $p = 2$, we denote $W^{k,2}(\mathcal{K})$ by $H^2(\mathcal{K})$ with the norm $\|\cdot\|_{2,\mathcal{K}} = \|\cdot\|_2$ and when $\mathcal{K} = \Omega$, we omit the subscript $\mathcal{K}$ from the norm and inner product.

The space $H^k(\mathcal{K})$ is a Hilbert space with the inner product given by

$$(\upsilon_1, \upsilon_2)_{k,\mathcal{K}} = \sum_{0 \leq \theta \leq k} \int_{\mathcal{K}} D^\theta \upsilon_1 D^\theta \upsilon_2 dx \ \ \forall \ \ \upsilon_1, \upsilon_2 \in H^k(\mathcal{K}).$$

We now define the following usual vector valued Sobolev spaces

$$\begin{aligned} \mathbf{H}^s(\text{div}; \delta; \Omega) &= \{\mathbf{v} \in \mathbf{H}^s(\Omega), \ \nabla \cdot \delta\mathbf{v} \in H^s(\Omega)\}. \\ \mathbf{H}^s(\text{curl}; \delta; \Omega) &= \{\mathbf{v} \in \mathbf{H}^s(\Omega) : \ \nabla \times \delta\mathbf{v} \in [H^s(\Omega)]^{2d-3}\}, \\ \mathbf{H}^s_0(\text{div}; \delta; \Omega) &= \{\mathbf{v} \in \mathbf{H}^s(\text{div}; \delta; \Omega) : \delta\mathbf{v} \cdot \boldsymbol{\eta} = 0 \text{ on } \partial\Omega\}, \\ \mathbf{H}^s_0(\text{curl}; \delta; \Omega) &= \{\mathbf{v} \in \mathbf{H}^s(\text{curl}; \delta; \Omega) : \delta\mathbf{v} \times \boldsymbol{\eta} = \mathbf{0} \text{ on } \partial\Omega\}, \end{aligned}$$

where δ is any weight function and $s \geq 0$ is an integer. Note that for $\delta = 1$, we have $\mathbf{H}(\text{div}; \Omega) = \mathbf{H}(\text{div}; 1; \Omega)$ and $\mathbf{H}(\text{curl}; \Omega) = \mathbf{H}(\text{curl}; 1; \Omega)$. Further, we write $\mathbf{H}^s(\mathcal{U}) = [H^s(\mathcal{U})]^{2d-3}$. Here we don't distinguish $H^s(\mathcal{U})$ and $\mathbf{H}^s(\mathcal{U})$ for standard Hilbert spaces for simplicity. In addition, the norms on $\mathbf{H}^s(\text{div}; \Omega)$ and $\mathbf{H}^s(\text{curl}; \Omega)$ can be introduced as follows

$$\begin{aligned} \|\mathbf{v}\|_{s,\mathbf{div}} &= \left(\|\mathbf{v}\|^2_{\mathbf{H}^s(\Omega)} + \|\nabla \cdot \mathbf{v}\|^2_{\mathbf{H}^s(\Omega)} \right)^{\frac{1}{2}}, \\ \|\mathbf{v}\|_{s,\mathbf{curl}} &= \left(\|\mathbf{v}\|^2_{\mathbf{H}^s(\Omega)} + \|\nabla \times \mathbf{v}\|^2_{\mathbf{H}^s(\Omega)} \right)^{\frac{1}{2}}. \end{aligned}$$

When $\Omega = \Omega_1 \cup \Omega_2 \cap \Gamma$, where Ω_i $(i = 1, 2)$ are two subdomains of Ω and Γ is an interface such that $\Gamma = \Omega_1 \cap \Omega_2$, then we define the following Sobolev spaces

$$\begin{aligned}
\mathbf{H}^s(\text{div}; \Omega_1, \Omega_2) &= \{\mathbf{v} \in \mathbf{H}^s(\Omega_i) : \nabla \cdot \mathbf{v} \in H^s(\Omega_i),\ i = 1,\ 2\},\\
\mathbf{H}^s(\text{curl}; \Omega_1, \Omega_2) &= \{\mathbf{v} \in \mathbf{H}^s(\Omega_i) : \nabla \times \mathbf{v} \in [H^s(\Omega_i)]^{2d-3},\ i = 1,\ 2\},\\
\mathbf{H}^s_0(\text{div}; \Omega_1, \Omega_2) &= \{\mathbf{v} \in \mathbf{H}^s(\text{div}; \Omega_1, \Omega_2) : \mathbf{v} \cdot \boldsymbol{\eta} = 0 \text{ on } \partial\Omega\},\\
\mathbf{H}^s_0(\text{curl}; \Omega_1, \Omega_2) &= \{\mathbf{v} \in \mathbf{H}^s(\text{curl}; \Omega_1, \Omega_2) : \mathbf{v} \times \boldsymbol{\eta} = \mathbf{0} \text{ on } \partial\Omega\}.
\end{aligned}$$

In two dimensions, for the vector-valued function $\mathbf{v} = (v_1, v_2)^t$, the curl of $\mathbf{v}$ defines as

$$\nabla \times \mathbf{v} = \frac{\partial v_2}{\partial x} - \frac{\partial v_1}{\partial y},$$

and for scalar-valued function v, the curl of v read as

$$\nabla \times v = \left(\frac{\partial v}{\partial y}, -\frac{\partial v}{\partial x}\right)^t.$$

For more detailed discussions on Sobolev spaces, we refers to [1, 99].

We end this section by introducing the variational formulations for some aforementioned model problems. The variational formulation of (1.1.6)-(1.1.7) can be defined as follows: Seek $\mathbf{p} \in \mathbf{H_0}(\text{div}; \Omega)$ such that

$$\int_\Omega \alpha \text{div } \mathbf{p} \cdot \text{div } \mathbf{v} dx + \int_\Omega \gamma \mathbf{p} \cdot \mathbf{v} dx = \int_\Omega \mathbf{f} \cdot \mathbf{v} dx \ \ \forall \mathbf{v} \in \mathbf{H_0}(\text{div}; \Omega). \tag{1.2.1}$$

Existence and uniqueness of the solution of (1.2.1) is ensured by the Lax-Milgram Lemma [39].

Now, the variational formulation of the problem (1.1.8)-(1.1.9) is read as: Find $\mathbf{p} \in \mathbf{H}_0(\text{curl}; \Omega)$ such that

$$\int_\Omega \beta \text{curl } \mathbf{p} \cdot \text{curl } \mathbf{v} dx + \int_\Omega \gamma \mathbf{p} \cdot \mathbf{v} dx = \int_\Omega \mathbf{f} \cdot \mathbf{v} dx \ \ \forall \mathbf{v} \in \mathbf{H_0}(\text{curl}; \Omega). \tag{1.2.2}$$

Existence and uniqueness of the solution of (1.2.2) can be found in [61].

The variational formulation of (1.1.16)-(1.1.18) seeks $\mathbf{p} \in \mathbf{H_0}(\text{div}; \Omega)$ such that

$$\int_\Omega \alpha \text{div } \mathbf{p} \cdot \text{div } \mathbf{v} dx + \int_\Omega \gamma \mathbf{p} \cdot \mathbf{v} dx = \int_\Gamma \psi (\mathbf{v} \cdot \mathbf{n}) ds + \int_\Omega \mathbf{f} \cdot \mathbf{v} dx \ \ \forall \mathbf{v} \in \mathbf{H_0}(\text{div}; \Omega). \tag{1.2.3}$$

Next, the variational formulation of the problem (1.1.12)-(1.1.13) can be obtained by finding $\mathbf{p} \in \mathbf{H}_0(\text{curl}; \Omega) \cap \mathbf{H}(\text{div}, \text{curl}; \Omega)$ such that

$$\int_\Omega \text{div } \alpha \mathbf{p} \cdot \text{div } \alpha \mathbf{v} dx \int_\Omega \beta \text{curl } \mathbf{p} \cdot \text{curl } \mathbf{v} dx + \int_\Omega \gamma \mathbf{p} \cdot \mathbf{v} dx = \int_\Omega \mathbf{f} \cdot \mathbf{v} dx, \tag{1.2.4}$$

for all $\mathbf{v} \in \mathbf{H}_0(\text{curl}; \Omega) \cap \mathbf{H}(\text{div}; \Omega)$, and finally, the variational formulation of the problem (1.1.21) seeks $\mathbf{p} \in \mathbf{H}_0(\text{curl}; \Omega) \cap \mathbf{H}(\text{div}, \text{curl}; \Omega)$ such that

$$\begin{aligned} &\int_\Omega \text{div } \alpha\mathbf{p} \cdot \text{div } \alpha\mathbf{v} dx + \int_\Omega \beta \text{curl } \mathbf{p} \cdot \text{curl } \mathbf{v} dx + \int_\Omega \gamma \mathbf{p} \cdot \mathbf{v} dx \\ &= \int_\Gamma \boldsymbol{\chi} \cdot \mathbf{v} ds + \int_\Gamma \psi(\mathbf{v} \cdot \boldsymbol{\eta}) ds + \int_\Omega \mathbf{f} \cdot \mathbf{v} dx, \end{aligned} \tag{1.2.5}$$

for all $\mathbf{v} \in \mathbf{H}_0(\text{curl}; \Omega) \cap \mathbf{H}(\text{div}; \Omega)$. For the existence and uniqueness of the solutions of (1.2.4)-(1.2.5) one can see in [61].

1.3 Background and Motivation

This section briefly explains the existing relevant literature including our contributions with the rationale behind the present study.

Most modern technology is inconceivable without harnessing electromagnetic phenomena. Hence the design and analysis of schemes for the approximate solution of electromagnetic field problems can claim a rightful place as a core discipline of numerical mathematics and scientific computing. Finite element discretizations of Maxwell's equations are not as simple as they look, though. Finite element methods for Maxwell's equations are highly sensitive to the conformity of approximation spaces (see [47]). By the continuous finite element method, an incorrect solution may be obtained the continuous finite element solution converges to a function of $[\mathbf{H}^1(\Omega)]^d$, but not to the solution which does not belong to $[\mathbf{H}^1(\Omega)]^d$, see [47]. For instance, whenever the domain has reentrant corners/edges, the solution $\mathbf{u}$ is typically not in $[\mathbf{H}^1(\Omega)]^d$ but rather in $[\mathbf{H}^r(\Omega)]^d$ for some $r < 1$, (see, e.g., [47]). This low regularity of solution is what makes the implementation of the finite element method to Maxwell problems extremely challenging.

The significance of $\mathbf{H}(\text{div})$-elliptic problems has caused robust research into coherent numerical schemes. Classical finite element approximations for $\mathbf{H}(\text{div}; \Omega)$-elliptic problems have been studied extensively in the existing literature. For more details, we refer to [4, 20, 67, 69, 73, 95, 108]. In recent past years, there are different types of discontinuous Galerkin (DG) method has been developed for elliptic and system of equations due to the flexibility in the choices of approximation spaces. $\mathbf{H}(\text{div}; \Omega)$-flux reconstruction for DG approximation of elliptic problem has been discussed in [56]. The stable DG method for time-harmonic Maxwell's equations has been discussed in [59]. $\mathbf{H}(\text{div}; \Omega)$-conforming DG method for the Stokes equation has been discussed in [83]. DG discretizations of $\mathbf{H}(\text{curl}; \Omega)$-elliptic partial differential equations have been discussed in [76]. The hybridizable DG method for linear elasticity has been discussed in [113]. Interior penalty DG method for $\mathbf{H}(\text{div}; \Omega)$-elliptic method has been discussed

in [126]. Over the last two decades, for $\mathbf{H}(\text{curl})$ and $\mathbf{H}(\text{curl, div})$ Maxwell problems, many alternative approaches have been developed which include $\mathbf{H}(\text{curl}; \Omega)$ conforming edge element methods [50, 99], H^1 conforming nodal finite element methods with weighted regularization [44, 53], the singular complement/field method [66], interior penalty methods [19], nonconforming finite element methods [17, 18, 19], mixed finite element method [54]. For the recent relevant works, we refer to [52] and the references therein.

Numerous electromagnetic phenomena are of interest, primarily at a single frequency, in which case, they are governed by the time-harmonic Maxwell's equations. The finite element method is amongst the most popular numerical techniques used to solve such problems. The time-harmonic Maxwell's equations and related problems have been studied extensively in literature by using various finite element methods. A natural choice is to utilize $\mathbf{H}(\text{curl})$-conforming elements, known as edge element approaches. We refer to Nédélec [104], Jin [82], Monk [98, 99], Hiptmair [68] for more details of these conforming methods. Edge elements have several desirable properties that make them ideally suited to solve these problems. However, the use of low-order edge elements often lead to the discrete systems with large numbers of unknowns, especially for electromagnetic problems at high frequencies. On the other hand, the implementation of high-order edge element method is still challenging (cf. [16]). For an extensive discussion on high-order edge elements for Maxwell's equations, please see [2, 62, 111]. Using the discontinuous functions in the finite element technique provides extra flexibility in the selection of mesh partitions and finite element spaces. Numerous research articles have been published over the years using the finite element spaces approximating by discontinuous functions, such as local discontinuous Galerkin (DG) methods [3, 30], interior penalty DG methods [59, 74], mixed DG methods [75, 80], hybrid mixed DG method [55], hybridizable DG methods [58, 105, 127], Trefftz-DG method [71]. The Maxwell's operator is strongly indefinite for high wave number, which brings difficulties to both in theoretical analysis and numerical simulation. In literature, least-squares-based finite element method is also applied for solving the indefinite time-harmonic Maxwell's equations. The least-squares finite element method (LS-FEM) is a general numerical method, which is based on the minimization of a quadratic functional, and we refer to [13] for an overview to this method. The resulting system arising from most of the Galerkin finite element methods are indefinite with a large wave number, while the LS-FEM can provide a positive definite linear system [6, 32, 33, 77, 91]. In last two decades, the LS-FEM has been successfully implemented for various physical phenomena using discontinuous elements (cf. [9, 11, 91, 93], to name a few).

Despite the fact that conforming finite element methods have simple formulations with significantly fewer unknowns, the construction of conforming finite element spaces of any order is virtually impossible in the most of the practical problems. In the past few decades, significant progress has been achieved in the development of improved finite element methods for many classes of problems, which has become an active topic of research for applied mathematicians. The capacity of this method to handle a large class of problems with complex structures in a straightforward and systematic manner makes it preferable to other numerical procedures in numerous scientific and technical disciplines. Keeping in mind the applicability of higher-order numerical methods with polygonal meshes, recent efforts have been made to develop technologies that enable the use of polygonal meshes, for more details see in [26, 45] for virtual element methods and [42] for discontinuous Galerkin methods. Polygonal meshes are compatible with numerous complex geometries, allowing them to be utilized with finite element methods. A more recent development in the family of DG methods is the hybrid high-order method (HHO) [23, 41, 49, 63]. In [40], the authors have proposed an HHO method for the indefinite time-harmonic Maxwell's equations and evaluated its numerical performance. The theoretical convergence analysis of HHO method for the Maxwell problem (1.1.10)-(1.1.11) is still open.

The past few decades have witnessed intensive research activity in interface problems. Finite element method (FEM) is an another class of important approaches for interface problems and a wide variety of FEM approaches have been proposed in the literature. There are two major classes of FEM depending on the choice of the discretization, namely, interface fitted FEMs and unfitted FEMs. In fitted FEMs, the discretization is made in such a way that the grid line either follows the actual interface or is an approximation of the smooth interface. In unfitted FEMs, the discretization is independent of the location of the interface. Owing to its mathematical complexity and essential importance in a number of application areas, the study of interface problems has evolved into a well-defined field in applied and computational mathematics. Elliptic interface models were first studied in [5]. Since then in FEMs with smooth interfaces, several different kinds of works have been done on elliptic interface models, for more details, we refer to [7, 27, 28, 38, 46, 79, 88, 89, 106, 118]. The accuracy and effective implementation of the FEMs depend on various factors such as variational formulation of the problem, finite element discretization and interface fitted discretization. The discontinuity of flux can be encountered in the variational formulations of the interface problems in the case of classical FEMs. But the discontinuity occurs in solution across the interface neither incorporated in FEM solution space nor arises in the variational

formulation.

For interface problems, the development of high-order cost-efficient numerical methods is always paid more attention. If the interfaces are smooth enough, then optimal high-order convergence can be obtained with body-fitted FEMs (see [89]). The body-fitted finite element methods (FEMs) are one of the effective numerical approximation techniques to deal with various mathematical models such as elliptic interface models and bio-heat electric interface models, etc. In most of the physical model problems, interfaces occur with geometric singularities (due to edges, cusps, and tips), not Lipschitz continuous and have low global regularities. To keep this in mind, discontinuous Galerkin FEMs [81], hybridizable DG method [81], [35] for virtual element methods with fitted interface discretization has been developed for general polygonal meshes. A main difficulty for solving even interface Maxwell problems stems from the low regularity of the exact solution. In a practical setting with the geometry singularities result the solutions in $\mathbf{H}^l(\Omega_1) \cap \mathbf{H}^l(\Omega_2)$ ($l \geq \frac{1}{2}$) regularity (e.g., [18, 50]. The low regularity of the solutions makes many existing analysis techniques developed for $H^2(\Omega_1) \cap H^2(\Omega_2)$ solutions unavailable. Classical FEM for $\mathbf{H}$(div)-elliptic problems has been studied in [69]. Optimal error estimate for $\mathbf{H}$(div)-norm is obtained for C^2 smooth interface with homogeneous jump conditions. Recently, interface-penalty FEMs are proposed to solve $\mathbf{H}$(div)-elliptic interface problem in [96] using unfitted tetrahedral meshes. Error estimates of optimal orders are derived in energy norms assuming three transmission conditions. Although interface-penalty FEMs is able to achieve accuracy near the interfaces, the stabilizer needs one more penalty term to maintain the stability. In addition, immersed virtual element techniques have been developed for Maxwell interface problems in 3D in [27]. Optimal convergence results have been derived with homogenous jump conditions. More recently, high-order discontinuous Galerkin finite element method for solving the $\mathbf{H}$(div) elliptic interface problems (1.1.16)-(1.1.18) on unfitted meshes has been discussed in [92]. The optimal and suboptimal convergence rates under the energy norm and L^2 norm are derived in [92]. For other types of Maxwell interface problems, we refer to [26, 34, 37, 50, 64, 123].

More recently, the weak Galerkin finite element methods (WG-FEMs) has gained attention in the field of numerical partial differential equations. The WG-FEMs refer to the numerical algorithms for differential equations which are derived from weak formulations of the problems by replacing the involved differential operators by their weak forms and adding parameter free stabilizers [120]. The HHO method is closely related to weak Galerkin finite element method (or skeletal DG methods [29]) as the reconstruction operator in the HHO method corresponds to the weak operator in WG methods. The only

difference between HHO and WG methods lies in the choice of the discrete unknowns and in the pattern of stabilization. WG-FEM is a member of the class of hybridized Galerkin methods. The approach decomposes the space in polygonal/polyhedral elements of close to arbitrary shape and introduce polynomial approximation in the interior as well as on the boundary of each element (cf. [121]). By discretizing the PDE in each cell, with a reconstructed or weak operator and using the face degrees of freedom to ensure the physical transmission conditions between the cells a local-global separation is obtained. It is then possible to eliminate local element degrees of freedom in a procedure known as static condensation and solve a linear system for the face degrees of freedom only. The WG formulation uses totally discontinuous functions to approximate solutions and their derivatives, which seems to be the key point in the WG-FEM. Many other characteristics are included in the WG method, such as symmetric positive definite formulation, higher order of convergence, and most vital, the capability to employ general meshes including hanging node meshes, polygonal, and polyhedral meshes, and hybrid meshes. The WG-FEMs have been implemented successfully for several Maxwell problems. We refer to [90, 102, 114, 116, 117, 125] for full scale study of the theory and algorithm of WG-FEMs applied to Maxwell's equations. Some advantages of the WG method over traditional FEM are as follows:

- Flexibility in constructing approximation spaces: For instance, high-order WG spaces are usually built more conveniently than the conforming FEM spaces since there is no continuity requirement on the approximation spaces.

- Flexibility on approximation functions: For example, the polynomial $\mathcal{P}_k$ can be used on cubic element in this method. There is no need to construct particular elements such as $\mathcal{Q}_k$.

- Adaptability on mesh generation: Hybrid meshes, polygonal mesh, or meshes with hanging nodes are allowed in this method.

Due to the use of the RT and BDM elements, the weak Galerkin finite element formulation of [120] was limited to classical finite element partitions of triangles ($d = 2$) and tetrahedra ($d = 3$). In [121], a WG-FEM was developed for the second-order elliptic equation in mixed form. The use of stabilization for the flux variable in the mixed formulation is the key to the WG mixed finite element method of [121]. The resulting WG mixed finite element schemes turned out to be applicable for general finite element partitions consisting of shape regular polytopes, and the stabilization idea opened a new door for weak Galerkin method. At first, we extend the work in [121] by analyzing a numerical study on weak Galerkin finite element method for $\mathbf{H}$(div)-elliptic

problems. Optimal orders of convergence are established for the WG approximations in both discrete energy norm and L^2 norm. Then the analysis has been extended for $\mathbf{H}(\text{div})$-elliptic interface problems (1.1.16)-(1.1.18). In this work, we have discussed the fitted WG-FEM for $\mathbf{H}(\text{div})$-elliptic interface model problem (1.1.16)-(1.1.18) based on polygonal (in 2D)/polyhedral (in 3D) meshes. In both L^2 and H^1 norms, the error estimates of the optimal orders are discussed for the proposed WG algorithm. Moreover, Several numerical experiments have been carried out that also involve complicated interfaces and solutions having low regularity to justify the theoretical results.

Next, WG-FEMs for $\mathbf{H}(\text{curl}; \Omega)$ and $\mathbf{H}(\text{curl}, \text{div}; \Omega)$-elliptic problems are investigated in this thesis. The WG method as applied to curl-curl and grad-div problems uses two operators: discrete weak curl and discrete weak divergence, with appropriately defined stabilizations that enforce a weak continuity of the approximating functions. This WG method is highly flexible by allowing the use of discontinuous approximating functions on the arbitrary shape of polyhedra and, at the same time, is parameter-free. The optimal order of convergence is established for the WG approximations in discrete H^1 norm and L^2 norm. In fact, theoretical convergence analysis holds under low regularity requirements of the analytical solution. Results of numerical experiments that corroborate the theoretical results are also presented. There are a few finite element methods for stationary Maxwell interface problems (e.g., [26, 50, 51, 70, 92]). It is worthwhile to note that all existing works for Maxwell interface problems have been developed for homogeneous jump conditions. On the other hand, discontinuity of the solution along the interfaces adds more challenges than one would imagine. Therefore, we propose to develop higher order weak Galerkin finite element schemes for static Maxwell's equations involving curl, grad and div operators with non-homogeneous jump conditions. Related theoretical convergence analysis has been carried out in this thesis. At the same time, the method would be able to accommodate very irregular interfaces and low regular solutions.

WG-FEMs for Maxwell's equations were first studied in [102]. Optimal order error estimates were derived by analyzing saddle point problems. In this thesis, we introduce weak Galerkin least-squares method for solving Maxwell's equations (1.1.10) and (1.1.15). Compared to existing researches, our work has a quite simple theoretical analysis with very low regularity requirement.

1.4 Layout of the Thesis

This thesis is composed of nine chapters, which are listed below.

Chapter 1 contains the description of the problems, notations and preliminary materials to be used in the thesis. It also provides a brief survey on the relevant literature concerning the problems and their numerical solutions. Further, motivations for the present study is discussed.

In **Chapter 2**, we discuss high-order WG-FEMs for $\mathbf{H}$(div)-elliptic problems with variable coefficients. The optimal order convergence results are derived with suitable weak Galerkin space. The numerical experiments are consistent with the theoretical results. Results and findings of this chapter are published in [86].

Chapter 3 is concerned with the higher order weak Galerkin finite element methods for the $\mathbf{H}$(curl)-elliptic equations on the general polygonal/polyhedral meshes. The optimal order theoretical error estimates are discussed for the approximation space $\Big(\big[\mathcal{P}_k(T)\big]^d,\ \big[\mathcal{P}_k(\partial T)\big]^d,\ \mathcal{P}_{k-1}(T)\Big)$. Numerical tests are conducted to justify the theoretical convergence results. Results and findings of this chapter are communicated in [85].

In **Chapter 4**, we describe the WG algorithm for the $\mathbf{H}$(curl, div)-elliptic problems with variable physical coefficients for the general polygonal/polyhedral partitions. The error estimates of optimal orders are illustrated for the energy and L^2 norms with appropriate WG space. Further, numerical studies confirm the theoretical estimates. Results and findings of this chapter are communicated in [85].

Chapter 5 is devoted to study the WG methods for the $\mathbf{H}$(div)-elliptic interface problems with non-homogeneous jump conditions for the general polygonal/polygonal meshes. The theoretical optimal error estimates are obtained in discrete H^1 and L^2 norms. Numerical simulations justify the accuracy, efficiency, and robustness of the WG algorithms. Results and findings of this chapter are published in [87].

In **Chapter 6**, we discuss the high-order WG methods for the $\mathbf{H}(\mathrm{div}, \mathrm{curl})$-elliptic interface problems with non-homogeneous jump conditions with polygonal/polyhedral meshes. Error estimates of $\mathrm{O}(h^k)$ in energy and $\mathrm{O}(h^{k+1})$ in L^2 norms are established with weak Galerkin space $\Big(\big[\mathcal{P}_k(T)\big]^d,\ \big[\mathcal{P}_k(\partial T)\big]^d,\ [\mathcal{P}_{k-1}(T)]^{2d-3},\ \mathcal{P}_{k-1}(T)\Big)$.

Chapter 7 explores the least-squares weak Galerkin finite element method for time-harmonic Maxwell's equation on general polygonal/polyhedral meshes. The error estimate in energy norm is derived for the proposed algorithm. Several numerical experiments are illustrated that are consistent with theoretical estimates.

In **Chapter 8**, we have discussed the least-squares weak Galerkin finite element method for Maxwell's equation with Lagrange multiplier on general polygonal/polyhedral meshes. The error estimate in energy norm is obtained for the LSWG algorithm. Numerical simulations are conducted that confirm the theoretical finding.

Finally, **Chapter 9** discusses the critical interpretation of the results, trying to

emphasize the contributions made by this thesis and the scope for future studies.

For clarity of presentation we have repeatedly mentioned the problems and relevant preliminary materials at the beginning of each chapter.

2

WG-FEMs for H(div)-Elliptic Problems

This chapter provides the weak Galerkin (WG) finite element schemes for $\mathbf{H}(\mathrm{div};\Omega)$-elliptic problems with general polygonal/polyhedral meshes. Optimal orders of convergence are established for the WG approximations in both discrete energy norm and L^2 norm. Numerical experiments are conducted to justify the accuracy, flexibility, and robustness of the proposed WG algorithm. Further, two numerical experiments have been performed for the $\mathbf{H}(\mathrm{div};\Omega)$-elliptic interface problem with homogenous jump conditions and $\mathbf{H}(\mathrm{div};\Omega)$ convection-diffusion problem, which predicates the optimal order error estimates with respect to aforementioned norms.

2.1 Introduction

To begin with, first, we recall the $\mathbf{H}(\mathrm{div};\Omega)$-elliptic problem of the form

$$-\nabla(\alpha\nabla\cdot\mathbf{p})+\gamma\mathbf{p} = \mathbf{f} \text{ in } \Omega, \tag{2.1.1}$$

$$\mathbf{p}\cdot\boldsymbol{\eta} = 0 \text{ on } \partial\Omega, \tag{2.1.2}$$

where $\Omega\subset\mathbb{R}^d$ $(d=2,3)$ is a convex polygonal/polyhedral domain with boundary $\partial\Omega$ and $\boldsymbol{\eta}$ stands for outward unit normal vector to the boundary $\partial\Omega$. Further, we assume that α and γ are uniformly positive coefficients in $L^\infty(\Omega)$, and $\mathbf{f}:\Omega\subset\mathbb{R}^d\to[L^2(\Omega)]^d$ is the given source function.

The significance of $\mathbf{H}(\mathrm{div};\Omega)$-elliptic problems have caused robust research into coherent numerical schemes. So, the aim of this work is to develop the convergence results of the WG finite element method for the $\mathbf{H}(\mathrm{div};\Omega)$-elliptic problem with polygonal/polyhedral meshes and meshes with hanging nodes. Classical finite element approximations for $\mathbf{H}(\mathrm{div};\Omega)$-elliptic problems have been studied extensively in the existing

Results of this Chapter are published online in [86], https://doi.org/10.1002/zamm.202200207

literature. For more details, we refer to [4, 20, 67, 69, 73, 95, 108]. But in the case of conforming finite element methods, there are certain restrictions on the selections of finite spaces and partitions of the domain, which makes them less consistent. To overcome these challenges, the various types of discontinuous Galerkin (DG) methods have been developed for elliptic and system of equations due to flexibility in the choices of approximation spaces. For more details see, the interior penalty DG method for $\mathbf{H}(\mathrm{div};\Omega)$-elliptic method has been discussed in [126] and the references therein. The accuracy and computational complexity of the corresponding WG scheme are significantly impacted by the selection of such polynomials. In the present chapter, we derive the optimal error bounds in the discrete H^1 norm and L^2 norm for a stabilizer-based weak Galerkin algorithm. More precisely, error estimates of $\mathrm{O}(h^k)$ in energy norm and $\mathrm{O}(h^{k+1})$ in L^2 norm are obtained for the WG method with weak Galerkin space $\Big(\big[\mathcal{P}_k(T)\big]^d,\ \big[\mathcal{P}_k(\partial T)\big]^d,\ \mathcal{P}_{k-1}(T)\Big)$. Numerous numerical experiments have been conducted to justify the theoretical results for the both two-dimensional and three-dimensional proposed algorithms.

The rest of the chapter is divided as follows. In Sec.2.2, we discuss the weak Galerkin finite element discretization and recall a few theoretical results which will be used in this article. Sec.2.3 discusses the error estimates for the stabilizer-based WG-FEM. Sec.2.4 focuses on numerical examples.

2.2 Weak Galerkin Discretization and Spaces

In this section, we shall describe the weak Galerkin finite element discretization for the problem (2.1.1)-(2.1.2) and review the definition of the weak divergence operator.

Let $\mathcal{T}_h$ be a partition of domain Ω consisting of polygons (in 2D)/polyhedrons (in 3D) satisfying shape regularity assumptions described in [121, 122]. Denote by $\mathcal{E}_h$ the set of all edges/faces in $\mathcal{T}_h$ and let $\mathcal{E}_h^0 = \mathcal{E}_h \backslash \partial\Omega$ be the set of all interior edges/faces. For every element $T \in \mathcal{T}_h$, we denote by $|T|$ the measure of T and by h_T its diameter, and mesh size $h = \max_{T\in\mathcal{T}_h} h_T$.

Let T be any polygonal/polyhedron domain with interior T^0 and boundary ∂T. A weak function on the region T refers to a pair of vector valued functions $\mathbf{v} = \{\mathbf{v}_0, \mathbf{v}_b\}$ such that $\mathbf{v}_0 \in [L^2(T)]^d$ and $\mathbf{v}_b \cdot \boldsymbol{\eta} \in L^2(\partial T)$, where $\boldsymbol{\eta}$ is the outward normal direction to $L^2(\partial T)$. The first component $\mathbf{v}_0$ can be understood as the value of $\mathbf{v}$ in the interior of T, and the second component $\mathbf{v}_b$ represents $\mathbf{v}$ on the boundary of T. Note that $\mathbf{v}_b$ may not necessarily be related to the trace of $\mathbf{v}_0$ on ∂T. For $e \in \partial T$, we define $\boldsymbol{\eta}_e = \boldsymbol{\eta}|_e$.

For $k \geq 1$, we now introduce two discrete weak Galerkin spaces as follows:

$$\begin{aligned}\mathbf{V}_h &= \{\mathbf{v}_h = \{\mathbf{v}_0, \mathbf{v}_b\} : \ \mathbf{v}_0|_T \in [\mathcal{P}_k(T)]^d, \ \mathbf{v}_b = v_b \boldsymbol{\eta}_e, \ v_b \in \mathcal{P}_k(e), \ e \in \partial T, \ T \in \mathcal{T}_h\},\\ \mathbf{V}_h^0 &= \{\mathbf{v}_h = \{\mathbf{v}_0, \mathbf{v}_b\} \in \mathbf{V}_h : \ \mathbf{v}_b \cdot \boldsymbol{\eta} = 0 \ \text{ on } \partial\Omega\}.\end{aligned}$$

Note that the only differential operator which is involved in the weak formulation (1.2.1) is the divergence operator. Therefore, we proceed to define the discrete weak divergence operator. For any $\mathbf{v}_h = \{\mathbf{v}_0, \mathbf{v}_b\} \in \mathbf{V}_h$, the discrete weak divergence operator, denoted by $\nabla_w \cdot \mathbf{v}_h$, defined as the unique polynomial $\nabla_w \cdot \mathbf{v}_h \in \mathcal{P}_{k-1}(T)$ that satisfies the following equation

$$(\nabla_w \cdot \mathbf{v}_h, \varphi)_T = -\int_T \mathbf{v}_0 \cdot (\nabla\varphi) dT + \int_{\partial T} \mathbf{v}_b \cdot \boldsymbol{\eta} \varphi ds \ \ \forall \varphi \in \mathcal{P}_{k-1}(T). \tag{2.2.1}$$

A parameter-free stabilizer based WG-FEM for the problem (2.1.1)-(2.1.2) has the following form: find $\mathbf{p}_h = \{\mathbf{p}_0, \mathbf{p}_b\} \in \mathbf{V}_h^0$ such that

$$(\alpha \nabla_w \cdot \mathbf{p}_h, \nabla_w \cdot \mathbf{v}_h) + (\gamma \mathbf{p}_0, \mathbf{v}_0) + \mathcal{S}(\mathbf{p}_h, \mathbf{v}_h) = (\mathbf{f}, \mathbf{v}_0) \ \ \forall \mathbf{v}_h = \{\mathbf{v}_0, \mathbf{v}_b\} \in \mathbf{V}_h^0, \tag{2.2.2}$$

where

$$\mathcal{S}(\mathbf{p}_h, \mathbf{v}_h) = \sum_{T \in \mathcal{T}_h} h_T^{-1} \langle (\mathbf{p}_0 - \mathbf{p}_b) \cdot \boldsymbol{\eta}, (\mathbf{v}_0 - \mathbf{v}_b) \cdot \boldsymbol{\eta} \rangle_{\partial T}. \tag{2.2.3}$$

Here, $\langle \cdot, \cdot \rangle_{\partial T}$ denotes the L^2 inner product on ∂T and we write

$$\langle \cdot, \cdot \rangle_{\partial T} = \sum_{e \subset \partial T} \langle \cdot, \cdot \rangle_e,$$

where $\langle \cdot, \cdot \rangle_e$ denotes the L^2 inner product on $e \in \mathcal{E}_h$.

Note that, $\mathcal{S}(\cdot, \cdot)$ is known as a stabilizer and it is often chosen in such a way that it fits well into the theory and implementation of the WG numerical scheme. Further, stabilizer $\mathcal{S}(\cdot, \cdot)$ in (2.2.2) is necessary to guarantee the well-posedness and convergence of the methods. For examples, we refer to (cf. [119, 124]).

In addition, we introduce a bilinear map $\mathcal{A} : \mathbf{V}_h \times \mathbf{V}_h \to \mathbb{R}$ to be used in this section as follows

$$\mathcal{A}(\mathbf{p}_h, \mathbf{v}_h) = (\alpha \nabla_w \cdot \mathbf{p}_h, \nabla_w \cdot \mathbf{v}_h) + (\gamma \mathbf{p}_0, \mathbf{v}_0) + \mathcal{S}(\mathbf{p}_h, \mathbf{v}_h). \tag{2.2.4}$$

It is easy to verify that the weak finite element space $\mathbf{V}_h^0$ is a normed linear space with respect to following the triple-bar norm given by

$$\begin{aligned}|||\mathbf{v}_h|||^2 &:= \sum_{T \in \mathcal{T}_h} \|\alpha^{\frac{1}{2}} \nabla_w \cdot \mathbf{v}_h\|_T^2 + \|\gamma^{\frac{1}{2}} \mathbf{v}_0\|_T^2 + \sum_{T \in \mathcal{T}_h} h_T^{-1} \|(\mathbf{v}_0 - \mathbf{v}_b) \cdot \boldsymbol{\eta}\|_{\partial T}^2 \\ &= \mathcal{A}(\mathbf{v}_h, \mathbf{v}_h), \ \ \mathbf{v}_h = \{\mathbf{v}_0, \mathbf{v}_b\} \in \mathbf{V}_h^0.\end{aligned} \tag{2.2.5}$$

For each element $T \in \mathcal{T}_h$, denote by $\mathbf{Q}_0^j$ the usual L^2 projection operator from $[L^2(T)]^d$ onto $[\mathcal{P}_j(T)]^d$. For each edge/face $e \in \mathcal{E}_h$, denote by Q_b^j the L^2 projection operator from $L^2(e)$ onto $\mathcal{P}_j(e)$. We shall combine $\mathbf{Q}_0^j$ with $\mathbf{Q}_b^j$ by writing $\mathbf{Q}_h\mathbf{p} = \{\mathbf{Q}_0^j\mathbf{p}, \mathbf{Q}_b^j\mathbf{p}\}$, where $\mathbf{Q}_b^j\mathbf{p} = Q_b^j(\mathbf{p}\cdot\boldsymbol{\eta}_e)\cdot\boldsymbol{\eta}_e$. Apart $\mathbf{Q}_h$ projection, let $\mathbb{Q}_h^j$ be the usual L^2 projection operator from $L^2(T)$ onto $\mathcal{P}_j(T)$, where j is a non-negative integer. For both projection operators, the following identity holds (cf. [122])

$$\mathbb{Q}_h^{k-1}(\nabla\cdot\mathbf{v}) = \nabla_w\cdot(\mathbf{Q}_h\mathbf{v}) \ \ \forall\mathbf{v}\in\mathbf{H}(\mathrm{div};\Omega), \tag{2.2.6}$$

where $\mathbf{Q}_h\mathbf{v} = \{\mathbf{Q}_0^k\mathbf{v}, \mathbf{Q}_b^k\mathbf{v}\}$ with $\mathbf{Q}_b^k\mathbf{v} = \mathbf{Q}_b^k(\mathbf{v}\cdot\boldsymbol{\eta}_e)\cdot\boldsymbol{\eta}_e$.

Now, we recall the following crucial approximation properties for local projections $\mathbf{Q}_0^k$ and $\mathbb{Q}_h^r$. For details, we refer to ([121, 122]).

Lemma 2.2.1. *Let $\mathcal{T}_h$ be a finite element partition of Ω satisfying the shape regularity assumption as specified in [121]. Then, for $\mathbf{w}\in[H^{j+1}(\Omega)]^d$ and $z\in[H^{r+1}(\Omega)]$, we have*

$$\sum_{T\in\mathcal{T}_h}\|\mathbf{w}-\mathbf{Q}_0^j\mathbf{w}\|_T^2 \le Ch^{2(s+1)}\|\mathbf{w}\|_{s+1}^2, \ \ 0\le s\le j,$$
$$\sum_{T\in\mathcal{T}_h}\|\nabla\big(\mathbf{w}-\mathbf{Q}_0^j\mathbf{w}\big)\|_T^2 \le Ch^{2s}\|\mathbf{w}\|_{s+1}^2, \ \ 0\le s\le j,$$
$$\sum_{T\in\mathcal{T}_h}\Big\{\|z-\mathbb{Q}_h^r z\|_T^2 + h_T^2\|\nabla(z-\mathbb{Q}_h^r z)\|_T^2\Big\} \le Ch^{2(s+1)}\|z\|_{s+1}^2, \ \ 0\le s\le r.$$

Let T be an element with e as an edge/face. For any function $\varphi\in H^1(T)$, the following trace inequality holds true (see, [121] for details)

$$\|\varphi\|_e^2 \le C(h_T^{-1}\|\varphi\|_T^2 + h_T\|\nabla\varphi\|_T^2). \tag{2.2.7}$$

For any piecewise polynomial φ of degree p on $\mathcal{T}_h$, there exists constant $C = C(p)$ such that (cf. [121])

$$\|\nabla\varphi\|_T \le C(p)h_T^{-1}\|\varphi\|_T \ \ \forall T\in\mathcal{T}_h. \tag{2.2.8}$$

Lemma 2.2.2. *The semi-norm $|||\cdot|||$ is a norm on $\mathbf{V}_h^0$.*

Proof. To prove the semi-norm is indeed a norm, it is sufficient to show that $|||\mathbf{v}_h||| = 0$ if and only if $\mathbf{v}_h = \mathbf{0}$ for all $\mathbf{v}_h\in\mathbf{V}_h^0$. Suppose $|||\mathbf{v}_h||| = 0$, then the definition (2.2.5) implies that $\mathbf{v}_0 = \mathbf{0}$ on $T\in\mathcal{T}_h$ and $\mathbf{v}_0\cdot\boldsymbol{\eta} = \mathbf{v}_b\cdot\boldsymbol{\eta}$ on ∂T, which together with the fact $\mathbf{v}_b|_e = \mathbf{v}_b\boldsymbol{\eta}$ yields $v_b = 0$ on ∂T. On the other hand $\mathbf{v}_b\cdot\boldsymbol{\eta} = 0$ on $\partial\Omega$. This completes the proof. □

Weak Galerkin Algorithm . A numerical approximation for (2.1.1)-(2.1.2) can be obtained by seeking $\mathbf{p}_h = \{\mathbf{p}_0, \mathbf{p}_b\} \in \mathbf{V}_h^0$ such that

$$\mathcal{A}(\mathbf{p}_h, \mathbf{v}_h) = (\mathbf{f}, \mathbf{v}_0) \; \forall \mathbf{v}_h = \{\mathbf{v}_0, \mathbf{v}_b\} \in \mathbf{V}_h^0. \tag{2.2.9}$$

2.3 Error Analysis for the WG-FEMs

Now, we turn our discussion toward error analysis. The optimal error estimates in discrete energy norm and L^2 norm have been derived in this section. First, we split our error into two components using an intermediate operator. We write

$$\mathbf{p} - \mathbf{p}_h = (\mathbf{p} - \mathbf{Q}_h\mathbf{p}) + (\mathbf{Q}_h\mathbf{p} - \mathbf{p}_h),$$

where $\mathbf{Q}_h\mathbf{p} = \{\mathbf{Q}_0^k\mathbf{p}, \mathbf{Q}_b^k\mathbf{p}\}$. For simplicity, we introduce following notation

$$\mathbf{e}_h := (\mathbf{Q}_h\mathbf{p} - \mathbf{p}_h) = \{\mathbf{Q}_0^k\mathbf{p} - \mathbf{p}_0, \mathbf{Q}_b^k\mathbf{p} - \mathbf{p}_b\}. \tag{2.3.1}$$

Before proceeding further, we derive following results for our later analysis.

Lemma 2.3.1. *For any* $\mathbf{v}_h = \{\mathbf{v}_0, \mathbf{v}_b\} \in \mathbf{V}_h$, *we have*

$$\sum_{T \in \mathcal{T}_h} \|\nabla \cdot \mathbf{v}_0\|_T^2 \leq C|||\mathbf{v}_h|||^2. \tag{2.3.2}$$

Proof. For $\mathbf{v}_h = \{\mathbf{v}_0, \mathbf{v}_b\} \in \mathbf{V}_h$, using the integration by parts and weak divergence operator, we obtain

$$\begin{aligned}
(\nabla \cdot \mathbf{v}_0, \nabla \cdot \mathbf{v}_0)_T &= -(\mathbf{v}_0, \nabla(\nabla \cdot \mathbf{v}_0))_T + \langle \mathbf{v}_0 \cdot \boldsymbol{\eta}, \nabla \cdot \mathbf{v}_0 \rangle_{\partial T} \\
&= -(\mathbf{v}_0, \nabla(\nabla \cdot \mathbf{v}_0))_T + \langle \mathbf{v}_b \cdot \boldsymbol{\eta}, \nabla \cdot \mathbf{v}_0 \rangle_{\partial T} \\
&\quad + \langle (\mathbf{v}_0 - \mathbf{v}_b) \cdot \boldsymbol{\eta}, \nabla \cdot \mathbf{v}_0 \rangle_{\partial T} \\
&= (\nabla_w \cdot \mathbf{v}_h, \nabla \cdot \mathbf{v}_0)_T + \langle (\mathbf{v}_0 - \mathbf{v}_b) \cdot \boldsymbol{\eta}, \nabla \cdot \mathbf{v}_0 \rangle_{\partial T}.
\end{aligned}$$

Then, trace inequality (2.2.7) and inverse estimate (2.2.8) yields

$$\|\nabla \cdot \mathbf{v}_0\|_T^2 \leq C\Big(\|\nabla_w \cdot \mathbf{v}_h\|_T \|\nabla \cdot \mathbf{v}_0\|_T + h_T^{-1/2}\|(\mathbf{v}_0 - \mathbf{v}_b) \cdot \boldsymbol{\eta}\|_{\partial T}\|\nabla \cdot \mathbf{v}_0\|_T\Big),$$

which leads to Lemma 2.3.1. □

Now, we are in a position to derive the crucial error equation for $\mathbf{e}_h$.

Lemma 2.3.2. *Let $\mathbf{e}_h$ be the error function given by (2.3.1). Then, for each $\mathbf{v}_h = \{\mathbf{v}_0, \mathbf{v}_b\} \in \mathbf{V}_h^0$, we obtain*

$$\mathcal{A}(\mathbf{e}_h, \mathbf{v}_h) = R_1(\mathbf{p}, \mathbf{v}_h) + R_2(\mathbf{p}, \mathbf{v}_h) + \mathcal{S}(\mathbf{Q}_h\mathbf{p}, \mathbf{v}_h), \tag{2.3.3}$$

where bilinear maps $R_1(\cdot,\cdot)$ and $R_2(\cdot,\cdot)$ are given by

$$R_1(\mathbf{p}, \mathbf{v}_h) = \sum_{T\in\mathcal{T}_h} \langle(\alpha\nabla\cdot\mathbf{p} - \mathbb{Q}_h^{k-1}\alpha\nabla\cdot\mathbf{p}), (\mathbf{v}_0 - \mathbf{v}_b)\cdot\boldsymbol{\eta}\rangle_{\partial T}, \tag{2.3.4}$$

$$R_2(\mathbf{p}, \mathbf{v}_h) = \sum_{T\in\mathcal{T}_h} (\alpha\mathbb{Q}_h^{k-1}(\nabla\cdot\mathbf{p}) - \mathbb{Q}_h^{k-1}(\alpha\nabla\cdot\mathbf{p}), \nabla_w\cdot\mathbf{v}_h)_T. \tag{2.3.5}$$

Proof. For $\mathbf{v}_h = \{\mathbf{v}_0, \mathbf{v}_b\} \in \mathbf{V}_h^0$, testing equation (2.1.1) by $\mathbf{v}_0$, we arrive at

$$-\sum_{T\in\mathcal{T}_h} (\nabla(\alpha\nabla\cdot\mathbf{p}), \mathbf{v}_0)_T + (\mathbf{Q}_0^k(\gamma\mathbf{u}), \mathbf{v}_0) = (\mathbf{f}, \mathbf{v}_0). \tag{2.3.6}$$

Then, apply integration by parts to obtain

$$\begin{aligned}(\mathbf{f}, \mathbf{v}_0) &= (\gamma\mathbf{Q}_0^k\mathbf{p}, \mathbf{v}_0) + \sum_{T\in\mathcal{T}_h} (\alpha\nabla\cdot\mathbf{p}, \nabla\cdot\mathbf{v}_0)_T \\ &\quad - \sum_{T\in\mathcal{T}_h} \langle\mathbf{v}_0 - \mathbf{v}_b, (\alpha\nabla\cdot\mathbf{p})\boldsymbol{\eta}\rangle_{\partial T}.\end{aligned} \tag{2.3.7}$$

Here, we have assumed that γ is piecewise constant and the fact that

$$\sum_{T\in\mathcal{T}_h} \langle(\alpha\nabla\cdot\mathbf{p})\boldsymbol{\eta}, \mathbf{v}_b\rangle_{\partial T} = 0.$$

Now, using the definition (2.2.1) for $\mathbf{v}_h$ with $l = k-1$, we obtain

$$\begin{aligned}&(\mathbb{Q}_h^{k-1}(\alpha\nabla\cdot\mathbf{p}), \nabla_w\cdot\mathbf{v}_h)_T \\ &= -(\mathbf{v}_0, \nabla(\mathbb{Q}_h^{k-1}(\alpha\nabla\cdot\mathbf{p})))_T + \langle\mathbf{v}_b, \mathbb{Q}_h^{k-1}(\alpha\nabla\cdot\mathbf{p})\boldsymbol{\eta}\rangle_{\partial T} \\ &= (\nabla\cdot\mathbf{v}_0, \mathbb{Q}_h^{k-1}(\alpha\nabla\cdot\mathbf{p}))_T - \langle(\mathbb{Q}_h^{k-1}(\alpha\nabla\cdot\mathbf{p}))\boldsymbol{\eta}, \mathbf{v}_0\rangle_{\partial T} \\ &\quad + \langle\mathbb{Q}_h^{k-1}(\alpha\nabla\cdot\mathbf{p})\boldsymbol{\eta}, \mathbf{v}_b\rangle_{\partial T} \\ &= (\nabla\cdot\mathbf{v}_0, \mathbb{Q}_h^{k-1}(\alpha\nabla\cdot\mathbf{p}))_T - \langle(\mathbb{Q}_h^{k-1}(\alpha\nabla\cdot\mathbf{p}))\boldsymbol{\eta}, \mathbf{v}_0 - \mathbf{v}_b\rangle_{\partial T} \\ &= (\nabla\cdot\mathbf{v}_0, \alpha\nabla\cdot\mathbf{p})_T - \langle(\mathbb{Q}_h^{k-1}(\alpha\nabla\cdot\mathbf{p}))\boldsymbol{\eta}, \mathbf{v}_0 - \mathbf{v}_b\rangle_{\partial T}.\end{aligned} \tag{2.3.8}$$

Then, combine (2.3.8) and (2.3.7) to obtain

$$\begin{aligned}(\mathbf{f},\mathbf{v}_0) &= (\gamma\mathbf{Q}_0^k\mathbf{p},\mathbf{v}_0)+(\mathbb{Q}_h^{k-1}(\alpha\nabla\cdot\mathbf{p}),\nabla_w\cdot\mathbf{v}_h)\\ &\quad-\sum_{T\in\mathcal{T}_h}\langle(\alpha\nabla\cdot\mathbf{p}-\mathbb{Q}_h^{k-1}(\alpha\nabla\cdot\mathbf{p}))\boldsymbol{\eta},\mathbf{v}_0-\mathbf{v}_b\rangle_{\partial T}\\ &= (\gamma\mathbf{Q}_0^k\mathbf{p},\mathbf{v}_0)+(\alpha\mathbb{Q}_h^{k-1}(\nabla\cdot\mathbf{p}),\nabla_w\cdot\mathbf{v}_h)\\ &\quad-(\alpha\mathbb{Q}_h^{k-1}(\nabla\cdot\mathbf{p})-\mathbb{Q}_h^{k-1}(\alpha\nabla\cdot\mathbf{p}),\nabla_w\cdot\mathbf{v}_h)\\ &\quad-\sum_{T\in\mathcal{T}_h}\langle\alpha\nabla\cdot\mathbf{p}-\mathbb{Q}_h^{k-1}(\alpha\nabla\cdot\mathbf{p}),(\mathbf{v}_0-\mathbf{v}_b)\cdot\boldsymbol{\eta}\rangle_{\partial T}\\ &= (\gamma\mathbf{Q}_0^k\mathbf{p},\mathbf{v}_0)+(\alpha\nabla_w\cdot(\mathbf{Q}_h\mathbf{p}),\nabla_w\cdot\mathbf{v}_h)\\ &\quad-R_1(\mathbf{p},\mathbf{v}_h)-R_2(\mathbf{p},\mathbf{v}_h).\end{aligned}\tag{2.3.9}$$

In the last equality, we have used identity (2.2.6).

Next, by adding $\mathcal{S}(\mathbf{Q}_h\mathbf{p},\mathbf{v}_h)$ both sides to (2.3.9), we obtain

$$\mathcal{A}(\mathbf{Q}_h\mathbf{p},\mathbf{v}_h)=(\mathbf{f},\mathbf{v}_0)+R_1(\mathbf{p},\mathbf{v}_h)+R_2(\mathbf{p},\mathbf{v}_h)+\mathcal{S}(\mathbf{Q}_h\mathbf{p},\mathbf{v}_h).\tag{2.3.10}$$

Finally, subtracting (2.2.9) from (2.3.10) leads to desire result. □

Next result deals with the bounds for the terms in error equation (2.3.3).

Lemma 2.3.3. *Let* $\mathbf{p}\in[H^{k+1}(\Omega)]^d$ *and* $\alpha\in W^{k,\infty}(\Omega)$. *Then, for any* $\mathbf{v}_h=\{\mathbf{v}_0,\mathbf{v}_b\}\in\mathbf{V}_h^0$, *we obtain*

$$|R_1(\mathbf{p},\mathbf{v}_h)| \le C(\|\alpha\|_{k,\infty})h^k\|\mathbf{p}\|_{k+1}|||\mathbf{v}_h|||,\tag{2.3.11}$$

$$|R_2(\mathbf{p},\mathbf{v}_h)| \le C(\|\alpha\|_{1,\infty})h^{k+1}\|\mathbf{p}\|_{k+1}|||\mathbf{v}_h|||,\tag{2.3.12}$$

$$|\mathcal{S}(\mathbf{Q}_h\mathbf{p},\mathbf{v}_h)| \le Ch^k\|\mathbf{p}\|_{k+1}|||\mathbf{v}_h|||.\tag{2.3.13}$$

Proof. For the estimate (2.3.11), we use the Cauchy-Schwarz inequality and trace inequality (2.2.7) along with Lemma 2.2.1 and Lemma 2.3.1 to obtain

$$\begin{aligned}|R_1(\mathbf{p},\mathbf{v}_h)| &= \left|\sum_{T\in\mathcal{T}_h}\langle\alpha(\nabla\cdot\mathbf{p})-\mathbb{Q}_h^{k-1}(\alpha\nabla\cdot\mathbf{p}),(\mathbf{v}_0-\mathbf{v}_b)\cdot\boldsymbol{\eta}\rangle_{\partial T}\right|\\ &\le C\sum_{T\in\mathcal{T}_h}\|\alpha(\nabla\cdot\mathbf{p})-\mathbb{Q}_h^{k-1}(\alpha\nabla\cdot\mathbf{p})\|_{\partial T}\|(\mathbf{v}_0-\mathbf{v}_b)\cdot\boldsymbol{\eta}\|_{\partial T}\\ &\le C\left(\sum_{T\in\mathcal{T}_h}h_T\|\alpha(\nabla\cdot\mathbf{p})-\mathbb{Q}_h^{k-1}(\alpha\nabla\cdot\mathbf{p})\|_{\partial T}^2\right)^{\frac{1}{2}}\\ &\quad\times\left(\sum_{T\in\mathcal{T}_h}h_T^{-1}\|(\mathbf{v}_0-\mathbf{v}_b)\cdot\boldsymbol{\eta}\|_{\partial T}\right)^{\frac{1}{2}}\\ &\le C(\|\alpha\|_{k,\infty})h^k\|\mathbf{p}\|_{k+1}|||\mathbf{v}_h|||.\end{aligned}\tag{2.3.14}$$

It follows from Lemma 2.2.1 and Lemma 2.3.1 that

$$\begin{aligned}
|R_2(\mathbf{p},\mathbf{v}_h)| &= \left|(\alpha\mathbb{Q}_h^{k-1}(\nabla\cdot\mathbf{p})-\alpha\nabla\cdot\mathbf{p},\nabla_w\cdot\mathbf{v}_h)\right| \\
&\leq \left|(\mathbb{Q}_h^{k-1}(\nabla\cdot\mathbf{p})-\nabla\cdot\mathbf{p},(\alpha-\bar{\alpha})\nabla_w\cdot\mathbf{v}_h)\right| \\
&\leq C(\|\alpha\|_{1,\infty})h\left|(\mathbb{Q}_h^{k-1}(\nabla\cdot\mathbf{p})-\nabla\cdot\mathbf{p},\nabla_w\cdot\mathbf{v}_h)\right| \\
&\leq C(\|\alpha\|_{1,\infty})h^{k+1}\|\mathbf{p}\|_{k+1}|||\mathbf{v}_h|||. \qquad (2.3.15)
\end{aligned}$$

Here, $\bar{\alpha}$ denotes the average of α and on each element $T\in\mathcal{T}_h$, following inequality holds true (see, [121]).

$$\|\bar{\alpha}-\alpha\|_{L^\infty(T)}\leq Ch\|\nabla\alpha\|_{L^\infty(T)}. \qquad (2.3.16)$$

To estimate the stabilizer term, we use (2.2.3), inequality (2.2.7) and Lemma 2.2.1 to arrive at

$$\begin{aligned}
|\mathcal{S}(\mathbf{Q}_h\mathbf{p},\mathbf{v}_h)| &= \left|\sum_{T\in\mathcal{T}_h}h_T^{-1}\langle(\mathbf{Q}_0^k\mathbf{p}-\mathbf{Q}_b^k\mathbf{p})\cdot\boldsymbol{\eta},(\mathbf{v}_0-\mathbf{v}_b)\cdot\boldsymbol{\eta}\rangle_{\partial T}\right| \\
&\leq \left|\sum_{T\in\mathcal{T}_h}h_T^{-1}\langle(\mathbf{Q}_0^k\mathbf{p}-\mathbf{p})\cdot\boldsymbol{\eta},(\mathbf{v}_0-\mathbf{v}_b)\cdot\boldsymbol{\eta}\rangle_{\partial T}\right| \\
&= \left|\sum_{T\in\mathcal{T}_h}h_T^{-1}\langle(\mathbf{Q}_0^k\mathbf{p}-\mathbf{p})\cdot\boldsymbol{\eta},(\mathbf{v}_0-\mathbf{v}_b)\cdot\boldsymbol{\eta}\rangle_{\partial T}\right| \\
&\leq \sum_{T\in\mathcal{T}_h}h_T^{-1}\|\mathbf{Q}_0^k\mathbf{p}-\mathbf{p}\|_{\partial T}\|(\mathbf{v}_0-\mathbf{v}_b)\cdot\boldsymbol{\eta}\|_{\partial T} \\
&\leq \left(\sum_{T\in\mathcal{T}_h}(h_T^{-2}\|\mathbf{Q}_0^k\mathbf{p}-\mathbf{p}\|_T^2+\|\nabla(\mathbf{Q}_0^k\mathbf{p}-\mathbf{p})\|_T^2)\right)^{\frac{1}{2}} \\
&\quad\times\left(\sum_{T\in\mathcal{T}_h}h_T^{-1}\|(\mathbf{v}_0-\mathbf{v}_b)\cdot\boldsymbol{\eta}\|_{\partial T}^2\right)^{\frac{1}{2}} \\
&\leq Ch^k\|\mathbf{p}\|_{k+1}|||\mathbf{v}_h|||.
\end{aligned}$$

This completes the proof of Lemma 2.3.3. □

Theorem 2.3.1. *Let $\mathbf{p}\in[H^{k+1}(\Omega)]^d$ be the exact solution for (2.1.1)-(2.1.2) and $\mathbf{p}_h\in\mathbf{V}_h^0$ be the weak Galerkin finite element solution of (2.2.9). Then, there exists a constant C such that*

$$|||\mathbf{Q}_h\mathbf{p}-\mathbf{p}_h|||\leq Ch^k\|\mathbf{p}\|_{k+1}. \qquad (2.3.17)$$

Proof. By letting $\mathbf{v}_h=\mathbf{e}_h$ in the error equation (2.3.3), we have

$$|||\mathbf{e}_h|||^2 \leq |R_1(\mathbf{p},\mathbf{e}_h)|+|R_2(\mathbf{p},\mathbf{e}_h)|+|\mathcal{S}(\mathbf{Q}_h\mathbf{p},\mathbf{e}_h)|. \qquad (2.3.18)$$

Here, $\mathbf{e}_h$ is as defined in (2.3.1). Then the desired estimate (2.3.17) follows immediately from Lemma 2.3.3 and above estimate (2.3.18). □

Now, we are in a position to derive the L^2 norm error estimate for the error function $\mathbf{e}_h$. To do so, we need following space

$$\mathcal{B}_h = \{\boldsymbol{\phi} \in \mathbf{H}_0(\mathrm{div};\Omega) : \boldsymbol{\phi}|_T \in [\mathcal{P}_k(T)]^d,\ \forall T \in \mathcal{T}_h\}. \tag{2.3.19}$$

It is well known that there exists a global finite element interpolation operator Π_h onto the space $\mathcal{B}_h$ (see, page 124 in [99]).

Lemma 2.3.4. *([99], Theorem 5.25 and Remark 5.26) For any $\boldsymbol{\phi} \in \mathbf{H}^s(\Omega)$ and $\nabla\cdot\boldsymbol{\phi} \in H^s(\Omega)$, $s \in \left(\frac{1}{2}, k\right]$, we obtain*

$$\|\boldsymbol{\phi} - \Pi_h\boldsymbol{\phi}\|_{s,\mathbf{div}} \le Ch^s(\|\boldsymbol{\phi}\|_s + \|\nabla\cdot\boldsymbol{\phi}\|_s).$$

Lemma 2.3.5. *For any $\boldsymbol{\phi} \in \mathcal{B}_h$, we have*

$$(\alpha\nabla_w\cdot\mathbf{e}_h, \nabla\cdot\boldsymbol{\phi}) + (\gamma\mathbf{e}_0, \boldsymbol{\phi}) = (\mathbb{Q}_h^{k-1}(\nabla\cdot\mathbf{p}) - \nabla\cdot\mathbf{p}, (\alpha-\bar{\alpha})\nabla\cdot\boldsymbol{\phi}).$$

Proof. Testing equation (2.1.1) against $\boldsymbol{\phi}$ and using the definitions of L^2 projections yield

$$\begin{aligned}
(\mathbf{f},\boldsymbol{\phi}) &= -(\nabla(\alpha\nabla\cdot\mathbf{p}),\boldsymbol{\phi}) + (\gamma\mathbf{p},\boldsymbol{\phi}) \\
&= (\alpha(\mathbb{Q}_h^{k-1}(\nabla\cdot\mathbf{p})),\nabla\cdot\boldsymbol{\phi}) + (\gamma\mathbf{Q}_0^k\mathbf{p},\boldsymbol{\phi}) \\
&- (\alpha(\mathbb{Q}_h^{k-1}(\nabla\cdot\mathbf{p})) - \mathbb{Q}_h^{k-1}(\alpha\nabla\cdot\mathbf{p}),\nabla\cdot\boldsymbol{\phi}) \\
&= (\alpha(\nabla_w\cdot(\mathbf{Q}_h\mathbf{p})),\nabla\cdot\boldsymbol{\phi}) + (\gamma\mathbf{Q}_0^k\mathbf{p},\boldsymbol{\phi}) \\
&- (\mathbb{Q}_h^{k-1}(\nabla\cdot\mathbf{p}) - \nabla\cdot\mathbf{p}, (\alpha-\bar{\alpha})\nabla\cdot\boldsymbol{\phi}).
\end{aligned} \tag{2.3.20}$$

Next, we set $\boldsymbol{\phi}_h = \{\boldsymbol{\phi}_0, \boldsymbol{\phi}_b\} \in \mathbf{V}_h^0$, where $\boldsymbol{\phi}_0 = \boldsymbol{\phi}$ and $\boldsymbol{\phi}_b = (\boldsymbol{\phi}\cdot\boldsymbol{\eta})\boldsymbol{\eta}$, and note that $\nabla_w\cdot\boldsymbol{\phi}_h = \nabla\cdot\boldsymbol{\phi}$. Then by putting $\mathbf{v}_h = \boldsymbol{\phi}_h$ in (2.2.9), we get

$$(\mathbf{f},\boldsymbol{\phi}) = (\alpha\nabla_w\cdot\mathbf{p}_h, \nabla\cdot\boldsymbol{\phi}) + (\gamma\mathbf{p}_0,\boldsymbol{\phi}). \tag{2.3.21}$$

Finally, equations (2.3.20)-(2.3.21) leads to the desired result. □

Now, we proceed to derive the following optimal L^2 norm estimate.

Theorem 2.3.2. *Let $\mathbf{p}_h \in \mathbf{V}_h^0$ be the weak Galerkin finite element solution of (2.2.9). Assume the exact solution $\mathbf{p} \in [H^{k+1}(\Omega)]^d$. Then, we have*

$$\|\mathbf{Q}_0^k\mathbf{p} - \mathbf{p}_0\| \le Ch^{k+1}\|\mathbf{p}\|_{k+1}.$$

Proof. Let $\boldsymbol{\psi} \in \mathbf{H}^1(\mathrm{div};\Omega) \cap \mathbf{H_0}(\mathrm{div};\Omega)$ be the solution of the dual problem (cf. [69])

$$\begin{cases} -\nabla(\alpha\nabla\cdot\boldsymbol{\psi}) + \gamma\boldsymbol{\psi} = \mathbf{e}_0 & \text{in } \Omega, \\ \boldsymbol{\psi}\cdot\boldsymbol{\eta} = 0 & \text{on } \partial\Omega. \end{cases} \tag{2.3.22}$$

Here $\mathbf{e}_0 = \mathbf{Q}_0^k\mathbf{u} - \mathbf{u}_0$ is the restriction of $\mathbf{e}_h$ inside of each element. Further, we assume following a priori estimate (see, [69])

$$\|\boldsymbol{\psi}\|_1 + \|\nabla\cdot\boldsymbol{\psi}\|_1 \leq C\|\mathbf{e}_0\|. \tag{2.3.23}$$

Then multiply the first equation of (2.3.22) with $\mathbf{e}_0$ to arrive at

$$\begin{aligned} (\mathbf{e}_0,\mathbf{e}_0) &= -(\nabla(\alpha\nabla\cdot\boldsymbol{\psi}),\mathbf{e}_0) + (\gamma\boldsymbol{\psi},\mathbf{e}_0) \\ &= (\alpha\nabla\cdot\boldsymbol{\psi},\nabla\cdot\mathbf{e}_0) - \sum_{T\in\mathcal{T}_h}\langle\alpha\nabla\cdot\boldsymbol{\psi},(\mathbf{e}_0-\mathbf{e}_b)\cdot\boldsymbol{\eta}\rangle_{\partial T} + (\gamma\boldsymbol{\psi},\mathbf{e}_0), \\ &= (\alpha\nabla\cdot\boldsymbol{\psi},\nabla_w\cdot\mathbf{e}_h) + (\gamma\boldsymbol{\psi},\mathbf{e}_0) \\ &- \sum_{T\in\mathcal{T}_h}\langle\alpha\nabla\cdot\boldsymbol{\psi} - \mathbb{Q}_h^{k-1}(\alpha\nabla\cdot\boldsymbol{\psi}),(\mathbf{e}_0-\mathbf{e}_b)\cdot\boldsymbol{\eta}\rangle_{\partial T}, \end{aligned} \tag{2.3.24}$$

where we have used the fact that $\sum_{T\in\mathcal{T}_h}\langle\alpha\nabla\cdot\boldsymbol{\psi},\mathbf{e}_b\cdot\boldsymbol{\eta}\rangle_{\partial T} = 0$. Further, using Lemma 2.3.5 with $\boldsymbol{\phi} = \Pi_h\boldsymbol{\psi}$ in the equation (2.3.24), we obtain

$$\begin{aligned} \|\mathbf{e}_0\|^2 &= (\alpha\nabla\cdot(\boldsymbol{\psi}-\Pi_h\boldsymbol{\psi}),\nabla_w\cdot\mathbf{e}_h) + (\gamma(\boldsymbol{\psi}-\Pi_h\boldsymbol{\psi}),\mathbf{e}_0) \\ &- \sum_{T\in\mathcal{T}_h}\langle\alpha\nabla\cdot\boldsymbol{\psi} - \mathbb{Q}_h^{k-1}(\alpha\nabla\cdot\boldsymbol{\psi}),(\mathbf{e}_0-\mathbf{e}_b)\cdot\boldsymbol{\eta}\rangle_{\partial T} \\ &+(\mathbb{Q}_h^{k-1}(\nabla\cdot\mathbf{p}) - \nabla\cdot\mathbf{p},(\alpha-\bar{\alpha})\nabla\cdot(\Pi_h\boldsymbol{\psi})) \\ &\leq C\|\boldsymbol{\psi}-\Pi_h\boldsymbol{\psi}\|_{1,\mathbf{div}}|||\mathbf{e}_h||| + \sum_{T\in\mathcal{T}_h}\|\alpha\nabla\cdot\boldsymbol{\psi} - \mathbb{Q}_h^{k-1}(\alpha\nabla\cdot\boldsymbol{\psi})\|_{\partial T}\|\mathbf{e}_0-\mathbf{e}_b\|_{\partial T} \\ &+Ch(\|\alpha\|_{1,\infty})\sum_{T\in\mathcal{T}_h}\|\mathbb{Q}_h^{k-1}(\nabla\cdot\mathbf{p}) - \nabla\cdot\mathbf{p}\|_T\|\nabla\cdot(\Pi_h\boldsymbol{\psi})\|_T. \end{aligned} \tag{2.3.25}$$

Next, from trace inequality (2.2.7) and inverse inequality (2.2.8), we note that

$$\begin{aligned} h_T\|\alpha\nabla\cdot\boldsymbol{\psi} - \mathbb{Q}_h^{k-1}(\alpha\nabla\cdot\boldsymbol{\psi})\|_{\partial T}^2 &\leq C\|\alpha\nabla\cdot\boldsymbol{\psi} - \mathbb{Q}_h^{k-1}(\alpha\nabla\cdot\boldsymbol{\psi})\|_T^2 \\ &\leq Ch^2\|\alpha\nabla\cdot\boldsymbol{\psi}\|_1^2 \\ &\leq Ch^2\|\alpha\|_{1,\infty}\|\boldsymbol{\psi}\|_{1,\mathbf{div}}^2, \end{aligned} \tag{2.3.26}$$

which together with estimate (2.3.25), Lemma 2.2.1, Lemma 2.3.4 and a priori estimate (2.3.23) yield

$$\begin{aligned} \|\mathbf{e}_0\|^2 &\leq Ch\|\boldsymbol{\psi}\|_{1,\mathbf{div}}|||\mathbf{e}_h||| + Ch^{k+1}\|\mathbf{p}\|_{k+1}\|\boldsymbol{\psi}\|_{1,\mathrm{div}} \\ &\leq Ch\|\mathbf{e}_0\|||\mathbf{e}_h||| + Ch^{k+1}\|\mathbf{p}\|_{k+1}\|\mathbf{e}_0\|. \end{aligned}$$

Finally, Theorem 2.3.1 leads to the desired estimate. □

2.4 Numerical Section

In this section, we have tested various numerical examples for the $\mathbf{H}(\text{div};\Omega)$-elliptic problem (2.1.1)-(2.1.2) in Ω, where $\Omega \subset \mathbb{R}^d$ $(d = 2, 3)$. In 2D, finite element partitions with different kinds of configurations like triangular, rectangular, and meshes with hanging nodes are used for solving $\mathbf{H}(\text{div};\Omega)$-elliptic problems to confirm the flexibility of WG method. In addition, we have also validated both algorithms for the 3D domain with cubical meshes also. These numerical results demonstrate that the scheme is robust and accurate.

For a given finite number of successive iterations (indexed by i), let e_i be the error corresponding to the suitable norm on the i-th iteration, and h_i is the corresponding mesh size. Then expected order of convergence (EOC) can be defined by

$$\text{EOC}(e_i) = \frac{\log\left(\frac{e_{i+1}}{e_i}\right)}{\log\left(\frac{h_{i+1}}{h_i}\right)}.$$

Example 2.4.1. Convergence test for $\mathbf{H}(\text{div};\Omega)$-elliptic problem on mixed mesh: Consider the problem (2.1.1)-(2.1.2) in $\Omega = (0,1)^2$. The exact solution of the given problem is defined as

$$\mathbf{p} = (p_1, p_2) = \big(\sin(x+y) + \cos(x+y), \exp(x)\cos(\pi y)\big).$$

The right-hand side $\mathbf{f}$ can be evaluated from the exact solution $\mathbf{p}$ and the coefficients $\alpha = x^2 + y^2 + 1$ and $\gamma = xy + 3$.

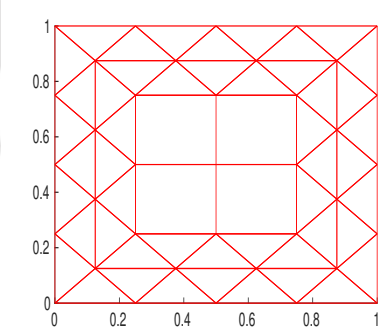

Figure 2.4.1: Initial mixed mesh.

Mixed meshes are used in this example, which is depicted in Figure 2.4.1. The errors, for the weak Galerkin algorithm, with respect to L^2 norm and discrete H^1 norm are reported in Table 2.4.1. WG solutions are shown in Figures 2.4.2 for $k = 2$ with $h = 1/64$.

Table 2.4.1: Errors and convergence profile for WG solution in Example 2.4.1.

k	$\frac{1}{h}$	$\|\|\|\mathbf{e}_h\|\|\|$	Order	$\|\mathbf{e}_0\|$	Order
	4	4.53e-01	—	4.75e-02	—
	8	2.27e-01	0.99	1.16e-02	2.02
	16	1.13e-01	0.99	2.89e-03	2.01
1	32	5.67e-02	1.00	7.21e-04	2.00
	64	2.83e-02	1.00	1.80e-04	2.00
	128	1.41e-02	1.00	4.50e-05	2.00
	4	1.08e-01	—	8.97e-03	—
	8	2.75e-02	1.97	1.12e-03	2.99
	16	6.91e-0	1.99	1.40e-04	3.00
2	32	1.73e-03	1.99	1.75e-05	3.00
	64	4.33e-04	1.99	2.18e-06	3.00
	128	1.08e-04	2.00	2.73e-07	3.00
	4	1.17e-02	—	8.50e-04	—
	8	1.48e-03	2.98	5.34e-05	3.99
3	16	1.86e-04	2.99	3.33e-06	3.99
	32	2.32e-05	2.99	2.08e-07	4.00
	64	2.91e-06	2.99	1.30e-08	4.00

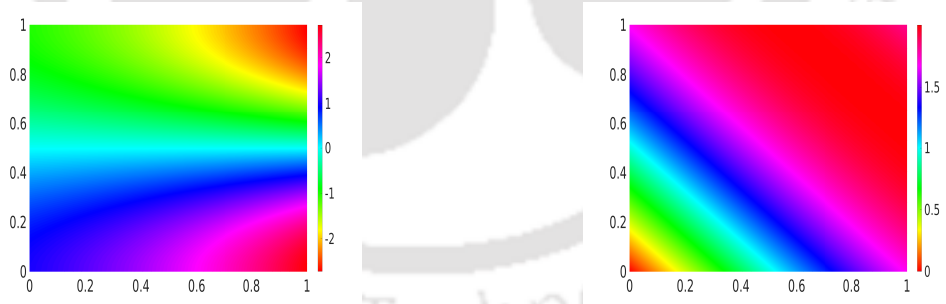

Figure 2.4.2: (Test Example 2.4.1) Component-wise surface plots of WG solution $\mathbf{p}_h$ for WG algorithm. Plot for the first-component of $\mathbf{p}_h$ (left) and plot for second-component of $\mathbf{p}_h$ (right).

Example 2.4.2. Convergence test for H(div; Ω) convection-diffusion problem on rectangular mesh with hanging nodes: In this example, we will discuss the numerical experiments for a $\mathbf{H}(\text{div};\Omega)$ convection-diffusion problem on the non-uniform rectangular mesh with hanging nodes. The initial mesh is shown as in Figure 2.4.3 (left).

The mesh on the right in Figure 2.4.3 is generated by uniform refinement procedure. It should be pointed out that the initial mesh has hanging nodes P, Q, R, and S. For the finite element partition $\mathcal{T}_h$ with hanging nodes, we notice that the WG algorithm still holds on to these refinements. We consider following convection-diffusion equation

$$-\nabla(\alpha\nabla\cdot\mathbf{p}+\gamma\cdot\mathbf{p})+\gamma\mathbf{p}=\mathbf{f} \ \text{ in } \Omega, \tag{2.4.1}$$

with Dirichlet boundary condition, and $\alpha = 2+\sin(x+y)$, $\gamma = x+y+1$ and convection speed $\gamma = (-y, x)$. We select the data in (2.4.1) such that the exact solution $\mathbf{p}$ is given by

$$\mathbf{p} = (p_1, p_2) = \big(\exp(x+y)\sin(\pi y), \sin(\pi x)\sin(\pi y)\big).$$

The WG solution for the WG scheme is compared with the exact solution of the

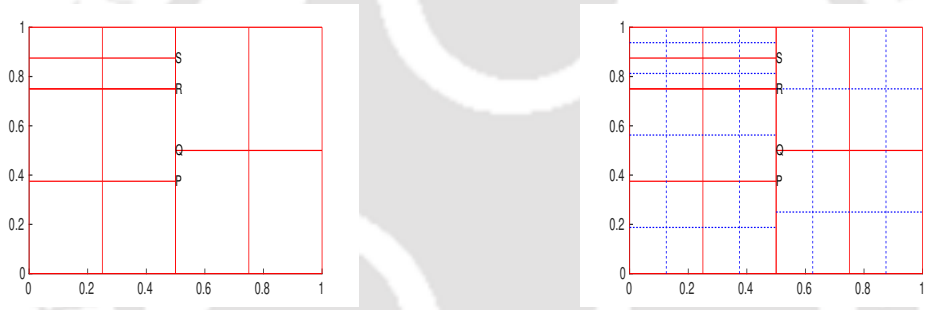

(a) (b)

Figure 2.4.3: An initial rectangular mesh with hanging nodes in (a) and its refinement in (b).

Figure 2.4.4: (Test Example 2.4.2) Component-wise surface plots of WG solution $\mathbf{p}_h$ for WG algorithm. Plot for the first-component of $\mathbf{p}_h$ (left) and plot for second-component of $\mathbf{p}_h$ (right).

$\mathbf{H}(\text{div};\Omega)$ convection-diffusion problem. Convergence results are presented in Table 2.4.2, which confirms the optimal order convergence for the proposed algorithm.

Table 2.4.2: Errors and convergence profile for WG solution in Example 2.4.2.

k	$\frac{1}{h}$	$\lvert\lvert\lvert\mathbf{e}_h\rvert\rvert\rvert$	Order	$\lVert\mathbf{e}_0\rVert$	Order
1	2	5.51e-01	—	6.42e-02	—
	4	2.75e-01	1.00	1.60e-02	2.00
	8	1.37e-01	1.00	3.99e-03	2.00
	16	6.87e-02	1.00	9.99e-04	2.00
	32	3.43e-02	1.00	2.49e-04	2.00
	64	1.71e-02	1.00	6.24e-05	2.00
2	2	4.66e-02	—	4.04e-03	—
	4	1.17e-02	1.99	5.06e-04	2.99
	8	2.93e-03	1.99	6.32e-05	3.00
	16	7.34e-04	1.99	7.90e-06	3.00
	32	1.83e-04	1.99	9.87e-07	3.00
	64	4.58e-05	2.00	1.23e-07	3.00
3	2	2.49e-03	—	1.84e-04	—
	4	3.13e-04	2.99	1.15e-05	3.99
	8	3.92e-05	2.99	7.21e-07	4.00
	16	4.90e-06	2.99	4.50e-08	4.00
	32	6.13e-07	3.00	2.81e-09	4.00

Example 2.4.3. Convergence results on L-shape domain: To demonstrate the efficiency and robustness of the weak Galerkin methods on a non-convex L-shaped domain $\Omega = [0,1]^2 \setminus [\frac{1}{2},1] \times [0,\frac{1}{2}]$, we consider the $\mathbf{H}(\text{div};\Omega)$-elliptic problem (2.1.1)-(2.1.2) with constant coefficients $\alpha = 1$ and $\gamma = 1$. In general, singularities arise for the non-convex domains. However, we choose our data selectively so that the solution is not singular at the corners. The data appeared in the problem (2.1.1)-(2.1.2) are selected by setting the exact solution as

$$\begin{aligned}\mathbf{p} &= (p_1, p_2)\\ &= \big((xy(x-0.5)(x-1)((y-0.5)(y-1))^2, xy(x-0.5)(x-1)(y-0.5)(y-1)\big).\end{aligned}$$

Numerical experiments are carried out for triangular partitions. The first two meshes are shown in Figure 2.4.5. Approximate solutions are shown in Figure 2.4.6 for $k = 3$

(a) Triangular mesh with $h = 1/2$. (b) Triangular mesh with $h = 1/4$.

Figure 2.4.5: Initial mesh and its refinement.

Figure 2.4.6: (Test Example 2.4.3) Component-wise surface plots of WG solution $\mathbf{p}_h$ for WG algorithm. Plot for the first-component of $\mathbf{p}_h$ (left) and plot for second-component of $\mathbf{p}_h$ (right).

with $h = 1/32$. Through the Table 2.4.3, we follow the rate of convergence for both the WG algorithms with various polynomial spaces.

Example 2.4.4. Convergence test for $\mathbf{H}(\mathbf{div};\Omega)$-elliptic interface problem with homogenous jump conditions: This numerical example is devoted to WG-FEM for $\mathbf{H}(\text{div};\Omega)$-elliptic interface problem with homogenous jump conditions on mixed meshes as shown in Figure 2.4.1. We consider following $\mathbf{H}(\text{div};\Omega)$-elliptic interface problem (cf. [69])

$$-\nabla(\alpha\nabla\cdot\mathbf{p}) + \mathbf{p} = \mathbf{f} \ \text{ in } \Omega, \tag{2.4.2}$$

with Dirichlet boundary condition and following jump conditions on interface Γ

$$[\boldsymbol{\eta}\cdot\mathbf{p}] = \boldsymbol{\eta}_1\cdot\mathbf{p}|_{\Omega_1} + \boldsymbol{\eta}_2\cdot\mathbf{p}|_{\Omega_2} = 0 \quad \text{on } \Gamma, \tag{2.4.3}$$

$$[\alpha\nabla\cdot\mathbf{p}] = \alpha_1\nabla\cdot\mathbf{p}|_{\Omega_1} - \alpha_2\nabla\cdot\mathbf{p}|_{\Omega_2} = 0 \quad \text{on } \Gamma, \tag{2.4.4}$$

Table 2.4.3: Errors and convergence profile for WG solution in Example 2.4.3.

k	$\frac{1}{h}$	$\|\|\|\mathbf{e}_h\|\|\|$	Order	$\|\mathbf{e}_0\|$	Order
1	2	2.67e-01	—	2.77e-02	—
	4	1.43e-01	0.90	7.47e-03	1.89
	8	7.31e-02	0.96	1.91e-03	1.96
	16	3.68e-02	0.98	4.84e-04	1.98
	32	1.84e-02	1.00	1.21e-04	1.99
	64	9.23e-03	1.00	3.03e-05	2.00
2	2	1.92e-02	—	1.24e-03	—
	4	5.03e-03	1.93	1.62e-04	2.93
	8	1.28e-03	1.96	2.06e-05	2.97
	16	3.25e-04	1.98	2.61e-06	2.98
	32	8.16e-05	1.99	3.28e-07	2.99
	64	2.04e-05	2.00	4.11e-08	3.00
3	2	7.47e-04	—	4.46e-05	—
	4	9.34e-05	2.99	2.79e-06	4.00
	8	1.16e-05	2.99	1.74e-07	4.00
	16	1.46e-06	2.99	1.08e-08	4.00
	32	1.82e-07	2.99	6.80e-10	4.00

where $\Omega_2 = \left[\frac{1}{4}, \frac{3}{4}\right] \times \left[\frac{1}{4}, \frac{3}{4}\right]$, $\Omega_1 = \Omega \setminus \Omega_2$ and interface $\Gamma = \Omega_1 \cap \Omega_2$. Further, $\boldsymbol{\eta}_1$ and $\boldsymbol{\eta}_2$ denote unit outward normals of Ω_1 and Ω_2, respectively. Here, Dirichlet boundary condition and load term $\mathbf{f}$ are chosen so that the exact solution is

$$\mathbf{p} = (p_1, p_2) = \begin{cases} \big(\sin(4\pi x)\sin(4\pi y), \sin(\pi x)\sin(\pi y)\cos(2\pi x)\cos(2\pi y)\big) & \text{in } \Omega_1, \\ \big(3\sin(4\pi x)\sin(4\pi y), 3\sin(\pi x)\sin(\pi y)\cos(2\pi x)\cos(2\pi y)\big) & \text{in } \Omega_2, \end{cases}$$

with large variation in the discontinuous coefficient α. We set $\alpha|_{\Omega_1} = 10^5 + x$ and $\alpha|_{\Omega_2} = x$. Due to the low global regularity of the exact solution, it is challenging to obtain higher order of convergence for $\mathbf{H}(\text{div}; \Omega)$-elliptic interface problem (cf. [69]). Table 2.4.4 represents the numerical solution errors and convergence rates in both L^2 and discrete H^1 norms for higher order WG finite element spaces. Note that the higher order WG finite element spaces are chosen to emphasize the fact that our numerical schemes are consistent for the problems with low global regularity. It is clear from the aforementioned table that we have achieved higher order of convergence in both L^2 and discrete H^1 norms which consolidates our theoretical findings. Here, we have used interface-fitted discretization as discussed in [103]. For exterior domain and interior domain, we have used triangular meshes and rectangular meshes, respectively. WG solutions are shown in Figure 2.4.7 for $k = 1$ with $h = 1/64$.

Figure 2.4.7: (Test Example 2.4.4) Component-wise surface plots of WG solution $\mathbf{p}_h$ for WG algorithm. Plot for the first-component of $\mathbf{p}_h$ (left) and plot for second-component of $\mathbf{p}_h$ (right).

Table 2.4.4: Errors and convergence profile for WG solutions in Example 2.4.4.

k	$\frac{1}{h}$	$\|\|\|\mathbf{e}_h\|\|\|$	Order	$\|\mathbf{e}_0\|$	Order
1	4	1.28e-01	—	1.44e-02	—
	8	6.41e-02	1.00	3.60e-03	2.00
	16	3.20e-02	1.00	9.01e-04	2.00
	32	1.60e-02	1.00	2.25e-04	2.00
	64	8.01e-03	1.00	5.63e-05	2.00
	128	4.00e-03	1.00	1.40e-05	2.00
2	4	1.23e-02	—	1.07e-03	—
	8	3.09e-03	1.99	1.33e-04	3.00
	16	7.74e-04	1.99	1.66e-05	3.00
	32	1.93e-04	1.99	2.08e-06	3.00
	64	4.84e-05	1.99	2.60e-07	3.00
	128	1.21e-05	2.00	3.25e-08	3.00
3	4	4.13e-04	—	3.04e-05	—
	8	5.18e-05	2.99	1.90e-06	3.99
	16	6.49e-06	2.99	1.19e-07	3.99
	32	8.12e-07	2.99	7.45e-09	4.00
	64	1.01e-07	3.00	4.65e-10	4.00

Example 2.4.5. Convergence test for 3D H(div; Ω)-elliptic problem on cubic mesh: Consider the problem (2.1.1)-(2.1.2) in $\Omega = (0,1)^3$. The exact solution of the given problem is taken as [90]

$$\mathbf{p}(x,y,z) = (p_1,p_2,p_3)^t = \begin{pmatrix} y(1-y)z(1-z) \\ x(1-x)z(1-z) \\ x(1-x)y(1-y) \end{pmatrix},$$

The coefficients are chosen as $\alpha = \gamma = 1$. The initial mesh is shown in Figure 2.4.8 (left). Numerical errors in Table 2.4.5 justify the theoretical results. First two components of WG solutions are shown in Figure 2.4.8 (middle)-(right) for $k = 1$ with $h = 1/32$.

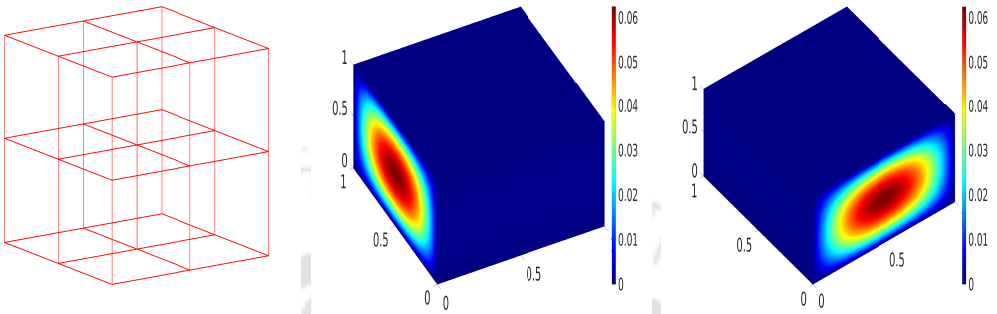

Figure 2.4.8: Initial cubic mesh (left) and component-wise surface plots of WG solution $\mathbf{p}_h$ for Example 2.4.5. Plot for the first-component of $\mathbf{p}_h$ (middle) and plot for second-component of $\mathbf{p}_h$ (right).

Table 2.4.5: Errors and convergence profile for WG solution in Example 2.4.5.

k	$\frac{1}{h}$	$\lvert\lvert\lvert\mathbf{e}_h\rvert\rvert\rvert$	Order	$\lVert\mathbf{e}_0\rVert$	Order
1	2	7.63e-01	—	8.64e-02	—
	4	3.80e-01	1.00	2.14e-02	2.00
	8	1.90e-01	1.00	5.35e-03	2.00
	16	9.50e-02	1.00	1.33e-03	2.00
	32	4.75e-02	1.00	3.34e-04	2.00
	64	2.37e-02	1.00	8.36e-05	2.00
2	2	6.91e-02	—	5.93e-03	—
	4	1.74e-02	1.98	7.42e-04	2.99
	8	4.36e-03	1.99	9.27e-05	3.00
	16	1.09e-03	1.99	1.15e-05	3.00
	32	2.73e-04	1.99	1.44e-06	3.00
	64	6.82e-05	2.00	1.81e-07	3.00
3	2	3.99e-03	—	2.93e-04	—
	4	5.05e-04	2.98	1.85e-05	3.98
	8	6.34e-05	2.99	1.15e-06	3.99
	16	7.93e-06	2.99	7.23e-08	4.00
	32	9.92e-07	3.00	4.51e-09	4.00

3

WG-FEMs for H(curl)-Elliptic Problems

Weak Galerkin finite element methods (WG-FEMs) for **H**(curl)-elliptic problems are investigated in this chapter. This WG method is highly flexible by allowing the use of discontinuous approximating functions on the arbitrary shape of polyhedra and, at the same time, is parameter-free. The optimal order of convergence is established for the WG approximations in discrete H^1 norm and L^2 norm. In fact, theoretical convergence analysis holds under low regularity requirements of the analytical solution. Results of numerical experiments that corroborate the theoretical results are also presented.

3.1 Introduction

Let $\Omega \subset \mathbb{R}^d$ $(d = 2, 3)$ be a bounded polygonal/polyhedral domain with Lipschitz continuous boundary $\partial\Omega$. The **H**(curl)-elliptic problem reads as

$$\nabla \times (\beta \nabla \times \mathbf{p}) + \gamma \mathbf{p} = \mathbf{f} \ \text{ in } \Omega, \tag{3.1.1}$$

with Dirichlet boundary condition

$$\mathbf{p} \times \boldsymbol{\eta} = 0 \ \text{ on } \partial\Omega. \tag{3.1.2}$$

Here, $\mathbf{f} \in \left[L^2(\Omega)\right]^d$, γ is a $d \times d$ positive constant matrix, and β is a $(2d-3) \times (2d-3)$ symmetric matrix with the assumption that there exist two positive constants $\underline{\lambda}$, $\bar{\lambda} > 0$ such that $\underline{\lambda}\zeta^t\zeta \leq \zeta^t\beta\zeta \leq \bar{\lambda}\zeta^t\zeta$ for all $\zeta \in \mathbb{R}^{2d-3}$. Further, $\boldsymbol{\eta}$ is the unit outward normal vector to $\partial\Omega$.

Finite element discretizations of all these equations are not as simple as they look, though. Finite element methods for Maxwell's equations are highly sensitive to the conformity of approximation spaces (see [47]). Over the last two decades, many alternatives approaches have been developed which include **H**(curl) conforming edge element

Results of this Chapter are submitted (revised) to Computers and Mathematics with Applications.

methods [99], H^1 conforming nodal finite element methods with weighted regularization [44, 53], the singular complement/field method [66], interior penalty methods [19], non-conforming finite element methods [17, 18, 19], mixed finite element method [54]. For the recent relevant works, we refer to [52] and the references therein.

In this study, we have proposed the WG-FEMs for model problems (3.1.1)-(3.1.2). In the case of **H**(curl)-elliptic problem, error estimates of $\mathrm{O}(h^k)$ in the energy norm and $\mathrm{O}(h^{k+1})$ in the L^2 norm are obtained for the WG-FEMs with typical local weak Galerkin space $\Big(\big[\mathcal{P}_k(T)\big]^d,\ \big[\mathcal{P}_k(\partial T)\big]^d,\ [\mathcal{P}_{k-1}(T)]^{2d-3}\Big)$. Further, the loss in convergence in case of classical FEMs for linear elements can be recovered in WG-FEMs under the same regularity assumption of $\mathbf{p}$ (see, Remark 3.3.2). Several numerical experiments are also carried out to validate the theoretical findings.

The rest of the chapter is organized as follows: In Sec. 3.2, we shall discuss the weak Galerkin discretization, discrete weak operators, and L^2 projection operators. The WG algorithm and error estimates have been discussed for the **H**(curl)-elliptic problem in the Sec. 3.3. Some numerical experiments have been discussed for both model problems in Sec.3.4.

3.2 Weak Galerkin Spaces

In this section, we shall discuss the weak Galerkin spaces for the model problems (3.1.1)-(3.1.2). First, we borrow the finite element partition from Chap. 2. For three-dimensional case, let T be any polyhedral domain with boundary ∂T. Then for any face $e \in \partial T$, suppose $\mathbf{t}_1$ and $\mathbf{t}_2$ be the two unit vectors on the face e such that set $\{\mathbf{t}_1, \mathbf{t}_2, \mathbf{n}\}$ is an orthogonal set. For any weak function $\mathbf{v} = \{\mathbf{v}_0, \mathbf{v}_b\}$, where $\mathbf{v}_0 \in [L^2(\Omega)]^3$ and $\mathbf{v}_b \in [L^2(e)]^3$, we can write $\mathbf{v}_b|_e = v_1\mathbf{t}_1 + v_2\mathbf{t}_2 + v_n\mathbf{n}$. Define $\bar{\mathbf{v}}_b = v_1\mathbf{t}_1 + v_2\mathbf{t}_2$ as the projection of the $\mathbf{v}_b$ in the tangential plane. Hence, we have $\bar{\mathbf{v}}_b \times \mathbf{n} = \mathbf{v}_b \times \mathbf{n}$. In similar manner, for 2D case, let $\mathbf{t}_1$ be the unit vector along the edge e such that the set of vectors $\{\mathbf{t}_1, \mathbf{n}\}$ is an orthogonal set. Then for any weak function $\mathbf{v} = \{\mathbf{v}_0, \mathbf{v}_b\}$ where $\mathbf{v}_0 \in [L^2(\Omega)]^2$ and $\mathbf{v}_b \in [L^2(e)]^2$, we can rewrite $\mathbf{v}_b|_e = v_1\mathbf{t}_1 + v_n\mathbf{n}$. Let $\bar{\mathbf{v}}_b = v_1\mathbf{t}_1$ be the projection of $\mathbf{v}_b$ on the edge e. Then, we get $\bar{\mathbf{v}}_b \times \mathbf{n} = \mathbf{v}_b \times \mathbf{n}$. Since, the quantity of interest for the approximation space corresponding to $\mathbf{p}$ is $\mathbf{v}_b \times \mathbf{n}$ not $\mathbf{v}_b$. Due to this reason in both 2D and 3D cases, we assume $\mathbf{v}_b = \bar{\mathbf{v}}_b$, that will reduce reduces the computationally cost significantly.

Next, we define the following WG space

$$\sum\nolimits_h = \{\boldsymbol{\sigma}_h = \{\boldsymbol{\sigma}_0, \boldsymbol{\sigma}_b = \sigma_1\mathbf{t}_1 + (d-2)\sigma_2\mathbf{t}_2\} : \boldsymbol{\sigma}_0 \in [\mathcal{P}_k(T)]^d,\ \sigma_1, \sigma_2 \in \mathcal{P}_k(e), e \in \partial T, T \in \mathcal{T}_h\},$$

where $k \geq 1$ is an integer. For the well-posedness of the WG approximation, $\boldsymbol{\sigma}_b$ defined on each interior edge/face $e \in \mathcal{E}_h^0$ must be single valued (cf. [121, 122]). Hence, the

global weak finite element space for the vector-component is defined as

$$\mathbf{V}_h = \Big\{ \boldsymbol{\sigma}_h = \{\boldsymbol{\sigma}_0, \boldsymbol{\sigma}_b\} \in \sum\nolimits_h : \ [\boldsymbol{\sigma}_b]_e = \mathbf{0} \ \forall e \in \mathcal{E}_h^0 \Big\}.$$

Here,

$$[\boldsymbol{\sigma}_b]_e = \boldsymbol{\sigma}_b|_{\partial T_i \cap e} - \boldsymbol{\sigma}_b|_{\partial T_j \cap e} \tag{3.2.1}$$

is the jump of $\boldsymbol{\sigma}_b$ across $e \in \mathcal{E}_h^0$, where $\boldsymbol{\sigma}_b|_{\partial T_s \cap e}$ is the value of $\boldsymbol{\sigma}_b$ on the edge/face e as seen from the element T_s, $s = i,\ j$. Subsequently, we define

$$\mathbf{V}_h^0 = \{\boldsymbol{\sigma}_h = \{\boldsymbol{\sigma}_0, \boldsymbol{\sigma}_b\} \in \mathbf{V}_h : \ \boldsymbol{\sigma}_b \times \boldsymbol{\eta} = \mathbf{0} \ \text{ on } \partial\Omega\}.$$

For any $\mathbf{v}_h = \{\mathbf{v}_0, \mathbf{v}_b\} \in \sum_h$, the discrete weak curl operator, denoted by $(\nabla_w \times (\cdot))$, is a unique polynomial $\nabla_w \times \mathbf{v}_h \in [\mathcal{P}_{k-1}(T)]^{2d-3}$ defined as

$$(\nabla_w \times \mathbf{v}_h, \boldsymbol{\varphi})_T = \int_T \mathbf{v}_0 \cdot (\nabla \times \boldsymbol{\varphi}) dT - \int_{\partial T} \mathbf{v}_b \times \boldsymbol{\eta} \cdot \boldsymbol{\varphi} ds \ \ \forall \boldsymbol{\varphi} \in [\mathcal{P}_{k-1}(T)]^{2d-3}. \tag{3.2.2}$$

Now, for $T \in \mathcal{T}_h$ and $e \in \mathcal{E}_h$, we define some important usual local L^2 projection operators given as follows:

$$\mathbf{Q}_b^k : [L^2(e)]^d \to [\mathcal{P}_k(e)]^d \ \& \ \boldsymbol{\mathcal{Q}}_h^{k-1} : [L^2(T)]^{2d-3} \to [\mathcal{P}_{k-1}(T)]^{2d-3}.$$

For $\mathbf{p} \in [H^1(\Omega)]^d$, we define $\mathbf{Q}_h\mathbf{p} = \{\mathbf{Q}_0^k\mathbf{p}, \mathbf{Q}_b^k\mathbf{v} = Q_b^k(p_1)\mathbf{t}_1 + (d-2)Q_b^k(p_2)\mathbf{t}_2\}$. Now, for the stabilized WG schemes, we define a stabilizer $\mathcal{S} : \mathbf{V}_h \times \mathbf{V}_h \to \mathbb{R}$ given by

$$\mathcal{S}(\mathbf{v}_h, \mathbf{w}_h) = \sum_{T \in \mathcal{T}_h} h_T^{-1} \langle (\mathbf{v}_0 - \mathbf{v}_b) \times \boldsymbol{\eta}, (\mathbf{w}_0 - \mathbf{w}_b) \times \boldsymbol{\eta} \rangle_{\partial T} \ \ \forall \mathbf{v}_h, \mathbf{w}_h \in \mathbf{V}_h. \tag{3.2.3}$$

For later analysis, we require the following approximation properties associated with the standard L^2 projection operators.

Lemma 3.2.1. *(cf. [102, 121]) Suppose $\mathcal{T}_h$ is a polygonal/polyhedral partition of $\Omega \subset \mathbb{R}^d$ with some shape-regularity constraints mentioned in [121]. Then, for $\mathbf{w} \in [H^{s+1}(\Omega)]^d$, we have*

$$\sum_{T \in \mathcal{T}_h} \|\mathbf{Q}_0^k\mathbf{w} - \mathbf{w}\|_T^2 \leq h^{2(s+1)} \|\mathbf{w}\|_{s+1}^2, \tag{3.2.4}$$

$$\sum_{T \in \mathcal{T}_h} \|\boldsymbol{\mathcal{Q}}_h^{k-1}(\nabla \times \mathbf{w}) - \nabla \times \mathbf{w}\|_T^2 \leq h^{2s} \|\mathbf{w}\|_{s+1}^2, \tag{3.2.5}$$

where $1 \leq s \leq k$.

Lemma 3.2.2. *The L^2 projection operators $\mathbf{Q}_h$, and $\boldsymbol{\mathcal{Q}}_h^{k-1}$ entertain the following commutative properties*

$$\boldsymbol{\mathcal{Q}}_h^{k-1}(\nabla \times \mathbf{w}) \ = \ \nabla_w \times (\mathbf{Q}_h\mathbf{w}) \ \ \forall \mathbf{w} \in \mathbf{H}(\text{curl}; \Omega). \tag{3.2.6}$$

3.3 Convergence Analysis

In this section, we have proposed a WG-FEM for the $\mathbf{H}(\text{curl};\Omega)$-elliptic model problem (3.1.1)-(3.1.2) with local weak Galerkin space $\left(\mathcal{P}_k^d,\ \mathcal{P}_k^d,\ \mathcal{P}_{k-1}^{2d-3}\right)$. Further, we establish optimal error estimates in discrete energy norm and L^2 norm.

We introduce a bilinear map $\mathcal{A}_1 : \mathbf{V}_h \times \mathbf{V}_h \to \mathbb{R}$ to be used in this section

$$\mathcal{A}_1(\mathbf{v}_h, \mathbf{w}_h) = (\beta\nabla_w \times \mathbf{v}_h, \nabla_w \times \mathbf{w}_h) + (\gamma\mathbf{v}_0, \mathbf{w}_0) + \mathcal{S}(\mathbf{v}_h, \mathbf{w}_h)\ \forall \mathbf{v}_h, \mathbf{w}_h \in \mathbf{V}_h. \quad (3.3.1)$$

Note that WG space $\mathbf{V}_h^0$ is a normed linear space with the triple-bar norm given as

$$\begin{aligned} |||\mathbf{v}_h|||_1^2 &:= \sum_{T\in\mathcal{T}_h} \|\beta^{\frac{1}{2}}\nabla_w \times \mathbf{v}_h\|_T^2 + \|\gamma^{\frac{1}{2}}\mathbf{v}_0\|_T^2 + \sum_{T\in\mathcal{T}_h} h_T^{-1}\|(\mathbf{v}_0 - \mathbf{v}_b) \times \boldsymbol{\eta}\|_{\partial T}^2 \\ &= \mathcal{A}_1(\mathbf{v}_h, \mathbf{v}_h), \quad \mathbf{v}_h = \{\mathbf{v}_0, \mathbf{v}_b\} \in \mathbf{V}_h^0. \end{aligned} \quad (3.3.2)$$

Weak Galerkin Algorithm 1. A WG approximation for (3.1.1)-(3.1.2) can be developed by finding $\mathbf{p}_h = \{\mathbf{p}_0, \mathbf{p}_b\} \in \mathbf{V}_h^0$ such that

$$\mathcal{A}_1(\mathbf{p}_h, \mathbf{v}_h) = (\mathbf{f}, \mathbf{v}_0)\ \ \forall \mathbf{v}_h = \{\mathbf{v}_0, \mathbf{v}_b\} \in \mathbf{V}_h^0. \quad (3.3.3)$$

For the purpose of error analysis, we introduce error function $\mathbf{e}_h$ given by

$$\mathbf{e}_h := \{\mathbf{e}_0, \mathbf{e}_b\} = \mathbf{Q}_h\mathbf{p} - \mathbf{p}_h = \{\mathbf{Q}_0^k\mathbf{p} - \mathbf{p}_0, \mathbf{Q}_b^k\mathbf{p} - \mathbf{p}_b\}. \quad (3.3.4)$$

To capture the error function $\mathbf{e}_h$, we introduce following bilinear maps

$$R_1(\mathbf{p}, \mathbf{v}_h) = \sum_{T\in\mathcal{T}_h} \langle(\beta\nabla \times \mathbf{p} - \boldsymbol{\mathcal{Q}}_h^{k-1}(\beta\nabla \times \mathbf{p})) \times \boldsymbol{\eta}, \mathbf{v}_0 - \mathbf{v}_b\rangle_{\partial T}, \quad (3.3.5)$$

$$R_2(\mathbf{p}, \mathbf{v}_h) = \sum_{T\in\mathcal{T}_h} (\beta\boldsymbol{\mathcal{Q}}_h^{k-1}(\nabla \times \mathbf{p}) - \boldsymbol{\mathcal{Q}}_h^{k-1}(\beta\nabla \times \mathbf{p}), \nabla_w \times \mathbf{v}_h)_T. \quad (3.3.6)$$

Then, we derive the following error equation.

Lemma 3.3.1. *For each* $\mathbf{v}_h = \{\mathbf{v}_0, \mathbf{v}_b\} \in \mathbf{V}_h^0$, *we have*

$$\begin{aligned} \mathcal{A}_1(\mathbf{e}_h, \mathbf{v}_h) &= R_1(\mathbf{p}, \mathbf{v}_h) + R_2(\mathbf{p}, \mathbf{v}_h) + \mathcal{S}(\mathbf{Q}_h\mathbf{p}, \mathbf{v}_h) \\ &:= R_3(\mathbf{p}, \mathbf{v}_h), \quad R_3(\cdot,\cdot) = R_1(\cdot,\cdot) + R_2(\cdot,\cdot) + \mathcal{S}(\mathbf{Q}_h\cdot, \cdot). \end{aligned} \quad (3.3.7)$$

Proof. For any $\mathbf{v}_h = \{\mathbf{v}_0, \mathbf{v}_b\} \in \mathbf{V}_h^0$, inspect equation (3.1.1) with $\mathbf{v}_0$ to obtain

$$\sum_{T\in\mathcal{T}_h} (\nabla \times (\beta\nabla \times \mathbf{p}), \mathbf{v}_0)_T + (\gamma\mathbf{p}, \mathbf{v}_0) = (\mathbf{f}, \mathbf{v}_0). \quad (3.3.8)$$

Now, apply integration by parts to arrive at

$$\begin{aligned}(\mathbf{f},\mathbf{v}_0) &= (\gamma\mathbf{Q}_0^k\mathbf{p},\mathbf{v}_0)+\sum_{T\in\mathcal{T}_h}(\beta\nabla\times\mathbf{p},\nabla\times\mathbf{v}_0)_T\\ &\quad-\sum_{T\in\mathcal{T}_h}\langle\mathbf{v}_0-\mathbf{v}_b,(\beta\nabla\times\mathbf{p})\times\boldsymbol{\eta}\rangle_{\partial T}. \end{aligned}\tag{3.3.9}$$

Here, we assume γ to be a piecewise constant and the fact that $\sum_{T\in\mathcal{T}_h}\langle(\beta\nabla\times\mathbf{p})\times\boldsymbol{\eta},\mathbf{v}_b\rangle_{\partial T}=0$. Next, by using the definition (3.2.2) for $\mathbf{v}_h$, we obtain

$$\begin{aligned}&(\boldsymbol{\mathcal{Q}}_h^{k-1}(\beta\nabla\times\mathbf{p}),\nabla_w\times\mathbf{v}_h)_T\\ &=(\mathbf{v}_0,\nabla\times(\boldsymbol{\mathcal{Q}}_h^{k-1}(\beta\nabla\times\mathbf{p})))_T-\langle\mathbf{v}_b\times\boldsymbol{\eta},\boldsymbol{\mathcal{Q}}_h^{k-1}(\beta\nabla\times\mathbf{p})\rangle_{\partial T}\\ &=(\mathbf{v}_0,\nabla\times(\boldsymbol{\mathcal{Q}}_h^{k-1}(\beta\nabla\times\mathbf{p})))_T+\langle\mathbf{v}_b,\boldsymbol{\mathcal{Q}}_h^{k-1}(\beta\nabla\times\mathbf{p})\times\boldsymbol{\eta}\rangle_{\partial T}\\ &=(\nabla\times\mathbf{v}_0,\boldsymbol{\mathcal{Q}}_h^{k-1}(\beta\nabla\times\mathbf{p}))_T-\langle(\boldsymbol{\mathcal{Q}}_h^{k-1}(\beta\nabla\times\mathbf{p}))\times\boldsymbol{\eta},\mathbf{v}_0\rangle_{\partial T}\\ &\quad+\langle\boldsymbol{\mathcal{Q}}_h^{k-1}(\beta\nabla\times\mathbf{p})\times\boldsymbol{\eta},\mathbf{v}_b\rangle_{\partial T}\\ &=(\nabla\times\mathbf{v}_0,\boldsymbol{\mathcal{Q}}_h^{k-1}(\beta\nabla\times\mathbf{p}))_T-\langle(\boldsymbol{\mathcal{Q}}_h^{k-1}(\beta\nabla\times\mathbf{p}))\times\boldsymbol{\eta},\mathbf{v}_0-\mathbf{v}_b\rangle_{\partial T}\\ &=(\nabla\times\mathbf{v}_0,\beta\nabla\times\mathbf{p})_T-\langle(\boldsymbol{\mathcal{Q}}_h^{k-1}(\beta\nabla\times\mathbf{p}))\times\boldsymbol{\eta},\mathbf{v}_0-\mathbf{v}_b\rangle_{\partial T}.\end{aligned}\tag{3.3.10}$$

Equations (3.3.9)-(3.3.10) together with commutative property (3.2.6) lead to

$$\begin{aligned}(\mathbf{f},\mathbf{v}_0) &= (\gamma\mathbf{Q}_0^k\mathbf{p},\mathbf{v}_0)+(\boldsymbol{\mathcal{Q}}_h^{k-1}(\beta\nabla\times\mathbf{p}),\nabla_w\times\mathbf{v}_h)\\ &\quad-\sum_{T\in\mathcal{T}_h}\langle(\beta\nabla\times\mathbf{p}-\boldsymbol{\mathcal{Q}}_h^{k-1}(\beta\nabla\times\mathbf{p}))\times\boldsymbol{\eta},\mathbf{v}_0-\mathbf{v}_b\rangle_{\partial T}\\ &=(\gamma\mathbf{Q}_0^k\mathbf{p},\mathbf{v}_0)+(\beta\boldsymbol{\mathcal{Q}}_h^{k-1}(\nabla\times\mathbf{p}),\nabla_w\times\mathbf{v}_h)\\ &\quad-(\beta\boldsymbol{\mathcal{Q}}_h^{k-1}(\nabla\times\mathbf{p})-\boldsymbol{\mathcal{Q}}_h^{k-1}(\beta\nabla\times\mathbf{p}),\nabla_w\times\mathbf{v}_h)\\ &\quad-\sum_{T\in\mathcal{T}_h}\langle(\beta\nabla\times\mathbf{p}-\boldsymbol{\mathcal{Q}}_h^{k-1}(\beta\nabla\times\mathbf{p}))\times\boldsymbol{\eta},\mathbf{v}_0-\mathbf{v}_b\rangle_{\partial T}\\ &=(\gamma\mathbf{Q}_0^k\mathbf{p},\mathbf{v}_0)+(\beta\nabla_w\times(\mathbf{Q}_h\mathbf{p}),\nabla_w\times\mathbf{v}_h)\\ &\quad-R_1(\mathbf{p},\mathbf{v}_h)-R_2(\mathbf{p},\mathbf{v}_h).\end{aligned}\tag{3.3.11}$$

Next, adding $\mathcal{S}(\mathbf{Q}_h\mathbf{p},\mathbf{v}_h)$ to both sides of (3.3.11) yields

$$\mathcal{A}_1(\mathbf{Q}_h\mathbf{p},\mathbf{v}_h)=(\mathbf{f},\mathbf{v}_0)+R_1(\mathbf{p},\mathbf{v}_h)+R_2(\mathbf{p},\mathbf{v}_h)+\mathcal{S}(\mathbf{Q}_h\mathbf{p},\mathbf{v}_h).\tag{3.3.12}$$

Finally, subtracting (3.3.3) from (3.3.12) leads to desire identity (3.3.7). □

Next result establishes crucial bounds for bilinear maps $R_i(\cdot,\cdot)$ $(i=1,2)$ and stabilizer $\mathcal{S}(\cdot,\cdot)$.

Lemma 3.3.2. *Suppose* $\mathbf{p} \in [H^{k+1}(\Omega)]^d$. *Then, for any* $\mathbf{v}_h = \{\mathbf{v}_0, \mathbf{v}_b\} \in \mathbf{V}_h^0$, *we have*

$$
\begin{aligned}
|R_1(\mathbf{p}, \mathbf{v}_h)| &\leq C(\|\beta\|_{k,\infty}) h^k \|\mathbf{p}\|_{k+1} |||\mathbf{v}_h|||_1, && (3.3.13)\\
|R_2(\mathbf{p}, \mathbf{v}_h)| &\leq C(\|\beta\|_{1,\infty}) h^{k+1} \|\mathbf{p}\|_{k+1} |||\mathbf{v}_h|||_1, && (3.3.14)\\
|\mathcal{S}(\mathbf{Q}_h\mathbf{p}, \mathbf{v}_h)| &\leq C h^k \|\mathbf{p}\|_k |||\mathbf{v}_h|||_1. && (3.3.15)
\end{aligned}
$$

Proof. For (3.3.13), use Cauchy-Schwarz inequality, trace inequality (2.2.7) and Lemma 3.2.1 to obtain

$$
\begin{aligned}
|R_1(\mathbf{p}, \mathbf{v}_h)| &\leq \sum_{T\in\mathcal{T}_h} \|(\beta\nabla\times\mathbf{p} - \boldsymbol{\mathcal{Q}}_h^{k-1}(\beta\nabla\times\mathbf{p}))\times\boldsymbol{\eta}\|_{\partial T} \|\mathbf{v}_0 - \mathbf{v}_b\|_{\partial T}\\
&\leq C\left(\sum_{T\in\mathcal{T}_h} h_T \|\beta\nabla\times\mathbf{p} - \boldsymbol{\mathcal{Q}}_h^{k-1}(\beta\nabla\times\mathbf{p})\|_{\partial T}^2\right)^{\frac{1}{2}}\\
&\quad\times\left(\sum_{T\in\mathcal{T}_h} h_T^{-1}\|\mathbf{v}_0 - \mathbf{v}_b\|_{\partial T}^2\right)^{\frac{1}{2}}\\
&\leq C(\|\beta\|_{k,\infty}) h^k \|\mathbf{p}\|_{k+1} |||\mathbf{v}_h|||_1.
\end{aligned}
$$

To estimate (3.3.14), we use Lemma 3.2.1 and use inequality (2.3.16) to obtain

$$
\begin{aligned}
|R_2(\mathbf{p}, \mathbf{v}_h)| &= \left|\sum_{T\in\mathcal{T}_h} (\beta\boldsymbol{\mathcal{Q}}_h^{k-1}(\nabla\times\mathbf{p}) - \boldsymbol{\mathcal{Q}}_h^{k-1}(\beta\nabla\times\mathbf{p}), \nabla_w\times\mathbf{v}_h)_T\right|\\
&= \left|\sum_{T\in\mathcal{T}_h} (\beta\boldsymbol{\mathcal{Q}}_h^{k-1}(\nabla\times\mathbf{p}) - \beta\nabla\times\mathbf{p}, \nabla_w\times\mathbf{v}_h)_T\right|\\
&= \left|\sum_{T\in\mathcal{T}_h} (\boldsymbol{\mathcal{Q}}_h^{k-1}(\nabla\times\mathbf{p}) - \nabla\times\mathbf{p}, (\beta - \bar{\beta})\nabla_w\times\mathbf{v}_h)_T\right|\\
&\leq C(\|\beta\|_{1,\infty}) h \left(\sum_{T\in\mathcal{T}_h} \|\boldsymbol{\mathcal{Q}}_h^{k-1}(\nabla\times\mathbf{p}) - \nabla\times\mathbf{p}\|_T^2\right)^{\frac{1}{2}}\\
&\quad\times\left(\sum_{T\in\mathcal{T}_h} \|\nabla_w\times\mathbf{v}_h\|_T^2\right)^{\frac{1}{2}}\\
&\leq C(\|\beta\|_{1,\infty}) h^{k+1} \|\mathbf{p}\|_{k+1} |||\mathbf{v}_h|||_1.
\end{aligned}
$$

Similar arguments yield

$$\begin{aligned}
|\mathcal{S}(\mathbf{Q}_h\mathbf{p},\mathbf{v}_h)| &= \left|\sum_{T\in\mathcal{T}_h} h_T^{-1}\langle \mathbf{Q}_0^k\mathbf{p}-\mathbf{Q}_b^k\mathbf{p},\mathbf{v}_0-\mathbf{v}_b\rangle_{\partial T}\right| \\
&\le \sum_{T\in\mathcal{T}_h} h_T^{-1}\|\mathbf{Q}_0^k\mathbf{p}-\mathbf{p}\|_{\partial T}\|\mathbf{v}_0-\mathbf{v}_b\|_{\partial T} \\
&\le \left(\sum_{T\in\mathcal{T}_h}(h_T^{-2}\|\mathbf{Q}_0^k\mathbf{p}-\mathbf{p}\|_T^2+\|\nabla(\mathbf{Q}_0^k\mathbf{p}-\mathbf{p})\|_T^2)\right)^{\frac{1}{2}} \\
&\quad\times\left(\sum_{T\in\mathcal{T}_h} h_T^{-1}\|\mathbf{v}_0-\mathbf{v}_b\|_{\partial T}^2\right)^{\frac{1}{2}} \\
&\le Ch^k\|\mathbf{p}\|_{k+1}|||\mathbf{v}_h|||_1.
\end{aligned}$$

This completes the proof of Lemma 3.3.2. □

As an immediate consequence of the above result, we obtain the following optimal error estimates in discrete H^1 norm.

Theorem 3.3.1. *Let* $\mathbf{p}\in[H^{k+1}(\Omega)]^d$ *be the exact solution of* (3.1.1)-(3.1.2) *and* $\mathbf{p}_h\in\mathbf{V}_h^0$ *be the WG solution of* (3.3.3)*. Then, we have*

$$|||\mathbf{Q}_h\mathbf{p}-\mathbf{p}_h|||_1\le Ch^k\|\mathbf{p}\|_{k+1}. \tag{3.3.16}$$

Proof. We inspect the error equation (3.3.7) with $\mathbf{v}_h=\mathbf{e}_h$ to obtain

$$|||\mathbf{e}_h|||_1\le|R_1(\mathbf{p},\mathbf{e}_h)|+|R_2(\mathbf{p},\mathbf{e}_h)|+|\mathcal{S}(\mathbf{Q}_h\mathbf{p},\mathbf{e}_h)|. \tag{3.3.17}$$

The estimate (3.3.16) directly follows from (3.3.17) and Lemma 3.3.2. □

Remark 3.3.1. *Suppose the problem* (3.1.1)-(3.1.2) *has the* $\left[H^{1+\delta}(\Omega)\right]^d$*-regularity property in the sense that the solution* $\mathbf{p}$ *of* (3.1.1)-(3.1.2) *belongs to* $\left[H^{1+\delta}(\Omega)\right]^d$ *for some* $\delta\in\left(\frac{1}{2},1\right]$*. Such low regularity is common for the solutions of Maxwell's equations in the non-convex domain (cf. [19]). Then, assuming the following approximation properties for the standard* L^2 *projection operators*

$$\begin{aligned}
&\text{(a)}\quad \left\|\beta\nabla\times\mathbf{p}-\boldsymbol{\mathcal{Q}}_h^{k-1}(\beta\nabla\times\mathbf{p})\right\|_T^2+h_T^{2\delta}\left|\beta\nabla\times\mathbf{p}-\boldsymbol{\mathcal{Q}}_h^{k-1}(\beta\nabla\times\mathbf{p})\right|_{\delta,T}^2 \\
&\qquad\le Ch_T^{2\delta}\left|\beta\nabla\times\mathbf{p}\right|_{\delta,T}^2\le Ch_T^{2\delta}\|\mathbf{p}\|_{1+\delta,T}^2, \qquad (3.3.18)\\
&\text{(b)}\quad \|\mathbf{Q}_0^k\mathbf{p}-\mathbf{p}\|_T^2+h_T^2|\mathbf{Q}_0^k\mathbf{p}-\mathbf{p}|_{1,T}^2\le Ch_T^{2(1+\delta)}\|\mathbf{p}\|_{1+\delta,T}^2, \qquad (3.3.19)
\end{aligned}$$

and the trace result (2.2.7) yields

$$|R_3(\mathbf{p},\mathbf{v}_h)|\le Ch^\delta\|\mathbf{p}\|_{1+\delta}.$$

Then, arguing as in (3.3.17), we arrive at

$$|||\mathbf{e}_h|||_1 \leq Ch^{\delta}\|\mathbf{p}\|_{1+\delta}. \tag{3.3.20}$$

Remark 3.3.2. *Assuming* $\beta\nabla\times\mathbf{p}\in[H^1(\Omega)]^{2d-3}$ *(see in [19] for two-dimensional curl-curl problems), it is easy to prove that*

$$|R_1(\mathbf{p},\mathbf{v}_h)|+|R_2(\mathbf{p},\mathbf{v}_h)|\leq C(\|\beta\|_{1,\infty})h\|\nabla\times\mathbf{p}\|_{\mathbf{H}^1(\Omega)}|||\mathbf{v}_h|||_1. \tag{3.3.21}$$

Hence, the estimate (3.3.20) is expected to be optimal for the WG-FEMs without a stabilizer, which we will report in another article. In fact, for stabilizer-free WG-FEMs with $\nabla\times\mathbf{p}\in[H^{\alpha}(\Omega)]^{2d-3}$*, we note that*

$$|||\mathbf{e}_h|||_1 \leq h^{\alpha}\|\nabla\times\mathbf{p}\|_{\mathbf{H}^{\alpha}(\Omega)} \quad \text{for } \alpha>\frac{1}{2}. \tag{3.3.22}$$

Now, by using the duality argument, we shall find the L^2 norm error estimate. For this, we consider the auxiliary problem with H^1 regularity in which unknown function $\boldsymbol{\psi}$ satisfy the following equations

$$\nabla\times(\beta\nabla\times\boldsymbol{\psi})+\gamma\boldsymbol{\psi}=\mathbf{e}_0 \ \text{ in } \Omega, \tag{3.3.23}$$

$$\boldsymbol{\psi}\times\boldsymbol{\eta}=0 \quad \text{on } \partial\Omega, \tag{3.3.24}$$

and $\boldsymbol{\psi}$ also satisfy the priori bound given by (see, [70])

$$\|\boldsymbol{\psi}\|_1+\|\nabla\times\boldsymbol{\psi}\|_1\leq C\|\mathbf{e}_0\|. \tag{3.3.25}$$

Let $\mathcal{N}_h=\{\boldsymbol{\phi}\in\mathbf{H}_0(\text{curl};\Omega),\ \boldsymbol{\phi}|_T\in[\mathcal{P}_k(T)]^d,\ \forall T\in\mathcal{T}_h\}$ be the second Nedelec edge element space. We define the $\boldsymbol{\Pi}_h$ be the interpolation operator onto the space $\mathcal{N}_h$ (see [99]).

Lemma 3.3.3. *([99], Theorem 5.41) For any* $\boldsymbol{\phi}\in\mathbf{H}^s(\Omega)$ *and* $\nabla\times\boldsymbol{\phi}\in[H^s(\Omega)]^{2d-3}$, $s\in\left(\frac{1}{2},k\right]$, *we obtain*

$$\|\boldsymbol{\phi}-\boldsymbol{\Pi}_h\boldsymbol{\phi}\|_{s,\mathbf{curl}}\leq Ch^s(\|\boldsymbol{\phi}\|_s+\|\nabla\times\boldsymbol{\phi}\|_s).$$

Lemma 3.3.4. *For any* $\boldsymbol{\phi}\in\mathcal{N}_h$, *we have*

$$(\alpha\nabla_w\times\mathbf{e}_h,\nabla\times\boldsymbol{\phi})+(\beta\mathbf{e}_0,\boldsymbol{\phi})=(\mathbb{Q}_h^{k-1}(\nabla\times\mathbf{p})-\nabla\times\mathbf{p},(\alpha-\bar{\alpha})\nabla\times\boldsymbol{\phi}).$$

Proof. Testing equation (3.1.1) against $\boldsymbol{\phi}$ and using the definitions of L^2 projections yield

$$\begin{aligned}
(\mathbf{f},\boldsymbol{\phi}) &= (\nabla\times(\beta\nabla\times\mathbf{p}),\boldsymbol{\phi})+(\gamma\mathbf{p},\boldsymbol{\phi})\\
&= (\beta(\boldsymbol{\mathcal{Q}}_h^{k-1}(\nabla\times\mathbf{p})),\nabla\times\boldsymbol{\phi})+(\gamma\mathbf{Q}_0^k\mathbf{p},\boldsymbol{\phi})\\
&- (\beta(\boldsymbol{\mathcal{Q}}_h^{k-1}(\nabla\times\mathbf{p}))-\boldsymbol{\mathcal{Q}}_h^{k-1}(\beta\nabla\times\mathbf{p}),\nabla\times\boldsymbol{\phi})\\
&= (\beta(\nabla_w\times(\mathbf{Q}_h\mathbf{p})),\nabla\times\boldsymbol{\phi})+(\gamma\mathbf{Q}_0^k\mathbf{p},\boldsymbol{\phi})\\
&- (\boldsymbol{\mathcal{Q}}_h^{k-1}(\nabla\times\mathbf{p})-\nabla\times\mathbf{p},(\beta-\bar{\beta})\nabla\times\boldsymbol{\phi}).
\end{aligned}\tag{3.3.26}$$

Next, we set $\boldsymbol{\phi}_h = \{\boldsymbol{\phi}_0, \boldsymbol{\phi}_b\} \in \mathbf{V}_h^0$ with $\boldsymbol{\phi}_0 = \boldsymbol{\phi}$ and $\boldsymbol{\phi}_b = (\boldsymbol{\phi} \times \boldsymbol{\eta}) \times \boldsymbol{\eta} = \boldsymbol{\phi} - (\boldsymbol{\phi} \cdot \boldsymbol{\eta})\boldsymbol{\eta}$, and note that $\nabla_w \times \boldsymbol{\phi}_h = \nabla \times \boldsymbol{\phi}$. Then by putting $\mathbf{v}_h = \boldsymbol{\phi}_h$ in (3.3.3), we get

$$(\mathbf{f}, \boldsymbol{\phi}) = (\beta \nabla_w \times \mathbf{p}_h, \nabla \times \boldsymbol{\phi}) + (\gamma \mathbf{p}_0, \boldsymbol{\phi}). \tag{3.3.27}$$

Finally, equations (3.3.26)-(3.3.27) leads to the desired result. □

Theorem 3.3.2. *Let $\mathbf{p} \in [H^{k+1}(\Omega)]^d$ be the exact solution of (3.1.1)-(3.1.2) and $\mathbf{p}_h \in \mathbf{V}_h^0$ be the WG solution of (3.3.3). Then, we have*

$$\|\mathbf{Q}_0^k \mathbf{p} - \mathbf{p}_0\| \leq C h^{k+1} \|\mathbf{p}\|_{k+1}. \tag{3.3.28}$$

Proof. Multiply the first equation of (3.3.23) with $\mathbf{e}_0$ to arrive at

$$\begin{aligned}
(\mathbf{e}_0, \mathbf{e}_0) &= (\nabla \times (\beta \nabla \times \boldsymbol{\psi}), \mathbf{e}_0) + (\gamma \boldsymbol{\psi}, \mathbf{e}_0) \\
&= (\beta \nabla \times \boldsymbol{\psi}, \nabla \times \mathbf{e}_0) - \sum_{T \in \mathcal{T}_h} \langle \beta \nabla \times \boldsymbol{\psi}, (\mathbf{e}_b - \mathbf{e}_0) \times \boldsymbol{\eta} \rangle_{\partial T} + (\gamma \boldsymbol{\psi}, \mathbf{e}_0), \\
&= (\beta \nabla \times \boldsymbol{\psi}, \nabla_w \times \mathbf{e}_h) + (\gamma \boldsymbol{\psi}, \mathbf{e}_0) \\
&- \sum_{T \in \mathcal{T}_h} \langle \beta \nabla \times \boldsymbol{\psi} - \boldsymbol{\mathcal{Q}}_h^{k-1}(\beta \nabla \times \boldsymbol{\psi}), (\mathbf{e}_b - \mathbf{e}_0) \times \boldsymbol{\eta} \rangle_{\partial T},
\end{aligned} \tag{3.3.29}$$

where we have used the fact that $\sum_{T \in \mathcal{T}_h} \langle \beta \nabla \times \boldsymbol{\psi}, \mathbf{e}_b \times \boldsymbol{\eta} \rangle_{\partial T} = 0$. Further, using Lemma 3.3.4 with $\boldsymbol{\phi} = \boldsymbol{\Pi}_h \boldsymbol{\psi}$ in the equation (3.3.29), we deduce

$$\begin{aligned}
\|\mathbf{e}_0\|^2 &= (\beta \nabla \times (\boldsymbol{\psi} - \boldsymbol{\Pi}_h \boldsymbol{\psi}), \nabla_w \times \mathbf{e}_h) + (\gamma(\boldsymbol{\psi} - \boldsymbol{\Pi}_h \boldsymbol{\psi}), \mathbf{e}_0) \\
&- \sum_{T \in \mathcal{T}_h} \langle \beta \nabla \times \boldsymbol{\psi} - \boldsymbol{\mathcal{Q}}_h^{k-1}(\beta \nabla \cdot \boldsymbol{\psi}), (\mathbf{e}_b - \mathbf{e}_0) \times \boldsymbol{\eta} \rangle_{\partial T} \\
&+ (\boldsymbol{\mathcal{Q}}_h^{k-1}(\nabla \cdot \mathbf{p}) - \nabla \cdot \mathbf{p}, (\beta - \bar{\beta}) \nabla \cdot (\boldsymbol{\Pi}_h \boldsymbol{\psi})) \\
&\leq C \|\boldsymbol{\psi} - \boldsymbol{\Pi}_h \boldsymbol{\psi}\|_{1,\mathbf{curl}} |||\mathbf{e}_h|||_1 + \sum_{T \in \mathcal{T}_h} \|\beta \nabla \times \boldsymbol{\psi} - \boldsymbol{\mathcal{Q}}_h^{k-1}(\beta \nabla \times \boldsymbol{\psi})\|_{\partial T} \|(\mathbf{e}_0 - \mathbf{e}_b) \times \boldsymbol{\eta}\|_{\partial T} \\
&+ C h (\|\beta\|_{1,\infty}) \sum_{T \in \mathcal{T}_h} \|\boldsymbol{\mathcal{Q}}_h^{k-1}(\nabla \times \mathbf{p}) - \nabla \times \mathbf{p}\|_T \|\nabla \times (\boldsymbol{\Pi}_h \boldsymbol{\psi})\|_T.
\end{aligned} \tag{3.3.30}$$

Next, from trace inequality (2.2.7) and inverse inequality (2.2.8), we note that

$$\begin{aligned}
h_T \|\beta \nabla \times \boldsymbol{\psi} - \boldsymbol{\mathcal{Q}}_h^{k-1}(\beta \nabla \times \boldsymbol{\psi})\|_{\partial T}^2 &\leq C \|\beta \nabla \times \boldsymbol{\psi} - \boldsymbol{\mathcal{Q}}_h^{k-1}(\beta \nabla \times \boldsymbol{\psi})\|_T^2 \\
&\leq C h^2 \|\beta \nabla \times \boldsymbol{\psi}\|_1^2 \\
&\leq C h^2 \|\beta\|_{1,\infty} \|\boldsymbol{\psi}\|_{1,\mathbf{curl}}^2,
\end{aligned}$$

which together with estimate (3.3.30), Lemma 2.2.1, Lemma 2.3.4 and a priori estimate (3.3.25) yield

$$\begin{aligned}
\|\mathbf{e}_0\|^2 &\leq C h \|\boldsymbol{\psi}\|_{1,\mathbf{curl}} |||\mathbf{e}_h|||_1 + C h^{k+1} \|\mathbf{p}\|_{k+1} \|\boldsymbol{\psi}\|_{1,\mathbf{curl}} \\
&\leq C h \|\mathbf{e}_0\| |||\mathbf{e}_h|||_1 + C h^{k+1} \|\mathbf{p}\|_{k+1} \|\mathbf{e}_0\|.
\end{aligned}$$

Finally, Theorem 3.3.1 leads to the desired estimate. □

Remark 3.3.3. *Now we relax the regularity of the global solution* $\mathbf{p}$ *in Theorem 3.3.2 and require only* $\mathbf{p} \in \left[H^{1+\delta}(\Omega)\right]^d$ *for some* $\delta \in \left(\frac{1}{2}, 1\right]$*. If the solution* $\boldsymbol{\psi}$ *of the auxiliary problem (3.3.23)-(3.3.24) has* $[H^{1+s}(\Omega)]^d$ *regularity for some* $s \in \left(\frac{1}{2}, 1\right]$*, then*

$$\|\mathbf{Q}_0^k \mathbf{p} - \mathbf{p}_0\| \leq C h^{\delta+s} \|\mathbf{p}\|_{1+\delta}. \tag{3.3.31}$$

3.4 Numerical Experiments

In this section, we have demonstrated the accuracy of the WG method by solving several **H**(curl)-elliptic problems for which the analytical solutions are available. We have used various kinds of configurations like triangular meshes, rectangular meshes with hanging nodes in 2D, and cubical meshes in 3D. Moreover, we have also validated the numerical scheme for **H**(curl)-elliptic convection-diffusion problem.

Example 3.4.1. H(curl)-elliptic problem on non-uniform rectangular mesh with hanging nodes: The purpose of this example is to exhibit high order convergence of the proposed WG approximation for sufficiently smooth solutions and coefficients. Consider the the $\mathbf{H}(\text{curl}; \Omega)$-elliptic problem $\beta \nabla \times (\nabla \times (\beta \mathbf{p})) + \gamma \mathbf{p} = \mathbf{f}$ with boundary condition (3.1.2) in $\Omega = (0,1)^2$. The exact solution to the given problem is defined as

$$\mathbf{p} = (p_1, p_2)^t = (\exp(x+y)\sin(\pi(x+y)), \exp(x+y)\cos(\pi(x+y)))^t,$$

with coefficients $\beta = \begin{pmatrix} 2x+3 & y+1 \\ y+1 & xy+1 \end{pmatrix}$ and $\gamma = \begin{pmatrix} x+y+4 & 3x+4 \\ 3x+4 & xy+5 \end{pmatrix}$.

In this example, we will deal with the non-uniform rectangular mesh with hanging nodes. The initial mesh, as shown in Figure 3.4.1 (left), has hanging nodes denoted by A, B, C and D. Convergence results for the weak Galerkin algorithm 1 with respect to triple-bar norm $|||\cdot|||_1$ and L^2 norm are presented in Tables 3.4.1-3.4.2, which clearly validates our theoretical convergence results for weak Galerkin algorithm 1. Component-wise surface plots for the exact solution and WG solution are shown in Figures 3.4.2-3.4.3.

Example 3.4.2. Convection-diffusion problem on mixed mesh: We consider the following convection-diffusion equation

$$\beta \nabla \times (\nabla \times (\beta \mathbf{p})) + \nabla \times (c \times \mathbf{p}) + \gamma \mathbf{p} = \mathbf{f} \ \text{ in } \Omega = (0,1)^2,$$

with Dirichlet boundary condition. The coefficients are chosen as $\beta = \begin{pmatrix} x^3+1 & y^2+1 \\ y^2+1 & xy+4 \end{pmatrix}$, $c = (x, y)^t$ and $\gamma = \begin{pmatrix} x+y+4 & x+3 \\ x+3 & 2y+3 \end{pmatrix}$. The analytical solution of the given problem

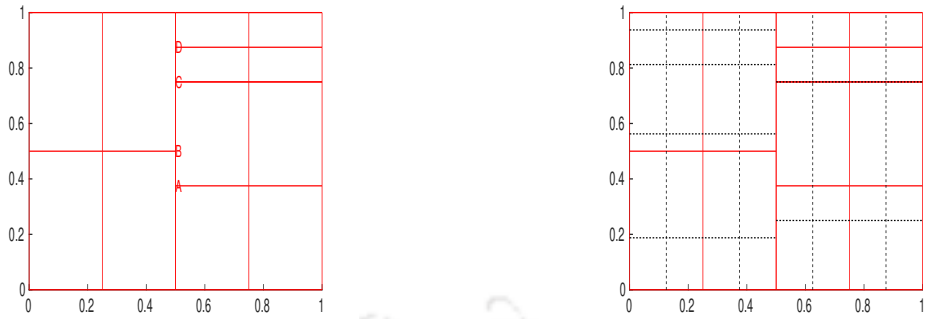

Figure 3.4.1: An initial non-uniform rectangular mesh with hanging nodes (left) and its next refinement (right).

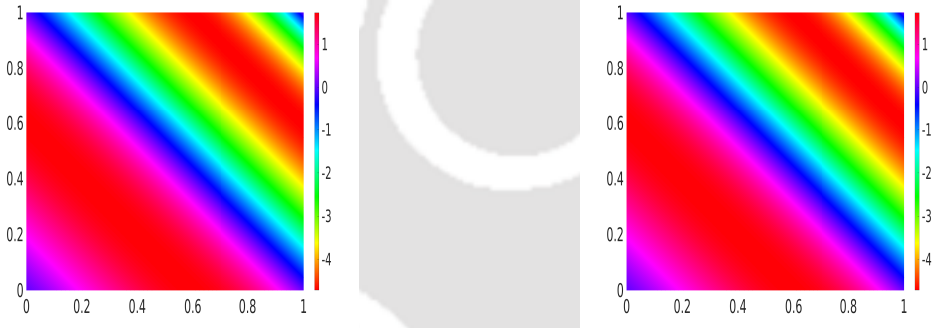

Figure 3.4.2: (Example 3.4.1) Surface plots for first component of exact solution (left) and WG solution (right).

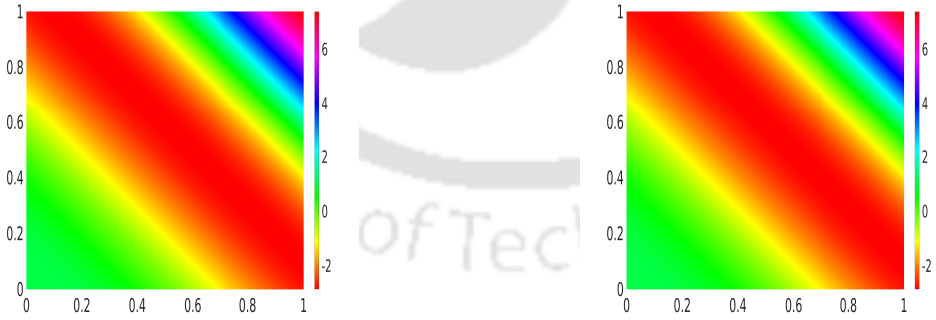

Figure 3.4.3: (Example 3.4.1) Surface plots for second component of exact solution (left) and WG solution (right).

defined as

$$\mathbf{p} = (p_1, p_2)^t = \left(x^3 \cos(\pi y) + y^4 \sin(\pi x), -\frac{\pi}{5} y^5 \cos(\pi x) - \frac{3}{\pi} x^2 \sin(\pi y) \right)^t .$$

Table 3.4.1: Convergence and error results for the Example 3.4.1.

k	Level	$\|\|\|\mathbf{e}_h\|\|\|_1$	Order	$\|\mathbf{e}_0\|$	Order
1	1	1.30e+01	—	3.03e+00	—
	2	6.80e+00	0.93	8.34e-01	1.86
	3	3.40e+00	0.99	2.11e-01	1.98
	4	1.70e+00	1.00	5.29e-02	1.99
	5	8.50e-01	1.00	1.32e-02	1.99
	6	4.25e-01	1.00	3.31e-03	1.99
2	1	6.25e+00	—	1.07e+00	—
	2	1.70e+00	1.87	1.46e-01	2.87
	3	4.36e-01	1.97	1.84e-02	2.98
	4	1.09e-01	1.99	2.31e-03	2.99
	5	2.74e-02	1.99	2.89e-04	3.00
	6	6.86e-03	1.99	3.61e-05	3.00

A sequence of mixed meshes (an initial mesh is presented in Figure 3.4.4) is generated for domain Ω. On the basis these meshes, the discrete H^1 errors and L^2 errors for WG solution are reported in Tables 3.4.3-3.4.4. Both components of the analytical solution and WG solution are shown in Figures 3.4.5-3.4.6 for $k = 2$ and mesh level 5.

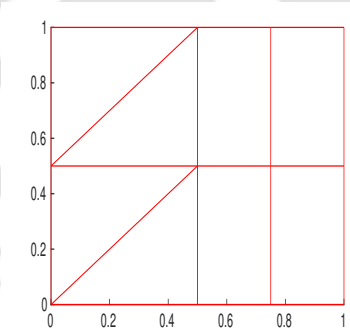

Figure 3.4.4: Initial mixed mesh in Example 3.4.2.

Example 3.4.3. H(curl)-elliptic problem with low regular solution: In this example, we investigate the performance of the WG method for low regular solution in a three-dimensional domain $\Omega = (0, 1)^3$. We have extracted the following exact solution

Table 3.4.2: Convergence and error results for the Example 3.4.1.

k	Level	$\|\|\|\mathbf{e}_h\|\|\|_1$	Order	$\|\mathbf{e}_0\|$	Order
3	1	1.86e+00	—	2.70e-01	—
	2	2.55e-01	2.86	1.86e-02	3.86
	3	3.26e-02	2.96	1.19e-03	3.96
	4	4.11e-03	2.99	7.47e-05	3.99
	5	5.14e-04	2.99	4.67e-06	3.99
	6	6.43e-05	2.99	2.92e-07	3.99
4	1	4.01e-01	—	5.15e-02	—
	2	2.73e-02	3.87	1.76e-03	4.86
	3	1.74e-03	3.96	5.65e-05	4.96
	4	1.09e-04	3.99	1.77e-06	4.99
	5	6.88e-06	3.99	5.56e-08	4.99
	6	4.30e-07	3.99	1.73e-09	4.99

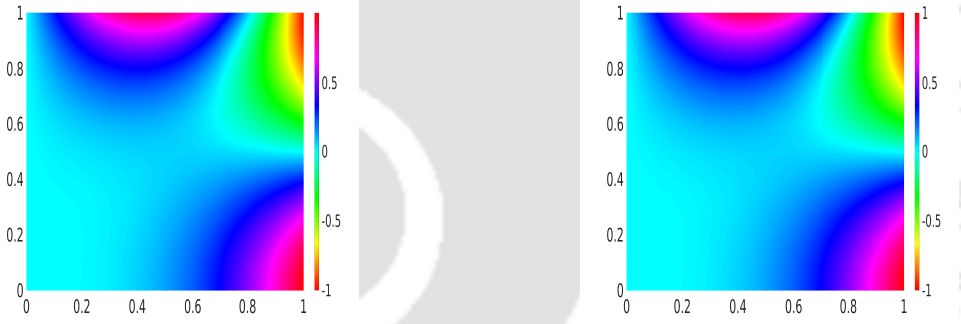

Figure 3.4.5: (Example 3.4.2) Surface plots for first component of analytical solution (left) and WG solution (right).

from Example 2 in [90]

$$\mathbf{p}(x,y,z) = \begin{pmatrix} y(1-y)z(1-z) \\ x(1-x)z(1-z) \\ r^{2/3}\sin(2\theta)(1-x)(1-y) \end{pmatrix},$$

where $r = \sqrt{x^2+y^2}$ and $\theta = \arctan(y/x)$. The coefficients are chosen to be $\beta = \gamma = 1$ in Ω. Note that $\mathbf{p} \in [H^{1+2/3}(\Omega)]^3$ and the suitable WG space is $\Big([\mathcal{P}_1(T)]^3,\ [\mathcal{P}_1(\partial T)]^3,\ \mathcal{P}_0(T)\Big)$. The initial mesh and its next refinement are shown in Figure 3.4.7. As expected, for the lowest order WG finite element space, we have achieved $\mathrm{O}(h^{0.65})$ in the energy norm

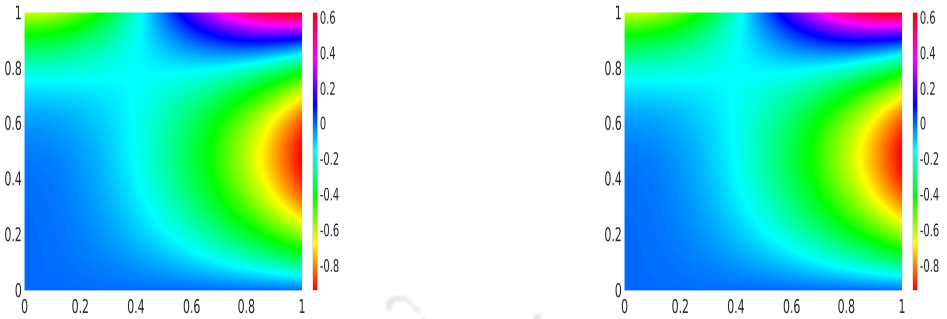

Figure 3.4.6: (Example 3.4.2) Surface plots for second component of analytical solution (left) and WG solution (right).

Table 3.4.3: Convergence and error results for the Example 3.4.2.

k	Level	$\|\|\|\mathbf{e}_h\|\|\|_1$	Order	$\|\mathbf{e}_0\|$	Order
1	1	1.16e+00	—	1.82e-01	—
	2	7.00e-01	0.73	5.17e-02	1.81
	3	3.74e-01	0.90	1.35e-02	1.92
	4	1.91e-01	0.96	3.45e-03	1.97
	5	9.62e-02	0.99	8.68e-04	1.99
	6	4.82e-02	0.99	2.17e-04	1.99
2	1	3.56e-01	—	4.44e-02	—
	2	9.84e-02	1.85	5.93e-03	2.90
	3	2.55e-02	1.94	7.516e-04	2.98
	4	6.50e-03	1.97	9.43e-05	2.99
	5	1.64e-03	1.98	1.18e-05	2.99
	6	4.11e-04	1.99	1.47e-06	2.99

Table 3.4.4: Convergence and error results for the Example 3.4.2.

k	Level	$\|\|\|\mathbf{e}_h\|\|\|_1$	Order	$\|\mathbf{e}_0\|$	Order
3	1	6.22e-02	—	7.73e-03	—
	2	8.90e-03	2.80	5.46e-04	3.82
	3	1.15e-03	2.94	3.49e-05	3.96
	4	1.46e-04	2.97	2.19e-06	3.99
	5	1.84e-05	2.99	1.37e-07	3.99
	6	2.31e-06	2.99	8.57e-09	4.00
4	1	1.19e-02	—	1.38e-03	—
	2	8.08e-04	3.88	4.65e-05	4.89
	3	5.17e-05	3.96	1.48e-06	4.97
	4	3.25e-06	3.98	4.66e-08	4.99
	5	2.04e-07	3.99	1.46e-09	4.99
	6	1.27e-08	3.99	4.57e-11	4.99

and $O(h^{1.62})$ for the L^2 norm, which are presented in Table 3.4.5.

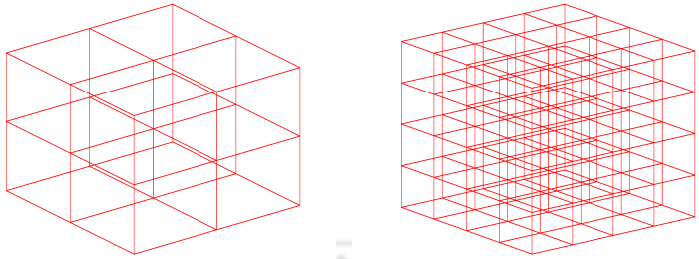

Figure 3.4.7: Cubical initial mesh (left) and its refinement (right) in Example 3.4.3.

Table 3.4.5: Errors and convergence profile for WG solution in Example 3.4.5.

Level	$\|\|\|\mathbf{e}_h\|\|\|_1$	Order	$\|\|\mathbf{e}_0\|\|$	Order
1	1.00e+00	—	1.02e+00	—
2	6.87e-01	0.55	3.91e-01	1.38
3	4.50e-01	0.60	1.36e-01	1.52
4	2.90e-01	0.63	4.54e-02	1.58
5	1.85e-01	0.64	1.48e-02	1.61
6	1.18e-01	0.65	4.85e-03	1.62

4

WG-FEMs for H(curl,div)-Elliptic Problems

In this chapter, the weak Galerkin finite element methods for the $\mathbf{H}(\text{div}, \text{curl})$-elliptic equations in general polygonal/polyhedral domains have been discussed. The optimal order error bounds in appropriate norms are derived for the proposed algorithms. Moreover, several numerical experiments are performed to justify the theoretical results.

4.1 Introduction

Let $\Omega \subset \mathbb{R}^d$ $(d = 2, 3)$ be a bounded polygonal/polyhedral domain with Lipschitz continuous boundary $\partial\Omega$. The $\mathbf{H}(\text{curl, div}; \Omega)$-elliptic problem is given by

$$\nabla \times (\beta \nabla \times \mathbf{p}) - \alpha \nabla(\nabla \cdot \alpha \mathbf{p}) + \gamma \mathbf{p} = \mathbf{f} \ \text{ in } \Omega, \tag{4.1.1}$$

$$\mathbf{p} \times \boldsymbol{\eta} = 0, \qquad \nabla \cdot \alpha \mathbf{p} = 0 \ \text{ on } \partial\Omega. \tag{4.1.2}$$

Other symbols are as defined in Chapter 1. The equation (4.1.1) is highly generic, as it applies to a vast array of models in numerous physical phenomena involving div and curl operators. The physical problem referenced by (4.1.1) encompasses several model problems in the fields of electromagnetism and fluid-structure mechanics in heterogeneous/homogeneous media (cf. [15, 31, 43, 100, 102, 109, 110, 112]).

The objective of this chapter is to extend the work of Brener *et al.* [18] and Duan *et al.* [50] for WF-FEMs in two and three-dimensional settings. In [18], the authors have discussed a linear nonconforming FEM for a two-dimensional curl-curl and grad-div problem. Optimal convergence rates (up to an arbitrary positive ϵ) in both the energy norm and the L^2 norm have been established on graded meshes under the regularity assumption that solution $\mathbf{p} \in \mathbf{H}^{2-\epsilon}(\Omega)$ to (4.1.1)-(4.1.2) satisfies following a priori estimate

$$|\nabla \times \mathbf{p}|_{H^1(\Omega)} + |\nabla \cdot \mathbf{p}|_{H^1(\Omega)} \leq C\|\mathbf{f}\|. \tag{4.1.3}$$

Results of this Chapter are submitted (revised) to Computers and Mathematics with Applications.

Later, Duan *et al.* [50] developed a linear continuous finite element for curl-curl and grad-div vector second-order elliptic problem in a three-dimensional polyhedral domain with discontinuous coefficients. An error estimate $\mathcal{O}(h^r)$ in energy norm has been established assuming analytical solution $\mathbf{u} \in \mathbf{H}^r(\Omega)$ for some $r \in (\frac{1}{2}, 1]$.

In this chapter, we have developed the WG-FEMs for the model problems (4.1.1)-(4.1.2). The optimal error estimates of $\mathrm{O}(h^k)$ in the energy norm and $\mathrm{O}(h^{k+1})$ in the L^2 norm are obtained for the WG-FEMs with local weak Galerkin space $\Big(\big[\mathcal{P}_k(T^0)\big]^d, \big[\mathcal{P}_k(\partial T)\big]^d, [\mathcal{P}_{k-1}(T)]^{2d-3}, \mathcal{P}_{k-1}(T)\Big)$. Moreover, numerical experiments have been performed to validate the theoretical error estimates.

The rest of the chapter is presented as follows. In Sec.4.1, we shall discuss the weak Galerkin discretization, discrete weak operators, and L^2 projection operators. The WG algorithm and error estimates have been discussed for the **H**(curl,div)-elliptic problem in the Sec.4.2. Several numerical experiments have been discussed for the proposed model problems in Sec.4.3.

4.2 Error Analysis

We have proposed a WG-FEM for the $\mathbf{H}(\mathrm{curl}, \mathrm{div})$-elliptic model problem (4.1.1)-(4.1.2) with local WG space $\Big(\mathcal{P}_k^d,\ \mathcal{P}_k^d,\ \mathcal{P}_{k-1}^{2d-3},\ \mathcal{P}_{k-1}\Big)$. Further, optimal error estimates in the L^2 norm and discrete energy norm are established. WG spaces and other notations are as defined in Chap. 3.

For the WG approximation, we define a bilinear map $\mathcal{A}_2 : \mathbf{V}_h \times \mathbf{V}_h \to \mathbb{R}$ to be used in this section as follows

$$\begin{aligned} \mathcal{A}_2(\mathbf{v}_h, \mathbf{w}_h) &= (\nabla_w \cdot \alpha \mathbf{v}_h, \nabla_w \cdot \alpha \mathbf{w}_h) + (\beta \nabla_w \times \mathbf{v}_h, \nabla_w \times \mathbf{w}_h) \\ &\quad + (\gamma \mathbf{v}_0, \mathbf{w}_0) + \mathcal{S}(\mathbf{v}_h, \mathbf{w}_h) \ \ \forall \mathbf{v}_h, \mathbf{w}_h \in \mathbf{V}_h. \end{aligned} \tag{4.2.1}$$

Note that $\mathcal{A}_2(\cdot, \cdot)$ induces the following triple-bar norm in WG space $\mathbf{V}_h^0$

$$\begin{aligned} |||\mathbf{v}_h|||_2^2 &:= \sum_{T \in \mathcal{T}_h} \|\nabla_w \cdot \alpha \mathbf{v}_h\|_T^2 + \sum_{T \in \mathcal{T}_h} \|\beta^{\frac{1}{2}} \nabla_w \times \mathbf{v}_h\|_T^2 \\ &\quad + \|\gamma^{\frac{1}{2}} \mathbf{v}_0\|_T^2 + \sum_{T \in \mathcal{T}_h} h_T^{-1} \|(\mathbf{v}_0 - \mathbf{v}_b) \times \boldsymbol{\eta}\|_{\partial T}^2 \\ &= \mathcal{A}_2(\mathbf{v}_h, \mathbf{v}_h), \quad \mathbf{v}_h = \{\mathbf{v}_0, \mathbf{v}_b\} \in \mathbf{V}_h^0. \end{aligned} \tag{4.2.2}$$

It is easy to observe that

$$|||\mathbf{v}_h|||_1 \leq C |||\mathbf{v}_h|||_2, \quad \forall \mathbf{v}_h \in \mathbf{V}_h. \tag{4.2.3}$$

Weak Galerkin Algorithm 2. A WG approximation for (4.1.1)-(4.1.2) can be developed by seeking $\mathbf{p}_h = \{\mathbf{p}_0, \mathbf{p}_b\} \in \mathbf{V}_h^0$ such that

$$\mathcal{A}_2(\mathbf{p}_h, \mathbf{v}_h) = (\mathbf{f}, \mathbf{v}_0) \ \ \forall \mathbf{v}_h = \{\mathbf{v}_0, \mathbf{v}_b\} \in \mathbf{V}_h^0. \tag{4.2.4}$$

Now, we are in the position to discuss the error equation for

$$\mathbf{e}_h = \mathbf{Q}_h\mathbf{p} - \mathbf{p}_h,$$

where $\mathbf{p}$ is the exact solution for (4.1.1)-(4.1.2) and $\mathbf{p}_h$ is the WG approximation given by (4.2.4). Due to the presence of a divergence operator in the curl-curl and gard-div system, we require an additional bilinear map defined as

$$R_4(\mathbf{p}, \mathbf{v}_h) = \sum_{T\in\mathcal{T}_h} \langle (\nabla\cdot\alpha\mathbf{p} - \mathbb{Q}_h^{k-1}(\nabla\cdot\alpha\mathbf{p}))\boldsymbol{\eta}, \alpha(\mathbf{v}_0 - \mathbf{v}_b)\rangle_{\partial T}. \tag{4.2.5}$$

Lemma 4.2.1. *For each $\mathbf{v}_h = \{\mathbf{v}_0, \mathbf{v}_b\} \in \mathbf{V}_h^0$, we have*

$$\begin{aligned} \mathcal{A}_2(\mathbf{e}_h, \mathbf{v}_h) &= R_1(\mathbf{p}, \mathbf{v}_h) + R_2(\mathbf{p}, \mathbf{v}_h) + R_4(\mathbf{p}, \mathbf{v}_h) + \mathcal{S}(\mathbf{Q}_h\mathbf{p}, \mathbf{v}_h) \\ &:= R_5(\mathbf{p}, \mathbf{v}_h), \end{aligned} \tag{4.2.6}$$

where the bilinear maps R_i $(i = 1, 2)$ and $\mathcal{S}$ are as defined in chapter 3.

Proof. For $\mathbf{v}_h = \{\mathbf{v}_0, \mathbf{v}_b\} \in \mathbf{V}_h^0$, testing (4.1.1) by $\mathbf{v}_0$ gives

$$(\mathbf{f}, \mathbf{v}_0) = -\sum_{T\in\mathcal{T}_h} (\alpha\nabla\cdot\alpha\mathbf{p}, \mathbf{v}_0)_T + \sum_{T\in\mathcal{T}_h} (\nabla\times(\beta\nabla\times\mathbf{p}), \mathbf{v}_0)_T + (\gamma\mathbf{p}, \mathbf{v}_0). \tag{4.2.7}$$

Then, integration by parts yields

$$\begin{aligned} (\mathbf{f}, \mathbf{v}_0) &= (\gamma\mathbf{Q}_0^k\mathbf{p}, \mathbf{v}_0) + \sum_{T\in\mathcal{T}_h} (\nabla\cdot\alpha\mathbf{p}, \nabla\cdot\alpha\mathbf{v}_0)_T \\ &\quad + \sum_{T\in\mathcal{T}_h} (\beta\nabla\times\mathbf{p}, \nabla\times\mathbf{v}_0)_T - \sum_{T\in\mathcal{T}_h} \langle (\nabla\cdot\alpha\mathbf{p})\boldsymbol{\eta}, \alpha(\mathbf{v}_0 - \mathbf{v}_b)\rangle_{\partial T} \\ &\quad - \sum_{T\in\mathcal{T}_h} \langle (\beta\nabla\times\mathbf{p})\times\boldsymbol{\eta}, \mathbf{v}_0 - \mathbf{v}_b\rangle_{\partial T}. \end{aligned} \tag{4.2.8}$$

Here, we assume γ and α to be piecewise constants and the fact that

$$\sum_{T\in\mathcal{T}_h} \langle (\nabla\cdot\alpha\mathbf{p})\boldsymbol{\eta}, \alpha\mathbf{v}_b\rangle_{\partial T} = 0.$$

Now, by using the definition (2.2.1) for $\alpha\mathbf{v}_h$, we obtain

$$\begin{aligned}
&(\mathbb{Q}_h^{k-1}(\nabla\cdot\alpha\mathbf{p}),\nabla_w\cdot\alpha\mathbf{v}_h)_T\\
&=-(\alpha\mathbf{v}_0,\nabla(\mathbb{Q}_h^{k-1}(\nabla\cdot\alpha\mathbf{p})))_T+\langle\alpha\mathbf{v}_b,\mathbb{Q}_h^{k-1}(\nabla\cdot\alpha\mathbf{p})\boldsymbol{\eta}\rangle_{\partial T}\\
&=(\nabla\cdot\alpha\mathbf{v}_0,\mathbb{Q}_h^{k-1}(\nabla\cdot\alpha\mathbf{p}))_T-\langle(\mathbb{Q}_h^{k-1}(\nabla\cdot\alpha\mathbf{p}))\boldsymbol{\eta},\alpha\mathbf{v}_0\rangle_{\partial T}\\
&\quad+\langle\mathbb{Q}_h^{k-1}(\nabla\cdot\alpha\mathbf{p})\boldsymbol{\eta},\alpha\mathbf{v}_b\rangle_{\partial T}\\
&=(\nabla\cdot\alpha\mathbf{v}_0,\mathbb{Q}_h^{k-1}(\nabla\cdot\alpha\mathbf{p}))_T-\langle(\mathbb{Q}_h^{k-1}(\nabla\cdot\alpha\mathbf{p}))\boldsymbol{\eta},\alpha\mathbf{v}_0-\alpha\mathbf{v}_b\rangle_{\partial T}\\
&=(\nabla\cdot\alpha\mathbf{v}_0,\nabla\cdot\alpha\mathbf{p})_T-\langle(\mathbb{Q}_h^{k-1}(\nabla\cdot\alpha\mathbf{p}))\boldsymbol{\eta},\alpha(\mathbf{v}_0-\mathbf{v}_b)\rangle_{\partial T}. \qquad (4.2.9)
\end{aligned}$$

Then, equations (3.3.10) and (4.2.8)-(4.2.9) leads to

$$\begin{aligned}
(\mathbf{f},\mathbf{v}_0) &= (\gamma\mathbf{Q}_0^k\mathbf{p},\mathbf{v}_0)+\sum_{T\in\mathcal{T}_h}(\beta\boldsymbol{\mathcal{Q}}_h^{k-1}(\nabla\times\mathbf{p}),\nabla_w\times\mathbf{v}_h)_T\\
&\quad+\sum_{T\in\mathcal{T}_h}(\nabla_w\cdot(\alpha\mathbf{Q}_h\mathbf{p}),\nabla_w\cdot(\alpha\mathbf{v}_h))_T\\
&\quad-\sum_{T\in\mathcal{T}_h}(\beta\boldsymbol{\mathcal{Q}}_h^{k-1}(\nabla\times\mathbf{p})-\boldsymbol{\mathcal{Q}}_h^{k-1}(\beta\nabla\times\mathbf{p}),\nabla_w\times\mathbf{v}_h)_T\\
&\quad-\sum_{T\in\mathcal{T}_h}\langle(\nabla\cdot\alpha\mathbf{p}-\mathbb{Q}_h^{k-1}(\nabla\cdot\alpha\mathbf{p}))\boldsymbol{\eta},\alpha(\mathbf{v}_0-\mathbf{v}_b)\rangle_{\partial T}\\
&\quad-\sum_{T\in\mathcal{T}_h}\langle(\beta\nabla\times\mathbf{p}-\boldsymbol{\mathcal{Q}}_h^{k-1}(\beta\nabla\times\mathbf{p}))\times\boldsymbol{\eta},\mathbf{v}_0-\mathbf{v}_b\rangle_{\partial T}\\
&= (\gamma\mathbf{Q}_0^k\mathbf{p},\mathbf{v}_0)+\sum_{T\in\mathcal{T}_h}(\beta\nabla_w\times\mathbf{Q}_h\mathbf{p},\nabla_w\times\mathbf{v}_h)_T\\
&\quad+\sum_{T\in\mathcal{T}_h}(\nabla_w\cdot(\alpha\mathbf{Q}_h\mathbf{p}),\nabla_w\cdot(\alpha\mathbf{v}_h))_T-R_2(\mathbf{p},\mathbf{v}_h)\\
&\quad-R_4(\mathbf{p},\mathbf{v}_h)-R_1(\mathbf{p},\mathbf{v}_h). \qquad (4.2.10)
\end{aligned}$$

Adding and subtracting $\mathcal{S}(\mathbf{Q}_h\mathbf{p},\mathbf{v}_h)$ to the equation (4.2.10) yields

$$\begin{aligned}
\mathcal{A}_2(\mathbf{Q}_h\mathbf{p},\mathbf{v}_h) &= (\mathbf{f},\mathbf{v}_0)+R_1(\mathbf{p},\mathbf{v}_h)+R_2(\mathbf{p},\mathbf{v}_h)\\
&\quad+R_4(\mathbf{p},\mathbf{v}_h)+\mathcal{S}(\mathbf{Q}_h\mathbf{p},\mathbf{v}_h). \qquad (4.2.11)
\end{aligned}$$

Finally, subtracting (4.2.4) from (4.2.11) leads to desire error equation. □

Lemma 4.2.2. *Assume* $\mathbf{p}\in[H^{k+1}(\Omega)]^d$. *Then, for any* $\mathbf{v}_h=\{\mathbf{v}_0,\mathbf{v}_b\}\in\mathbf{V}_h^0$, *we obtain*

$$|R_4(\mathbf{p},\mathbf{v}_h)|\leq C(\|\alpha\|_{k,\infty})h^k\|\mathbf{p}\|_{k+1}|||\mathbf{v}_h|||_2. \qquad (4.2.12)$$

Proof. The proof follows from Lemma 3.2.1, Cauchy-Schwarz inequality and trace-inequality (2.2.7). We omit the details. □

Theorem 4.2.1. *Let* $\mathbf{p} \in [H^{k+1}(\Omega)]^d$ *be the exact solution of* (4.1.1)-(4.1.2) *and* $\mathbf{p}_h \in \mathbf{V}_h^0$ *be the WG solution of* (4.2.4)*. Then, we have*

$$|||\mathbf{Q}_h\mathbf{p} - \mathbf{p}_h|||_2 \leq Ch^k\|\mathbf{p}\|_{k+1}. \tag{4.2.13}$$

Proof. We inspect the error equation (4.2.6) with $\mathbf{v}_h = \mathbf{e}_h$ to obtain

$$|||\mathbf{e}_h|||_2 \;\leq\; |R_1(\mathbf{p}, \mathbf{e}_h)| + |R_2(\mathbf{p}, \mathbf{e}_h)| + |R_4(\mathbf{p}, \mathbf{e}_h)| + |\mathcal{S}(\mathbf{Q}_h\mathbf{p}, \mathbf{e}_h)|. \tag{4.2.14}$$

The estimate (4.2.13) directly follows from (4.2.14), Lemma 4.2.2 and Lemma 3.3.2 along with (4.2.3). This completes the Theorem 4.2.1. □

Next, we shall derive the L^2 error estimate for the weak Galerkin algorithm 2 with the help of the duality-argument. To do so, we consider an auxiliary problem with H^2 regular solution $\boldsymbol{\psi}$ satisfying

$$-\alpha\nabla(\nabla\cdot\alpha\boldsymbol{\psi}) + \nabla\times(\beta\nabla\times\boldsymbol{\psi}) + \gamma\boldsymbol{\psi} = \mathbf{e}_0 \;\text{ in }\; \Omega, \tag{4.2.15}$$

$$\boldsymbol{\psi}\times\boldsymbol{\eta} = 0, \;\; \nabla\cdot\alpha\boldsymbol{\psi} = 0 \;\text{ on }\; \partial\Omega. \tag{4.2.16}$$

Under the assumptions in the present geometric setting, we have (see, [18])

$$\|\boldsymbol{\psi}\|_2 \leq \|\mathbf{e}_0\|. \tag{4.2.17}$$

Theorem 4.2.2. *Let* $\mathbf{p} \in [H^{k+1}(\Omega)]^d$ *be the exact solution of* (4.1.1)-(4.1.2) *and* $\mathbf{p}_h \in \mathbf{V}_h^0$ *be the WG solution of* (4.2.4)*. Then, we have*

$$\|\mathbf{Q}_0^k\mathbf{p} - \mathbf{p}_0\| \leq Ch^{k+1}\|\mathbf{p}\|_{k+1}. \tag{4.2.18}$$

Proof. For the equation (4.2.15), analogue to (4.2.10), we have

$$\begin{aligned}(\mathbf{e}_0, \mathbf{v}_0) \;&=\; (\gamma\mathbf{Q}_0^k\boldsymbol{\psi}, \mathbf{v}_0) + \sum_{T\in\mathcal{T}_h}(\beta\nabla_w\times\mathbf{Q}_h\boldsymbol{\psi}, \nabla_w\times\mathbf{v}_h)_T \\ &\quad + \sum_{T\in\mathcal{T}_h}(\nabla_w\cdot(\alpha\mathbf{Q}_h\boldsymbol{\psi}), \nabla_w\cdot(\alpha\mathbf{v}_h))_T - R_1(\boldsymbol{\psi}, \mathbf{v}_h) \\ &\quad - R_2(\boldsymbol{\psi}, \mathbf{v}_h) - R_4(\boldsymbol{\psi}, \mathbf{v}_h) \;\; \forall\mathbf{v}_h \in \{\mathbf{v}_0, \mathbf{v}_b\} \in \mathbf{V}_h^0,\end{aligned} \tag{4.2.19}$$

where $\mathbf{Q}_h\boldsymbol{\psi} = \{\mathbf{Q}_0^k\boldsymbol{\psi}, \mathbf{Q}_b^k\boldsymbol{\psi}\}$. Then, add $\mathcal{S}(\mathbf{Q}_h\boldsymbol{\psi}, \mathbf{e}_h)$ to both sides of (4.2.19) to arrive at

$$\begin{aligned}\|\mathbf{e}_0\|^2 \;&=\; \mathcal{A}_2(\mathbf{e}_h, \mathbf{Q}_h\boldsymbol{\psi}) - R_5(\boldsymbol{\psi}, \mathbf{e}_h) \\ &=\; R_5(\mathbf{p}, \mathbf{Q}_h\boldsymbol{\psi}) - R_5(\boldsymbol{\psi}, \mathbf{e}_h) \\ &:=\; J_1 + J_2.\end{aligned} \tag{4.2.20}$$

It follows from a priori bound (4.2.17), Lemma 4.2.2, Theorem 4.2.1, Lemma 3.3.2 and inequality (4.2.3) that

$$|J_2| \leq Ch\|\boldsymbol{\psi}\|_2 |||\mathbf{e}_h|||_2 \leq Ch\|\mathbf{e}_0\| |||\mathbf{e}_h|||_2 \leq Ch^{k+1}\|\mathbf{p}\|_{k+1}\|\mathbf{e}_0\|.$$

For the term J_1, we need some preparations. Definition of the $\mathbf{Q}_b^k$, estimate (2.3.16), trace inequality (2.2.7) and a priori bound (4.2.17) leads to

$$\begin{aligned}
|R_1(\mathbf{p}, \mathbf{Q}_h\boldsymbol{\psi})| &= \left| \sum_{T\in\mathcal{T}_h} \langle (\beta\nabla\times\mathbf{p} - \boldsymbol{\mathcal{Q}}_h^{k-1}(\beta\nabla\times\mathbf{p}))\times\boldsymbol{\eta}, \mathbf{Q}_0^k\boldsymbol{\psi} - \mathbf{Q}_b^k\boldsymbol{\psi}\rangle_{\partial T} \right| \\
&\leq \sum_{T\in\mathcal{T}_h} \|(\beta\nabla\times\mathbf{p} - \boldsymbol{\mathcal{Q}}_h^{k-1}(\beta\nabla\times\mathbf{p}))\times\boldsymbol{\eta}\|_{\partial T} \|\mathbf{Q}_0^k\boldsymbol{\psi} - \boldsymbol{\psi}\|_{\partial T} \\
&\leq C\left(\sum_{T\in\mathcal{T}_h} h_T \|\beta\nabla\times\mathbf{p} - \boldsymbol{\mathcal{Q}}_h^{k-1}(\beta\nabla\times\mathbf{p})\|_{\partial T}^2 \right)^{\frac{1}{2}} \\
&\quad \times \left(\sum_{T\in\mathcal{T}_h} h_T^{-1} \|\mathbf{Q}_0^k\boldsymbol{\psi} - \boldsymbol{\psi}\|_{\partial T}^2 \right)^{\frac{1}{2}} \\
&\leq C(\|\beta\|_{k,\infty}) h^{k+1}\|\mathbf{p}\|_{k+1}\|\boldsymbol{\psi}\|_2 \\
&\leq C(\|\beta\|_{k,\infty}) h^{k+1}\|\mathbf{p}\|_{k+1}\|\mathbf{e}_0\|. \qquad (4.2.21)
\end{aligned}$$

Next, using commutative property (3.2.6), we have

$$\begin{aligned}
&|R_2(\mathbf{p}, \mathbf{Q}_h\boldsymbol{\psi})| \\
&= \left| \sum_{T\in\mathcal{T}_h} (\beta\boldsymbol{\mathcal{Q}}_h^{k-1}(\nabla\times\mathbf{p}) - \beta\nabla\times\mathbf{p}, \nabla_w\times\mathbf{Q}_h\boldsymbol{\psi})_T \right| \\
&= \left| \sum_{T\in\mathcal{T}_h} (\boldsymbol{\mathcal{Q}}_h^{k-1}(\nabla\times\mathbf{p}) - \nabla\times\mathbf{p}, (\beta-\bar{\beta})\boldsymbol{\mathcal{Q}}_h^{k-1}(\nabla\times\boldsymbol{\psi}))_T \right| \\
&= \left| \sum_{T\in\mathcal{T}_h} (\boldsymbol{\mathcal{Q}}_h^{k-1}(\nabla\times\mathbf{p}) - \nabla\times\mathbf{p}, (\beta-\bar{\beta})(\boldsymbol{\mathcal{Q}}_h^{k-1}(\nabla\times\boldsymbol{\psi}) - \nabla\times\boldsymbol{\psi} + \nabla\times\boldsymbol{\psi}))_T \right| \\
&\leq \left| \sum_{T\in\mathcal{T}_h} (\boldsymbol{\mathcal{Q}}_h^{k-1}(\nabla\times\mathbf{p}) - \nabla\times\mathbf{p}, (\beta-\bar{\beta})(\boldsymbol{\mathcal{Q}}_h^{k-1}(\nabla\times\boldsymbol{\psi}) - \nabla\times\boldsymbol{\psi}))_T \right| \\
&\quad + \left| \sum_{T\in\mathcal{T}_h} (\boldsymbol{\mathcal{Q}}_h^{k-1}(\nabla\times\mathbf{p}) - \nabla\times\mathbf{p}, (\beta-\bar{\beta})(\nabla\times\boldsymbol{\psi}))_T \right| \\
&:= L_1 + L_2. \qquad (4.2.22)
\end{aligned}$$

For L_1, we use Lemma 3.2.1, Cauchy-Schwarz inequality, a priori bound (4.2.17) and

estimate (2.3.16) to get

$$\begin{aligned} L_1 &\leq \sum_{T\in\mathcal{T}_h} \|\boldsymbol{\mathcal{Q}}_h^{k-1}(\nabla\times\mathbf{p})-\nabla\times\mathbf{p}\|_T\|(\beta-\bar{\beta})(\boldsymbol{\mathcal{Q}}_h^{k-1}(\nabla\times\boldsymbol{\psi})-\nabla\times\boldsymbol{\psi})\|_T \\ &\leq Ch\left(\|\beta\|_{1,\infty}\right)\left(\sum_{T\in\mathcal{T}_h}\|\boldsymbol{\mathcal{Q}}_h^{k-1}(\nabla\times\mathbf{p})-\nabla\times\mathbf{p}\|_T^2\right)^{\frac{1}{2}} \\ &\quad\times\left(\sum_{T\in\mathcal{T}_h}\|\boldsymbol{\mathcal{Q}}_h^{k-1}(\nabla\times\boldsymbol{\psi})-\nabla\times\boldsymbol{\psi}\|_T^2\right)^{\frac{1}{2}} \\ &\leq Ch^{k+2}(\|\beta\|_{1,\infty})\|\mathbf{p}\|_{k+1}\|\boldsymbol{\psi}\|_2 \\ &\leq Ch^{k+2}(\|\beta\|_{1,\infty})\|\mathbf{p}\|_{k+1}\|\mathbf{e}_0\|. \end{aligned} \tag{4.2.23}$$

Similar arguments yields

$$|L_2| \leq Ch^{k+1}(\|\beta\|_{1,\infty})\|\mathbf{p}\|_{k+1}\|\mathbf{e}_0\|. \tag{4.2.24}$$

Combining the estimates (4.2.22)-(4.2.24), we arrive at

$$|R_2(\mathbf{p},\mathbf{Q}_h\boldsymbol{\psi})| \leq Ch^{k+1}(\|\beta\|_{1,\infty})\|\mathbf{p}\|_{k+1}\|\mathbf{e}_0\|. \tag{4.2.25}$$

Next, for the stabilizer $\mathcal{S}(\cdot,\cdot)$, we obtain

$$\begin{aligned} &|\mathcal{S}(\mathbf{Q}_h\mathbf{p},\mathbf{Q}_h\boldsymbol{\psi})| \\ &= \left|\sum_{T\in\mathcal{T}_h} h_T^{-1}\langle(\mathbf{Q}_0^k\mathbf{p}-\mathbf{Q}_b^k\mathbf{p})\times\boldsymbol{\eta},(\mathbf{Q}_0^k\boldsymbol{\psi}-\mathbf{Q}_b^k\boldsymbol{\psi})\times\boldsymbol{\eta}\rangle_{\partial T}\right| \\ &\leq \sum_{T\in\mathcal{T}_h} h_T^{-1}\|\mathbf{Q}_0^k\mathbf{p}-\mathbf{p}\|_{\partial T}\|\mathbf{Q}_0^k\boldsymbol{\psi}-\boldsymbol{\psi}\|_{\partial T} \\ &\leq C\left(\sum_{T\in\mathcal{T}_h} h_T^{-1}(h_T^{-1}\|\mathbf{Q}_0^k\mathbf{p}-\mathbf{p}\|_T^2+h_T\|\nabla(\mathbf{Q}_0^k\mathbf{p}-\mathbf{p})\|_T^2)\right)^{\frac{1}{2}} \\ &\quad\times\left(\sum_{T\in\mathcal{T}_h} h_T^{-1}(h_T^{-1}\|\mathbf{Q}_0^k\boldsymbol{\psi}-\boldsymbol{\psi}\|_T^2+h_T\|\nabla(\mathbf{Q}_0^k\boldsymbol{\psi}-\boldsymbol{\psi})\|_T^2)\right)^{\frac{1}{2}} \\ &\leq Ch^{k+1}\|\mathbf{p}\|_{k+1}\|\boldsymbol{\psi}\|_2 \\ &\leq Ch^{k+1}\|\mathbf{p}\|_{k+1}\|\mathbf{e}_0\|. \end{aligned} \tag{4.2.26}$$

For R_4, we use Lemmas 3.2.1-2.2.1, Cauchy-Schwarz inequality, trace-inequality

(2.2.7) and a priori bound (4.2.17) to have

$$\begin{aligned}
&|R_4(\mathbf{p}, \mathbf{Q}_h\boldsymbol{\psi})| \\
&= \left| \sum_{T\in\mathcal{T}_h} \langle (\nabla\cdot\alpha\mathbf{p} - \mathbb{Q}_h^{k-1}(\nabla\cdot\alpha\mathbf{p}))\boldsymbol{\eta}, \alpha(\mathbf{Q}_0^k\boldsymbol{\psi} - \mathbf{Q}_b^k\boldsymbol{\psi})\rangle_{\partial T} \right| \\
&\leq \sum_{T\in\mathcal{T}_h} \|\nabla\cdot\alpha\mathbf{p} - \mathbb{Q}_h^{k-1}(\nabla\cdot\alpha\mathbf{p})\|_{\partial T}\|\alpha(\mathbf{Q}_0^k\boldsymbol{\psi} - \boldsymbol{\psi})\|_{\partial T} \\
&\leq \left(\sum_{T\in\mathcal{T}_h} h_T\|\nabla\cdot\alpha\mathbf{p} - \mathbb{Q}_h^{k-1}(\nabla\cdot\alpha\mathbf{p})\|_{\partial T}^2 \right)^{\frac{1}{2}} \left(\sum_{T\in\mathcal{T}_h} h_T^{-1}\|\alpha(\mathbf{Q}_0^k\boldsymbol{\psi} - \boldsymbol{\psi})\|_{\partial T}^2 \right)^{\frac{1}{2}} \\
&\leq C(\|\alpha\|_{k,\infty})h^{k+1}\|\mathbf{p}\|_{k+1}\|\boldsymbol{\psi}\|_2 \\
&\leq C(\|\alpha\|_{k,\infty})h^{k+1}\|\mathbf{p}\|_{k+1}\|\mathbf{e}_0\|.
\end{aligned}$$

Finally, we arrive at

$$|J_1| \leq Ch^{k+1}\|\mathbf{p}\|_{k+1}\|\mathbf{e}_0\|.$$

This completes the rest of the proof for Theorem 4.2.2. □

Remark 4.2.1. *Let* $\mathbf{p} \in [H^{1+\delta}(\Omega)]^d$ *for some* $\delta \in \left(\frac{1}{2}, 1\right]$*. Then, as in Remark 3.3.1 and Remark 3.3.3, we have following estimates*

$$\begin{aligned}
|||\mathbf{Q}_h\mathbf{p} - \mathbf{p}_h|||_2 &\leq Ch^{\delta}\|\mathbf{p}\|_{1+\delta}, \\
\|\mathbf{Q}_0^k\mathbf{p} - \mathbf{p}_0\| &\leq Ch^{\delta+s}\|\mathbf{p}\|_{1+\delta},
\end{aligned}$$

for some $s \in \left(\frac{1}{2}, 1\right]$.

4.3 Numerical Examples

In this section, we have conducted specific numerical experiments for the both 2D and 3D $\mathbf{H}(\text{curl}, \text{div}; \Omega)$-elliptic problem (4.1.1)-(4.1.2) using the weak Galerkin finite element method. In our numerical experiments, we shall perform the WG algorithm with a higher degree finite element space $\mathbf{V}_h$. For 2D experiments, a finite sequence of triangular meshes whereas for 3D tests, cubic meshes have been used. In addition, we have also validated the proposed algorithm for $\mathbf{H}(\text{div}, \text{curl})$-elliptic interface problem with homogenous jump conditions.

Example 4.3.1. $\mathbf{H}(\text{curl}, \text{div})$-elliptic problem on deformed triangular mesh: Consider the problem $-\alpha\nabla(\nabla\cdot\alpha\mathbf{p}) + \beta\nabla\times(\nabla\times(\beta\mathbf{p})) + \gamma\mathbf{p} = \mathbf{f}$ with boundary condition (4.1.2) in the domain $\Omega = (0,1)^2$. We set the analytical solution as

$$\mathbf{p} = (p_1, p_2)^t = \left((x^2+y^2)\sin(\pi(x+y)), (x^3+y+6)\cos(\pi x)\cos(\pi y)\right)^t,$$

with coefficients $\alpha = \begin{pmatrix} x^2+y^2+1 & 3y+2 \\ 3y+2 & 2y^2+1 \end{pmatrix}$, $\beta = \begin{pmatrix} xy+2 & 3 \\ 3 & x+y+1 \end{pmatrix}$ and $\gamma = \begin{pmatrix} x+1 & (x+1)(y+1) \\ (x+1)(y+1) & y^2+1 \end{pmatrix}$. We again examine the high-order convergence of the WG method by considering the deformed triangular meshes. An initial mesh is shown in Figure 4.3.1 (left). We report the numerical errors in Tables 4.3.1-4.3.2. For $k = 3$ and mesh level 6, component-wise surface plots of analytical solution and WG solution are shown in Figures 4.3.1 (middle-right)-4.3.2.

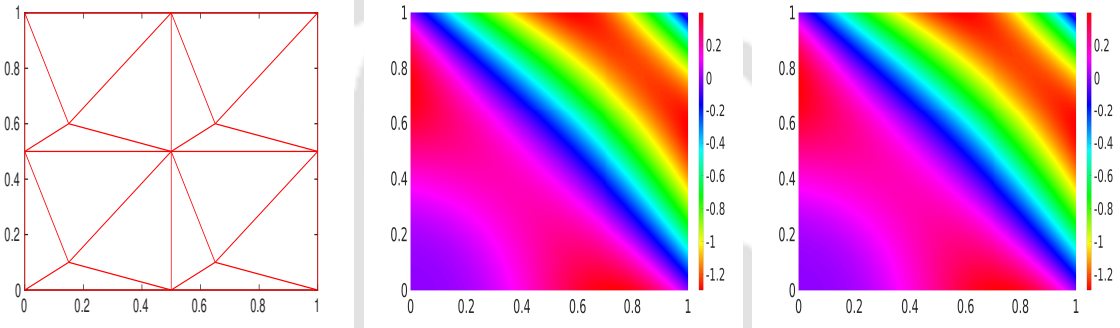

Figure 4.3.1: (Example 4.3.1) Initial deformed triangular mesh (left), surface plots for first component of analytical solution (middle) and WG solution (right)

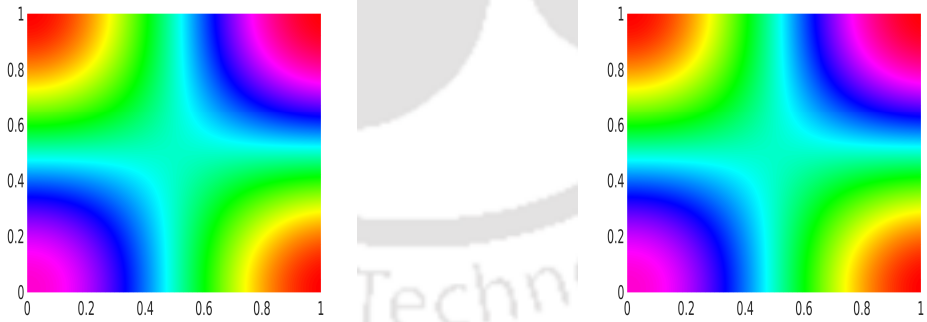

Figure 4.3.2: (Example 4.3.1) Surface plots for second component of analytical solution (left) and WG solution (right).

Example 4.3.2. $\mathbf{H}$(curl, div)-elliptic interface problem: We consider the following $\mathbf{H}$(curl, div; Ω)-elliptic interface problem (cf. [50])

$$\begin{aligned} -\alpha\nabla(\nabla\cdot\alpha\mathbf{p}) + \beta\nabla\times(\nabla\times(\beta\mathbf{p})) + \gamma\mathbf{p} &= \mathbf{f} \text{ in } \Omega, \\ \mathbf{p}\times\boldsymbol{\eta} = \mathbf{0},\ \nabla\cdot\alpha\mathbf{p} &= 0 \text{ on } \partial\Omega, \end{aligned}$$

Table 4.3.1: Convergence and error profiles for the Example 4.3.1.

k	Level	$\|\|\|\mathbf{e}_h\|\|\|_2$	Order	$\|\|\mathbf{e}_0\|\|$	Order
1	1	1.31e+00	—	1.59e-01	—
	2	6.62e-01	0.99	4.06e-02	1.97
	3	3.31e-01	1.00	1.01e-02	1.99
	4	1.65e-01	1.00	2.55e-03	1.99
	5	8.27e-02	0.99	6.37e-04	1.99
	6	4.13e-02	0.99	1.59e-04	1.99
2	1	3.67e-01	—	3.14e-02	—
	2	9.47e-02	1.95	4.00e-03	2.97
	3	2.38e-02	1.98	5.01e-04	2.99
	4	5.97e-03	1.99	6.26e-05	3.00
	5	1.49e-03	1.99	7.83e-06	3.00
	6	3.73e-04	1.99	9.79e-07	3.00

Table 4.3.2: Convergence and error profiles for the Example 4.3.1.

k	Level	$\|\|\|\mathbf{e}_h\|\|\|_2$	Order	$\|\|\mathbf{e}_0\|\|$	Order
3	1	6.67e-02	—	4.87e-03	—
	2	8.60e-03	2.95	3.13e-04	3.95
	3	1.08e-03	2.98	1.97e-05	3.99
	4	1.359e-04	2.99	1.23e-06	3.99
	5	1.70e-05	2.99	7.71e-08	3.99
	6	2.12e-06	2.99	4.81e-09	4.00
4	1	1.26e-01	—	1.62e-02	—
	2	8.71e-03	3.86	5.62e-04	4.85
	3	5.58e-04	3.96	1.80e-05	4.96
	4	3.51e-05	3.99	5.68e-07	4.99
	5	2.20e-06	3.99	1.77e-08	4.99
	6	1.37e-07	3.99	5.56e-10	4.99

with homogeneous jump conditions along the interface Γ. Here, a L-shaped domain is embedded in the domain $\Omega = (0,1)^2$. Interface Γ and two sub-domains Ω_1 and Ω_2 are shown in Figure 4.3.6 (left). In this example, we have used non-uniform fitted triangular meshes with high contrast coefficients. We set $\alpha|_{\Omega_1} = \alpha_1 = \begin{pmatrix} 1 & 0 \\ 0 & 1 \end{pmatrix}$ in Ω_1 and $\alpha|_{\Omega_2} = \alpha_2 = \begin{pmatrix} 10^7 & 0 \\ 0 & x+y+1 \end{pmatrix}$ in Ω_2, and $\beta = \gamma = I$ in Ω. Then the exact solution $\mathbf{p} = (p_1, p_2)$ is chosen as

$$p_1 = \begin{cases} 10^5(\exp(\pi(y-0.60)(x-0.50)) - 1)\sin(4\pi x)\sin(4\pi y) & \text{for } (x,y) \in \Omega_1, \\ (\exp(\pi(y-0.60)(x-0.50)) - 1)\sin(4\pi x)\sin(4\pi y) & \text{for } (x,y) \in \Omega_2, \end{cases}$$

and

$$p_2 = \begin{cases} 10^5(y-0.60)^2(x-0.50)^2\sin(4\pi x)\sin(4\pi y) & \text{for } (x,y)\in\Omega_1, \\ (y-0.60)^2(x-0.50)^2\sin(4\pi x)\sin(4\pi y) & \text{for } (x,y)\in\Omega_2. \end{cases}$$

The discrete H^1 errors and L^2 errors of weak Galerkin algorithm 2 are listed in Tables 4.3.3-4.3.4. In Figures 4.3.4 (middle-right)-4.3.5, component-wise surface plots (in 2D view) for exact solution and WG solution are depicted with $k = 1$ and mesh level 6.

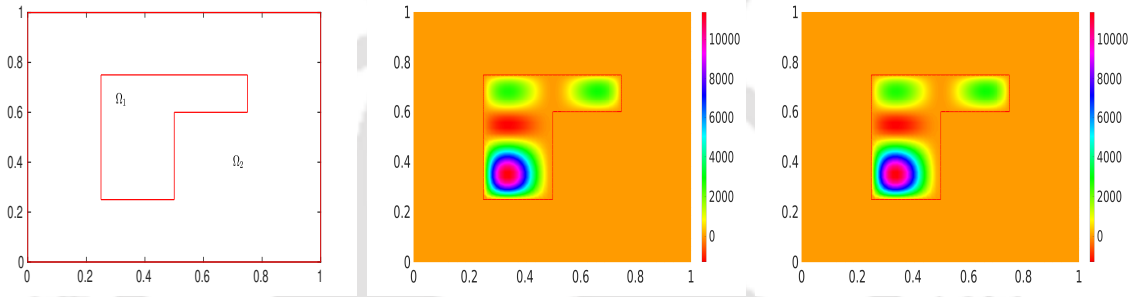

Figure 4.3.3: (Example 4.3.2) Domain with interface (left) and surface plots for first component of exact solution (middle) and WG solution (right).

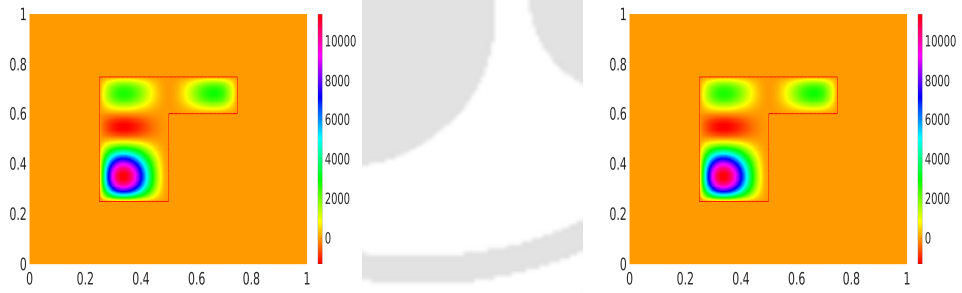

Figure 4.3.4: (Example 4.3.2) Surface plots for first component of exact solution (left) and WG solution (right).

Example 4.3.3. H(curl, div)-elliptic problem in three dimensional *L*-shaped domain: In Example 3.4.3, we have demonstrated the convergence of weak Galerkin approximation for a non-smooth solution in a convex polyhedral domain. This numerical example illustrates the convergence of the WG scheme in a non-convex polyhedral domain $\Omega = (0,1)^3 \setminus (1/2,1)\times(0,1/2)\times(0,1)$. The exact solution is set as (see, Example

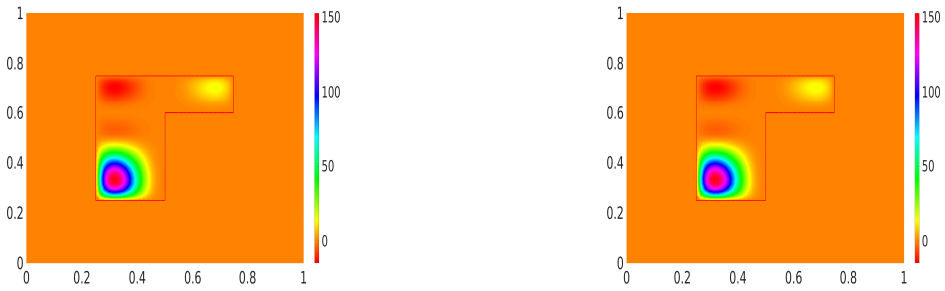

Figure 4.3.5: (Example 4.3.2) Surface plots for second component of exact solution (left) and WG solution (right).

Table 4.3.3: Convergence and error results for the Example 4.3.2.

k	Level	$\|\|\|\mathbf{e}_h\|\|\|_2$	Order	$\|\|\mathbf{e}_0\|\|$	Order
1	1	2.63e+00	—	6.20e-01	—
	2	1.34e+00	0.97	1.64e-01	1.91
	3	6.67e-01	1.00	4.13e-02	1.99
	4	3.33e-01	1.00	1.03e-02	2.00
	5	1.66e-01	1.00	2.58e-03	1.99
	6	8.32e-02	1.00	6.45e-04	1.99
2	1	1.30e+00	—	2.25e-01	—
	2	3.68e-01	1.82	3.19e-02	2.82
	3	9.50e-02	1.95	4.09e-03	2.96
	4	2.39e-02	1.98	5.13e-04	2.99
	5	6.00e-03	1.99	6.42e-05	2.99
	6	1.50e-03	1.99	8.03e-06	2.99

Table 4.3.4: Convergence and error results for the Example 4.3.2.

k	Level	$\|\|\|\mathbf{e}_h\|\|\|_2$	Order	$\|\|\mathbf{e}_0\|\|$	Order
3	1	4.67e-01	—	6.86e-02	—
	2	6.68e-02	2.80	4.92e-03	3.80
	3	8.63e-03	2.95	3.17e-04	3.95
	4	1.08e-03	2.98	1.99e-05	3.99
	5	1.36e-04	2.99	1.24e-06	3.99
	6	1.70e-05	2.99	7.80e-08	3.99
4	1	1.26e-01	—	1.63e-02	—
	2	8.72e-03	3.86	5.64e-04	4.85
	3	5.59e-04	3.96	1.81e-05	4.96
	4	3.51e-05	3.99	5.71e-07	4.98
	5	2.20e-06	3.99	1.78e-08	4.99
	6	1.37e-07	3.99	5.58e-10	4.99

1 in [90])

$$\mathbf{p}(x,y,z) = \begin{pmatrix} y(1-y)z(1-z) \\ x(1-x)z(1-z) \\ x(1-x)y(1-y) \end{pmatrix}.$$

The coefficients are set as $\alpha = \beta = \gamma = 1$ in Ω. The initial mesh is shown in Figure 4.3.6. The errors and orders of convergence for the WG method are shown in Table 4.3.5. For a smooth solution, it is clear from Table 4.3.5 that we have achieved optimal orders of convergence in a domain with the corner.

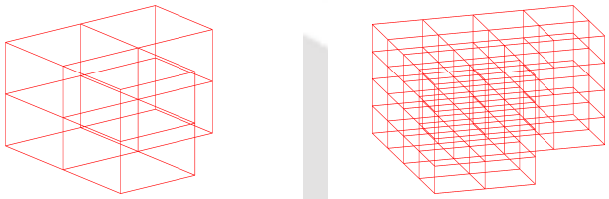

Figure 4.3.6: An initial mesh (left) and its refinement (right) in Example 4.3.3.

Table 4.3.5: Convergence and error profiles for the Example 4.3.3.

k	Level	$\|\|\|\mathbf{e}_h\|\|\|_2$	Order	$\|\mathbf{e}_0\|$	Order
1	1	1.11e-01	—	2.46e-01	—
	2	5.65e-02	0.97	6.32e-02	1.96
	3	2.84e-02	0.99	1.59e-02	1.99
	4	1.42e-02	0.99	3.98e-03	1.99
	5	7.11e-03	0.99	9.95e-04	1.99
	6	3.55e-03	1.00	2.48e-04	1.99
2	1	1.99e-02	—	3.35e-02	—
	2	5.13e-03	1.95	4.33e-03	2.95
	3	1.29e-03	1.98	5.44e-04	2.99
	4	3.24e-04	1.99	6.80e-05	2.99
	5	8.11e-05	1.99	8.50e-06	3.00
	6	2.02e-05	1.99	1.06e-06	3.00
3	1	2.29e-03	—	3.31e-03	—
	2	2.92e-04	2.96	2.12e-04	3.96
	3	3.68e-05	2.99	1.33e-05	3.99
	4	4.61e-06	2.99	8.33e-07	3.99
	5	5.77e-07	2.99	5.20e-08	4.00
	6	7.21e-08	2.99	3.25e-09	4.00

5

WG-FEMs for H(div)-Elliptic Interface Problems

A fitted weak Galerkin (WG) finite element scheme has been demonstrated in the present chapter for solving **H**(div)-elliptic equation with discontinuous coefficients and interface. In both L^2 norm and H^1 norm, error estimates of optimal orders are discussed for the **H**(div)-elliptic interface problems. High-order convergence rates have been achieved by using suitable WG approximation spaces of higher degrees. We have performed some typical numerical tests to confirm the theoretical findings of the proposed WG algorithm. Moreover, numerically it is shown that the proposed WG algorithm is able to accommodate geometrically complicated and very irregular interfaces having sharp edges, cusps, and tips.

5.1 Introduction

Let Ω be a polygonal/polyhedral domain in $\mathbb{R}^d (d = 2,\ 3)$ with Lipschitz boundary $\partial\Omega$ and $\Omega_1 \subset \Omega$ is an open domain with C^2 smooth boundary $\Gamma = \partial\Omega_1$ and $\Omega_2 = \Omega \backslash \Omega_1$ (see Fig. 1.1.1 for an illustration). In Ω, we now recall the **H**(div)-elliptic interface problem of the form

$$-\nabla(\alpha \nabla \cdot \mathbf{p}) + \gamma \mathbf{p} = \mathbf{f} \ \text{ in } \Omega, \tag{5.1.1}$$

$$\mathbf{p} \cdot \boldsymbol{\eta} = 0 \ \text{ on } \partial\Omega, \tag{5.1.2}$$

with non-homogeneous interface jump conditions

$$[\alpha \nabla \cdot \mathbf{p}] = \psi \ \ \& \ \ [\mathbf{p} \cdot \boldsymbol{\eta}] \ = \ -\phi \ \text{ on } \ \Gamma. \tag{5.1.3}$$

Other symbols are as defined in Chapter 1.

Results of this Chapter are published in J. Comput. Appl. Math., https://doi.org/10.1016/j.cam.2023.115269.

Classical FEM for $\mathbf{H}(\text{div})$-elliptic problems has been studied in [69]. Optimal error estimate for $\mathbf{H}(\text{div})$-norm is obtained for C^2 smooth interface with homogeneous jump conditions. Recently, interface-penalty FEMs are proposed to solve $\mathbf{H}(\text{div})$-elliptic interface problem in [96] using unfitted tetrahedral meshes. Error estimates of optimal orders are derived in energy norms assuming three transmission conditions. Although interface-penalty FEMs is able to achieve accuracy near the interfaces but the stabilizer needs one more penalty term to maintain stability. In addition, immersed virtual element techniques have been developed for Maxwell's interface problems in 3D in [27]. Optimal convergence results have been derived with homogenous jump conditions.

From the analysis in [69], it is evident that high-order convergence depends on the fact that how appropriately the interface settled by the finite element mesh, and subsequently, WG-FEM provides a scope due to the flexibility of mesh generation in WG-FEMs. In this work, we have discussed the fitted WG-FEM for $\mathbf{H}(\text{div})$-elliptic interface model problem (5.1.1)-(5.1.3) based on polygonal (in 2D)/polyhedral (in 3D) meshes. In both L^2 and H^1 norms, the error estimates of the optimal orders are discussed for the proposed WG algorithm. Moreover, several numerical experiments have been carried out that also involve complicated interfaces and solutions having low regularity to justify the theoretical results. As per our literature survey, it seems that there has been no work until now on high-order FEMs for $\mathbf{H}(\text{div})$-elliptic interface problems with general polygonal/polyhedral meshes.

The rest of the chapter is organized as follows. In Sec.5.2, we have described regularity results for the $\mathbf{H}(\text{div})$-elliptic problem. The weak Galerkin discretization, L^2-projections, and weak Galerkin algorithm are described in Sec.5.3. Error equation and error estimates are derived in Sec. 5.4. In Sec.5.5, we demonstrate specific numerical experiments that confirm the theory established in the previous sections.

5.2 Regularity Results

In this section, the existence and uniqueness of the weak solution to the aforementioned interface problem have been discussed. For this purpose, we introduce the weak formulation of the model problem (5.1.1)-(5.1.3).

Definition 5.2.1. A function $\mathbf{p} \in \mathbf{H}_0(\text{div}; \Omega_1, \Omega_2)$ is known as a weak solution of (5.1.1)-(5.1.3) if $[\mathbf{p} \cdot \boldsymbol{\eta}] = -\phi$ and satisfy

$$(\alpha \nabla \cdot \mathbf{p}, \nabla \cdot \mathbf{v}) + (\gamma \mathbf{p}, \mathbf{v}) = (\mathbf{f}, \mathbf{v}) + \langle \psi, \mathbf{v} \cdot \boldsymbol{\eta} \rangle_\Gamma \quad \forall \mathbf{v} \in \mathbf{H}_0(\text{div}; \Omega). \tag{5.2.1}$$

Here, $\langle \cdot, \cdot \rangle_\Gamma$ denotes the L^2 inner product on Γ.

Theorem 5.2.1. *Formulation (5.2.1) has a unique solution* $\mathbf{p} \in \mathbf{H}_0(\mathrm{div}; \Omega_1, \Omega_2)$. *In addition, we have*

$$\|\mathbf{p}\|_{\mathbf{H}(\mathrm{div};\Omega_1,\Omega_2)} \leq C \left\{ \|\mathbf{f}\| + \|\phi\|_{H^{\frac{1}{2}}(\Gamma)} + \|\psi\|_{H^{\frac{1}{2}}(\Gamma)} \right\}.$$

Proof. Using Lax-Milgram Lemma, for $\hat{\mathbf{f}} \in [L^2(\Omega)]^d$ and $\psi \in H^{\frac{1}{2}}(\Gamma)$, it is easy to justify that there must exists a unique solution $\hat{\mathbf{w}} \in \mathbf{H}_0(\mathrm{div}; \Omega)$ satisfying

$$(\alpha \nabla \cdot \hat{\mathbf{w}}, \nabla \cdot \mathbf{v}) + (\gamma \hat{\mathbf{w}}, \mathbf{v}) = (\hat{\mathbf{f}}, \mathbf{v}) + \langle \psi, \mathbf{v} \cdot \boldsymbol{\eta} \rangle_\Gamma \ \ \forall \mathbf{v} \in \mathbf{H}_0(\mathrm{div}; \Omega). \tag{5.2.2}$$

Above problem can be realized as the weak formulation to the model problem given by

$$\begin{cases} -\nabla(\alpha \nabla \cdot \hat{\mathbf{w}}) &= \hat{\mathbf{f}} \ \text{ in } \Omega, \\ [\alpha \nabla \cdot \hat{\mathbf{w}}] &= \psi \ \text{ on } \ \Gamma, \\ [\hat{\mathbf{w}} \cdot \boldsymbol{\eta}] &= 0 \ \text{ on } \ \Gamma. \end{cases} \tag{5.2.3}$$

Again, as Γ is of class C^2, we can determine a function $\hat{\mathbf{p}} \in \mathbf{H}_0(\mathrm{div}; \Omega_1, \Omega_2) \cap \mathbf{H}^1(\mathrm{div}; \Omega_1, \Omega_2)$ in such a way that satisfies

$$[\hat{\mathbf{p}} \cdot \boldsymbol{\eta}] = -\phi \ \text{ on } \ \Gamma \ \text{ and } \ \|\hat{\mathbf{p}}\|_{\mathbf{H}^1(\mathrm{div};\Omega_1,\Omega_2)} \leq C \|\phi\|_{H^{\frac{1}{2}}(\Gamma)}. \tag{5.2.4}$$

From Theorem 5.2.1, we observe that $\mathbf{p} = \hat{\mathbf{w}} + \hat{\mathbf{p}}$ solves the equation (5.2.1) with $\hat{\mathbf{f}}$ replaced as $\mathbf{f} + \nabla(\alpha \nabla \cdot \hat{\mathbf{p}}) - \gamma \hat{\mathbf{p}}$ and integration by parts. The proof for the stability is straightforward. □

Remark 5.2.1. For the construction of $\hat{\mathbf{p}} \in \mathbf{H}_0(\mathrm{div}; \Omega_1, \Omega_2) \cap \mathbf{H}^1(\mathrm{div}; \Omega_1, \Omega_2)$, we refer to Remark 2.1 in [38].

To prove the existence of the strong solution for the interface model, we first derive the following results.

Lemma 5.2.1. *Let* $\mathbf{p} \in \mathbf{H}_0(\mathrm{div}; \Omega_1, \Omega_2) \cap \mathbf{H}^1(\mathrm{div}; \Omega_1, \Omega_2)$ *be the weak solution for* (5.1.1)-(5.1.3)*, then* $\mathbf{p}$ *is also a strong solution of* (5.1.1)-(5.1.3).

Proof. For $\mathbf{p} \in \mathbf{H}_0(\mathrm{div}; \Omega_1, \Omega_2) \cap \mathbf{H}^1(\mathrm{div}; \Omega_1, \Omega_2)$ and integration by parts give rise to

$$\begin{aligned} &\int_{\Omega_i} \left(-\nabla(\alpha \nabla \cdot \mathbf{p}) + \gamma \mathbf{p}\right) \mathbf{v} dx \\ &= (\gamma \mathbf{p}, \mathbf{v})_{\Omega_i} + (\alpha \nabla \cdot \mathbf{p}, \nabla \cdot \mathbf{v})_{\Omega_i} = (\mathbf{f}, \mathbf{v})_{\Omega_i} \ \ \forall \mathbf{v} \in \mathbf{H}_0(\mathrm{div}; \Omega_i), \end{aligned}$$

which implies that

$$-\nabla(\alpha \nabla \cdot \mathbf{p}) + \gamma \mathbf{p} = \mathbf{f} \ \ a.e. \ \text{ in } \ \Omega_i, \ i = 1, 2.$$

Next, we shall prove that $\mathbf{p}$ satisfies the jump conditions (5.1.3). Integration by parts give rise to

$$\begin{aligned} 0 &= \sum_{i=1}^{2}\int_{\Omega_i}(-\mathbf{f})\mathbf{v}dx + \sum_{i=1}^{2}\int_{\Omega_i}\left(-\nabla(\alpha\nabla\cdot\mathbf{p})+\gamma\mathbf{p}\right)\mathbf{v}dx \\ &= -\sum_{i=1}^{2}(\mathbf{f},\mathbf{v})_{\Omega_i} + \sum_{i=1}^{2}(\alpha\nabla\cdot\mathbf{p},\nabla\cdot\mathbf{v})_{\Omega_i} + \sum_{i=1}^{2}(\gamma\mathbf{p},\mathbf{v})_{\Omega_i} \\ &\quad -\left\langle[\alpha\nabla\cdot\mathbf{p}],\mathbf{v}\cdot\boldsymbol{\eta}\right\rangle_{\Gamma} \ \ \forall\mathbf{v}\in\mathbf{H}_0(\mathrm{div};\Omega). \end{aligned}$$

Using the definition of weak solution and above relation leads to

$$\left\langle\mathbf{v}\cdot\boldsymbol{\eta},([\alpha\nabla\cdot\mathbf{p}]-\psi)\right\rangle_{\Gamma}=0 \ \ \forall\mathbf{v}\in\mathbf{H}_0(\mathrm{div};\Omega).$$

The arbitrariness of $\mathbf{v}$ shows that $\mathbf{p}$ satisfies the first jump condition in (5.1.3). From the definition (5.2.1), the second condition directly follows. □

Lemma 5.2.2. *For* $\psi\in H^{\frac{3}{2}}(\Gamma)$*, the interface problem (5.2.3) has an unique solution* $\hat{\mathbf{w}}\in\mathbf{H}_0(\mathrm{div};\Omega_1,\Omega_2)\cap\mathbf{H}^1(\mathrm{div};\Omega_1,\Omega_2)$ *and satisfies the following apriori estimate*

$$\|\hat{\mathbf{w}}\|_{\mathbf{H}^1(\mathrm{div};\Omega_1,\Omega_2)}\leq C\left\{\|\mathbf{f}\|+\|\psi\|_{H^{\frac{3}{2}}(\Gamma)}\right\}.$$

Proof. First, we consider the following elliptic interface problem

$$\begin{cases} -\nabla\cdot(\alpha\nabla v)=0 \ \text{ in } \Omega_1\cup\Omega_2, \\ v=0 \ \text{ on } \partial\Omega, \\ [v]=-\psi, \ [\alpha\nabla v\cdot\mathbf{n}]=0 \ \text{ on } \ \Gamma. \end{cases} \tag{5.2.5}$$

Then, $v\in H^2(\Omega_1)\cap H^2(\Omega_2)$ (cf. [38, 84]) and satisfies following estimate

$$\|v\|_{2,\Omega_1}+\|v\|_{2,\Omega_2}\leq C\|\psi\|_{H^{\frac{3}{2}}(\Gamma)}.$$

Next, consider following auxiliary elliptic problem

$$\begin{cases} -\Delta u_i+\alpha_i^{-1}u_i=\alpha_i^{-1}v \ \text{ in } \Omega_i, \ \ i=1,\ 2, \\ \nabla u_2\cdot\mathbf{n}=0 \ \text{ on } \partial\Omega, \\ u_1-u_2=0, \ \ \nabla u_1\cdot\mathbf{n}-\nabla u_2\cdot\mathbf{n}=0 \ \text{ on } \ \Gamma. \end{cases} \tag{5.2.6}$$

Due to the construction of u_i in Ω_i $(i=1,\ 2)$, it is clear that $u=u_i\in H^2(\Omega_i)$ (see, [78]). In fact, for sufficiently smooth coefficient α, we have

$$\Delta u=\alpha^{-1}(u-v)\in H^2(\Omega_1)\cap H^2(\Omega_2).$$

Then, trace result and interface conditions lead to

$$[\alpha \Delta u] = [u] - [v] = \psi \ \text{ and } \ [\nabla u \cdot \mathbf{n}] = 0 \ \text{ on } \Gamma. \tag{5.2.7}$$

Then, $\tilde{\mathbf{p}} = \nabla u \in \mathbf{H}_0(\text{div}; \Omega_1, \Omega_2) \cap \mathbf{H}^1(\text{div}; \Omega_1, \Omega_2)$ and following estimate holds

$$\|\tilde{\mathbf{p}}\|_{\mathbf{H}^1(\text{div};\Omega_1,\Omega_2)} \leq C \|\psi\|_{H^{\frac{3}{2}}(\Gamma)}. \tag{5.2.8}$$

Again, the problem admits the unique solution given as follows: Find $\tilde{\mathbf{w}} \in \mathbf{H}_0(\text{div}; \Omega) \cap \mathbf{H}^1(\text{div}; \Omega_1, \Omega_2)$ such that (cf. [69])

$$\begin{cases} -\nabla(\alpha \nabla \cdot \tilde{\mathbf{w}}) + \gamma \tilde{\mathbf{w}} &= \tilde{\mathbf{f}} \ \text{ in } \Omega, \\ [\tilde{\mathbf{w}} \cdot \mathbf{n}] &= 0 \ \text{ on } \ \Gamma, \\ [\alpha \nabla \cdot \tilde{\mathbf{w}}] &= 0 \ \text{ on } \ \Gamma, \end{cases} \tag{5.2.9}$$

with $\tilde{\mathbf{f}} = \mathbf{f} + \nabla(\alpha \nabla \cdot \tilde{\mathbf{p}}) - \gamma \tilde{\mathbf{p}} \in [L^2(\Omega)]^d$. Further, $\tilde{\mathbf{w}}$ satisfies following weak formulation

$$(\alpha \nabla \cdot \tilde{\mathbf{w}}, \nabla \cdot \mathbf{v}) + (\gamma \tilde{\mathbf{w}}, \mathbf{v}) = (\tilde{\mathbf{f}}, \mathbf{v}) \ \ \forall \mathbf{v} \in \mathbf{H}_0(\text{div}; \Omega). \tag{5.2.10}$$

In order to use interface condition (5.2.7), we integrate in each subdomain to get

$$(\tilde{\mathbf{f}}, \mathbf{v}) = (\mathbf{f}, \mathbf{v}) - (\gamma \tilde{\mathbf{p}}, \mathbf{v}) - (\alpha \nabla \cdot \tilde{\mathbf{p}}, \nabla \cdot \mathbf{v}) + \langle \psi, \mathbf{v} \cdot \mathbf{n} \rangle_\Gamma \ \ \forall \mathbf{v} \in \mathbf{H}_0(\text{div}; \Omega). \tag{5.2.11}$$

Then, $\hat{\mathbf{w}} = \tilde{\mathbf{w}} + \tilde{\mathbf{p}} \in \mathbf{H}_0(\text{div}; \Omega_1, \Omega_2) \cap \mathbf{H}^1(\text{div}; \Omega_1, \Omega_2)$ is a weak solution of (5.2.3). Hence, due to previous Lemma 5.2.1, the interface problem (5.2.3) has a strong solution $\hat{\mathbf{w}}$, and satisfies the desired apriori estimate. □

Hence, from Lemma 5.2.1, we can conclude that the existence of a strong solution demands high regularity from weak solution, which justify by the following Theorem 5.2.2.

Theorem 5.2.2. *Assume that* $\mathbf{f} \in [L^2(\Omega)]^d$, $\phi \in H^{\frac{1}{2}}(\Gamma)$ *and* $\psi \in H^{\frac{3}{2}}(\Gamma)$. *Then, the interface problem* (5.1.1)-(5.1.3) *has a unique strong solution.*

Proof. Combining Theorem 5.2.1 and Lemma 5.2.2, we observe that $\mathbf{p} = \hat{\mathbf{w}} + \hat{\mathbf{p}} \in \mathbf{H}_0(\text{div}; \Omega) \cap \mathbf{H}^1(\text{div}; \Omega_1, \Omega_2)$ solves the equation (5.2.1) and $[\mathbf{p} \cdot \mathbf{n}] = [\hat{\mathbf{w}} \cdot \mathbf{n}] + [\hat{\mathbf{p}} \cdot \mathbf{n}] = -\phi$ on Γ. Then, due to Lemma 5.2.1, we conclude that $\mathbf{p}$ is a strong solution to the interface problem (5.1.1)-(5.1.3). □

Remark 5.2.2. If $\mathbf{p} \in \mathbf{H}_0(\text{div}; \Omega_1, \Omega_2) \cap \mathbf{H}^1(\text{div}; \Omega_1, \Omega_2)$ is the strong solution for (5.1.1)-(5.1.3), then $\mathbf{p}$ satisfies the apriori estimate given by

$$\|\mathbf{p}\|_{\mathbf{H}^1(\text{div};\Omega_1,\Omega_2)} \leq C \left\{ \|\mathbf{f}\| + \|\phi\|_{H^{\frac{1}{2}}(\Gamma)} + \|\psi\|_{H^{\frac{1}{2}}(\Gamma)} \right\}.$$

5.3 Weak Galerkin Algorithm

Let $\mathcal{T}_h$ be a finite fitted mesh of domain Ω having mesh size h with some regularity constraints mentioned in [121]. A simple cost-efficient fitted mesh generation algorithm has been proposed in [36]. Elements in $\mathcal{T}_h$ can be any kind of polygons/polyhedra instead of standard simplicies. Let $\mathcal{E}_h$ be the set containing all edges/flat-faces of $\mathcal{T}_h$ and assume $\mathcal{E}_h^0 = \mathcal{E}_h \backslash \partial\Omega$ be the set containing all the interior edges/flat-faces. Let $|T|$ and h_T denote the measure and diameter of $T \in \mathcal{T}_h$, respectively. With supplementary computational cost, we shall generate body-fitted grids such that edges/flat-faces of $\mathcal{E}_h^0$ aligned along the interface Γ. Thus, in a simplified way, we can write

$$\begin{aligned} \mathcal{T}_h &= \{T \in \mathcal{T}_h : T \nsubseteq \Omega_2 \text{ or } \partial T \cap \Gamma = \emptyset\} \\ &\quad \cup \{T \in \mathcal{T}_h : T \subseteq \Omega_2 \text{ and } \partial T \cap \Gamma \neq \emptyset\} \\ &:= \mathcal{T}_1 \cup \mathcal{T}_2. \end{aligned} \tag{5.3.1}$$

Note that, all the elements of Ω_1 and non-interface elements of Ω_2 are contained in $\mathcal{T}_1$. We denote Γ_h be the finite element partition of the interface Γ, which can be obtained from the intersection of the $\mathcal{T}_1$ and $\mathcal{T}_2$.

Here, we have adopted the same definition of weak functions as defined in Chapter 2. Let T be any polyhedra (in 3D)/polygons (in 2D) domain with interior T^0 and boundary ∂T. A weak vector-valued function on the domain T refers to a vector-valued function $\mathbf{v} = \{\mathbf{v}_0, \mathbf{v}_b\}$ such that $\mathbf{v}_0 \in [L^2(T)]^d$ and $\mathbf{v}_b \cdot \boldsymbol{\eta} \in L^2(\partial T)$, where $\boldsymbol{\eta}$ is unit outward normal of ∂T. For each $e \in \partial T$, we define $\boldsymbol{\eta}_e = \boldsymbol{\eta}|_e$. Then, for each integer $k \geq 1$, we recall the following weak Galerkin (WG) spaces based on the partition $\mathcal{T}_h$ given by

$$\mathbf{V}_h = \{\mathbf{v}_h = \{\mathbf{v}_0, \mathbf{v}_b\} : \mathbf{v}_0|_T \in [\mathcal{P}_k(T)]^d, \mathbf{v}_b|_e = v_b \boldsymbol{\eta}_e, v_b \in \mathcal{P}_k(e), e \in \partial T, T \in \mathcal{T}_h\},$$

and

$$\mathbf{V}_h^0 = \{\mathbf{v}_h = \{\mathbf{v}_0, \mathbf{v}_b\} \in \mathbf{V}_h : \mathbf{v}_b \cdot \boldsymbol{\eta} = 0 \text{ on } \partial\Omega\}.$$

For the well-posedness of the WG approximation, $\mathbf{v}_b$ defined on each edge/flat-face $e \in \mathcal{E}_h$ must be single valued (cf. [121, 122]). Now, for each $\mathbf{v}_h = \{\mathbf{v}_0, \mathbf{v}_b\} \in \mathbf{V}_h$, we recalls the weak divergence of it, denoted by $\nabla_w \cdot \mathbf{v}_h$, is a unique polynomial in $\mathcal{P}_{k-1}(T)$ which satisfy

$$(\nabla_w \cdot \mathbf{v}_h, p)_T = -(\mathbf{v}_0, \nabla p)_T + \langle \mathbf{v}_b \cdot \boldsymbol{\eta}, p \rangle_{\partial T} \quad \forall p \in \mathcal{P}_{k-1}(T). \tag{5.3.2}$$

Now, we define two bilinear maps $\mathcal{S}, \mathcal{A} : \mathbf{V}_h \times \mathbf{V}_h \to \mathbb{R}$ given by

$$\mathcal{S}(\mathbf{w}_h, \mathbf{v}_h) = \sum_{T \in \mathcal{T}_h} h^{-1} \langle (\mathbf{w}_0 - \mathbf{w}_b) \cdot \boldsymbol{\eta}, (\mathbf{v}_0 - \mathbf{v}_b) \cdot \boldsymbol{\eta} \rangle_{\partial T}, \tag{5.3.3}$$

and

$$\mathcal{A}(\mathbf{w}_h, \mathbf{v}_h) = (\alpha \nabla_w \cdot \mathbf{w}_h, \nabla_w \cdot \mathbf{v}_h) + (\gamma \mathbf{w}_0, \mathbf{v}_0) + \mathcal{S}(\mathbf{w}_h, \mathbf{v}_h), \tag{5.3.4}$$

for all $\mathbf{w}_h = \{\mathbf{w}_0, \mathbf{w}_b\},\ \mathbf{v}_h = \{\mathbf{v}_0, \mathbf{v}_b\} \in \mathbf{V}_h$.

Next, we introduce triple-bar norm on $\mathbf{V}_h^0$ given by

$$\begin{aligned} |||\mathbf{v}_h|||^2 &= \sum_{T\in\mathcal{T}_h} \|\alpha^{\frac{1}{2}} \nabla_w \cdot \mathbf{v}_h\|_T^2 + \|\gamma^{\frac{1}{2}} \mathbf{v}_0\|_T^2 + \sum_{T\in\mathcal{T}_h} h^{-1} \|(\mathbf{v}_0 - \mathbf{v}_b) \cdot \boldsymbol{\eta}\|_{\partial T}^2 \\ &= \mathcal{A}(\mathbf{v}_h, \mathbf{v}_h) \ \ \forall \mathbf{v}_h \in \mathbf{V}_h^0. \end{aligned} \tag{5.3.5}$$

For any $T \in \mathcal{T}_h$ and $e \in \mathcal{E}_h$, we introduce the local L^2-projections given as follows:

$$\mathbf{Q}_0^k : [L^2(T)]^d \to [\mathcal{P}_k(T)]^d,\ \mathbb{Q}_h^{k-1} : L^2(T) \to \mathcal{P}_{k-1}(T),\ Q_b^k : L^2(e) \to \mathcal{P}_k(e).$$

For $\mathbf{w} \in [H^1(T)]^d$, we define $\mathbf{Q}_h \mathbf{w} = \{\mathbf{Q}_0^k \mathbf{w}, Q_b^k(\mathbf{w} \cdot \boldsymbol{\eta}_e)\boldsymbol{\eta}_e\}$. Now, we reintroduce some important approximations results from ([121, 122]) for $\mathbf{Q}_0^k$ and $\mathbb{Q}_h^{k-1}$.

Lemma 5.3.1. *Assume $\mathcal{T}_h$ be the partition of Ω mentioned in [121]. Then, we get*

$$\begin{aligned} &\sum_{T\in\mathcal{T}_h} \|\mathbf{w} - \mathbf{Q}_0^k \mathbf{w}\|_T^2 \le C h^{2(s+1)} \|\mathbf{w}\|_{s+1}^2, \ \ 0 \le s \le k, \\ &\sum_{T\in\mathcal{T}_h} \|\nabla(\mathbf{w} - \mathbf{Q}_0^k \mathbf{w})\|_T^2 \le C h^{2s} \|\mathbf{w}\|_{s+1}^2, \ \ 0 \le s \le k, \\ &\sum_{T\in\mathcal{T}_h} \left\{ \|z - \mathbb{Q}_h^{k-1} z\|_T^2 + h_T^2 \|\nabla(z - \mathbb{Q}_h^{k-1} z)\|_T^2 \right\} \le C h^{2(s+1)} \|z\|_{s+1}^2, \ 0 \le s \le k-1. \end{aligned}$$

For $e \notin \Gamma_h$, shared edge between two elements T_1 and T_2, $\mathbf{p}|_{T_1 \cap e} = \mathbf{p}|_{T_2 \cap e}$. Therefore, $Q_b^k(\mathbf{p} \cdot \boldsymbol{\eta}_e)$ is a single valued function on each $e \notin \Gamma_h$ and $\mathbf{Q}_h \mathbf{p} = \{\mathbf{Q}_0^k \mathbf{p}, Q_b^k(\mathbf{p} \cdot \boldsymbol{\eta}_e)\boldsymbol{\eta}_e\} \in \mathbf{V}_h$. If $e \in \Gamma_h$, $\mathbf{p}|_{T_1 \cap e} \ne \mathbf{p}|_{T_2 \cap e}$ with $T_1 \subset \Omega_1$ and $T_2 \subset \Omega_2$. To ensure $\mathbf{Q}_h \mathbf{p} \in \mathbf{V}_h$, i.e., $Q_b^k(\mathbf{p} \cdot \boldsymbol{\eta}_e)$ single valued on each $e \in \Gamma_h$, $Q_b^k(\mathbf{p} \cdot \boldsymbol{\eta}_e)$ defined in a way given below

$$Q_b^k(\mathbf{p} \cdot \boldsymbol{\eta})|_e = \begin{cases} Q_b^k(\mathbf{p}|_{T\cap e} \cdot \boldsymbol{\eta}) & \text{if} \quad e \in \Gamma_h \ \& \ T \subset \Omega_1, \\ Q_b^k(\mathbf{p}|_{T\cap e} \cdot \boldsymbol{\eta}) + Q_b^k \phi & \text{if} \quad e \in \Gamma_h \ \& \ T \subset \Omega_2, \\ Q_b^k(\mathbf{p}|_{T\cap e} \cdot \boldsymbol{\eta}) & \text{if} \quad e \notin \Gamma_h \ \& \ T \in \mathcal{T}_h. \end{cases} \tag{5.3.6}$$

Next result set a relation between projection operators $\mathbf{Q}_h$ and $\mathbb{Q}_h^{k-1}$.

Lemma 5.3.2. *Let $\mathbf{p}$ be an exact solution for (5.1.1)-(5.1.3). Then, for each $q \in \mathcal{P}_{k-1}(T)$, the following properties satisfy*

$$\begin{aligned} (\nabla_w \cdot \mathbf{Q}_h \mathbf{p}, q)_T &= (\mathbb{Q}_h^{k-1}(\nabla \cdot \mathbf{p}), q)_T, \ \ T \in \mathcal{T}_1, \\ (\nabla_w \cdot \mathbf{Q}_h \mathbf{p}, q)_T &= (\mathbb{Q}_h^{k-1}(\nabla \cdot \mathbf{p}), q)_T + \langle \phi, q \rangle_{\partial T \cap \Gamma}, \ \ T \in \mathcal{T}_2. \end{aligned}$$

Proof. For $q \in \mathcal{P}_{k-1}(T)$ and $T \in \mathcal{T}_1$, using (5.3.6) together with the definition (5.3.2), we have

$$\begin{aligned}(\nabla_w \cdot \mathbf{Q}_h\mathbf{p}, q)_T &= -(\mathbf{Q}_0^k\mathbf{p}, \nabla q)_T + \langle Q_b^k(\mathbf{p}\cdot\boldsymbol{\eta}), q\rangle_{\partial T} \\ &= -(\mathbf{p}, \nabla q)_T + \langle \mathbf{p}\cdot\boldsymbol{\eta}, q\rangle_{\partial T} \\ &= (\nabla\cdot\mathbf{p}, q)_T \\ &= (\mathbb{Q}_h^{k-1}(\nabla\cdot\mathbf{p}), q)_T.\end{aligned}$$

In a similar way, for $T \in \mathcal{T}_2$ leads to

$$\begin{aligned}(\nabla_w \cdot \mathbf{Q}_h\mathbf{p}, q)_T &= -(\mathbf{Q}_0^k, \nabla q)_T + \langle Q_b^k(\mathbf{p}\cdot\boldsymbol{\eta}), q\rangle_{\partial T} \\ &= -(\mathbf{p}, \nabla q)_T + \langle \mathbf{p}\cdot\boldsymbol{\eta}, q\rangle_{\partial T} + \langle \phi, q\rangle_{\partial T\cap\Gamma} \\ &= (\nabla\cdot\mathbf{p}, q)_T + \langle \phi, q\rangle_{\partial T\cap\Gamma} \\ &= (\mathbb{Q}_h^{k-1}(\nabla\cdot\mathbf{p}), q)_T + \langle \phi, q\rangle_{\partial T\cap\Gamma}.\end{aligned}$$

This completes the Lemma 5.3.2. □

For $\mathbf{v}_h = \{\mathbf{v}_0, \mathbf{v}_b\} \in \mathbf{V}_h$, we define the bilinear forms as follow

$$\begin{aligned}\langle \psi, \mathbf{v}_b\cdot\boldsymbol{\eta}\rangle_\Gamma &= \sum_{e\in\Gamma_h}\langle \psi, \mathbf{v}_b\cdot\boldsymbol{\eta}\rangle_e, \\ \langle \phi, \alpha\nabla_w\cdot\mathbf{v}_h\rangle_\Gamma &= \sum_{T\in\mathcal{T}_2}\langle \phi, \alpha_2\nabla_w\cdot\mathbf{v}_h|_T\rangle_{\partial T\cap\Gamma_h}, \\ h^{-1}\langle \phi, (\mathbf{v}_0-\mathbf{v}_b)\cdot\boldsymbol{\eta}\rangle_\Gamma &= \sum_{T\in\mathcal{T}_2} h^{-1}\langle \phi, (\mathbf{v}_0|_T-\mathbf{v}_b)\cdot\boldsymbol{\eta}\rangle_{\partial T\cap\Gamma_h}.\end{aligned}$$

5.4 Error Equation and Error Analysis

In this section, we have studied a WG-FEM for the $\mathbf{H}(\text{div})$-elliptic interface problem (5.1.1)-(5.1.3) with on local WG space $\left(\mathcal{P}_k^d,\ \mathcal{P}_k^d,\ \mathcal{P}_{k-1}\right)$. Further, we shall derive error estimates of optimal order in L^2 norm and discrete energy norm. We assume α and γ to be piecewise constants in theoretical analysis.

Weak Galerkin Algorithm. A weak Galerkin numerical approximation equation for (5.1.1)-(5.1.3) can be derived by finding $\mathbf{p}_h = \{\mathbf{p}_0, \mathbf{p}_b\} \in \mathbf{V}_h^0$ such that

$$\begin{aligned}\mathcal{A}(\mathbf{p}_h, \mathbf{v}_h) &= (\mathbf{f}, \mathbf{v}_0) + \langle \psi, \mathbf{v}_b\cdot\boldsymbol{\eta}\rangle_\Gamma + \langle \phi, \alpha\nabla_w\cdot\mathbf{v}_h\rangle_\Gamma \\ &\quad -h^{-1}\langle \phi, (\mathbf{v}_0-\mathbf{v}_b)\cdot\boldsymbol{\eta}\rangle_\Gamma \ \ \forall \mathbf{v}_h = \{\mathbf{v}_0, \mathbf{v}_b\} \in \mathbf{V}_h^0. \qquad (5.4.1)\end{aligned}$$

Next, we rigorously discuss the error equation and corresponding error estimates. For this purpose, we define error function $\mathbf{e}_h$ by

$$\mathbf{e}_h = \mathbf{Q}_h\mathbf{p} - \mathbf{p}_h = \{\mathbf{e}_0, \mathbf{e}_b\} = \{\mathbf{Q}_0^k\mathbf{p} - \mathbf{p}_0, Q_b^k(\mathbf{p}\cdot\boldsymbol{\eta})\boldsymbol{\eta} - \mathbf{p}_b\}. \tag{5.4.2}$$

Then, to capture the error $\mathbf{e}_h$, we define two bilinear maps $R_1(\cdot,\cdot)$ and $R_2(\cdot,\cdot)$ as

$$R_1(\mathbf{p}, \mathbf{v}_h) = \sum_{T\in\mathcal{T}_h} \langle \alpha(\nabla\cdot\mathbf{p} - \mathbb{Q}_h^{k-1}(\nabla\cdot\mathbf{p}))\boldsymbol{\eta}, \mathbf{v}_0 - \mathbf{v}_b\rangle_{\partial T}, \tag{5.4.3}$$

$$R_2(\mathbf{p}, \mathbf{v}_h) = \sum_{T\in\mathcal{T}_h} h^{-1}\langle \mathbf{Q}_0^k\mathbf{p}\cdot\boldsymbol{\eta} - Q_b^k(\mathbf{p}\cdot\boldsymbol{\eta}), (\mathbf{v}_0 - \mathbf{v}_b)\cdot\boldsymbol{\eta}\rangle_{\partial T}. \tag{5.4.4}$$

Lemma 5.4.1. *For $\mathbf{v}_h = \{\mathbf{v}_0, \mathbf{v}_b\} \in \mathbf{V}_h^0$, we obtain*

$$\mathcal{A}(\mathbf{e}_h, \mathbf{v}_h) = R_1(\mathbf{p}, \mathbf{v}_h) + R_2(\mathbf{p}, \mathbf{v}_h). \tag{5.4.5}$$

Proof. For any $\mathbf{v}_h = \{\mathbf{v}_0, \mathbf{v}_b\} \in \mathbf{V}_h^0$, test equation (5.1.1) with $\mathbf{v}_0$ to get

$$\begin{aligned}
&-(\nabla(\alpha\nabla\cdot\mathbf{p}), \mathbf{v}_0)\\
&= -\sum_{T\in\mathcal{T}_h}\langle\alpha(\nabla\cdot\mathbf{p})\boldsymbol{\eta}, \mathbf{v}_0\rangle_{\partial T} + \sum_{T\in\mathcal{T}_h}(\alpha\nabla\cdot\mathbf{p}, \nabla\cdot\mathbf{v}_0)_T\\
&= -\sum_{T\in\mathcal{T}_h}\langle\alpha(\nabla\cdot\mathbf{p})\boldsymbol{\eta}, \mathbf{v}_0 - \mathbf{v}_b\rangle_{\partial T} + \sum_{T\in\mathcal{T}_h}(\alpha\nabla\cdot\mathbf{p}, \nabla\cdot\mathbf{v}_0)_T\\
&\quad - \sum_{T\in\mathcal{T}_h}\langle\alpha(\nabla\cdot\mathbf{p})\boldsymbol{\eta}, \mathbf{v}_b\rangle_{\partial T}\\
&= -\sum_{T\in\mathcal{T}_h}\langle\alpha(\nabla\cdot\mathbf{p})\boldsymbol{\eta}, \mathbf{v}_0 - \mathbf{v}_b\rangle_{\partial T} + \sum_{T\in\mathcal{T}_h}(\alpha\nabla\cdot\mathbf{p}, \nabla\cdot\mathbf{v}_0)_T - \langle\psi, \mathbf{v}_b\cdot\boldsymbol{\eta}\rangle_\Gamma\\
&= \sum_{T\in\mathcal{T}_h}(\alpha\mathbb{Q}_h^{k-1}(\nabla\cdot\mathbf{p}), \nabla\cdot\mathbf{v}_0)_T - \sum_{T\in\mathcal{T}_h}\langle\alpha(\nabla\cdot\mathbf{p})\boldsymbol{\eta}, \mathbf{v}_0 - \mathbf{v}_b\rangle_{\partial T}\\
&\quad -\langle\psi, \mathbf{v}_b\cdot\boldsymbol{\eta}\rangle_\Gamma.
\end{aligned}$$

Equation (5.3.2) and $\mathbb{Q}_h^{k-1}$ operator give rise to

$$\begin{aligned}
&(\alpha\mathbb{Q}_h^{k-1}(\nabla\cdot\mathbf{p}), \nabla_w\cdot\mathbf{v}_h)_T\\
&= -(\mathbf{v}_0, \nabla\left(\alpha\mathbb{Q}_h^{k-1}(\nabla\cdot\mathbf{p})\right))_T + \langle\mathbf{v}_b\cdot\boldsymbol{\eta}, \alpha\mathbb{Q}_h^{k-1}(\nabla\cdot\mathbf{p})\rangle_{\partial T}\\
&= (\nabla\cdot\mathbf{v}_0, \alpha\mathbb{Q}_h^{k-1}(\nabla\cdot\mathbf{p}))_T - \langle(\mathbf{v}_0 - \mathbf{v}_b)\cdot\boldsymbol{\eta}, \alpha\mathbb{Q}_h^{k-1}(\nabla\cdot\mathbf{p})\rangle_{\partial T}.
\end{aligned}$$

Above two equations together with Lemma 5.3.2 implies

$$\begin{aligned}
&-(\nabla(\alpha\nabla\cdot\mathbf{p}),\mathbf{v}_0)\\
&=\sum_{T\in\mathcal{T}_h}(\alpha\mathbb{Q}_h^{k-1}(\nabla\cdot\mathbf{p}),\nabla_w\cdot\mathbf{v}_h)_T-\sum_{T\in\mathcal{T}_h}\langle\alpha(\nabla\cdot\mathbf{p}-\mathbb{Q}_h^{k-1}(\nabla\cdot\mathbf{p}))\boldsymbol{\eta},\mathbf{v}_0-\mathbf{v}_b\rangle_{\partial T}\\
&\quad-\langle\psi,\mathbf{v}_b\cdot\boldsymbol{\eta}\rangle_\Gamma\\
&=\sum_{T\in\mathcal{T}_h}(\alpha\nabla_w\cdot\mathbf{Q}_h\mathbf{p},\nabla_w\cdot\mathbf{v}_h)_T-\sum_{T\in\mathcal{T}_h}\langle\alpha(\nabla\cdot\mathbf{p}-\mathbb{Q}_h^{k-1}(\nabla\cdot\mathbf{p}))\boldsymbol{\eta},\mathbf{v}_0-\mathbf{v}_b\rangle_{\partial T}\\
&\quad-\langle\psi,\mathbf{v}_b\cdot\boldsymbol{\eta}\rangle_\Gamma-\langle\phi,\alpha\nabla_w\cdot\mathbf{v}_h\rangle_\Gamma.
\end{aligned}$$

which yields

$$\begin{aligned}
&\sum_{T\in\mathcal{T}_h}(\alpha\nabla_w\cdot\mathbf{Q}_h\mathbf{p},\nabla_w\cdot\mathbf{v}_h)_T+\sum_{T\in\mathcal{T}_h}(\gamma\mathbf{Q}_h\mathbf{p},\mathbf{v}_0)_T\\
&=(\mathbf{f},\mathbf{v}_0)+\sum_{T\in\mathcal{T}_h}\langle\alpha(\nabla\cdot\mathbf{p}-\mathbb{Q}_h^{k-1}(\nabla\cdot\mathbf{p}))\boldsymbol{\eta},\mathbf{v}_0-\mathbf{v}_b\rangle_{\partial T}\\
&\quad+\langle\psi,\mathbf{v}_b\cdot\boldsymbol{\eta}\rangle_\Gamma+\langle\phi,\alpha\nabla_w\cdot\mathbf{v}_h\rangle_\Gamma.
\end{aligned}\tag{5.4.6}$$

Then, equation (5.4.6) leads to

$$\begin{aligned}
\mathcal{A}(\mathbf{Q}_h\mathbf{p},\mathbf{v}_h)&=(\mathbf{f},\mathbf{v}_0)+R_1(\mathbf{p},\mathbf{v}_h)+\mathcal{S}(\mathbf{Q}_h\mathbf{p},\mathbf{v}_h)\\
&\quad+\langle\psi,\mathbf{v}_b\cdot\boldsymbol{\eta}\rangle_\Gamma+\langle\phi,\alpha\nabla_w\cdot\mathbf{v}_h\rangle_\Gamma.
\end{aligned}\tag{5.4.7}$$

The stabilizer term $\mathcal{S}(\cdot,\cdot)$ and (5.3.6) leads to

$$\begin{aligned}
\mathcal{S}(\mathbf{Q}_h\mathbf{p},\mathbf{v}_h)&=\sum_{T\in\mathcal{T}_h}h^{-1}\langle\mathbf{Q}_0^k\mathbf{p}\cdot\boldsymbol{\eta}-Q_b^k(\mathbf{p}|_T\cdot\boldsymbol{\eta}),(\mathbf{v}_0-\mathbf{v}_b)\cdot\boldsymbol{\eta}\rangle_{\partial T}\\
&\quad-h^{-1}\langle\phi,(\mathbf{v}_0-\mathbf{v}_b)\cdot\boldsymbol{\eta}\rangle_\Gamma.
\end{aligned}\tag{5.4.8}$$

Substituting (5.4.8) in (5.4.7) yields

$$\begin{aligned}
\mathcal{A}(\mathbf{Q}_h\mathbf{p},\mathbf{v}_h)&=(\mathbf{f},\mathbf{v}_0)+R_1(\mathbf{p},\mathbf{v}_h)+R_2(\mathbf{p},\mathbf{v}_h)+\langle\psi,\mathbf{v}_b\cdot\boldsymbol{\eta}\rangle_\Gamma\\
&\quad+\langle\phi,\alpha\nabla_w\cdot\mathbf{v}_h\rangle_\Gamma-h^{-1}\langle\phi,(\mathbf{v}_0-\mathbf{v}_b)\cdot\boldsymbol{\eta}\rangle_\Gamma.
\end{aligned}\tag{5.4.9}$$

The difference of (5.4.9) and (5.4.1) implies (5.4.5). □

Remark 5.4.1. *Work of Mu et al. [103] and (5.4.9) motivate us to derive the approximation equation (5.4.1). In a more precise manner, to avoid the residue in the error we add the jump functions ψ and ϕ to the WG formulation.* □

Next result deals with the bounds for the terms in error equation (5.4.5), which are based on Lemma 5.3.1.

Lemma 5.4.2. *For* $\mathbf{p} \in [H^{k+1}(\Omega_i)]^d$ *with* $i = 1, 2$, *we have*

$$\begin{aligned} |R_1(\mathbf{p}, \mathbf{v}_h)| &\leq Ch^k \left(\|\mathbf{p}\|_{k+1,\Omega_1} + \|\mathbf{p}\|_{k+1,\Omega_2} \right) |||\mathbf{v}_h|||, \\ |R_2(\mathbf{p}, \mathbf{v}_h)| &\leq Ch^k \left(\|\mathbf{p}\|_{k+1,\Omega_1} + \|\mathbf{p}\|_{k+1,\Omega_2} \right) |||\mathbf{v}_h|||, \end{aligned}$$

for all $\mathbf{v}_h = \{\mathbf{v}_0, \mathbf{v}_b\} \in \mathbf{V}_h$.

Proof. Trace inequality (2.2.7) and Cauchy-Schwarz inequality yield following estimate for R_1

$$\begin{aligned} |R_1(\mathbf{p}, \mathbf{v}_h)| &= \left| \sum_{T \in \mathcal{T}_h} \langle \alpha(\nabla \cdot \mathbf{p} - \mathbb{Q}_h^{k-1}(\nabla \cdot \mathbf{p}))\boldsymbol{\eta}, \mathbf{v}_0 - \mathbf{v}_b \rangle_{\partial T} \right| \\ &= \left| \sum_{T \in \mathcal{T}_h} \langle \alpha(\nabla \cdot \mathbf{p} - \mathbb{Q}_h^{k-1}(\nabla \cdot \mathbf{p})), (\mathbf{v}_0 - \mathbf{v}_b) \cdot \boldsymbol{\eta} \rangle_{\partial T} \right| \\ &\leq C \sum_{T \in \mathcal{T}_h} \|\alpha(\nabla \cdot \mathbf{p} - \mathbb{Q}_h^{k-1}(\nabla \cdot \mathbf{p}))\|_{\partial T} \|(\mathbf{v}_0 - \mathbf{v}_b) \cdot \boldsymbol{\eta}\|_{\partial T} \\ &\leq \left(\sum_{T \in \mathcal{T}_h} h_T \|\alpha(\nabla \cdot \mathbf{p} - \mathbb{Q}_h^{k-1}(\nabla \cdot \mathbf{p}))\|_{\partial T}^2 \right)^{\frac{1}{2}} \\ &\quad \times \left(\sum_{T \in \mathcal{T}_h} h_T^{-1} \|(\mathbf{v}_0 - \mathbf{v}_b) \cdot \boldsymbol{\eta}\|_{\partial T}^2 \right)^{\frac{1}{2}} \\ &\leq Ch^k (\|\mathbf{p}\|_{k+1,\Omega_1} + \|\mathbf{p}\|_{k+1,\Omega_2}) |||\mathbf{v}_h|||. \end{aligned}$$

By using the similar arguments, we obtain

$$\begin{aligned} |R_2(\mathbf{p}, \mathbf{v}_h)| &= \left| \sum_{T \in \mathcal{T}_h} h^{-1} \langle \mathbf{Q}_0^k \mathbf{p} \cdot \boldsymbol{\eta} - Q_b^k(\mathbf{p} \cdot \boldsymbol{\eta}), (\mathbf{v}_0 - \mathbf{v}_b) \cdot \boldsymbol{\eta} \rangle_{\partial T} \right| \\ &\leq \left| \sum_{T \in \mathcal{T}_h} h_T^{-1} \langle (\mathbf{Q}_0^k \mathbf{p} - \mathbf{p}) \cdot \boldsymbol{\eta}, (\mathbf{v}_0 - \mathbf{v}_b) \cdot \boldsymbol{\eta} \rangle_{\partial T} \right| \\ &\leq C \left(\sum_{T \in \mathcal{T}_h} (h_T^{-2} \|\mathbf{Q}_0^k \mathbf{p} - \mathbf{p}\|_T^2 + \|\nabla(\mathbf{Q}_0^k \mathbf{p} - \mathbf{p})\|_T^2) \right)^{\frac{1}{2}} \\ &\quad \times \left(\sum_{T \in \mathcal{T}_h} h_T^{-1} \|(\mathbf{v}_0 - \mathbf{v}_b) \cdot \boldsymbol{\eta}\|_{\partial T}^2 \right)^{\frac{1}{2}} \\ &\leq Ch^k (\|\mathbf{p}\|_{k+1,\Omega_1} + \|\mathbf{p}\|_{k+1,\Omega_2}) |||\mathbf{v}_h|||. \end{aligned}$$

This completes the Lemma 5.4.2. □

As an immediate consequence of the previous lemma and error equation (5.4.5), we obtain the following error estimate in the discrete energy norm.

Theorem 5.4.1. *Let $\mathbf{p}_h$ the WG solution of the problem (5.4.1). Assume the exact solution $\mathbf{p} \in [H^{k+1}(\Omega_i)]^d$ with $i = 1, 2$ of the problem* (5.1.1)-(5.1.3)*. Then, we have*

$$|||\mathbf{Q}_h\mathbf{p} - \mathbf{p}_h||| \leq Ch^k \left(\|\mathbf{p}\|_{k+1,\Omega_1} + \|\mathbf{p}\|_{k+1,\Omega_2}\right). \tag{5.4.10}$$

Next, we will use the duality principle argument to estimate the error $\mathbf{e}_h = \mathbf{Q}_h\mathbf{p} - \mathbf{p}_h$ in L^2 norm. To do so, we consider the dual problem that seeks $\boldsymbol{\Psi} \in \mathbf{H}^1(\text{div};\ \Omega_1,\ \Omega_2)$ such that

$$\begin{cases} -\nabla(\alpha\nabla\cdot\boldsymbol{\Psi}) + \gamma\boldsymbol{\Psi} &= \mathbf{e}_0 \text{ on } \Omega, \\ \boldsymbol{\Psi}\cdot\boldsymbol{\eta} &= 0 \text{ on } \partial\Omega, \\ [\boldsymbol{\Psi}\cdot\boldsymbol{\eta}] &= 0 \text{ on } \Gamma, \\ [\alpha\nabla\cdot\boldsymbol{\Psi}] &= 0 \text{ on } \Gamma. \end{cases} \tag{5.4.11}$$

Then, due to Remark 5.2.2, $\boldsymbol{\Psi}$ satisfies following apriori estimate

$$\|\boldsymbol{\Psi}\|_{1,\Omega_1} + \|\boldsymbol{\Psi}\|_{1,\Omega_2} + \|\nabla\cdot\boldsymbol{\Psi}\|_{1,\Omega_1} + \|\nabla\cdot\boldsymbol{\Psi}\|_{1,\Omega_2} \leq C\|\mathbf{e}_0\|. \tag{5.4.12}$$

Moreover, we recalls the definitions of $\mathcal{B}_h$ and interpolation operator Π_h (see, 2.3.19) and Lemma 2.3.4 from the Chapter 2.

Lemma 5.4.3. *For any $\boldsymbol{\phi} \in \mathcal{B}_h$, we have*

$$(\alpha\nabla_w\cdot\mathbf{e}_h, \nabla\cdot\boldsymbol{\phi}) + (\gamma\mathbf{e}_0, \boldsymbol{\phi}) = 0.$$

Proof. Testing equation (5.1.1) against $\boldsymbol{\phi}$, using the definitions of L^2 projections and Lemma 5.3.2 yield

$$\begin{aligned} (\mathbf{f}, \boldsymbol{\phi}) &= -(\nabla(\alpha\nabla\cdot\mathbf{p}), \boldsymbol{\phi}) - \sum_{T\in\mathcal{T}_h}\langle\alpha\nabla\cdot\mathbf{p}, \boldsymbol{\phi}\rangle_{\partial T} + (\gamma\mathbf{p}, \boldsymbol{\phi}) \\ &= (\alpha\nabla_w\cdot(\mathbf{Q}_h\mathbf{p}), \nabla\cdot\boldsymbol{\phi}) - \langle\psi, \boldsymbol{\phi}\cdot\boldsymbol{\eta}\rangle_\Gamma - \langle\phi, \alpha\nabla\cdot\boldsymbol{\phi}\rangle_\Gamma + (\gamma\mathbf{Q}_0^k\mathbf{p}, \boldsymbol{\phi}) \end{aligned} \tag{5.4.13}$$

Next, we set $\boldsymbol{\phi}_h = \{\boldsymbol{\phi}_0, \boldsymbol{\phi}_b\} \in \mathbf{V}_h^0$, where $\boldsymbol{\phi}_0 = \boldsymbol{\phi}$ and $\boldsymbol{\phi}_b = (\boldsymbol{\phi}\cdot\boldsymbol{\eta})\boldsymbol{\eta}$, and note that $\nabla_w\cdot\boldsymbol{\phi}_h = \nabla\cdot\boldsymbol{\phi}$.

Then by putting $\mathbf{v}_h = \boldsymbol{\phi}_h$ in (5.4.1), we get

$$(\mathbf{f}, \boldsymbol{\phi}) = (\alpha\nabla_w\cdot\mathbf{u}_h, \nabla\cdot\boldsymbol{\phi}) + (\gamma\mathbf{u}_0, \boldsymbol{\phi}) - \langle\psi, \boldsymbol{\phi}\cdot\boldsymbol{\eta}\rangle_\Gamma - \langle\phi, \alpha\nabla\cdot\boldsymbol{\phi}\rangle_\Gamma. \tag{5.4.14}$$

Finally, equations (5.4.13)-(5.4.14) leads to the desired result. □

Theorem 5.4.2. *Let $\mathbf{p} \in [H^{k+1}(\Omega_i)]^d$ with $i = 1, 2$ be the exact solution for* (5.1.1)-(5.1.3) *and $\mathbf{p}_h \in \mathbf{V}_h^0$ be the WG solution for* (5.4.1)*. Then, we have*

$$\|\mathbf{Q}_0^k\mathbf{p} - \mathbf{p}_h\| \leq Ch^{k+1} \left(\|\mathbf{p}\|_{k+1,\Omega_1} + \|\mathbf{p}\|_{k+1,\Omega_2}\right). \tag{5.4.15}$$

Proof. Testing first equation in (5.4.11) with $\mathbf{e}_0$ gives rise to

$$\begin{aligned}(\mathbf{e}_0,\mathbf{e}_0) &= -(\nabla(\alpha\nabla\cdot\boldsymbol{\psi}),\mathbf{e}_0)+(\gamma\boldsymbol{\psi},\mathbf{e}_0)\\ &= (\alpha\nabla\cdot\boldsymbol{\psi},\nabla\cdot\mathbf{e}_0)-\sum_{T\in\mathcal{T}_h}\langle\alpha\nabla\cdot\boldsymbol{\psi},(\mathbf{e}_0-\mathbf{e}_b)\cdot\boldsymbol{\eta}\rangle_{\partial T}+(\gamma\boldsymbol{\psi},\mathbf{e}_0),\\ &= (\alpha\nabla\cdot\boldsymbol{\psi},\nabla_w\cdot\mathbf{e}_h)+(\gamma\boldsymbol{\psi},\mathbf{e}_0)\\ &- \sum_{T\in\mathcal{T}_h}\langle\alpha\nabla\cdot\boldsymbol{\psi}-\mathbb{Q}_h^{k-1}(\alpha\nabla\cdot\boldsymbol{\psi}),(\mathbf{e}_0-\mathbf{e}_b)\cdot\boldsymbol{\eta}\rangle_{\partial T}, \end{aligned}\tag{5.4.16}$$

where we have used the fact that $\sum_{T\in\mathcal{T}_h}\langle\alpha\nabla\cdot\boldsymbol{\psi},\mathbf{e}_b\cdot\boldsymbol{\eta}\rangle_{\partial T}=0$. Further, using Lemma 5.4.3 with $\boldsymbol{\phi}=\Pi_h\mathbf{p}$ in the equation (5.4.16), we obtain

$$\begin{aligned}\|\mathbf{e}_0\|^2 &= (\alpha\nabla\cdot(\boldsymbol{\psi}-\Pi_h\boldsymbol{\psi}),\nabla_w\cdot\mathbf{e}_h)+(\gamma(\boldsymbol{\psi}-\Pi_h\boldsymbol{\psi}),\mathbf{e}_0)\\ &\quad-\sum_{T\in\mathcal{T}_h}\langle\alpha\nabla\cdot\boldsymbol{\psi}-\mathbb{Q}_h^{k-1}(\alpha\nabla\cdot\boldsymbol{\psi}),(\mathbf{e}_0-\mathbf{e}_b)\cdot\boldsymbol{\eta}\rangle_{\partial T}\\ &\le C\|\boldsymbol{\psi}-\Pi_h\boldsymbol{\psi}\|_{1,\mathbf{div}}|||\mathbf{e}_h|||\\ &+ \sum_{T\in\mathcal{T}_h}\|\alpha\nabla\cdot\boldsymbol{\psi}-\mathbb{Q}_h^{k-1}(\alpha\nabla\cdot\boldsymbol{\psi})\|_{\partial T}\|\mathbf{e}_0-\mathbf{e}_b\|_{\partial T}\end{aligned}\tag{5.4.17}$$

Next, from trace inequality (2.2.7) and inverse inequality (2.2.8), we derive that

$$\begin{aligned}h_T\|\alpha\nabla\cdot\boldsymbol{\psi}-\mathbb{Q}_h^{k-1}(\alpha\nabla\cdot\boldsymbol{\psi})\|_{\partial T}^2 &\le C\|\alpha\nabla\cdot\boldsymbol{\psi}-\mathbb{Q}_h^{k-1}(\alpha\nabla\cdot\boldsymbol{\psi})\|_T^2\\ &\le Ch^2\|\alpha\nabla\cdot\boldsymbol{\psi}\|_1^2\\ &\le Ch^2\|\alpha\|_{1,\infty}\|\boldsymbol{\psi}\|_{1,\mathbf{div}}^2,\end{aligned}\tag{5.4.18}$$

which together with estimate (5.4.17), Lemma 2.2.1, Lemma 5.3.1 and a priori estimate (5.4.12) yield

$$\begin{aligned}\|\mathbf{e}_0\|^2 &\le Ch\|\boldsymbol{\psi}\|_{1,\mathbf{div}}|||\mathbf{e}_h|||+Ch^{k+1}\|\mathbf{p}\|_{k+1}\|\boldsymbol{\psi}\|_{1,\mathbf{div}}\\ &\le Ch\|\mathbf{e}_0\|\,|||\mathbf{e}_h|||+Ch^{k+1}\|\mathbf{p}\|_{k+1}\|\mathbf{e}_0\|.\end{aligned}$$

Finally, Theorem 5.4.1 leads to the desired result. □

5.5 Numerical Experiments

The main objective of the present section is to numerically validate the accuracy and robustness of the aforementioned WG approximation by solving specific standard $\mathbf{H}(\mathrm{div})$-elliptic interface problems in $\mathbb{R}^d$ $(d=2,\ 3)$. To demonstrate high-order convergence, we consider different kinds of Lipschitz continuous interfaces with complex structures in 2D

model problems with sufficiently smooth analytical/exact solutions. Further, numerical studies for non-convex geometries in 3D and low global regular solutions justify the robustness of the WG method. For the detailed discussions on computational procedure, we refer to [28, 36, 87]

Example 5.5.1. We consider the 5-point star-shape interface embedded in $\Omega = (-1, 1)^2$. The two subdomains and interface are shown in Figure 5.5.1 (left). The coefficients are chosen to be $\alpha = x + 4$, $\gamma = 2$ in Ω_1 and $\alpha = y + 4$, $\gamma = 1$ in Ω_2. The analytical solution $\mathbf{p} = (p_1, p_2)$ is selected as

$$p_1 = \begin{cases} x - y^2 + 10 & \text{for } (x, y) \in \Omega_1, \\ \exp(x)\cos(\pi y) & \text{for } (x, y) \in \Omega_2, \end{cases}$$

and

$$p_2 = \begin{cases} 10 - y^2 - x^2 & \text{for } (x, y) \in \Omega_1, \\ \sin(\pi y)\sin(\pi x) & \text{for } (x, y) \in \Omega_2, \end{cases}$$

where p_1 is taken from [103]. The non-uniform triangular meshes (see, initial mesh Figure 5.5.1 (right)) aligned with interface Γ have been taken for the WG algorithm. The numerical errors with respect to L^2 norm and discrete H^1 norm are reported in Table 5.5.1. For mesh level 6 and $k = 2$, component-wise analytical solution (left) and WG solution (right) are shown in Figures 5.5.2-5.5.3, which indeed shows that numerical solution does not differ from the analytical solution.

Figure 5.5.1: The interface and subdomains (left) and the initial mesh (right) in Example 5.5.1.

Example 5.5.2. We next consider a 5-petals flower shape interface in the domain $\Omega = (-3, 3)^2$, whose parametric equation is given as

$$\begin{cases} x(\theta) = (\sin(5\theta) + 1.5)\cos\theta, \\ y(\theta) = (\sin(5\theta) + 1.5)\sin\theta, \end{cases}$$

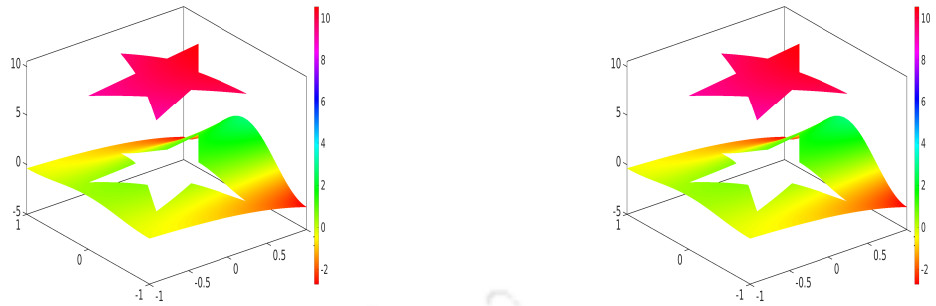

Figure 5.5.2: (Example 5.5.1) Surface plots for first component of analytical solution (left) and WG solution (right).

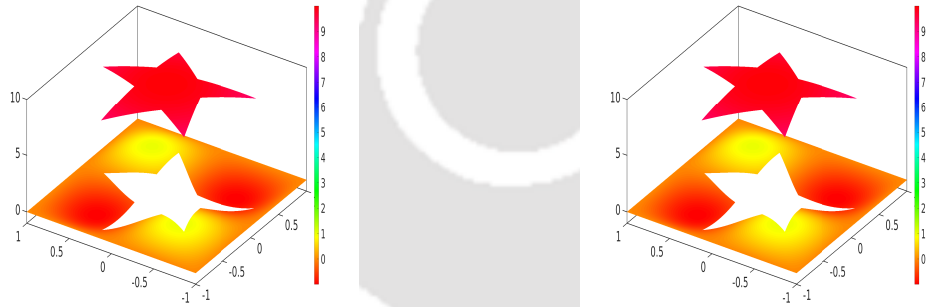

Figure 5.5.3: (Example 5.5.1) Surface plots for second component of analytical solution (left) and WG solution (right).

for $\theta = [0, 2\pi]$. The subdomains and interface are demonstrated in Figure 5.5.4 (left). In our example, the coefficients are taken as $\alpha = (x^2 - y^2 + 3)^2/7$ and $\gamma = x^2 + 1$ in Ω_1, and $\alpha = (xy+2)^2/5$ and $\gamma = y^2+1$ in Ω_2. The exact solution $\mathbf{p} = (p_1, p_2)$ is set as [103]

$$p_1 = \begin{cases} 10 + \cos(x+y) + \sin(x+y) & \text{for } (x,y) \in \Omega_1, \\ y + x + 1 & \text{for } (x,y) \in \Omega_2, \end{cases}$$

and

$$p_2 = \begin{cases} \sin(\pi(x+y)) + 15 & \text{for } (x,y) \in \Omega_1, \\ y^2 + x^2 - 10 & \text{for } (x,y) \in \Omega_2. \end{cases}$$

A finite sequence of non-uniform triangular meshes (see, initial mesh 5.5.4 (right)) aligned with interface Γ have been taken for the WG algorithm. The numerical errors are reported in Table 5.5.2, which demonstrates the high-order optimal convergence rate

Table 5.5.1: Convergence and error profiles for the Example 5.5.1.

k	Level	h	$\|\mathbf{e}_0\|$	Order	$\|\|\|\mathbf{e}_h\|\|\|$	Order
	1	4.876e-01	3.88e-01	—	1.45e+00	—
	2	2.43e-01	9.81e-02	1.98	7.20e-01	1.01
	3	1.21e-01	2.45e-02	2.00	3.58e-01	1.00
1	4	6.09e-02	6.13e-03	2.00	1.78e-01	1.00
	5	3.04e-02	1.53e-03	2.00	8.94e-02	1.00
	6	1.52e-02	3.83e-04	2.00	4.46e-02	1.00
	1	4.87e-01	8.82e-02	—	5.06e-01	—
	2	2.43e-01	1.14e-02	2.94	1.33e-01	1.92
	3	1.21e-01	1.44e-03	2.98	3.37e-02	1.98
2	4	6.09e-02	1.80e-04	2.99	8.47e-03	1.99
	5	3.04e-02	2.25e-05	2.99	2.12e-03	1.99
	6	1.52e-02	2.82e-06	2.99	5.30e-04	1.99
3	1	4.876e-01	1.896e-02	—	1.289e-01	—
	2	2.438e-01	1.254e-03	3.91	1.715e-02	2.91
	3	1.219e-01	7.945e-05	3.98	2.179e-03	2.97
	4	6.095e-02	4.981e-06	3.99	2.735e-04	2.99
	5	3.047e-02	3.115e-07	3.99	3.423e-05	2.99
	6	1.523e-02	1.947e-08	3.99	4.280e-06	2.99
4	1	4.876e-01	3.296e-03	—	2.545e-02	—
	2	2.438e-01	1.092e-04	4.91	1.687e-03	3.91
	3	1.219e-01	3.463e-06	4.97	1.070e-04	3.97
	4	6.095e-02	1.086e-07	4.99	6.714e-06	3.99
	5	3.047e-02	3.398e-09	4.99	4.200e-07	3.99
	6	1.523e-02	1.064e-10	4.99	2.626e-08	3.99

of the WG method for solving the model interface problems. For mesh level 5 and $k = 2$ component-wise surface plots of the exact solution (left) and WG solution (right) are shown in Figures 5.5.5-5.5.6.

Example 5.5.3. Next consider the interface Γ with parametric equation is taken as [103]

$$\begin{cases} y(t) = r(t)\sin(\theta(t)), \\ x(t) = r(t)\cos(\theta(t)), \end{cases}$$

where

$$r(t) = 0.2401256\cos(4t + \pi/2) + 0.6012563,\ \theta = \sin(4t) + t.$$

Domain Ω and its subdomains Ω_1 and Ω_2 along with interface Γ are illustrated in Figure

Figure 5.5.4: The interface and subdomains (left) and the initial mesh (right) in Example 5.5.2.

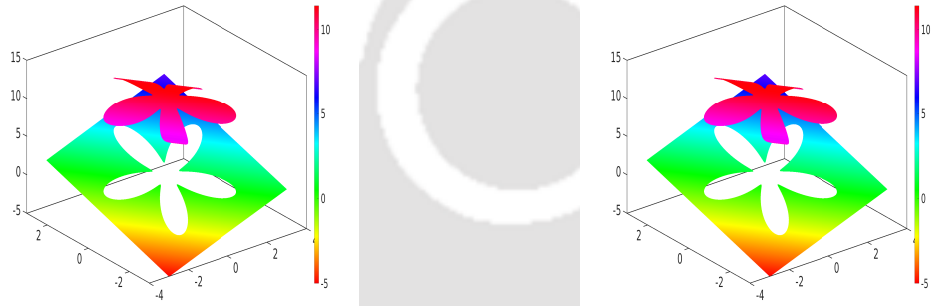

Figure 5.5.5: (Example 5.5.2) Surface plots for first component of exact solution (left) and WG solution (right).

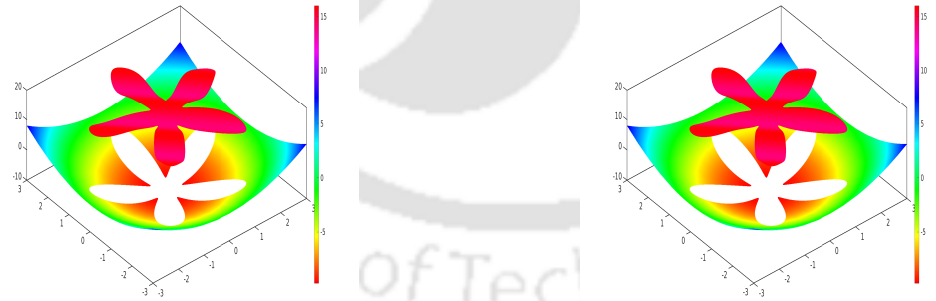

Figure 5.5.6: (Example 5.5.2) Surface plots for second component of exact solution (left) and WG solution (right).

5.5.7 (left). The analytical solution $\mathbf{p} = (p_1, p_2)$ is chosen as

$$p_1 = \begin{cases} \exp(x)\cos(y) & \text{for } (x,y) \in \Omega_1, \\ 0 & \text{for } (x,y) \in \Omega_2, \end{cases}$$

Table 5.5.2: Convergence and error profiles for the Example 5.5.2.

k	Level	h	$\|\mathbf{e}_0\|$	Order	$\|\|\|\mathbf{e}_h\|\|\|$	Order
2	1	2.54e-01	7.77e-02	—	4.45e-01	—
	2	1.27e-01	1.03e-02	2.90	1.19e-01	1.89
	3	6.36e-02	1.31e-03	2.98	3.04e-02	1.97
	4	3.18e-02	1.65e-04	2.99	7.65e-03	1.99
	5	1.59e-02	2.06e-05	2.99	1.91e-03	1.99
	6	7.95e-03	2.58e-06	3.00	4.79e-04	1.99
3	1	2.54e-01	1.84e-02	—	1.25e-01	—
	2	1.27e-01	1.24e-03	3.88	1.69e-02	2.89
	3	6.36e-02	7.94e-05	3.97	2.16e-03	2.97
	4	3.18e-02	4.98e-06	3.99	2.71e-04	2.99
	5	1.59e-02	3.11e-07	3.99	3.39e-05	2.99
	6	7.95e-03	1.94e-08	3.99	4.25e-06	2.99

and

$$p_2 = \begin{cases} \cos(\pi(x+y))^2 + \sin(\pi(x+y))^2 & \text{for } (x,y) \in \Omega_1, \\ 0 & \text{for } (x,y) \in \Omega_2. \end{cases}$$

The coefficients are set as $\alpha = 1+x^2+y^2$ and $\gamma = x+3$ in Ω_1, and $\alpha = 1000$ and $\gamma = y+3$ in Ω_2. The non-uniform triangular meshes (see, initial mesh Figure 5.5.7 (right)) aligned with interface Γ have been taken for the WG algorithm. The numerical errors are listed in Table 5.5.3. From this example, we observed the high-order optimal convergence in the case of high-contrast coefficients. For the elliptic interface problem, for $k = 1$ WG-FEM has been implemented in [103]. For mesh level 6 and $k = 3$ component-wise surface plots of analytical solution (left) and WG solution (right) are shown in Figures 5.5.8-5.5.9.

Figure 5.5.7: The interface and subdomains (left) and the initial mesh (right) in Example 5.5.3.

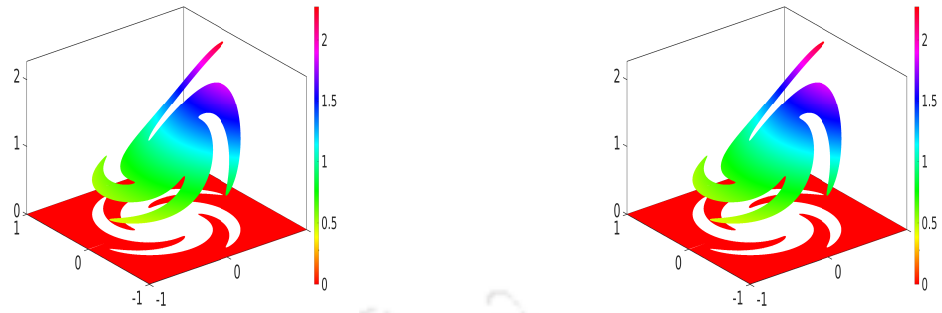

Figure 5.5.8: (Example 5.5.3) Surface plots for first component of analytical solution (left) and WG solution (right).

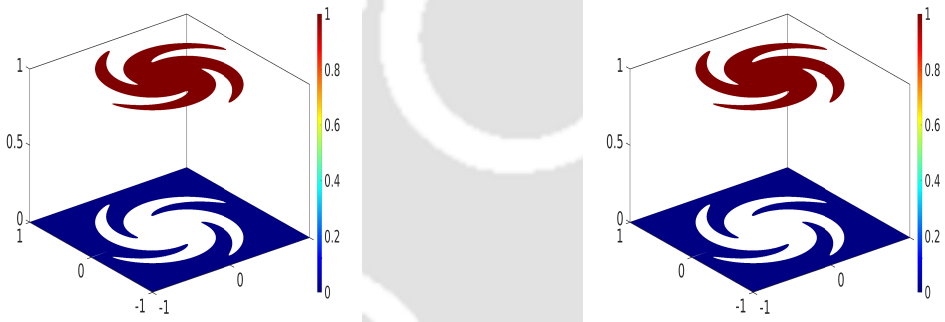

Figure 5.5.9: (Example 5.5.3) Surface plots for second component of analytical solution (left) and WG solution (right).

Table 5.5.3: Convergence and error profiles for the Example 5.5.3.

k	Level	h	$\|\mathbf{e}_0\|$	Order	$\|\|\|\mathbf{e}_h\|\|\|$	Order
3	1	1.82e-01	2.68e-04	—	1.83e-03	—
	2	9.13e-02	1.69e-05	3.98	2.31e-04	2.99
	3	4.56e-02	1.06e-06	3.99	2.89e-05	2.99
	4	2.28e-02	6.65e-08	3.99	3.62e-06	2.99
	5	1.14e-02	4.15e-09	4.00	4.53e-07	2.99
4	1	1.82e-01	6.55e-06	—	5.10e-05	—
	3	9.13e-02	2.21e-07	4.88	3.42e-06	3.89
	3	4.56e-02	7.05e-09	4.97	2.17e-07	3.97
	4	2.28e-02	2.21e-10	4.99	1.36e-08	3.99
	5	1.14e-02	7.07e-12	4.96	8.59e-10	3.98

Example 5.5.4. Consider the cardioid as an interface embedded in $\Omega = (-1, 1)^2$, whose

parametric equation is defined as

$$\begin{cases} x(t) = 1/4 + 2a(1-\cos\theta)\cos\theta, \\ y(t) = 2a(1-\cos\theta)\sin\theta, \end{cases}$$

with $a = 1/6$. The shape of the two subdomains and cardioid are shown in Figure 5.5.10 (left). The analytical solution $\mathbf{p} = (p_1, p_2)$ is set to be

$$p_1 = \begin{cases} 5\exp(y^2+x^2) & \text{for } (x,y) \in \Omega_1, \\ \cos(y+x)\sin(y+x) & \text{for } (x,y) \in \Omega_2, \end{cases}$$

and

$$p_2 = \begin{cases} 5 + 5(y^2+x^2) & \text{for } (x,y) \in \Omega_1, \\ y^2 + x^2 + \sin(y+x) & \text{for } (x,y) \in \Omega_2. \end{cases}$$

The coefficients are taken as

$$\alpha = \begin{cases} x^3 + y^2 + 1 & \text{for } (x,y) \in \Omega_1, \\ y^2 + x^4 + 3 & \text{for } (x,y) \in \Omega_2, \end{cases}$$

and

$$\gamma = \begin{cases} (y+3)(x+4) & \text{for } (x,y) \in \Omega_1, \\ y^2 + 2 & \text{for } (x,y) \in \Omega_2. \end{cases}$$

For mesh level 6 and $k = 4$, component-wise analytical solution (left) and WG solution (right) surface plots are shown in Figures 5.5.11-5.5.12. A finite sequence of non-uniform triangular meshes (see, initial mesh 5.5.10 (right)) aligned with interface Γ have been taken for the WG algorithm. The L^2 errors and discrete H^1 errors of WG algorithm are reported in Table 5.5.4

Example 5.5.5. We consider a L-shaped type interface in three-dimensional domain $\Omega = (0,1)^3$. The two subdomain Ω_1, Ω_2 and interface are depicted in Figure 5.5.13. The exact solution $\mathbf{p} = (p_1, p_2, p_3)$ is taken as

$$p_1 = \begin{cases} zyx\sin(\pi y)\sin(\pi x) & \text{for } (x,y,z) \in \Omega_1, \\ zyx(1-z)(1-y)(1-x)r^{-2+c} & \text{for } (x,y,z) \in \Omega_2, \end{cases}$$

Figure 5.5.10: The interface and subdomains (left) and the initial mesh (right) in Example 5.5.4.

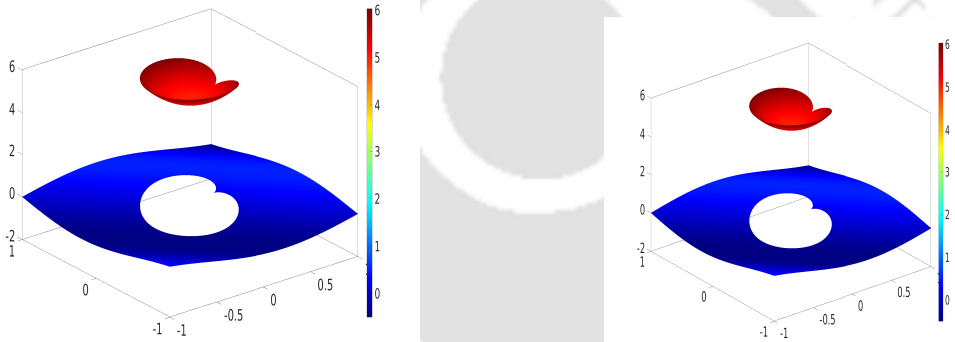

Figure 5.5.11: (Example 5.5.4) Surface plots for first component of analytical solution (left) and WG solution (right).

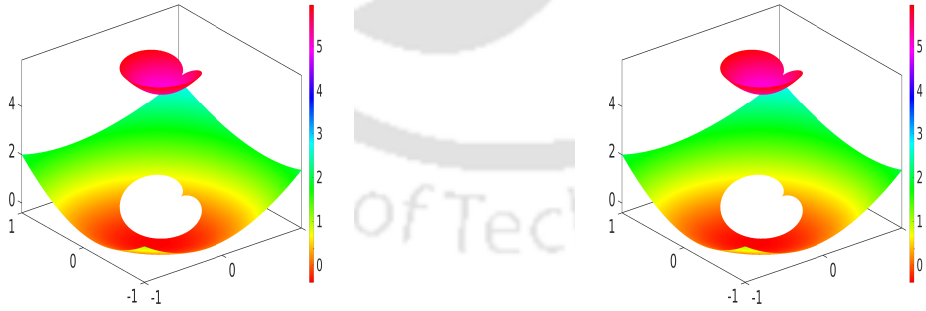

Figure 5.5.12: (Example 5.5.4) Surface plots for second component of analytical solution (left) and WG solution (right).

$$p_2 = \begin{cases} \exp(xyz)\cos(\pi z)\sin(\pi x) & \text{for } (x,y,z) \in \Omega_1, \\ \sin(\pi(z+y+x)) + \cos(\pi(z+y+x)) + 3 & \text{for } (x,y,z) \in \Omega_2, \end{cases}$$

Table 5.5.4: Convergence and error profiles for the Example 5.5.4.

k	Level	h	$\|\mathbf{e}_0\|$	Order	$\|\|\|\mathbf{e}_h\|\|\|$	Order
3	1	2.15e-01	6.17e-02	—	4.22e-01	—
	2	1.07e-01	4.57e-03	3.75	6.17e-02	2.77
	3	5.39e-02	2.99e-04	3.93	8.09e-03	2.93
	4	2.69e-02	1.89e-05	3.98	1.02e-03	2.98
	5	1.34e-02	1.18e-06	3.99	1.28e-04	2.99
	6	6.74e-03	7.42e-08	3.99	1.60e-05	2.99
4	1	2.15e-01	9.62e-03	—	7.48e-02	—
	2	1.07e-01	3.75e-04	4.67	5.77e-03	3.69
	3	5.39e-02	1.25e-05	4.90	3.84e-04	3.91
	4	2.69e-02	3.97e-07	4.97	2.44e-05	3.97
	5	1.34e-02	1.24e-08	4.99	1.53e-06	3.99
	6	6.74e-03	3.99e-10	4.96	9.58e-08	3.99

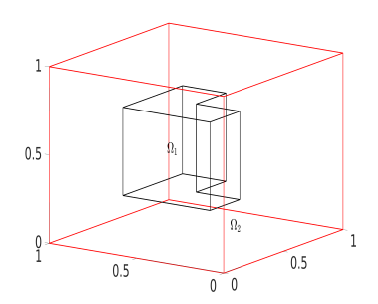

Figure 5.5.13: The interface and subdomains in Example 5.5.5.

and

$$p_3 = \begin{cases} zx(1-x)(1-z)r^{-2+c} & \text{for } (x,y,z) \in \Omega_1, \\ yz(1-y)(1-z) & \text{for } (x,y,z) \in \Omega_2, \end{cases}$$

where, $r = (x^2+y^2)^{\frac{1}{2}}$ and $c \in (0,1]$. The coefficients are set to be $\alpha = \gamma = 1$ in Ω. Note that, $\mathbf{p} \in [H^{1+c-\epsilon}(\Omega)]^3$, where ϵ is a very small positive real number. Here, the suitable WG-space is $([\mathcal{P}_1]^3, [\mathcal{P}_1]^3, \mathcal{P}_0)$. We test this example with different values of $c = 1/4,\ 1/2,\ 2/3,\ 4/5$. The convergence and error results are shown in Table 5.5.5. It is evident from Table 5.5.5 that the accuracy decreases as c tends to zero. In addition, we select higher order WG-space i.e., $([\mathcal{P}_2]^3, [\mathcal{P}_2]^3, \mathcal{P}_1)$, with $c = 1/4,\ 4/5$. Since, the regularity of the exact solution is $[H^{1+c-\epsilon}(\Omega)]^3$. So for any $k \geq 1$, we shall obtain the same convergence rates corresponding to H^1 norm and L^2 norm. The Table 5.5.5 justify the theoretical results.

Table 5.5.5: Convergence and error profiles for the Example 5.5.5.

c	Level	$1/h$	$\|\mathbf{e}_0\|$	Order	$\|\|\|\mathbf{e}_h\|\|\|$	Order
$\frac{1}{4}$	1	4	7.69e-01	—	3.34e+00	—
	2	8	3.47e-01	1.14	2.97e+00	0.16
	3	16	1.49e-01	1.21	2.55e+00	0.21
	4	32	6.33e-02	1.23	2.16e+00	0.23
	5	64	2.67e-02	1.24	1.82e+00	0.24
	6	128	1.12e-02	1.24	1.54e+00	0.24
$\frac{1}{2}$	1	4	3.74e-01	—	1.64e+00	—
	2	8	1.41e-01	1.40	1.22e+00	0.42
	3	16	5.13e-02	1.46	8.89e-01	0.46
	4	32	1.83e-02	1.48	6.37e-01	0.48
	5	64	6.51e-03	1.49	4.53e-01	0.49
	6	128	2.31e-03	1.49	3.21e-01	0.49
$\frac{2}{3}$	1	4	2.45e-01	—	1.07e+00	—
	2	8	8.13e-02	1.56	7.10e-01	0.59
	3	16	2.63e-02	1.62	4.58e-01	0.62
	4	32	8.42e-03	1.64	2.93-01	0.64
	5	64	2.68e-03	1.64	1.87e-01	0.65
	6	128	8.52e-04	1.65	1.18e-01	0.65
$\frac{4}{5}$	1	4	6.92e-02	—	4.57e-01	—
	2	8	2.05e-02	1.74	2.72e-01	0.74
	3	16	5.97e-03	1.78	1.58e-01	0.78
	4	32	1.72e-03	1.79	9.16e-02	0.79
	5	64	4.96e-04	1.80	5.28e-02	0.80
	6	128	1.42e-04	1.80	3.03e-02	0.80

6

WG-FEMs for H(curl,div)-Elliptic Interface Problems

We are concerned with the weak Galerkin (WG) finite element methods for the two dimensional (2D) and three dimensional (3D) $\mathbf{H}(\text{curl}, \text{div})$-elliptic interface problems. The WG algorithm allows the general meshes such as hybrid meshes, polygonal/polyhedral meshes and meshes with hanging nodes. Optimal order error estimates are established for the discrete energy norm and L^2 norm. In addition, we have also performed some numerical experiments for the model $\mathbf{H}(\text{curl}, \text{div})$-elliptic problems in 2D and 3D with complicated interfaces to validate the theoretical estimates.

6.1 Introduction

We shall begin with first recalling the $\mathbf{H}(\text{curl}, \text{div})$-elliptic interface model problem of the form

$$\nabla \times (\beta \nabla \times \mathbf{p}) - \nabla(\alpha \nabla \cdot \mathbf{p}) + \gamma \mathbf{p} = \mathbf{f} \text{ in } \Omega, \tag{6.1.1}$$

$$\nabla \cdot \mathbf{p} = 0, \quad \mathbf{p} \times \boldsymbol{\eta} = \mathbf{0} \text{ on } \partial\Omega, \tag{6.1.2}$$

$$[\mathbf{p} \times \boldsymbol{\eta}] = \boldsymbol{\rho}, \quad [(\beta \nabla \times \mathbf{p}) \times \boldsymbol{\eta}] = \boldsymbol{\chi} \text{ on } \Gamma, \tag{6.1.3}$$

$$[\mathbf{p} \cdot \boldsymbol{\eta}] = \phi, \quad [\alpha \nabla \cdot \mathbf{p}] = \psi \text{ on } \Gamma, \tag{6.1.4}$$

where Ω is a polygonal/polyhedral domain in $\mathbb{R}^d (d = 2,\ 3)$ with Lipschitz boundary $\partial\Omega$ and $\Omega_1 \subset \Omega$ is an open domain with C^2 smooth boundary $\Gamma = \partial\Omega_1$ and $\Omega_2 = \Omega \backslash \Omega_1$ (see Fig. 1.1.1 for an illustration). Other symbols and notations are as defined in Chapter 1. Setting $\zeta \in \{\alpha, \beta, \gamma\}$, we assume that there exist two constants $p_1,\ p_2$ with $0 < p_1 \leq p_2$ such that $p_1 \leq \zeta \leq p_2$ a.e. in Ω and $\mathbf{f} \in \left[L^2(\Omega)\right]^d$. Further, the coefficient functions are assumed to be discontinuous along Γ and we write

$$\zeta = \begin{cases} \zeta_1 \text{ in } \Omega_1, \\ \zeta_2 \text{ in } \Omega_2. \end{cases} \tag{6.1.5}$$

H(curl, div)-elliptic interface problems are non-standard elliptic problems occurs in various areas of electromagnetism and fluid-structure interaction problems. In electromagnetism, vector potential Maxwell's problem can be derived from **H**(curl, div)-elliptic equation (for details see [15, 31]). In fluid-structure, grad-div elliptic problem with curl free constraint can be obtained from **H**(curl, div)-elliptic equation, a model reads as (see [100]). Finite element method for **H**(curl, div)-elliptic interface problem with homogenous jump conditions have been discussed in [50]. However, as per our literature survey, there has been no work in FEMs for **H**(curl, div)-elliptic interface problem with non-homogenous jump conditions for general polygonal (in 2D)/polyhedral (in 3D) meshes.

In this chapter, we have discussed the WG-FEM for **H**(curl, div)-elliptic interface problem with non-homogenous jump conditions. In this study, we consider the typical local weak Galerkin space $\Big(\big[\mathcal{P}_k(T)\big]^d,\ \big[\mathcal{P}_k(\partial T)\big]^d,\ [\mathcal{P}_{k-1}(T)]^{2d-3},\ \mathcal{P}_{k-1}(T)\Big)$. Error estimates of the optimal orders in both L^2 norm and energy norm have been established for WG algorithm. To justify the theoretical results, we have performed several numerical experiments with some complicated interfaces geometries. In addition, we have also performed the numerical tests with low global regular solutions to validate the convergence results, flexibility, and accuracy of the WG algorithm.

The layout of this chapter is as follows. A weak Galerkin discretization, discrete curl and divergence operators and L^2 projections will be introduced in Section 6.2. WG algorithm and convergence analysis for discrete energy norm will be presented in the Section 6.3. In Section 6.4, we will discuss the error estimate for L^2 norm by using duality argument. We conduct the several numerical tests to justify the accuracy and efficiency of the proposed WG algorithm in Section 6.5.

6.2 Weak Galerkin Methodology

In this section, the weak Galerkin algorithm has been derived for the interface problem (6.1.1)-(6.1.4). First, we have adopted the fitted finite element partitions $\mathcal{T}_h$ of the domain Ω from the Chapter 5. Next, for each integer $k \geq 1$, we recall the weak Galerkin (WG) finite element spaces based on the partition $\mathcal{T}_h$ form the Chapter 3 defined as

$$\mathbf{V}_h = \{\mathbf{v}_h = \{\mathbf{v}_0, \mathbf{v}_b\} : \mathbf{v}_0|_T \in [\mathcal{P}_k(T)]^d,\ \mathbf{v}_b|_e \in [\mathcal{P}_k(e)]^d,\ e \in \partial T,\ T \in \mathcal{T}_h\}$$

and

$$\mathbf{V}_h^0 = \{\mathbf{v}_h = \{\mathbf{v}_0, \mathbf{v}_b\} \in \mathbf{V}_h : \mathbf{v}_b \times \boldsymbol{\eta} = \mathbf{0} \ \text{ on } \ \partial\Omega\}.$$

Next, we introduce following two bilinear maps

$$\begin{aligned}\mathcal{S}_1(\mathbf{w}_h,\mathbf{v}_h) &= \sum_{T\in\mathcal{T}_h} h^{-1}\langle(\mathbf{w}_0-\mathbf{w}_b)\cdot\boldsymbol{\eta},(\mathbf{v}_0-\mathbf{v}_b)\cdot\boldsymbol{\eta}\rangle_{\partial T},\\ \mathcal{S}_2(\mathbf{w}_h,\mathbf{v}_h) &= \sum_{T\in\mathcal{T}_h} h^{-1}\langle(\mathbf{w}_0-\mathbf{w}_b)\times\boldsymbol{\eta},(\mathbf{v}_0-\mathbf{v}_b)\times\boldsymbol{\eta}\rangle_{\partial T}.\end{aligned}$$

Based on above two stabilizers, we define an another bilinear map

$$\begin{aligned}\mathcal{A}(\mathbf{w}_h,\mathbf{v}_h) &= (\alpha\nabla_w\cdot\mathbf{w}_h,\nabla_w\cdot\mathbf{v}_h)+(\beta\nabla_w\times\mathbf{w}_h,\nabla_w\times\mathbf{v}_h)\\ &+ \mathcal{S}_1(\mathbf{w}_h,\mathbf{v}_h)+\mathcal{S}_2(\mathbf{w}_h,\mathbf{v}_h)+(\gamma\mathbf{w}_0,\mathbf{v}_0)\quad\forall\mathbf{w}_h,\mathbf{v}_h\in\mathbf{V}_h^0.\end{aligned}$$

For the discrete curl and discrete divergence operators, we refer to Chapter 3.

Now, we introduce triple-bar norm on $\mathbf{V}_h^0$ given as follows

$$\begin{aligned}|||\mathbf{v}_h|||^2 &= \sum_{T\in\mathcal{T}_h}\|\alpha^{\frac{1}{2}}\nabla_w\cdot\mathbf{v}_h\|_T^2+\sum_{T\in\mathcal{T}_h}\|\beta^{\frac{1}{2}}\nabla_w\times\mathbf{v}_h\|_T^2+\|\gamma^{\frac{1}{2}}\mathbf{v}_0\|_T^2\\ &+\sum_{T\in\mathcal{T}_h}h^{-1}\|(\mathbf{v}_0-\mathbf{v}_b)\cdot\boldsymbol{\eta}\|_{\partial T}^2+\sum_{T\in\mathcal{T}_h}h^{-1}\|(\mathbf{v}_0-\mathbf{v}_b)\times\boldsymbol{\eta}\|_{\partial T}^2\\ &=\mathcal{A}(\mathbf{v}_h,\mathbf{v}_h)\ \ \forall\mathbf{v}_h\in\mathbf{V}_h^0.\end{aligned}\tag{6.2.1}$$

For each $T\in\mathcal{T}_h$ and $e\in\mathcal{E}_h$, we define the local L^2 projections given as follows:

$$\mathbf{Q}_0^k:[L^2(T)]^d\to[\mathcal{P}_k(T)]^d,\ \ \mathbb{Q}_h^{k-1}:L^2(T)\to\mathcal{P}_{k-1}(T),$$

$$\boldsymbol{\mathcal{Q}}_h^{k-1}:[L^2(T)]^{2d-3}\to[\mathcal{P}_{k-1}(T)]^{2d-3}\ \&\ \ \mathbf{Q}_b^k:[L^2(e)]^d\to[\mathcal{P}_k(e)]^d.$$

In addition, for $\mathbf{w}\in[H^1(T)]^d$, we define $\mathbf{Q}_h\mathbf{w}=\{\mathbf{Q}_0^k\mathbf{w},\mathbf{Q}_b^k\mathbf{w}\}$. Now, we review some approximations results for $\mathbf{Q}_0^k$, $\boldsymbol{\mathcal{Q}}_h^{k-1}$, and $\mathbb{Q}_h^{k-1}$, which will be necessary for the later analysis.

Lemma 6.2.1. *(cf. [102, 121]). For* $\mathbf{w}\in[H^{s+1}(\Omega)]^d$, *we have*

$$\sum_{T\in\mathcal{T}_h}\|\mathbb{Q}_h^{k-1}(\nabla\cdot\mathbf{w})-\nabla\cdot\mathbf{w}\|_T^2\le h^{2s}\|\mathbf{w}\|_{s+1}^2,\tag{6.2.2}$$

$$\sum_{T\in\mathcal{T}_h}\|\mathbf{Q}_0^k\mathbf{w}-\mathbf{w}\|_T^2\le h^{2(s+1)}\|\mathbf{w}\|_{s+1}^2,\tag{6.2.3}$$

$$\sum_{T\in\mathcal{T}_h}\|\boldsymbol{\mathcal{Q}}_h^{k-1}(\nabla\times\mathbf{w})-\nabla\times\mathbf{w}\|_T^2\le h^{2s}\|\mathbf{w}\|_{s+1}^2,\tag{6.2.4}$$

where $1\le s\le k$.

Weak Galerkin Algorithm. A WG approximation for (6.1.1)-(6.1.4) can be acquired by seeking $\mathbf{p}_h = \{\mathbf{p}_0, \mathbf{p}_b\} \in \mathbf{V}_h^0$ such that

$$\begin{aligned}\mathcal{A}(\mathbf{p}_h, \mathbf{v}_h) &= (\mathbf{f}, \mathbf{v}_0) + \langle \psi, \mathbf{v}_b \cdot \boldsymbol{\eta}\rangle_\Gamma + \langle \phi, \alpha \nabla_w \cdot \mathbf{v}_h\rangle_\Gamma + \langle \boldsymbol{\chi}, \mathbf{v}_b\rangle_\Gamma \\ &\quad -h^{-1}\langle \phi, (\mathbf{v}_0 - \mathbf{v}_b)\cdot\boldsymbol{\eta}\rangle_\Gamma + h^{-1}\langle (\boldsymbol{\rho}\times\boldsymbol{\eta})\times\boldsymbol{\eta}, (\mathbf{v}_0 - \mathbf{v}_b)\times\boldsymbol{\eta}\rangle_\Gamma \\ &\quad +\langle (\boldsymbol{\rho}\times\boldsymbol{\eta})\times\boldsymbol{\eta}, \beta\nabla_w \times \mathbf{v}_h\rangle_\Gamma, \end{aligned} \tag{6.2.5}$$

for all $\mathbf{v}_h = \{\mathbf{v}_0, \mathbf{v}_b\} \in \mathbf{V}_h^0$.

6.3 Error Analysis

In this section, we shall discuss error equation and derive optimal order error estimates in discrete energy norm.

For $e \notin \Gamma_h$ be shared edges/flat-faces by two elements T_1 and T_2, $\mathbf{p}|_{T_1\cap e} = \mathbf{p}|_{T_2\cap e}$. Therefore, $\mathbf{Q}_b^k\mathbf{p}$ is a single valued function on each $e \notin \Gamma_h$ and $\mathbf{Q}_h\mathbf{p} = \{\mathbf{Q}_0^k\mathbf{p}, \mathbf{Q}_b^k\mathbf{p}\} \in \mathbf{V}_h$. If $e \in \Gamma_h$, $\mathbf{p}|_{T_1\cap e} \neq \mathbf{p}|_{T_2\cap e}$ with $T_1 \subset \Omega_1$ and $T_2 \subset \Omega_2$. Note that $\mathbf{Q}_b^k\mathbf{p}$ is single valued on each $e \in \Gamma_h$, which follows from the following definition

$$\mathbf{Q}_b^k\mathbf{p} = \begin{cases} \mathbf{Q}_b^k(\mathbf{p}|_{T\cap e}) & \text{if} \quad e \in \Gamma \ \&\ T \subset \Omega_1, \\ \mathbf{Q}_b^k(\mathbf{p}|_{T\cap e}) + \mathbf{Q}_b^k\bar{\boldsymbol{g}} & \text{if} \quad e \in \Gamma \ \&\ T \subset \Omega_2, \\ \mathbf{Q}_b^k(\mathbf{p}|_{T\cap e}) & \text{if} \quad e \notin \Gamma \ \&\ T \in \mathcal{T}_h, \end{cases} \tag{6.3.1}$$

where $\bar{\boldsymbol{g}} = \phi\boldsymbol{\eta} - \boldsymbol{\rho}\times\boldsymbol{\eta}$.

Remark 6.3.1. For a vector function $\mathbf{p}$, we can write $\mathbf{p} = (\mathbf{p}\cdot\boldsymbol{\eta})\boldsymbol{\eta} + \boldsymbol{\eta}\times(\mathbf{p}\times\boldsymbol{\eta})$. Let $T_1 \subset \Omega_1$ and $T_2 \subset \Omega_2$ are two interface elements having a common edge/flat-face $e \in \mathcal{E}_h^0$. Then, using interface conditions $[\mathbf{p}\times\mathbf{n}] = \boldsymbol{\rho}$ in (6.1.3) and $[\mathbf{p}\cdot\mathbf{n}] = \phi$ in (6.1.4), we get

$$[\mathbf{p}] = \mathbf{p}|_{\Omega_1} - \mathbf{p}|_{\Omega_2} = \bar{\boldsymbol{g}}.$$

Now, from the definition (6.3.1), we have

$$\begin{aligned}(\mathbf{Q}_b^k\mathbf{p})|_{T_1\cap e} - (\mathbf{Q}_b^k\mathbf{p})|_{T_2\cap e} &= \mathbf{Q}_b^k(\mathbf{p}|_{T_1\cap e}) - \mathbf{Q}_b^k(\mathbf{p}|_{T_2\cap e}) - \mathbf{Q}_b^k\bar{\boldsymbol{g}} \\ &= \mathbf{Q}_b^k(\mathbf{p}|_{T_1\cap e} - \mathbf{p}|_{T_2\cap e}) - \mathbf{Q}_b^k\bar{\boldsymbol{g}} \\ &= \mathbf{Q}_b^k\bar{\boldsymbol{g}} - \mathbf{Q}_b^k\bar{\boldsymbol{g}} = \mathbf{0}. \end{aligned}$$

From above equation, we observe that $\mathbf{Q}_h\mathbf{p} \in \mathbf{V}_h$.

Next, result sets relation between two projection operators $\mathbf{Q}_h$ and $\mathbb{Q}_h^{k-1}$.

Lemma 6.3.1. *For each element $T \in \mathcal{T}_h$, the following properties hold true*

$$(\nabla_w \cdot \mathbf{Q}_h\mathbf{p}, q)_T = (\mathbb{Q}_h^{k-1}(\nabla \cdot \mathbf{p}), q)_T \ \ \forall T \in \mathcal{T}_1, \tag{6.3.2}$$

$$(\nabla_w \cdot \mathbf{Q}_h\mathbf{p}, q)_T = (\mathbb{Q}_h^{k-1}(\nabla \cdot \mathbf{p}), q)_T + \langle \phi, q\rangle_{\partial T\cap\Gamma} \ \ \forall T \in \mathcal{T}_2, \tag{6.3.3}$$

for all $q \in \mathcal{P}_{k-1}(T)$.

Proof. For each $T \in \mathcal{T}_1$, we get

$$\begin{aligned}(\nabla_w \cdot \mathbf{Q}_h\mathbf{p}, q)_T &= -\left(\mathbf{Q}_0^k\mathbf{p}, \nabla q\right)_T + \langle (\mathbf{Q}_b^k\mathbf{p})\cdot\boldsymbol{\eta}, q\rangle_{\partial T}\\ &= -(\mathbf{p}, \nabla q)_T + \langle \mathbf{p}\cdot\boldsymbol{\eta}, q\rangle_{\partial T}\\ &= (\nabla\cdot\mathbf{p}, q)_T = \left(\mathbb{Q}_h^{k-1}(\nabla\cdot\mathbf{p}), q\right)_T,\end{aligned}$$

and for any $T \in \mathcal{T}_2$, we reach at

$$\begin{aligned}(\nabla_w \cdot \mathbf{Q}_h\mathbf{p}, q)_T &= -\left(\mathbf{Q}_0^k\mathbf{p}, \nabla q\right)_T + \langle (\mathbf{Q}_b^k\mathbf{p})\cdot\boldsymbol{\eta}, q\rangle_{\partial T}\\ &= -(\mathbf{p}, \nabla q)_T + \langle \mathbf{p}\cdot\boldsymbol{\eta}, q\rangle_{\partial T} + \langle \bar{\boldsymbol{g}}\cdot\boldsymbol{\eta}, q\rangle_{\partial T\cap\Gamma}\\ &= (\nabla\cdot\mathbf{p}, q)_T + \langle (\phi\boldsymbol{\eta} - \boldsymbol{\rho}\times\boldsymbol{\eta})\cdot\boldsymbol{\eta}, q\rangle_{\partial T\cap\Gamma}\\ &= (\mathbb{Q}_h^{k-1}(\nabla\cdot\mathbf{p}), q)_T + \langle \phi, q\rangle_{\partial T\cap\Gamma}.\end{aligned}$$

This completes the Lemma 6.3.1. □

Lemma 6.3.2. *For each element $T \in \mathcal{T}_h$, the following properties hold true*

$$\begin{aligned}(\nabla_w \times \mathbf{Q}_h\mathbf{p}, \mathbf{q})_T &= (\boldsymbol{\mathcal{Q}}_h^{k-1}(\nabla\times\mathbf{p}), \mathbf{q})_T \ \ \forall T \in \mathcal{T}_1,\\ (\nabla_w \times \mathbf{Q}_h\mathbf{p}, \mathbf{q})_T &= (\boldsymbol{\mathcal{Q}}_h^{k-1}(\nabla\times\mathbf{p}), \mathbf{q})_T + \langle (\boldsymbol{\rho}\times\boldsymbol{\eta})\times\boldsymbol{\eta}, \mathbf{q}\rangle_{\partial T\cap\Gamma} \ \ \forall T \in \mathcal{T}_2,\end{aligned}$$

for all $\mathbf{q} \in [\mathcal{P}_{k-1}(T)]^{2d-3}$.

Proof. For each $T \in \mathcal{T}_1$, we obtain

$$\begin{aligned}(\nabla_w \times \mathbf{Q}_h\mathbf{p}, \mathbf{q})_T &= (\mathbf{Q}_0^k\mathbf{p}, \nabla\times\mathbf{q})_T - \langle (\mathbf{Q}_b^k\mathbf{p})\times\boldsymbol{\eta}, \mathbf{q}\rangle_{\partial T}\\ &= (\mathbf{p}, \nabla\times\mathbf{q})_T - \langle \mathbf{p}\times\boldsymbol{\eta}, \mathbf{q}\rangle_{\partial T}\\ &= (\nabla\times\mathbf{p}, \mathbf{q})_T = (\boldsymbol{\mathcal{Q}}_h^{k-1}(\nabla\times\mathbf{p}), \mathbf{q})_T,\end{aligned}$$

and for any $T \in \mathcal{T}_2$, we have

$$\begin{aligned}(\nabla_w \times \mathbf{Q}_h\mathbf{p}, \mathbf{q})_T &= (\mathbf{Q}_0^k\mathbf{p}, \nabla\times\mathbf{q})_T - \langle (\mathbf{Q}_b^k\mathbf{p})\times\boldsymbol{\eta}, \mathbf{q}\rangle_{\partial T}\\ &= (\mathbf{p}, \nabla\times\mathbf{q})_T - \langle \mathbf{p}\times\boldsymbol{\eta}, \mathbf{q}\rangle_{\partial T} - \langle \bar{\boldsymbol{g}}\times\boldsymbol{\eta}, \mathbf{q}\rangle_{\partial T\cap\Gamma}\\ &= (\nabla\times\mathbf{p}, \mathbf{q})_T - \langle (\phi\boldsymbol{\eta} - \boldsymbol{\rho}\times\boldsymbol{\eta})\times\boldsymbol{\eta}, \mathbf{q}\rangle_{\partial T\cap\Gamma}\\ &= (\boldsymbol{\mathcal{Q}}_h^{k-1}(\nabla\times\mathbf{p}), \mathbf{q})_T + \langle (\boldsymbol{\rho}\times\boldsymbol{\eta})\times\boldsymbol{\eta}, \mathbf{q}\rangle_{\partial T\cap\Gamma}.\end{aligned}$$

This completes the Lemma 6.3.2. □

Next, we define the following error function

$$\mathbf{e}_h = \{\mathbf{e}_0, \mathbf{e}_b\} := \mathbf{Q}_h\mathbf{p} - \mathbf{p}_h.$$

Lemma 6.3.3. *For each* $\mathbf{v}_h \in \mathbf{V}_h^0$, *we have*

$$\mathcal{A}(\mathbf{e}_h, \mathbf{v}_h) = -\mathcal{R}_1(\mathbf{p}, \mathbf{v}_h) - \mathcal{R}_2(\mathbf{p}, \mathbf{v}_h) - \mathcal{R}_3(\mathbf{p}, \mathbf{v}_h) - \mathcal{R}_4(\mathbf{p}, \mathbf{v}_h) := \mathcal{R}_5(\mathbf{p}, \mathbf{v}_h). \quad (6.3.4)$$

Proof. For any $\mathbf{v}_h = \{\mathbf{v}_0, \mathbf{v}_b\} \in \mathbf{V}_h^0$, we test (6.1.1) with $\mathbf{v}_0$ to get

$$(\nabla \times (\beta\nabla \times \mathbf{p}), \mathbf{v}_0) - (\nabla(\alpha\nabla \cdot \mathbf{p}), \mathbf{v}_0) + (\gamma\mathbf{p}, \mathbf{v}_0) = (\mathbf{f}, \mathbf{v}_0). \quad (6.3.5)$$

Now, from Lemma 6.3.2, we reach at

$$\begin{aligned}
&(\nabla \times (\beta\nabla \times \mathbf{p}), \mathbf{v}_0)\\
&= \sum_{T\in\mathcal{T}_h} (\beta\nabla \times \mathbf{p}, \nabla \times \mathbf{v}_0)_T - \sum_{T\in\mathcal{T}_h} (\langle \mathbf{v}_0 - \mathbf{v}_b, (\beta\nabla \times \mathbf{p}) \times \boldsymbol{\eta}\rangle_{\partial T} + \langle (\beta\nabla \times \mathbf{p}) \times \boldsymbol{\eta}, \mathbf{v}_b\rangle_{\partial T})\\
&= \sum_{T\in\mathcal{T}_h} (\beta\nabla \times \mathbf{p}, \nabla \times \mathbf{v}_0)_T - \sum_{T\in\mathcal{T}_h} \langle \beta\nabla \times \mathbf{p}, (\mathbf{v}_b - \mathbf{v}_0) \times \boldsymbol{\eta}\rangle_{\partial T} - \langle \boldsymbol{\chi}, \mathbf{v}_b\rangle_\Gamma\\
&\quad - \sum_{T\in\mathcal{T}_h} \langle \beta\nabla \times \mathbf{p} - \beta\boldsymbol{\mathcal{Q}}_h^{k-1}(\nabla \times \mathbf{p}), (\mathbf{v}_b - \mathbf{v}_0) \times \boldsymbol{\eta}\rangle_{\partial T}\\
&= \sum_{T\in\mathcal{T}_h} (\beta\nabla_w \times \mathbf{Q}_h\mathbf{p}, \nabla_w \times \mathbf{v}_h)_T - \langle \boldsymbol{\chi}, \mathbf{v}_b\rangle_\Gamma - \langle (\boldsymbol{\rho} \times \boldsymbol{\eta}) \times \boldsymbol{\eta}, \beta\nabla_w \times \mathbf{v}_h\rangle_\Gamma\\
&\quad - \sum_{T\in\mathcal{T}_h} \langle \beta\nabla \times \mathbf{p} - \beta\boldsymbol{\mathcal{Q}}_h^{k-1}(\nabla \times \mathbf{p}), (\mathbf{v}_b - \mathbf{v}_0) \times \boldsymbol{\eta}\rangle_{\partial T}\\
&= \sum_{T\in\mathcal{T}_h} (\beta\nabla_w \times \mathbf{Q}_h\mathbf{p}, \nabla_w \times \mathbf{v}_h)_T - \mathcal{R}_1(\mathbf{p}, \mathbf{v}_h)\\
&\quad - \langle \boldsymbol{\chi}, \mathbf{v}_b\rangle_\Gamma - \langle (\boldsymbol{\rho} \times \boldsymbol{\eta}) \times \boldsymbol{\eta}, \beta\nabla_w \times \mathbf{v}_h\rangle_\Gamma. \quad (6.3.6)
\end{aligned}$$

Next, Lemma 6.3.1 yields

$$\begin{aligned}
&-(\nabla(\alpha\nabla \cdot \mathbf{p}), \mathbf{v}_0)\\
&= \sum_{T\in\mathcal{T}_h} (\alpha\nabla \cdot \mathbf{p}, \nabla \cdot \mathbf{v}_0)_T - \sum_{T\in\mathcal{T}_h} \langle \alpha\nabla \cdot \mathbf{p}, (\mathbf{v}_0 - \mathbf{v}_b) \cdot \boldsymbol{\eta}\rangle_{\partial T} - \langle \alpha\nabla \cdot \mathbf{p}, \mathbf{v}_b \cdot \boldsymbol{\eta}\rangle_{\partial T}\\
&= \sum_{T\in\mathcal{T}_h} (\alpha\nabla \cdot \mathbf{p}, \nabla \cdot \mathbf{v}_0)_T - \sum_{T\in\mathcal{T}_h} \langle \alpha\nabla \cdot \mathbf{p}, (\mathbf{v}_0 - \mathbf{v}_b) \cdot \boldsymbol{\eta}\rangle_{\partial T} - \langle \psi, \mathbf{v}_b \cdot \boldsymbol{\eta}\rangle_\Gamma\\
&= \sum_{T\in\mathcal{T}_h} (\alpha\nabla_w \cdot \mathbf{Q}_h\mathbf{p}, \nabla_w \cdot \mathbf{v}_h)_T - \langle \psi, \mathbf{v}_b \cdot \boldsymbol{\eta}\rangle_\Gamma - \langle \phi, \alpha\nabla_w \cdot \mathbf{v}_h\rangle_\Gamma\\
&\quad - \sum_{T\in\mathcal{T}_h} \langle \alpha\nabla \cdot \mathbf{p} - \alpha\mathbb{Q}_h^{k-1}(\nabla \cdot \mathbf{p}), (\mathbf{v}_0 - \mathbf{v}_b) \cdot \boldsymbol{\eta}\rangle_{\partial T}\\
&= \sum_{T\in\mathcal{T}_h} (\alpha\nabla_w \cdot \mathbf{Q}_h\mathbf{p}, \nabla_w \cdot \mathbf{v}_h)_T - \mathcal{R}_2(\mathbf{p}, \mathbf{v}_h) - \langle \psi, \mathbf{v}_b \cdot \boldsymbol{\eta}\rangle_\Gamma\\
&\quad - \langle \phi, \alpha\nabla_w \cdot \mathbf{v}_h\rangle_\Gamma. \quad (6.3.7)
\end{aligned}$$

By substituting (6.3.6) and (6.3.7) in (6.3.5), we get

$$\begin{aligned}&\sum_{T\in\mathcal{T}_h}(\alpha\nabla_w\times\mathbf{Q}_h\mathbf{p},\nabla_w\times\mathbf{v}_h)_T+\sum_{T\in\mathcal{T}_h}(\beta\nabla_w\cdot\mathbf{Q}_h\mathbf{p},\nabla_w\cdot\mathbf{v}_h)_T+(\gamma\mathbf{Q}_0^k\mathbf{p},\mathbf{v}_0)\\&=(\mathbf{f},\mathbf{v}_0)+\mathcal{R}_1(\mathbf{p},\mathbf{v}_h)+\mathcal{R}_2(\mathbf{p},\mathbf{v}_h)+\langle\psi,\mathbf{v}_b\cdot\boldsymbol{\eta}\rangle_\Gamma\\&\quad+\langle\phi,\alpha\nabla_w\cdot\mathbf{v}_h\rangle_\Gamma+\langle\boldsymbol{\chi},\mathbf{v}_b\rangle_\Gamma+\langle(\boldsymbol{\rho}\times\boldsymbol{\eta})\times\boldsymbol{\eta},\beta\nabla_w\times\mathbf{v}_h\rangle_\Gamma.\end{aligned}\tag{6.3.8}$$

Now, for any $T\in\mathcal{T}_1$, we have

$$\langle(\mathbf{Q}_0^k\mathbf{p}-\mathbf{Q}_b^k\mathbf{p})\cdot\boldsymbol{\eta},(\mathbf{v}_0-\mathbf{v}_b)\cdot\boldsymbol{\eta}\rangle_{\partial T}=\langle(\mathbf{Q}_0^k\mathbf{p}-\mathbf{Q}_b^k(\mathbf{p}|_T))\cdot\boldsymbol{\eta},(\mathbf{v}_0-\mathbf{v}_b)\cdot\boldsymbol{\eta}\rangle_{\partial T},$$

and for each $T\in\mathcal{T}_2$, we obtain

$$\begin{aligned}&\langle(\mathbf{Q}_0^k\mathbf{p}-\mathbf{Q}_b^k\mathbf{p})\cdot\boldsymbol{\eta},(\mathbf{v}_0-\mathbf{v}_b)\cdot\boldsymbol{\eta}\rangle_{\partial T}\\&=\langle(\mathbf{Q}_0^k\mathbf{p}-\mathbf{Q}_b^k(\mathbf{p}|_T))\cdot\boldsymbol{\eta},(\mathbf{v}_0-\mathbf{v}_b)\cdot\boldsymbol{\eta}\rangle_{\partial T}-\langle\bar{\boldsymbol{g}}\cdot\boldsymbol{\eta},(\mathbf{v}_0-\mathbf{v}_b)\cdot\boldsymbol{\eta}\rangle_{\partial T\cap\Gamma}\\&=\langle(\mathbf{Q}_0^k\mathbf{p}-\mathbf{Q}_b^k(\mathbf{p}|_T))\cdot\boldsymbol{\eta},(\mathbf{v}_0-\mathbf{v}_b)\cdot\boldsymbol{\eta}\rangle_{\partial T}-\langle\phi,(\mathbf{v}_0-\mathbf{v}_b)\cdot\boldsymbol{\eta}\rangle_{\partial T\cap\Gamma}.\end{aligned}$$

Next, we combine the above two equations to get

$$\begin{aligned}&\mathcal{S}_1(\mathbf{Q}_h\mathbf{p},\mathbf{v}_h)\\&=\sum_{T\in\mathcal{T}_h}h^{-1}\langle(\mathbf{Q}_0^k\mathbf{p}-\mathbf{Q}_b^k(\mathbf{p}|_T))\cdot\boldsymbol{\eta},(\mathbf{v}_0-\mathbf{v}_b)\cdot\boldsymbol{\eta}\rangle_{\partial T}-h^{-1}\langle\phi,(\mathbf{v}_0-\mathbf{v}_b)\cdot\boldsymbol{\eta}\rangle_\Gamma\\&=\mathcal{R}_3(\mathbf{p},\mathbf{v}_h)-h^{-1}\langle\phi,(\mathbf{v}_0-\mathbf{v}_b)\cdot\boldsymbol{\eta}\rangle_\Gamma.\end{aligned}\tag{6.3.9}$$

Now, for each $T\in\mathcal{T}_1$, we get

$$\langle(\mathbf{Q}_0^k\mathbf{p}-\mathbf{Q}_b^k\mathbf{p})\times\boldsymbol{\eta},(\mathbf{v}_0-\mathbf{v}_b)\times\boldsymbol{\eta}\rangle_{\partial T}=\langle(\mathbf{Q}_0^k\mathbf{p}-\mathbf{Q}_b^k(\mathbf{p}|_T))\times\boldsymbol{\eta},(\mathbf{v}_0-\mathbf{v}_b)\times\boldsymbol{\eta}\rangle_{\partial T},$$

and for each $T\in\mathcal{T}_2$, we have

$$\begin{aligned}&\langle(\mathbf{Q}_0^k\mathbf{p}-\mathbf{Q}_b^k\mathbf{p})\times\boldsymbol{\eta},(\mathbf{v}_0-\mathbf{v}_b)\times\boldsymbol{\eta}\rangle_{\partial T}\\&=\langle(\mathbf{Q}_0^k\mathbf{p}-\mathbf{Q}_b^k(\mathbf{p}|_T))\times\boldsymbol{\eta},(\mathbf{v}_0-\mathbf{v}_b)\times\boldsymbol{\eta}\rangle_{\partial T}-\langle\bar{\boldsymbol{g}}\times\boldsymbol{\eta},(\mathbf{v}_0-\mathbf{v}_b)\times\boldsymbol{\eta}\rangle_{\partial T\cap\Gamma}\\&=\langle(\mathbf{Q}_0^k\mathbf{p}-\mathbf{Q}_b^k(\mathbf{p}|_T))\times\boldsymbol{\eta},(\mathbf{v}_0-\mathbf{v}_b)\times\boldsymbol{\eta}\rangle_{\partial T}+\langle(\boldsymbol{\rho}\times\boldsymbol{\eta})\times\boldsymbol{\eta},(\mathbf{v}_0-\mathbf{v}_b)\times\boldsymbol{\eta}\rangle_{\partial T\cap\Gamma}.\end{aligned}$$

Next, we combine the above two equations to get

$$\begin{aligned}\mathcal{S}_2(\mathbf{Q}_h\mathbf{p},\mathbf{v}_h)&=\sum_{T\in\mathcal{T}_h}h^{-1}\langle(\mathbf{Q}_0^k\mathbf{p}-\mathbf{Q}_b^k(\mathbf{p}|_T))\times\boldsymbol{\eta},(\mathbf{v}_0-\mathbf{v}_b)\times\boldsymbol{\eta}\rangle_{\partial T}\\&\quad+h^{-1}\langle(\boldsymbol{\rho}\times\boldsymbol{\eta})\times\boldsymbol{\eta},(\mathbf{v}_0-\mathbf{v}_b)\times\boldsymbol{\eta}\rangle_\Gamma\\&=\mathcal{R}_4(\mathbf{p},\mathbf{v}_h)+h^{-1}\langle(\boldsymbol{\rho}\times\boldsymbol{\eta})\times\boldsymbol{\eta},(\mathbf{v}_0-\mathbf{v}_b)\times\boldsymbol{\eta}\rangle_\Gamma.\end{aligned}\tag{6.3.10}$$

From (6.3.8), (6.3.9), and (6.3.10), we have

$$\begin{aligned}\mathcal{A}(\mathbf{Q}_h\mathbf{p},\mathbf{v}_h) &= (\mathbf{f},\mathbf{v}_0)+\mathcal{R}_1(\mathbf{p},\mathbf{v}_h)+\mathcal{R}_2(\mathbf{p},\mathbf{v}_h)+\mathcal{R}_3(\mathbf{p},\mathbf{v}_h)+\mathcal{R}_4(\mathbf{p},\mathbf{v}_h)\\ &\quad+\langle\psi,\mathbf{v}_b\cdot\boldsymbol{\eta}\rangle_\Gamma+\langle\phi,\alpha\nabla_w\cdot\mathbf{v}_h\rangle_\Gamma+\langle\boldsymbol{\chi},\mathbf{v}_b\rangle_\Gamma\\ &\quad-h^{-1}\langle\phi,(\mathbf{v}_0-\mathbf{v}_b)\cdot\boldsymbol{\eta}\rangle_\Gamma+h^{-1}\langle(\boldsymbol{\rho}\times\boldsymbol{\eta})\times\boldsymbol{\eta},(\mathbf{v}_0-\mathbf{v}_b)\times\boldsymbol{\eta}\rangle_\Gamma\\ &\quad+\langle(\boldsymbol{\rho}\times\boldsymbol{\eta})\times\boldsymbol{\eta},\beta\nabla_w\times\mathbf{v}_h\rangle_\Gamma. \qquad (6.3.11)\end{aligned}$$

Now, subtraction of (6.2.5) form (6.3.11) implies (6.3.4). This completes the Lemma 6.3.3. □

Lemma 6.3.4. *For* $\mathbf{p}\in[H^{k+1}(\Omega_i)]^d$ $(i=1,2)$ *and for each* $\mathbf{v}_h=\{\mathbf{v}_0,\mathbf{v}_b\}\in\mathbf{V}_h^0$, *we have*

$$|\mathcal{R}_l(\mathbf{p},\mathbf{v}_h)|\le Ch^k\left(\|\mathbf{p}\|_{k+1,\Omega_1}+\|\mathbf{p}\|_{k+1,\Omega_2}\right)|||\mathbf{v}_h|||,\quad 1\le l\le 4. \qquad (6.3.12)$$

Proof. From trace inequality (2.2.7) and Cauchy-Schwarz inequality, we obtain

$$\begin{aligned}|\mathcal{R}_1(\mathbf{p},\mathbf{v}_h)| &= \left|\sum_{T\in\mathcal{T}_h}\langle\beta(\nabla\times\mathbf{p}-\boldsymbol{\mathcal{Q}}_h^{k-1}(\nabla\times\mathbf{p})),(\mathbf{v}_b-\mathbf{v}_0)\times\boldsymbol{\eta}\rangle_{\partial T}\right|\\ &\le C\sum_{T\in\mathcal{T}_h}\|\nabla\times\mathbf{p}-\boldsymbol{\mathcal{Q}}_h^{k-1}(\nabla\times\mathbf{p})\|_{\partial T}\|(\mathbf{v}_b-\mathbf{v}_0)\times\boldsymbol{\eta}\|_{\partial T}\\ &\le \left(\sum_{T\in\mathcal{T}_h}h_T\|\nabla\times\mathbf{p}-\boldsymbol{\mathcal{Q}}_h^{k-1}(\nabla\times\mathbf{p})\|_{\partial T}^2\right)^{\frac12}\\ &\quad\times\left(\sum_{T\in\mathcal{T}_h}h_T^{-1}\|(\mathbf{v}_b-\mathbf{v}_0)\times\boldsymbol{\eta}\|_{\partial T}^2\right)^{\frac12}\\ &\le Ch^k\left(\|\mathbf{p}\|_{k+1,\Omega_1}+\|\mathbf{p}\|_{k+1,\Omega_2}\right)|||\mathbf{v}_h|||,\end{aligned}$$

and by using the definition of $\mathbb{Q}_h^{k-1}$, we get

$$\begin{aligned}|\mathcal{R}_2(\mathbf{p},\mathbf{v}_h)| &= \left|\sum_{T\in\mathcal{T}_h}\langle\alpha(\nabla\cdot\mathbf{p}-\mathbb{Q}_h^{k-1}(\nabla\cdot\mathbf{p})),(\mathbf{v}_0-\mathbf{v}_b)\cdot\boldsymbol{\eta}\rangle_{\partial T}\right|\\ &\le C\sum_{T\in\mathcal{T}_h}\|\alpha(\nabla\cdot\mathbf{p}-\mathbb{Q}_h^{k-1}(\nabla\cdot\mathbf{p}))\|_{\partial T}\|(\mathbf{v}_0-\mathbf{v}_b)\cdot\boldsymbol{\eta}\|_{\partial T}\\ &\le \left(\sum_{T\in\mathcal{T}_h}h_T\|\alpha(\nabla\cdot\mathbf{p}-\mathbb{Q}_h^{k-1}(\nabla\cdot\mathbf{p}))\|_{\partial T}^2\right)^{\frac12}\\ &\quad\times\left(\sum_{T\in\mathcal{T}_h}h_T^{-1}\|(\mathbf{v}_0-\mathbf{v}_b)\cdot\boldsymbol{\eta}\|_{\partial T}^2\right)^{\frac12}\\ &\le Ch^k\left(\|\mathbf{p}\|_{k+1,\Omega_1}+\|\mathbf{p}\|_{k+1,\Omega_2}\right)|||\mathbf{v}_h|||.\end{aligned}$$

Similarly, using the definition of $\mathbf{Q}_b^k$, we get

$$\begin{aligned}
|\mathcal{R}_3(\mathbf{p},\mathbf{v}_h)| &= \left|\sum_{T\in\mathcal{T}_h} h^{-1}\langle(\mathbf{Q}_0^k\mathbf{p}-\mathbf{Q}_b^k(\mathbf{p}|_T))\cdot\boldsymbol{\eta},(\mathbf{v}_0-\mathbf{v}_b)\cdot\boldsymbol{\eta}\rangle_{\partial T}\right| \\
&= \left|\sum_{T\in\mathcal{T}_h} h^{-1}\langle(\mathbf{Q}_0^k\mathbf{p}\cdot\boldsymbol{\eta}-\mathbf{Q}_b^k\mathbf{p}\cdot\boldsymbol{\eta},(\mathbf{v}_0-\mathbf{v}_b)\cdot\boldsymbol{\eta}\rangle_{\partial T}\right| \\
&\le \left|\sum_{T\in\mathcal{T}_h} h_T^{-1}\langle(\mathbf{Q}_0^k\mathbf{p}-\mathbf{p})\cdot\boldsymbol{\eta},(\mathbf{v}_0-\mathbf{v}_b)\cdot\boldsymbol{\eta}\rangle_{\partial T}\right| \\
&\le \sum_{T\in\mathcal{T}_h} h_T^{-1}\|(\mathbf{Q}_0^k\mathbf{p}-\mathbf{p})\cdot\boldsymbol{\eta}\|_{\partial T}\|(\mathbf{v}_0-\mathbf{v}_b)\cdot\boldsymbol{\eta}\|_{\partial T} \\
&\le C\left(\sum_{T\in\mathcal{T}_h}(h_T^{-2}\|\mathbf{Q}_0^k\mathbf{p}-\mathbf{p}\|_T^2+\|\nabla(\mathbf{Q}_0^k\mathbf{p}-\mathbf{p})\|_T^2)\right)^{\frac{1}{2}} \\
&\quad\times\left(\sum_{T\in\mathcal{T}_h} h_T^{-1}\|(\mathbf{v}_0-\mathbf{v}_b)\cdot\boldsymbol{\eta}\|_{\partial T}^2\right)^{\frac{1}{2}} \\
&\le Ch^k\left(\|\mathbf{p}\|_{k+1,\Omega_1}+\|\mathbf{p}\|_{k+1,\Omega_2}\right)|||\mathbf{v}_h|||,
\end{aligned}$$

and

$$\begin{aligned}
|\mathcal{R}_4(\mathbf{p},\mathbf{v}_h)| &= \left|\sum_{T\in\mathcal{T}_h} h^{-1}\langle(\mathbf{Q}_0^k\mathbf{p}-\mathbf{Q}_b^k(\mathbf{p}|_T))\times\boldsymbol{\eta},(\mathbf{v}_0-\mathbf{v}_b)\times\boldsymbol{\eta}\rangle_{\partial T}\right| \\
&\le \left|\sum_{T\in\mathcal{T}_h} h_T^{-1}\langle(\mathbf{Q}_0^k\mathbf{p}-\mathbf{Q}_b^k\mathbf{p})\times\boldsymbol{\eta},(\mathbf{v}_0-\mathbf{v}_b)\times\boldsymbol{\eta}\rangle_{\partial T}\right| \\
&\le \sum_{T\in\mathcal{T}_h} h_T^{-1}\|(\mathbf{Q}_0^k\mathbf{p}-\mathbf{p})\times\boldsymbol{\eta}\|_{\partial T}\|(\mathbf{v}_0-\mathbf{v}_b)\times\boldsymbol{\eta}\|_{\partial T} \\
&\le C\left(\sum_{T\in\mathcal{T}_h} h_T^{-1}\|(\mathbf{Q}_0^k\mathbf{p}-\mathbf{p})\times\boldsymbol{\eta}\|_{\partial T}^2\right)^{\frac{1}{2}} \\
&\quad\times\left(\sum_{T\in\mathcal{T}_h} h_T^{-1}\|(\mathbf{v}_0-\mathbf{v}_b)\times\boldsymbol{\eta}\|_{\partial T}^2\right)^{\frac{1}{2}} \\
&\le Ch^k\left(\|\mathbf{p}\|_{k+1,\Omega_1}+\|\mathbf{p}\|_{k+1,\Omega_2}\right)|||\mathbf{v}_h|||.
\end{aligned}$$

This completes the proof. □

Then Lemmas 6.3.3-6.3.4 lead to the following result.

Theorem 6.3.1. *Let* $\mathbf{p}\in[H^{k+1}(\Omega_i)]^d$ $(i=1,2)$ *be the exact solution for* (6.1.1)-(6.1.4) *and* $\mathbf{p}_h\in\mathbf{V}_h^0$ *be the WG-solution for* (6.2.5)*. Then, we have*

$$|||\mathbf{Q}_h\mathbf{p}-\mathbf{p}_h|||\le Ch^k\left(\|\mathbf{p}\|_{k+1,\Omega_1}+\|\mathbf{p}\|_{k+1,\Omega_2}\right). \tag{6.3.13}$$

6.4 L^2 norm Error Analysis

This section deals with the optimal L^2 norm error estimate, which is based on duality principle.

For this purpose, we consider the following auxiliary problem

$$\begin{aligned}
\nabla \times (\beta \nabla \times \boldsymbol{\psi}) - \nabla(\alpha \nabla \cdot \boldsymbol{\psi}) + \gamma \boldsymbol{\psi} &= \mathbf{e}_0, && (6.4.1)\\
\boldsymbol{\psi} \times \boldsymbol{\eta} = 0, \quad \nabla \cdot \boldsymbol{\psi} &= 0 \quad \text{on} \quad \partial\Omega, && (6.4.2)\\
[\boldsymbol{\psi} \times \boldsymbol{\eta}] = 0, \quad [(\beta \nabla \times \boldsymbol{\psi}) \times \boldsymbol{\eta}] &= 0 \quad \text{on} \quad \Gamma, && (6.4.3)\\
[\boldsymbol{\psi} \cdot \boldsymbol{\eta}] = 0, \quad [\alpha \nabla \cdot \boldsymbol{\psi}] &= 0 \quad \text{on} \quad \Gamma. && (6.4.4)
\end{aligned}$$

Moreover, we assume that the dual problem is $\mathbf{H}^2$-regular, i.e., for any $\mathbf{e}_0 \in [L^2(\Omega)]^d$, there exist an unique $\boldsymbol{\psi} \in [H^2(\Omega_i)]^d$ for $i = 1, 2$ such that

$$\|\boldsymbol{\psi}\|_{2,\Omega_1} + \|\boldsymbol{\psi}\|_{2,\Omega_2} \leq C\|\mathbf{e}_0\|, \tag{6.4.5}$$

which is a natural assumption in the present geometric setting (cf. [18]).

Theorem 6.4.1. *Let* $\mathbf{p}_h \in \mathbf{V}_h^0$ *be the WG solution for* (6.2.5) *and* $\mathbf{p} \in [H^{k+1}(\Omega_i)]^d$ $(i = 1, 2)$ *be the exact solution for* (6.1.1)-(6.1.4)*. Then, we have*

$$\|\mathbf{Q}_0^k \mathbf{p} - \mathbf{p}_h\| \leq Ch^{k+1}(\|\mathbf{p}\|_{k+1,\Omega_1} + \|\mathbf{p}\|_{k+1,\Omega_2}). \tag{6.4.6}$$

Proof. Examine the (6.4.1) with $\mathbf{e}_0$ to obtain

$$(\mathbf{e}_0, \mathbf{e}_0) = (\nabla \times (\beta \nabla \times \boldsymbol{\psi}, \mathbf{e}_0) - (\nabla(\alpha \nabla \cdot \boldsymbol{\psi}), \mathbf{e}_0) + (\gamma \boldsymbol{\psi}, \mathbf{e}_0).$$

Now, by using the same argument as in (6.3.11), we get

$$\begin{aligned}
(\mathbf{e}_0, \mathbf{e}_0) = \mathcal{A}(Q_h\boldsymbol{\psi}, \mathbf{e}_h) - \mathcal{R}_5(\boldsymbol{\psi}, \mathbf{e}_h) &= \mathcal{R}_5(\mathbf{p}, Q_h\boldsymbol{\psi}) - \mathcal{R}_5(\boldsymbol{\psi}, \mathbf{e}_h)\\
&:= \mathcal{L}_1 + \mathcal{L}_2. && (6.4.7)
\end{aligned}$$

Now, examine the Lemma 6.3.4 with $k = 1$, $\mathbf{p} = \boldsymbol{\psi}$, $\mathbf{v}_h = \mathbf{e}_h$ and use a priori bound (6.4.5) to obtain

$$|\mathcal{L}_2| \leq Ch\|\mathbf{e}_0\|\|\|\mathbf{e}_h\|\|. \tag{6.4.8}$$

Next, we consider

$$\begin{aligned}
\mathcal{L}_1 &= \mathcal{R}_1(\mathbf{p}, Q_h\boldsymbol{\psi}) + \mathcal{R}_2(\mathbf{p}, Q_h\boldsymbol{\psi}) + \mathcal{R}_3(\mathbf{p}, Q_h\boldsymbol{\psi}) + \mathcal{R}_4(\mathbf{p}, Q_h\boldsymbol{\psi})\\
&:= \mathcal{L}_3 + \mathcal{L}_4 + \mathcal{L}_5 + \mathcal{L}_6. && (6.4.9)
\end{aligned}$$

Before proceeding to estimate each term in the right hand side of (6.4.9), using definition of $\mathbf{Q}_b^k$, we note that

$$\|(\mathbf{Q}_0^k\boldsymbol{\psi} - \mathbf{Q}_b^k\boldsymbol{\psi}) \times \boldsymbol{\eta}\|_{\partial T}^2 \leq C\|(\mathbf{Q}_0^k\boldsymbol{\psi} - \boldsymbol{\psi}) \times \boldsymbol{\eta}\|_{\partial T}^2,$$
$$\|(\mathbf{Q}_0^k\boldsymbol{\psi} - \mathbf{Q}_b^k\boldsymbol{\psi}) \cdot \boldsymbol{\eta}\|_{\partial T}^2 \leq C\|(\mathbf{Q}_0^k\boldsymbol{\psi} - \boldsymbol{\psi}) \cdot \boldsymbol{\eta}\|_{\partial T}^2.$$

Now, using standard trace inequality and approximation properties of L^2 projections along with a priori estimate (6.4.5), we have

$$\begin{aligned}
|\mathcal{L}_3| = |\mathcal{R}_1(\mathbf{p}, \mathbf{Q}_h\boldsymbol{\psi})| &= \left|\sum_{T\in\mathcal{T}_h} \langle \beta(\nabla\times\mathbf{p} - \boldsymbol{\mathcal{Q}}_h^{k-1}(\nabla\times\mathbf{p})), (\mathbf{Q}_0^k\boldsymbol{\psi} - \mathbf{Q}_b^k\boldsymbol{\psi}) \times \boldsymbol{\eta}\rangle_{\partial T}\right| \\
&\leq C\sum_{T\in\mathcal{T}_h} \|\nabla\times\mathbf{p} - \boldsymbol{\mathcal{Q}}_h^{k-1}(\nabla\times\mathbf{p})\|_{\partial T}\|(\mathbf{Q}_0^k\boldsymbol{\psi} - \boldsymbol{\psi}) \times \boldsymbol{\eta}\|_{\partial T} \\
&\leq \left(\sum_{T\in\mathcal{T}_h} h_T\|\nabla\times\mathbf{p} - \boldsymbol{\mathcal{Q}}_h^{k-1}(\nabla\times\mathbf{p})\|_{\partial T}^2\right)^{\frac{1}{2}} \\
&\quad \times \left(\sum_{T\in\mathcal{T}_h} h_T^{-1}\|(\mathbf{Q}_0^k\boldsymbol{\psi} - \boldsymbol{\psi}) \times \boldsymbol{\eta}\|_{\partial T}^2\right)^{\frac{1}{2}} \\
&\leq Ch^{k+1}(\|\mathbf{p}\|_{k+1,\Omega_1} + \|\mathbf{p}\|_{k+1,\Omega_2})(\|\boldsymbol{\psi}\|_{2,\Omega_1} + \|\boldsymbol{\psi}\|_{2,\Omega_2}) \\
&\leq Ch^{k+1}(\|\mathbf{p}\|_{k+1,\Omega_1} + \|\mathbf{p}\|_{k+1,\Omega_2})\|\mathbf{e}_0\|, \\
|\mathcal{L}_4| = |\mathcal{R}_2(\mathbf{p}, \mathbf{Q}_h\boldsymbol{\psi})| &= \left|\sum_{T\in\mathcal{T}_h} \langle \beta(\nabla\cdot\mathbf{p} - \mathbb{Q}_h^{k-1}\nabla\cdot\mathbf{p}), (\mathbf{Q}_0^k\boldsymbol{\psi} - \mathbf{Q}_b^k\boldsymbol{\psi}) \cdot \boldsymbol{\eta}\rangle_{\partial T}\right| \\
&\leq C\sum_{T\in\mathcal{T}_h} \|\nabla\cdot\mathbf{p} - \mathbb{Q}_h^{k-1}\nabla\cdot\mathbf{p}\|_{\partial T}\|\mathbf{Q}_0^k\boldsymbol{\psi} - \boldsymbol{\psi}\|_{\partial T} \\
&\leq Ch^{k+1}\left(\|\mathbf{p}\|_{k+1,\Omega_1} + \|\mathbf{p}\|_{k+1,\Omega_2}\right)(\|\boldsymbol{\psi}\|_{2,\Omega_1} + \|\boldsymbol{\psi}\|_{2,\Omega_2}) \\
&\leq Ch^{k+1}\left(\|\mathbf{p}\|_{k+1,\Omega_1} + \|\mathbf{p}\|_{k+1,\Omega_2}\right)\|\mathbf{e}_0\|, \\
|\mathcal{L}_5| = |\mathcal{R}_3(\mathbf{p}, \mathbf{Q}_h\boldsymbol{\psi})| &= \left|\sum_{T\in\mathcal{T}_h} h^{-1}\langle(\mathbf{Q}_0^k\mathbf{p} - \mathbf{Q}_b^k(\mathbf{p}|_T)) \cdot \boldsymbol{\eta}, (\mathbf{Q}_0^k\boldsymbol{\psi} - \mathbf{Q}_b^k(\boldsymbol{\psi}|_T)) \cdot \boldsymbol{\eta}\rangle_{\partial T}\right| \\
&\leq \sum_{T\in\mathcal{T}_h} h_T^{-1}\|\mathbf{Q}_0^k\mathbf{p} - \mathbf{p}\|_{\partial T}\|\mathbf{Q}_0^k\boldsymbol{\psi} - \boldsymbol{\psi}\|_{\partial T} \\
&\leq C\left(\sum_{T\in\mathcal{T}_h} (h_T^{-2}\|\mathbf{Q}_0^k\mathbf{p} - \mathbf{p}\|_T^2 + \|\nabla(\mathbf{Q}_0^k\mathbf{p} - \mathbf{p})\|_T^2)\right)^{\frac{1}{2}} \\
&\quad \times \left(\sum_{T\in\mathcal{T}_h} (h_T^{-2}\|\mathbf{Q}_0^k\boldsymbol{\psi} - \boldsymbol{\psi}\|_T^2 + \|\nabla(\mathbf{Q}_0^k\boldsymbol{\psi} - \boldsymbol{\psi})\|_T^2)\right)^{\frac{1}{2}} \\
&\leq Ch^{k+1}\left(\|\mathbf{p}\|_{k+1,\Omega_1} + \|\mathbf{p}\|_{k+1,\Omega_2}\right)\|\mathbf{e}_0\|.
\end{aligned}$$

Similar arguments yield

$$\begin{aligned}
|\mathcal{L}_6| = |\mathcal{R}_4(\mathbf{p}, \mathbf{Q}_h\boldsymbol{\psi})| &= \left| \sum_{T\in\mathcal{T}_h} h^{-1} \langle (\mathbf{Q}_0^k\mathbf{p} - \mathbf{Q}_b^k(\mathbf{p}|_T)) \times \boldsymbol{\eta}, (\mathbf{Q}_0^k\boldsymbol{\psi} - \mathbf{Q}_b^k\boldsymbol{\psi}) \times \boldsymbol{\eta} \rangle_{\partial T} \right| \\
&\leq \sum_{T\in\mathcal{T}_h} h_T^{-1} \|(\mathbf{Q}_0^k\mathbf{p} - \mathbf{p}) \times \boldsymbol{\eta}\|_{\partial T} \|(\mathbf{Q}_0^k\boldsymbol{\psi} - \boldsymbol{\psi}) \times \boldsymbol{\eta}\|_{\partial T} \\
&\leq C \left(\sum_{T\in\mathcal{T}_h} h_T^{-1} \|(\mathbf{Q}_0^k\mathbf{p} - \mathbf{p}) \times \boldsymbol{\eta}\|_{\partial T}^2 \right)^{\frac{1}{2}} \\
&\quad \times \left(\sum_{T\in\mathcal{T}_h} h_T^{-1} \|(\mathbf{Q}_0^k\boldsymbol{\psi} - \boldsymbol{\psi}) \times \boldsymbol{\eta}\|_{\partial T}^2 \right)^{\frac{1}{2}} \\
&\leq Ch^{k+1} \left(\|\mathbf{p}\|_{k+1,\Omega_1} + \|\mathbf{p}\|_{k+1,\Omega_2} \right) \left(\|\boldsymbol{\psi}\|_{2,\Omega_1} + \|\boldsymbol{\psi}\|_{2,\Omega_2} \right) \\
&\leq Ch^{k+1} \left(\|\mathbf{p}\|_{k+1,\Omega_1} + \|\mathbf{p}\|_{k+1,\Omega_2} \right) \|\mathbf{e}_0\|.
\end{aligned}$$

Then, we substitute the bounds for $\mathcal{L}_j$ $(j = 3, 4, 5, 6)$ in (6.4.9) to arrive at

$$|\mathcal{L}_1| \leq Ch^{k+1} \left(\|\mathbf{p}\|_{k+1,\Omega_1} + \|\mathbf{p}\|_{k+1,\Omega_2} \right) \|\mathbf{e}_0\|,$$

which together with estimate (6.4.8) and Theorem 6.3.1 completes the rest of the proof. □

6.5 Numerical Experiments

We conduct several numerical experiments to verify the accuracy and efficiency of the proposed WG algorithm by implementing it on both two dimensional (2D) and three dimensional (3D) interface problem (6.1.1)-(6.1.4). The WG algorithm has been discussed for the WG space with $k = 1, 2, 3, 4$. A finite sequence of non-uniform triangular meshes for the 2D problems has been used for numerical studies. For 3D experiments, the cubic and tetrahedral meshes are considered to justify the theoretical estimates. High-order of convergence are achieved with complex interface geometries. In addition, a numerical experiment has been performed with low regular solution to validate the theoretical results.

Example 6.5.1. We consider the interface problem (6.1.1)-(6.1.4) in $\Omega = (-1, 1)^2$ with an arbitrary shape interface whose parametric equation in polar coordinate θ is taken as (cf. [103])

$$\begin{cases} x(\theta) = (0.40178 + (0.40178)\cos(2\theta)\sin(6\theta))\cos(\theta), \\ y(\theta) = (0.40178 + (0.40178)\cos(2\theta)\sin(6\theta))\sin(\theta), \end{cases}$$

where $\theta = [0, 2\pi]$. The domain Ω, interface Γ, and subdomains Ω_1 and Ω_2 are shown in Figure 6.5.1. The analytical solution $\mathbf{p} = (p_1, p_2)$ to the $\mathbf{H}(\text{curl}, \text{div})$-elliptic problem is chosen as

$$p_1 = \begin{cases} \exp(y^2 + x^2) & \text{for } (x, y) \in \Omega_1, \\ 0.1(y^2 + x^2)^2 - 0.01 \ln(2\sqrt{y^2 + x^2}) & \text{for } (x, y) \in \Omega_2 \end{cases}$$

and

$$(p_2|_{\Omega_1},\ p_2|_{\Omega_2}) = \left(3 \exp x(y^2 + x^2 \sin y) + 2,\ 0\right).$$

The coefficients are taken as

$$(\alpha|_{\Omega_1},\ \alpha|_{\Omega_2}) = \left(x + y^2 + 2,\ 4\right),\ \ (\beta|_{\Omega_1},\ \beta|_{\Omega_2}) = (2,\ x + 6)$$

and $(\gamma|_{\Omega_1},\ \gamma|_{\Omega_2}) = (5,\ 10^3)$ is piecewise constants with the large variation. For mesh level 5 and $k = 1$ component-wise surface plots of analytical solution (left) and WG solution (right) are shown in Figures 6.5.2-6.5.3. The numerical errors and rate of convergence for linear WG method are demonstrated in Table 6.5.1, which justify the theoretical estimates derived in Theorems 6.3.1-6.4.1.

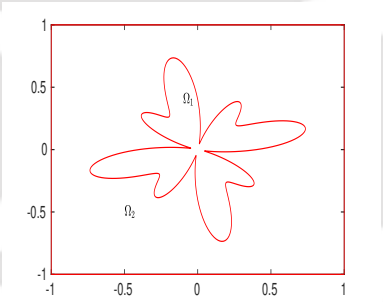

Figure 6.5.1: Computational domain in Example 6.5.1.

Example 6.5.2. We next consider the model interface problem (6.1.1)-(6.1.4) in $\Omega = (-1, 1)^2$ with an astroid shape interface Γ whose parametric equation is taken as

$$x(\theta) = r\cos^3(\theta)\ \ \&\ \ y(\theta) = r\sin^3(\theta),$$

where $r = 1/2$ and $\theta \in [0, 2\pi]$. The domain, interface and subdomains are illustrated in Figure 6.5.4. The permittivity and permeability are set as, and exact solution $\mathbf{p} = (p_1, p_2)$ are set as $\alpha = \begin{cases} y + x + 5, & \text{for } (x, y) \in \Omega_1, \\ y + 4, & \text{for } (x, y) \in \Omega_2, \end{cases}$ $\beta = \begin{cases} 5, & \text{for } (x, y) \in \Omega_1, \\ x + 4, & \text{for } (x, y) \in \Omega_2. \end{cases}$

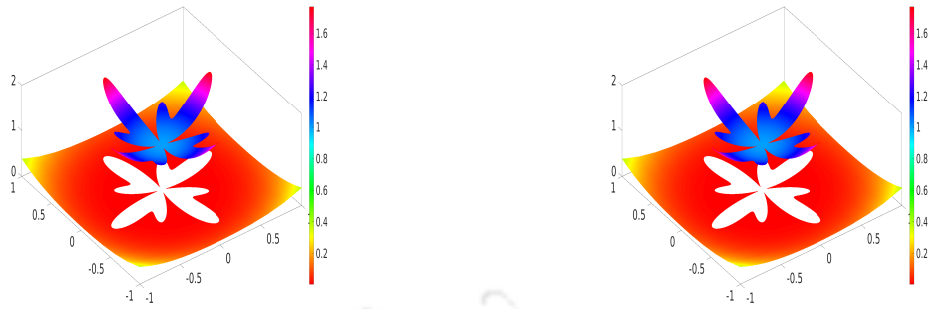

Figure 6.5.2: (Example 6.5.1) Surface plots for first component of analytical solution (left) and WG solution (right).

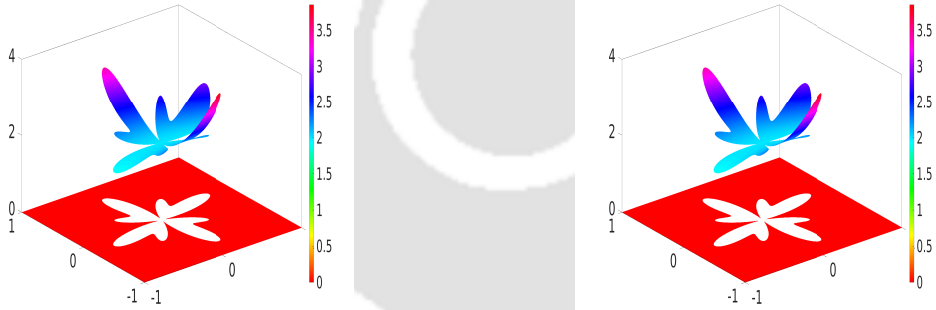

Figure 6.5.3: (Example 6.5.1) Surface plots for second component of analytical solution (left) and WG solution (right).

Table 6.5.1: Convergence and error profiles for Example 6.5.1.

k	Level	h	$\|\mathbf{e}_0\|$	Order	$\|\|\|\mathbf{e}_h\|\|\|$	Order
1	1	2.05e-01	3.60e-01	—	1.60e+00	—
	2	1.02e-01	9.27e-02	1.95	8.05e-01	0.99
	3	5.14e-02	2.35e-02	1.97	4.02e-01	0.99
	4	2.57e-02	5.90e-03	1.99	2.01e-01	0.99
	5	1.28e-02	1.47e-03	1.99	1.00e-01	0.99
	6	6.42e-03	3.69e-04	1.99	5.03e-02	0.99

The exact solution $\mathbf{p}$ with two components p_1 and p_2 are taken as

$$\begin{aligned}(p_1|_{\Omega_1},\ p_1|_{\Omega_2}) &= \big(2x - y^2 + 10,\ \exp(x)\cos(2\pi y)\big)\,,\\ (p_2|_{\Omega_1},\ p_2|_{\Omega_2}) &= \big(\exp(x)(x^2\sin(y) + y^2) + 5,\ \exp(x+y)\cos(\pi y)\big)\,.\end{aligned}$$

In addition, we select $\gamma = 1$ in Ω.

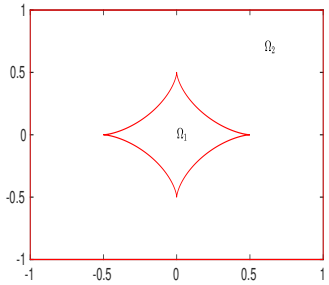

Figure 6.5.4: The interface and subdomains in Example 6.5.2.

Table 6.5.2 illustrates the numerical error and rate of convergence for the WG solution $\mathbf{u}_h$. Optimal order of convergence $\mathcal{O}(h^k)$ and $\mathcal{O}(h^{k+1})$ for $|||\mathbf{e}_h|||$ and $\|\mathbf{e}_0\|$ are observed, respectively, which justify the theoretical estimates of the previous sections. For mesh level 6 and $k = 2$ component-wise surface plots of exact solution (left) and WG solution (right) are shown in Figures 6.5.5-6.5.6.

Table 6.5.2: Convergence and error profiles for Example 6.5.2.

k	Level	h	$\|\mathbf{e}_0\|$	Order	$\|\|\|\mathbf{e}_h\|\|\|$	Order
2	1	4.95e-01	5.36e-01	—	3.38e+00	—
	2	2.47e-01	6.58e-02	3.02	7.82e-01	2.11
	3	1.23e-01	8.66e-03	2.92	2.05e-01	1.93
	4	6.19e-02	1.09e-03	2.97	5.18e-02	1.98
	5	3.09e-02	1.37e-04	2.99	1.30e-02	1.99
	6	1.54e-02	1.72e-05	2.99	3.25e-03	1.99
3	1	4.95e-01	9.65e-02	—	6.47e-01	—
	2	2.47e-01	1.06e-02	3.17	1.50e-01	2.10
	3	1.23e-01	6.83e-04	3.96	1.92e-02	2.96
	4	6.19e-02	4.30e-05	3.98	2.41e-03	2.99
	5	3.09e-02	2.69e-06	3.99	3.02e-04	2.99
	6	1.54e-02	1.68e-07	3.99	3.78e-05	2.99

Example 6.5.3. We consider the five-leaf shaped interface, whose parametric equation is given by (cf. [57])

$$x(\theta) = r(1 + (0.2)\sin(5\theta))\cos(\theta) \quad \& \quad y(\theta) = r(1 + (0.2)\sin(5\theta))\sin(\theta),$$

where $r = 1/2$ and $\theta \in [0, 2\pi]$. The interface and two subdomains with domain $\Omega = (-1, 1)^2$ are depicted in Figure 6.5.7.

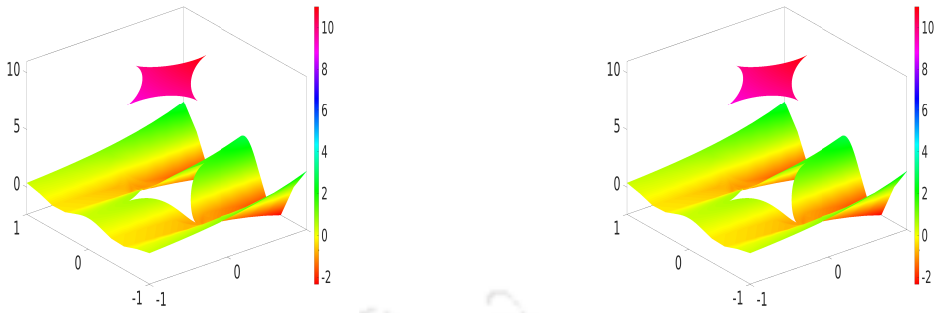

Figure 6.5.5: (Example 6.5.2) Surface plots for first component of exact solution (left) and WG solution (right).

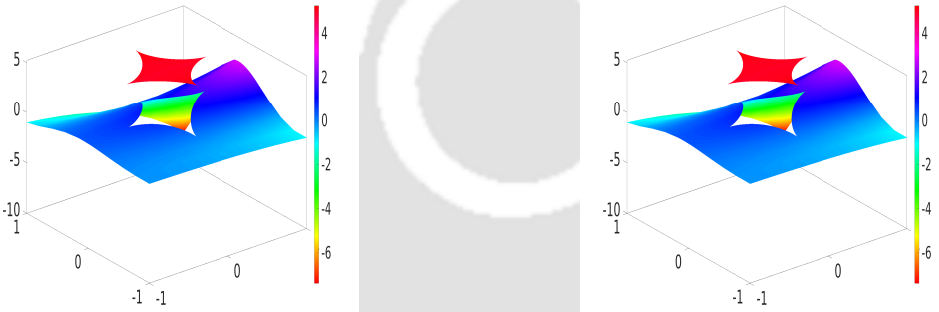

Figure 6.5.6: (Example 6.5.2) Surface plots for second component of exact solution (left) and WG solution (right).

The analytical solution $\mathbf{p} = (p_1, p_2)$ of the interface problem (6.1.1)-(6.1.4) is selected as

$$p_1 = \begin{cases} \exp(x)\cos(x+y) \text{ in } \Omega_1, \\ \cos(5x)\sin(5y) \text{ in } \Omega_2, \end{cases} \qquad p_2 = \begin{cases} \sin(5x)\cos(5y) \text{ in } \Omega_1, \\ \exp(y)\cos(5x) \text{ in } \Omega_2. \end{cases}$$

The coefficients are chosen as

$$\alpha = \begin{cases} y + x^2 + 2 \text{ in } \Omega_1, \\ y + 5 \text{ in } \Omega_2, \end{cases} \qquad \gamma = \begin{cases} x^2 + 5 \text{ in } \Omega_1, \\ 7 \text{ in } \Omega_2. \end{cases}$$

Moreover, $\beta = 1$ in Ω_1 and $\beta = 20$ in Ω_2.

Component-wise surface plots of analytical solution (left) and WG solution (right) with $k = 3$ on the refined mesh are shown in Figures 6.5.8-6.5.9. The numerical errors for WG method with $k = 3, 4$ are depicted in Table 6.5.3. One can say that $\mathcal{O}(h^k)$ for $|||\mathbf{e}_h|||$ and $\mathcal{O}(h^{k+1})$ for $\|\mathbf{e}_0\|$ are achieved in the numerical experiment.

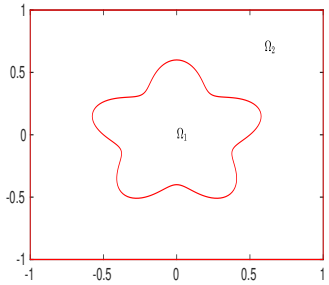

Figure 6.5.7: Computational domain in Example 6.5.3.

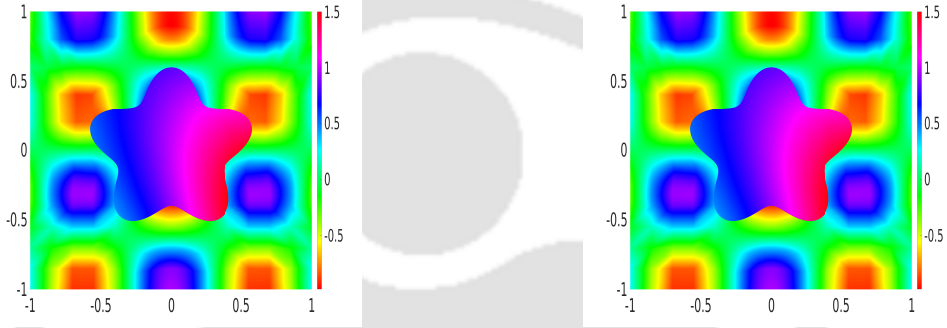

Figure 6.5.8: (Example 6.5.3) Surface plots for first component of analytical solution (left) and WG solution (right).

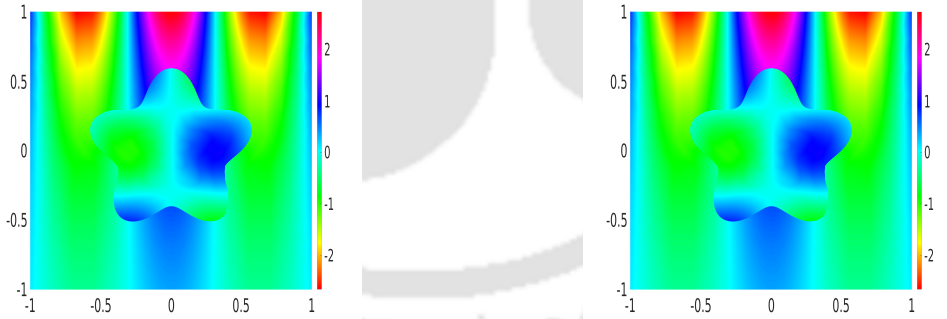

Figure 6.5.9: (Example 6.5.3) Surface plots for second component of analytical solution (left) and WG solution (right).

Example 6.5.4. We next consider the three-leaf flower shaped interface, whose parametric form is taken as

$$x(\theta) = (0.6 + (0.1)\sin(3\theta))\cos(\theta) \quad \& \quad y(\theta) = (0.6 + (0.1)\sin(3\theta))\sin(\theta),$$

where $\theta \in [0, 2\pi]$. Domain $\Omega = (-1, 1)^2$, and its subdomains Ω_1 and Ω_2 with interface Γ are illustrated in Figure 6.5.10.

Table 6.5.3: Convergence and error profiles for the Example 6.5.3.

k	Level	h	$\|\mathbf{e}_0\|$	Order	$\|\|\|\mathbf{e}_h\|\|\|$	Order
3	1	2.75e-01	7.11e-02	—	4.89e-01	—
	2	1.37e-01	4.78e-03	3.89	6.62e-02	2.88
	3	6.89e-02	3.08e-04	3.95	8.57e-03	2.95
	4	3.44e-02	1.94e-05	3.99	1.08e-03	2.99
	5	1.72e-02	1.21e-06	4.00	1.35e-04	3.00
	6	8.61e-03	7.61e-08	4.00	1.69e-05	3.00
4	1	2.75e-01	1.41e-02	—	1.11e-01	—
	2	1.37e-01	6.08e-04	4.53	9.47e-03	3.55
	3	6.89e-02	1.98e-05	4.93	6.17e-04	3.93
	4	3.44e-02	6.27e-07	4.98	3.90e-05	3.98
	5	1.72e-02	1.96e-08	5.00	2.44e-06	4.00
	6	8.61e-03	6.15e-10	5.00	1.52e-07	4.00

The exact solution $\mathbf{p} = (p_1, p_2)$ is taken as

$$p_1 = \begin{cases} 3 + 3(x^2 + y^2 + xy) \text{ in } \Omega_1, \\ x^2 + y^2 + \cos(x + y) \text{ in } \Omega_2, \end{cases} \qquad p_2 = \begin{cases} 7 - x^2 - y^2 \text{ in } \Omega_1, \\ 2\sin(x + y)\cos(x + y) \text{ in } \Omega_2. \end{cases}$$

The permittivity and permeability coefficients are selected as

$$\alpha = \begin{cases} x + 3 \text{ in } \Omega_1, \\ y + 4 \text{ in } \Omega_2, \end{cases} \qquad \beta = \begin{cases} 1 \text{ in } \Omega_1, \\ 100 \text{ in } \Omega_2. \end{cases}$$

In addition, $\gamma = 1$ in Ω.

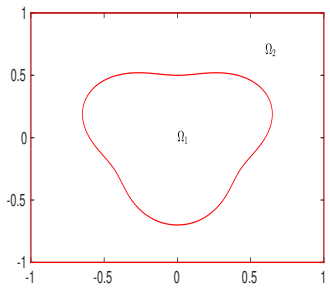

Figure 6.5.10: Computational domain in Example 6.5.4.

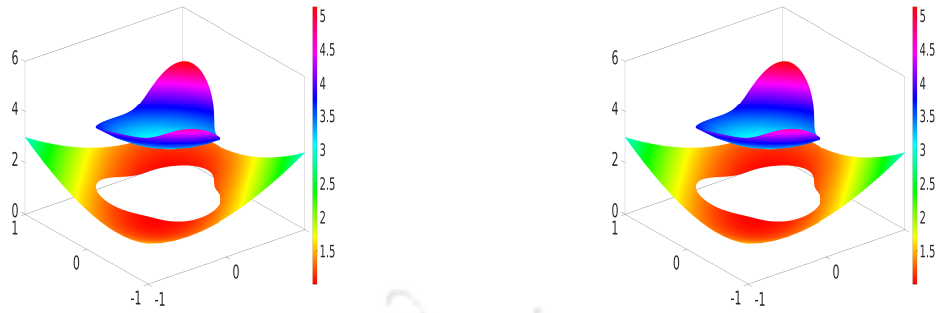

Figure 6.5.11: (Example 6.5.4) Surface plots for first component of exact solution (left) and WG solution (right).

For mesh level 6 and $k = 3$ component-wise surface plots of exact solution (left) and WG solution (right) are shown in Figures 6.5.11-6.5.12. As in Example 6.5.1, the numerical errors $|||\mathbf{e}_h|||$, $\|\mathbf{e}_0\|$ converges to 0 with orders k and $k+1$, respectively, which are reported in Table 6.5.4.

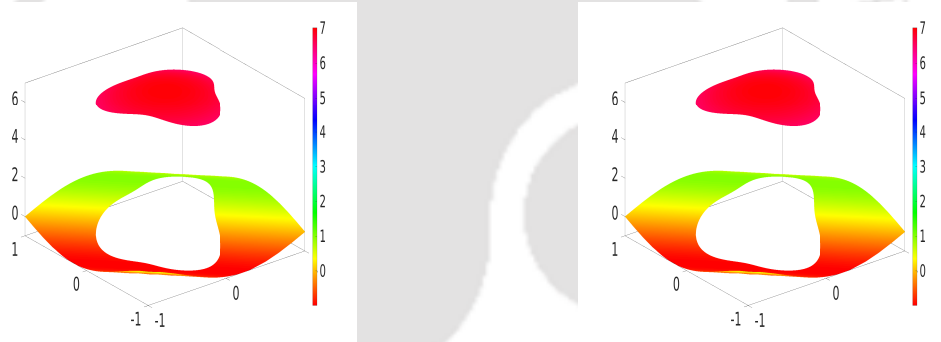

Figure 6.5.12: (Example 6.5.4) Surface plots for second component of exact solution (left) and WG solution (right).

Example 6.5.5. We examine the problem (6.1.1)-(6.1.4) in a 3D domain $\Omega = (0,1)^3$ with its subdomains $\Omega_1 = (0.25, 0.75)^3$ and $\Omega_2 = \Omega \setminus \Omega_1$ (cf. Figure 6.5.13 (left)). The three components of the exact solution $\mathbf{p} = (p_1, p_2, p_3)$ is assumed to be

$$p_1 = \begin{cases} \exp(xz + y) + \sin(z + x) \text{ in } \Omega_1, \\ xy + z^2 \text{ in } \Omega_2, \end{cases} \qquad p_2 = \begin{cases} \cos(xy + z^2) + (x + y)z \text{ in } \Omega_1, \\ x^2 + zy + 3 \text{ in } \Omega_2, \end{cases}$$

$$p_3 = \begin{cases} \sin(xyz) + \cos(x + z) + 4 \text{ in } \Omega_1, \\ x^2 + z^2 + 2 \text{ in } \Omega_2. \end{cases}$$

Table 6.5.4: Convergence and error profiles for Example 6.5.4.

k	Level	h	$\|\mathbf{e}_0\|$	Order	$\|\|\|\mathbf{e}_h\|\|\|$	Order
1	1	4.25e-01	6.66e-02	—	2.93e-01	—
	2	2.12e-01	1.72e-02	1.94	1.49e-01	0.97
	3	1.06e-01	4.36e-03	1.98	7.53e-02	0.99
	4	5.32e-02	1.09e-03	2.00	3.77e-02	1.00
	5	2.66e-02	2.73e-04	2.00	1.88e-02	1.00
	6	1.33e-02	6.84e-05	2.00	9.43e-03	1.00
2	1	4.25e-01	3.52e-03	—	2.04e-02	—
	2	2.12e-01	4.69e-04	2.91	5.42e-03	1.91
	3	1.06e-01	5.94e-05	2.98	1.37e-03	1.97
	4	5.32e-02	7.44e-06	3.00	3.45e-04	2.00
	5	2.66e-02	9.31e-07	3.00	8.64e-05	2.00
	6	1.33e-02	1.16e-07	3.00	2.16e-05	2.00
3	1	4.25e-01	6.26e-04	—	4.28e-03	—
	2	2.12e-01	3.95e-05	3.98	5.39e-04	2.99
	3	1.06e-01	2.48e-06	4.00	6.75e-05	3.00
	4	5.32e-02	1.55e-07	4.00	8.44e-06	2.99
	5	2.66e-02	9.68e-09	4.00	1.05e-06	3.00
	6	1.33e-02	6.05e-10	4.00	1.32e-07	3.00

We set the coefficients as $\alpha = \beta = 1$ in Ω_1 and $\alpha = \beta = 10^3$ in Ω_2, and $\gamma = 1$ in Ω.

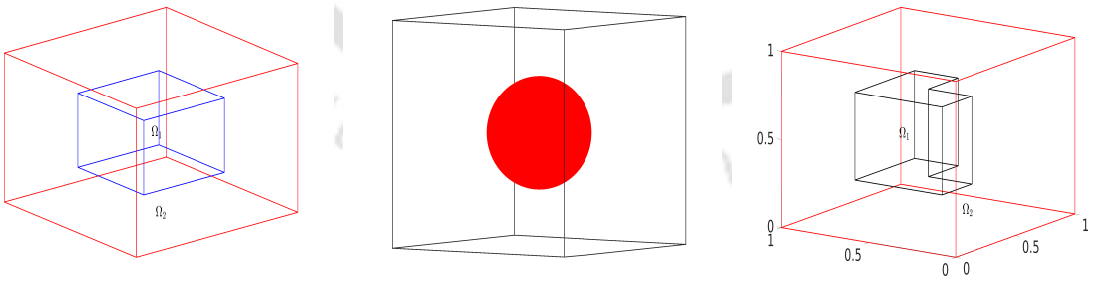

Figure 6.5.13: Computational domains in Example 6.5.5 (left), Example 6.5.6 (middle) and Example 6.5.7.

The numerical errors for WG method with $k = 2, 3$ are reported in Table 6.5.5. The order of convergence of $\mathcal{O}(h^k)$ and $\mathcal{O}(h^{k+1})$ for $|||\mathbf{e}_h|||$ and $\|\mathbf{e}_0\|$ are obtained in the numerical experiment, which justify the theoretical aspects of this study.

Table 6.5.5: Convergence and error profiles for Example 6.5.5.

k	Level	$\frac{1}{h}$	$\|\mathbf{e}_0\|$	Order	$\|\|\|\mathbf{e}_h\|\|\|$	Order
2	1	4	1.29e-02	—	7.93e-03	—
	2	8	1.71e-03	2.92	2.11e-03	1.90
	3	16	2.15e-04	2.99	5.38e-04	1.97
	4	32	2.68e-05	3.00	1.35e-04	1.99
	5	64	3.35e-06	3.00	3.39e-05	2.00
	6	128	4.18e-07	3.00	8.48e-06	2.00
3	1	4	1.93e-03	—	1.34e-03	—
	2	8	1.30e-04	3.88	1.81e-04	2.89
	3	16	8.32e-06	3.97	2.32e-05	2.96
	4	32	5.21e-07	3.99	2.92e-06	2.99
	5	64	3.25e-08	4.00	3.66e-07	2.99
	6	128	2.03e-09	4.00	4.58e-08	3.00

Example 6.5.6. We consider the $\mathbf{H}(\text{curl}, \text{div})$-elliptic interface problem in $\Omega = (0,1)^3$. Here, the subdomain Ω_1 is the sphere having center $(0.5, 0.5, 0.5)$ with radius $r = 0.25$, and $\Omega_2 = \Omega \setminus \Omega_1$ as illustrated in Figure 6.5.13 (middle). The three components of the exact solution is taken as

$$p_1 = \begin{cases} \exp(z)\sin(xy+1) + z^3 \text{ in } \Omega_1, \\ \sin(xy)\cos(y+z) + xy \text{ in } \Omega_2, \end{cases} \quad p_2 = \begin{cases} \exp(xyz) + x^2 + yz \text{ in } \Omega_1, \\ \sin(y+z) + \cos(xy) + 3 \text{ in } \Omega_2, \end{cases}$$

$$p_3 = \begin{cases} \exp(x+y+z) + xy + 2, & \text{for } (x,y,z) \in \Omega_1, \\ \sin(y+z) + 4, & \text{for } (x,y,z) \in \Omega_2. \end{cases}$$

For this numerical example, we take $\alpha = \gamma = 1$ in Ω, and $\beta = x+3$ in Ω_1 and $\beta = y+z+1$ in Ω_2. The numerical error and convergence results are reported in Table 6.5.6, which are consistent with Theorems 6.3.1-6.4.1.

Example 6.5.7. We consider the interface problem (6.1.1)-(6.1.4) on the domain $\Omega = (0,1)^3$ with the L-shaped interface Γ described in Figure 6.5.13 (right). The exact solution of the problem is selected as

$$p_1 = p_2 = p_3 = \begin{cases} \exp(x+y) + x^2 + yz & \text{for } (x,y,z) \in \Omega_1, \\ (xy + xz^2) r^{-2+c} & \text{for } (x,y,z) \in \Omega_2. \end{cases}$$

Table 6.5.6: Convergence and error profiles for Example 6.5.6.

k	Level	h	$\|\mathbf{e}_0\|$	Order	$\|\|\|\mathbf{e}_h\|\|\|$	Order
3	1	2.45e-01	6.78e-04	—	4.68e-03	—
	2	1.22e-01	4.59e-05	3.88	6.32e-04	2.88
	3	6.13e-02	2.92e-06	3.97	8.08e-05	2.96
	4	3.06e-02	1.83e-07	3.99	1.01e-05	2.99
	5	1.53e-02	1.14e-08	3.99	1.27e-06	2.99
4	1	2.45e-01	7.28e-05	—	5.70e-04	—
	2	1.22e-01	2.53e-06	4.84	3.92e-05	3.86
	3	6.13e-02	8.12e-08	4.96	2.51e-06	3.96
	4	3.06e-02	2.55e-09	4.98	1.58e-07	3.98
	5	1.53e-02	8.00e-11	4.99	9.92e-09	3.99

The physical coefficients are chosen to be $\alpha = \beta = \gamma = 1$ in Ω. It is easy to see that, $\mathbf{p} \in [H^{1+c-\epsilon}(\Omega)]^3$, where ϵ is a very small positive real number. The WG space is chosen to be $([\mathcal{P}_1]^3, [\mathcal{P}_1]^3, [\mathcal{P}_0]^3, \mathcal{P}_0)$. The numerical results obtained in Table 6.5.7 verifies that the proposed algorithm is compatible with the global low regular exact solution.

Table 6.5.7: Convergence and error profiles for Example 6.5.7.

c	Level	$\frac{1}{h}$	$\|\mathbf{e}_0\|$	Order	$\|\|\|\mathbf{e}_h\|\|\|$	Order
$\frac{1}{4}$	1	4	7.90e-01	—	3.45e+00	—
	2	8	3.50e-01	1.17	3.00e+00	0.20
	3	16	1.49e-01	1.22	2.56e+00	0.22
	4	32	6.34e-02	1.24	2.16e+00	0.24
	5	64	2.67e-02	1.24	1.83e+00	0.24
	6	128	1.12e-02	1.24	1.54e+00	0.24
$\frac{4}{5}$	1	4	2.18e-01	—	9.92e-01	—
	2	8	6.45e-02	1.76	5.69e-01	0.80
	3	16	1.86e-02	1.79	3.24e-01	0.81
	4	32	5.35e-03	1.79	1.84e-01	0.81
	5	64	1.53e-03	1.80	1.05e-01	0.80
	6	128	4.42-04	1.80	6.04e-02	0.80

7

Least-squares WG-FEMs for Time-harmonic Maxwell's Equations

In this chapter, we propose and analyze a least-squares-based weak Galerkin finite element method for solving the indefinite time-harmonic Maxwell's equations in $\mathbb{R}^d$ ($d = 2, 3$). Super-convergence of order one for the discrete H^1 like norm has been established. Numerical simulations show that the approximate solutions converge to the exact solutions with optimal rates in the L^2 norm on hybrid meshes. In addition, this method is shown to be an absolutely stable under low regularity requirements with high wave number.

7.1 Introduction

In this Chapter, we consider the following classical time-harmonic Maxwell's equation

$$\nabla \times (\mu_r^{-1} \nabla \times \mathbf{p}) - \gamma^2 \epsilon_r \mathbf{p} = \mathbf{g} \text{ in } \Omega, \tag{7.1.1}$$

$$\mathbf{p} \times \boldsymbol{\eta} = 0 \text{ on } \partial\Omega, \tag{7.1.2}$$

where $\Omega \subset \mathbb{R}^d$ ($d = 2, 3$) is bounded polygonal (2D)/Polyhedral (3D) domain with Lipschitz continuous boundary $\partial\Omega$ ($\boldsymbol{\eta}$ is the unit outward normal vector on $\partial\Omega$). Here, the relative magnetic permeability and electric permittivity are considered in the vacuum *i.e.*, ($\mu_r^{-1} = \epsilon_r = 1$). The source term $\mathbf{g} \in [L^2(\Omega)]^d$. In order to establish the well-posedness of the aforementioned problem, we assume that wave number $\gamma > 0$ which should not be the eigenvalue of the Maxwell's system (more precisely, γ is not an eigenvalue of the differential operator $\mathcal{L} : \nabla \times (\nabla \times \mathbf{p})$).

The Maxwell's operator is strongly indefinite for high wave number γ, which brings difficulties to the both in theoretical analysis and numerical simulation. In this chapter, we propose a least-squares weak Galerkin finite element method for equations (7.1.1)-

(7.1.2). By introducing an another unknown $\mathbf{q} = \frac{1}{\gamma}\nabla \times \mathbf{p}$, the Maxwell problem (7.1.1)-(7.1.2) can be rewritten as

$$\begin{aligned} \nabla \times \mathbf{p} - \gamma \mathbf{q} &= 0 \text{ in } \Omega, && (7.1.3)\\ \nabla \times \mathbf{q} - \gamma \mathbf{p} &= \mathbf{f} \text{ in } \Omega, && (7.1.4)\\ \mathbf{p} \times \boldsymbol{\eta} &= 0 \text{ on } \partial\Omega. && (7.1.5) \end{aligned}$$

where $\mathbf{f} = \frac{1}{\gamma}\mathbf{g}$. The system (7.1.3)-(7.1.5) is known as the first order time-harmonic system.

We aim to develop a LSWG method which is absolutely stable without any mesh constraint for the mixed curl-curl formulation (7.1.3)- (7.1.5). In comparison to LS-DG method [91], LSWG methods have a parameter-free positive definite symmetric system and provide more accurate approximations for both $\mathbf{p}$ and $\mathbf{q}$. In [91], the authors have derived optimal convergence rate for the energy-norm and suboptimal convergence rate for L^2 norm for the indefinite time-harmonic Maxwell's equations. Under the same regularity assumptions for the both primal variable ($\mathbf{p}$) and auxiliary variable ($\mathbf{q}$) as in [91], there is a one-order superconvergence for the proposed algorithm in the triple-bar norm, *i.e.*, discrete H^1 like norm. At the same time, this method is capable of handling very general geometries by allowing general polygonal/polytopal meshes and has low regularity requirements. In addition, numerous numerical experiments are conducted for 2D and 3D time-harmonic Maxwell's equations that justify the super-convergence of order one for the energy-norm and optimal convergence rate for L^2 norm.

The rest of chapter is organised as follows. In Section 7.2, we discuss the WG discretization, weak curl and LSWG algorithm of the proposed problem. The error equation and corresponding error estimates have been derived in Section 7.3. In Section 7.4, several numerical experiments have been conducted to justify the theoretical results.

7.2 Least-squares Weak Galerkin Algorithm

In this section, we introduce the LSWG algorithm for the problem (7.1.3)-(7.1.5). The WG partitions $\mathcal{T}_h$ of the domain Ω is borrowed from the Chap. 2. Next, we introduce two WG spaces corresponding to $\mathbf{p}$ and $\mathbf{q}$, respectively (for more details, see Chap. 3)

$$\begin{aligned} \mathbf{V}_h &= \{\mathbf{v}_h = \{\mathbf{v}_0, \mathbf{v}_b = v_1\mathbf{t}_1 + (d-2)v_2\mathbf{t}_2\} : \mathbf{v}_0|_T \in [\mathcal{P}_k(T)]^d, \\ &\qquad\qquad v_1, v_2 \in \mathcal{P}_k(e), e \in \partial T, T \in \mathcal{T}_h\}, \\ \mathbf{W}_h &= \{\mathbf{w}_h = \{\mathbf{w}_0, \mathbf{w}_b\} : \mathbf{w}_0|_T \in [\mathcal{P}_k(T)]^l, \mathbf{w}_b|_e \in [\mathcal{P}_k(e)]^l, e \in \partial T, T \in \mathcal{T}_h\}, \end{aligned}$$

where $k \geq 1$ an integer and $l = 2d - 3$ $(d = 2, 3)$. In addition, we introduce a subspace of $\mathbf{V}_h$ defined as follows

$$\mathbf{V}_h^0 = \{\mathbf{v}_h = \{\mathbf{v}_0, \mathbf{v}_b\} \in \mathbf{V}_h : \mathbf{v}_b \times \boldsymbol{\eta} = \mathbf{0} \text{ on } \partial\Omega\}.$$

The discrete weak curl operator $(\nabla_w \times (\cdot))$ for any $\mathbf{v}_h \in \mathbf{V}_h$ is a unique polynomial $\nabla_w \times \mathbf{v}_h \in [\mathcal{P}_k(T)]^{2d-3}$ satisfying the following equation

$$(\nabla_w \times \mathbf{v}_h, \boldsymbol{\phi})_T = (\mathbf{v}_0, \nabla \times \boldsymbol{\phi})_T - \langle \mathbf{v}_b \times \boldsymbol{\eta}, \boldsymbol{\phi} \rangle_{\partial T} \ \ \forall \boldsymbol{\phi} \in [\mathcal{P}_k(T)]^{2d-3}, \tag{7.2.1}$$

and for each $\mathbf{w}_h = \{\mathbf{w}_0, \mathbf{w}_b\} \in \mathbf{W}_h$, the discrete curl denoted by $\nabla_w \times \mathbf{w}_h$ is a unique piecewise vector polynomial of degree k satisfying

$$(\nabla_w \times \mathbf{w}_h, \boldsymbol{\psi})_T = (\mathbf{w}_0, \nabla \times \boldsymbol{\psi})_T - \langle \mathbf{w}_b \times \boldsymbol{\eta}, \boldsymbol{\psi} \rangle_{\partial T} \ \ \forall \boldsymbol{\psi} \in [\mathcal{P}_k(T)]^d, \ \forall\, T \in \mathcal{T}_h. \tag{7.2.2}$$

For each $T \in \mathcal{T}_h$ and $e \in \mathcal{E}_h$, we define the following L^2 projections:

- $\mathbf{Q}_0^k : [L^2(T)]^d \to [\mathcal{P}_k(T)]^d$; $\mathbf{Q}_b^k : [L^2(e)]^d \to [\mathcal{P}_k(e)]^d$, $Q_b^k : L^2(e) \to \mathcal{P}_k(e)$.
- $\mathbf{L}_0^k : [L^2(T)]^{2d-3} \to [\mathcal{P}_k(T)]^{2d-3}$, $\mathbf{L}_b^k : [L^2(e)]^{2d-3} \to [\mathcal{P}_k(e)]^{2d-3}$.
- $\boldsymbol{\mathcal{Q}}_h^k : [L^2(T)]^{2d-3} \to [\mathcal{P}_k(T)]^{2d-3}$& $\boldsymbol{\mathcal{L}}_h^k : [L^2(T)]^d \to [\mathcal{P}_k(T)]^d$.

In addition, we define $\mathbf{Q}_h\mathbf{v} = \{\mathbf{Q}_0^k\mathbf{v}, \mathbf{Q}_b^k\mathbf{v} = Q_b^k(v_1)\mathbf{t}_1 + (d-2)Q_b^k(v_2)\mathbf{t}_2\}$ for all $\mathbf{v} \in [H^\alpha(T)]^d$ and $\mathbf{L}_h\mathbf{w} = \{\mathbf{L}_0^k\mathbf{w}, \mathbf{L}_b^k\mathbf{w}\}$ for all $\mathbf{w} \in [H^\alpha(T)]^{2d-3}$, where $\alpha > 1/2$.

To define the least-squares weak Galerkin (LSWG) scheme, we need the following bilinear forms:

$$\begin{aligned}
\mathcal{A}(\boldsymbol{\rho}_h, \boldsymbol{\sigma}_h; \boldsymbol{w}_h, \boldsymbol{v}_h) \ &= \ \sum_{T\in\mathcal{T}_h} (\nabla_w \times \boldsymbol{\rho}_h - \gamma\boldsymbol{\sigma}_0, \nabla_w \times \mathbf{w}_h - \gamma\mathbf{v}_0)_T \\
&\quad + \sum_{T\in\mathcal{T}_h} (\nabla_w \times \boldsymbol{\sigma}_h - \gamma\boldsymbol{\rho}_0, \nabla_w \times \mathbf{v}_h - \gamma\mathbf{w}_0)_T \\
&\quad + \mathcal{S}_1(\boldsymbol{\sigma}_h, \mathbf{v}_h) + \mathcal{S}_2(\boldsymbol{\rho}_h, \mathbf{w}_h),
\end{aligned}$$

where

$$\begin{aligned}
\mathcal{S}_1(\boldsymbol{\sigma}_h, \mathbf{v}_h) \ &= \ \sum_{T\in\mathcal{T}_h} h_T \langle (\boldsymbol{\sigma}_0 - \boldsymbol{\sigma}_b) \times \boldsymbol{\eta}, (\mathbf{v}_0 - \mathbf{v}_b) \times \boldsymbol{\eta} \rangle_{\partial T}, \\
\mathcal{S}_2(\boldsymbol{\rho}_h, \mathbf{w}_h) \ &= \ \sum_{T\in\mathcal{T}_h} h_T^3 \langle \boldsymbol{\rho}_0 - \boldsymbol{\rho}_b, \mathbf{w}_0 - \mathbf{w}_b \rangle_{\partial T},
\end{aligned}$$

for all $\boldsymbol{\rho}_h, \mathbf{w}_h \in \mathbf{W}_h$, $\boldsymbol{\sigma}_h, \mathbf{v}_h \in \mathbf{V}_h$. Moreover, we define a triple-bar semi-norm on $\mathbf{W}_h \times \mathbf{V}_h$ given by

$$|||(\mathbf{w}_h, \mathbf{v}_h)|||^2 = \mathcal{A}(\mathbf{w}_h, \mathbf{v}_h; \mathbf{w}_h, \mathbf{v}_h) \ \ \forall (\mathbf{w}_h, \mathbf{v}_h) \in \mathbf{W}_h \times \mathbf{V}_h. \tag{7.2.3}$$

Indeed, next result shows that $|||\cdot|||$ is a norm in the finite element space $\mathbf{W}_h \times \mathbf{V}_h^0$.

Lemma 7.2.1. *The functional $|||\cdot|||$ in (7.2.3) defines a norm in $\mathbf{W}_h \times \mathbf{V}_h^0$.*

Proof. To justify the Lemma, it suffices to check the positivity property for $|||\cdot|||$, *i.e.*,

$$|||(\mathbf{w}_h, \mathbf{v}_h)||| = 0 \ \text{ iff } \ \mathbf{w}_h = \mathbf{v}_h = \mathbf{0}.$$

We assume that

$$|||(\mathbf{w}_h, \mathbf{v}_h)|||^2 = \mathcal{A}(\mathbf{w}_h, \mathbf{v}_h; \mathbf{w}_h, \mathbf{v}_h) = \mathbf{0},$$

which leads to following system of equations

$$\begin{cases} \nabla_w \times \mathbf{w}_h = \gamma \mathbf{v}_0, \quad \nabla_w \times \mathbf{v}_h = \gamma \mathbf{w}_0 & \forall\, T \in \mathcal{T}_h, \\ \mathbf{v}_0 \times \boldsymbol{\eta} = \mathbf{v}_b \times \boldsymbol{\eta}, \qquad \mathbf{w}_0 = \mathbf{w}_b & \forall\, \partial T,\ T \in \mathcal{T}_h. \end{cases} \tag{7.2.4}$$

Then, set $\mathbf{z}_h = \gamma \mathbf{w}_0 - \nabla \times \mathbf{v}_0$ and observe from (7.2.4) that

$$\begin{aligned} (\gamma \mathbf{w}_0, \mathbf{z}_h) = \sum_{T \in \mathcal{T}_h} (\gamma \mathbf{w}_0, \mathbf{z}_h)_T &= \sum_{T \in \mathcal{T}_h} (\nabla_w \times \mathbf{v}_h, \mathbf{z}_h)_T \\ &= \sum_{T \in \mathcal{T}_h} (\mathbf{v}_0, \nabla \times \mathbf{z}_h)_T - \sum_{T \in \mathcal{T}_h} \langle \mathbf{v}_b \times \boldsymbol{\eta}, \mathbf{z}_h \rangle_{\partial T} \\ &= \sum_{T \in \mathcal{T}_h} (\nabla \times \mathbf{v}_0, \mathbf{z}_h)_T + \sum_{T \in \mathcal{T}_h} \langle (\mathbf{v}_0 - \mathbf{v}_b) \times \boldsymbol{\eta}, \mathbf{z}_h \rangle_{\partial T} \\ &= (\nabla \times \mathbf{v}_0, \mathbf{z}_h)\,. \end{aligned}$$

As a consequence, we arrive at

$$\gamma \mathbf{w}_0 - \nabla \times \mathbf{v}_0 = \mathbf{0} \ \text{ in } \Omega. \tag{7.2.5}$$

Similarly, testing the first equation in (7.2.4) by $\mathbf{s}_h = \gamma \mathbf{v}_0 - \nabla \times \mathbf{w}_0$, we obtain

$$\gamma \mathbf{v}_0 - \nabla \times \mathbf{w}_0 = \mathbf{0} \ \text{ in } \Omega. \tag{7.2.6}$$

Now, from (7.2.4), (7.2.5) and (7.2.6), we have

$$\begin{cases} \nabla \times \mathbf{w}_0 - \gamma \mathbf{v}_0 = \mathbf{0} & \text{in } \Omega, \\ \nabla \times \mathbf{v}_0 - \gamma \mathbf{w}_0 = \mathbf{0} & \text{in } \Omega, \\ \mathbf{v}_0 \times \boldsymbol{\eta} = \mathbf{0} & \text{on } \partial\Omega. \end{cases} \tag{7.2.7}$$

For the $\mathbf{v}_0$, we first apply the curl operator to the second equation in (7.2.7), and then use first equation and boundary condition to obtain

$$\begin{cases} \nabla \times (\nabla \times \mathbf{v}_0) - \gamma^2 \mathbf{v}_0 = \mathbf{0} & \text{in } \Omega, \\ \mathbf{v}_0 \times \boldsymbol{\eta} = \mathbf{0} & \text{on } \partial\Omega, \end{cases} \tag{7.2.8}$$

which yields $\mathbf{v}_0 = \mathbf{0}$ in Ω (see, [17]). Then, plug this information in the second equation in (7.2.7) to arrive at $\mathbf{w}_0 = \mathbf{0}$ in Ω. This completes the lemma 7.2.1. □

Now, we are in position to introduce the LSWG algorithm for the aforementioned problem.

Least-squares Weak Galerkin Algorithm. A LSWG approximation for (7.1.3)-(7.1.5) seeks $(\mathbf{q}_h, \mathbf{p}_h) \in \mathbf{W}_h \times \mathbf{V}_h^0$ satisfying

$$\mathcal{A}(\mathbf{q}_h, \mathbf{p}_h; \mathbf{w}_h, \mathbf{v}_h) \;=\; (\mathbf{f}, \nabla_w \times \mathbf{w}_h - \gamma \mathbf{v}_0) \;\; \forall (\mathbf{w}_h, \mathbf{v}_h) \in \mathbf{W}_h \times \mathbf{V}_h^0. \tag{7.2.9}$$

Lemma 7.2.2. *The LSWG approximation* (7.2.9) *has a unique solution.*

Proof. Let $(\mathbf{q}_h^1, \mathbf{p}_h^1)$ and $(\mathbf{q}_h^2, \mathbf{p}_h^2)$ be two pairs of solutions of the (7.2.9). Set $\mathbf{U}_h = \mathbf{q}_h^1 - \mathbf{q}_h^2$ and $\mathbf{P}_h = \mathbf{p}_h^1 - \mathbf{p}_h^2$, then we have

$$\mathcal{A}(\mathbf{U}_h, \mathbf{P}_h; \mathbf{w}_h, \mathbf{v}_h) = 0 \;\; \forall (\mathbf{w}_h, \mathbf{v}_h) \in \mathbf{W}_h \times \mathbf{V}_h^0.$$

Now by letting $\mathbf{w}_h = \mathbf{U}_h$ and $\mathbf{v}_h = \mathbf{P}_h$ in the above equation gives rise to

$$|||(\mathbf{U}_h, \mathbf{P}_h)||| = 0.$$

Hence, we obtain $\mathbf{U}_h \equiv 0$ and $\mathbf{P}_h \equiv 0$. This completes the Lemma 7.2.2. □

Lemma 7.2.3. *For $\alpha > \frac{1}{2}$, we have*

$$\begin{aligned} \boldsymbol{\mathcal{Q}}_h^k(\nabla \times \mathbf{v}) &= \nabla_w \times (\mathbf{Q}_h \mathbf{v}) \;\; \forall \mathbf{v} \in [H^\alpha(\Omega)]^d, \\ \boldsymbol{\mathcal{L}}_h^k(\nabla \times \mathbf{w}) &= \nabla_w \times (\mathbf{L}_h \mathbf{w}) \;\; \forall \mathbf{w} \in [H^1(\Omega)]^{2d-3}. \end{aligned}$$

Proof. By using the definitions of $\boldsymbol{\mathcal{Q}}_h^k$ and discrete weak curl (7.2.1), we obtain

$$\begin{aligned} (\nabla_w \times (\mathbf{Q}_h \mathbf{v}), \mathbf{p})_T &= \left(\mathbf{Q}_0^k \mathbf{v}, \nabla \times \mathbf{p}\right)_T - \langle (\mathbf{Q}_b^k \mathbf{v}) \times \boldsymbol{\eta}, \mathbf{p} \rangle_{\partial T} \\ &= (\mathbf{v}, \nabla \times \mathbf{p})_T - \langle \mathbf{v} \times \boldsymbol{\eta}, \mathbf{p} \rangle_{\partial T} \\ &= (\nabla \times \mathbf{v}, \mathbf{p})_T = (\boldsymbol{\mathcal{Q}}_h^k (\nabla \times \mathbf{v}), \mathbf{p})_T, \end{aligned}$$

for all $\mathbf{p} \in [\mathcal{P}_k(T)]^{2d-3}$. Next, from the definitions of $\boldsymbol{\mathcal{L}}_h^k$ and weak curl (7.2.2), we have

$$\begin{aligned} (\nabla_w \times (\mathbf{L}_h \mathbf{v}), \mathbf{p})_T &= \left(\mathbf{L}_0^k \mathbf{v}, \nabla \times \mathbf{p}\right)_T - \langle (\mathbf{L}_b^k \mathbf{v}) \times \boldsymbol{\eta}, \mathbf{p} \rangle_{\partial T} \\ &= (\mathbf{v}, \nabla \times \mathbf{p})_T - \langle \mathbf{v} \times \boldsymbol{\eta}, \mathbf{p} \rangle_{\partial T} \\ &= (\nabla \times \mathbf{v}, \mathbf{p})_T = (\boldsymbol{\mathcal{L}}_h^k (\nabla \times \mathbf{v}), \mathbf{p})_T, \end{aligned}$$

for any $\mathbf{p} \in [\mathcal{P}_k(T)]^d$. □

Let us now end this section with a trace result to be used in the paper. Let T be an element with e as an edge/face. For any function $\varphi \in H^\alpha(T)$ $(\frac{1}{2} < \alpha \leq 1)$, the following trace inequality holds true (cf. [121])

$$\|\varphi\|_e^2 \leq C \left(h_T^{-1} \|\varphi\|_T^2 + h_T^{2\alpha - 1} \|\nabla \varphi\|_{\alpha, T}^2\right). \tag{7.2.10}$$

7.3 Error Analysis

In this section, we shall derive the error equation and establish the convergence under the energy norm.

We first define the error functions given as follows:

$$\mathbf{e}_h = \mathbf{Q}_h\mathbf{p} - \mathbf{p}_h, \quad \mathbf{e}_h^1 = \mathbf{L}_h\mathbf{q} - \mathbf{q}_h.$$

Lemma 7.3.1. *For each* $(\mathbf{w}_h, \mathbf{v}_h) \in \mathbf{W}_h \times \mathbf{V}_h^0$, *we have*

$$\mathcal{A}(\mathbf{e}_h^1, \mathbf{e}_h; \mathbf{w}_h, \mathbf{v}_h) = \mathcal{R}(\mathbf{q}, \mathbf{p}; \mathbf{w}_h, \mathbf{v}_h),$$

where

$$\mathcal{R}(\mathbf{q}, \mathbf{p}; \mathbf{w}_h, \mathbf{v}_h) \;:=\; \mathcal{S}_1(\mathbf{Q}_h\mathbf{p}, \mathbf{v}_h) + \mathcal{S}_2(\mathbf{L}_h\mathbf{q}, \mathbf{w}_h).$$

Proof. From Lemma 7.2.3 and (7.1.3), we have

$$\nabla_w \times \mathbf{Q}_h\mathbf{p} - \gamma\mathbf{L}_h\mathbf{q} = (\nabla_w \times \mathbf{Q}_h\mathbf{p} - \nabla \times \mathbf{p}) - \gamma(\mathbf{L}_h\mathbf{q} - \mathbf{q}).$$

Now for $(\mathbf{w}_h, \mathbf{v}_h) \in \mathbf{W}_h \times \mathbf{V}_h^0$, we have

$$\begin{aligned}
&\sum_{T\in\mathcal{T}_h} (\nabla_w \times \mathbf{Q}_h\mathbf{p} - \gamma\mathbf{L}_0^k\mathbf{q}, \nabla_w \times \mathbf{v}_h - \gamma\mathbf{w}_0)_T \\
&= \sum_{T\in\mathcal{T}_h} ((\nabla_w \times \mathbf{Q}_h\mathbf{p} - \nabla \times \mathbf{p}) - \gamma(\mathbf{L}_0^k\mathbf{q} - \mathbf{q}), \nabla_w \times \mathbf{v}_h - \gamma\mathbf{w}_0)_T \\
&= \sum_{T\in\mathcal{T}_h} ((\boldsymbol{\mathcal{Q}}_h^k(\nabla \times \mathbf{p}) - \nabla \times \mathbf{p}) - \gamma(\mathbf{L}_0^k\mathbf{q} - \mathbf{q}), \nabla_w \times \mathbf{v}_h - \gamma\mathbf{w}_0)_T \\
&= \mathcal{R}_1(\mathbf{q}, \mathbf{p}; \mathbf{w}_h, \mathbf{v}_h). \qquad (7.3.1)
\end{aligned}$$

From the L^2 orthogonality of the projection operator $\boldsymbol{\mathcal{Q}}_h^k$ and $\mathbf{L}_0^k$, we observed that $\mathcal{R}_1(\mathbf{q}, \mathbf{p}; \mathbf{w}_h, \mathbf{v}_h) \equiv 0$.

Next, from Lemma 7.2.3 and (7.1.4), we obtain

$$\begin{aligned}
\nabla_w \times \mathbf{L}_h\mathbf{q} - \gamma\mathbf{Q}_h\mathbf{p} &= \boldsymbol{\mathcal{L}}_h^k(\nabla \times \mathbf{q}) - \gamma\mathbf{Q}_h\mathbf{p} \\
&= \mathbf{f} + (\boldsymbol{\mathcal{L}}_h^k(\nabla \times \mathbf{q}) - \nabla \times \mathbf{q}) - \gamma(\mathbf{Q}_h\mathbf{p} - \mathbf{p}).
\end{aligned}$$

Now again for $(\mathbf{w}_h, \mathbf{v}_h) \in \mathbf{W}_h \times \mathbf{V}_h^0$, we arrived at

$$\begin{aligned}
&\sum_{T\in\mathcal{T}_h} (\nabla_w \times \mathbf{L}_h\mathbf{q} - \gamma\mathbf{Q}_0^k\mathbf{p}, \nabla_w \times \mathbf{w}_h - \gamma\mathbf{v}_0) \\
&= \sum_{T\in\mathcal{T}_h} ((\boldsymbol{\mathcal{L}}_h^k(\nabla \times \mathbf{q}) - \nabla \times \mathbf{q}) - \gamma(\mathbf{Q}_0^k\mathbf{p} - \mathbf{p}), \nabla_w \times \mathbf{w}_h - \gamma\mathbf{v}_0)_T \\
&\quad + (\mathbf{f}, \nabla \times \mathbf{w}_h - \gamma\mathbf{v}_0) \\
&= \mathcal{R}_2(\mathbf{q}, \mathbf{p}; \mathbf{w}_h, \mathbf{v}_h) + (\mathbf{f}, \nabla_w \times \mathbf{w}_h - \gamma\mathbf{v}_0). \qquad (7.3.2)
\end{aligned}$$

From the L^2 orthogonality of the projection operator $\boldsymbol{\mathcal{L}}_h^k$ and $\mathbf{Q}_0^k$, we can show that $\mathcal{R}_2(\mathbf{q},\mathbf{p};\mathbf{w}_h,\mathbf{v}_h)\equiv 0$.

Summing the (7.3.1) with (7.3.2) and, then adding $\mathcal{S}_1(\mathbf{Q}_h\mathbf{p},\mathbf{v}_h)$ and $\mathcal{S}_2(\mathbf{Q}_h\mathbf{q},\mathbf{w}_h)$ to the both sides of the resultant equation to get

$$\begin{aligned}\mathcal{A}(\mathbf{L}_h\mathbf{q},\mathbf{Q}_h\mathbf{p};\mathbf{w}_h,\mathbf{v}_h) &= \mathcal{S}_1(\mathbf{Q}_h\mathbf{p},\mathbf{v}_h)+\mathcal{S}_2(\mathbf{L}_h\mathbf{q},\mathbf{w}_h)\\ &\quad +(\mathbf{f},\nabla_w\times\mathbf{w}_h-\gamma\mathbf{v}_0). \qquad (7.3.3)\end{aligned}$$

The difference between (7.3.3) and (7.2.9) completes the Lemma 7.3.1. □

Lemma 7.3.2. *Let* $\mathbf{q}\in[H^\alpha(\Omega)]^{2d-3}$ *and* $\mathbf{p}\in[H^{\alpha+1}(\Omega)]^d$ $(\frac{1}{2}<\alpha\le k)$. *Then, for each* $(\mathbf{w}_h,\mathbf{v}_h)\in\mathbf{W}_h\times\mathbf{V}_h^0$, *we have*

$$\begin{aligned}\mathcal{S}_1(\mathbf{Q}_h\mathbf{p},\mathbf{v}_h) &\le Ch^{\alpha+1}\|\mathbf{p}\|_{\alpha+1}|||(\mathbf{w}_h,\mathbf{v}_h)|||,\\ \mathcal{S}_2(\mathbf{L}_h\mathbf{q},\mathbf{w}_h) &\le Ch^{\alpha+1}\|\mathbf{q}\|_{\alpha}|||(\mathbf{w}_h,\mathbf{v}_h)|||.\end{aligned}$$

Proof. Using the trace inequality (7.2.10) and definition of $\mathbf{Q}_b^k$, we obtain

$$\begin{aligned}&|\mathcal{S}_1(\mathbf{Q}_h\mathbf{p},\mathbf{v}_h)|\\ &=\left|\sum_{T\in\mathcal{T}_h}h_T\langle(\mathbf{Q}_0^k\mathbf{p}-\mathbf{Q}_b^k\mathbf{p})\times\boldsymbol{\eta},(\mathbf{v}_0-\mathbf{v}_b)\times\boldsymbol{\eta}\rangle_{\partial T}\right|\\ &=\left|\sum_{T\in\mathcal{T}_h}h_T\langle(\mathbf{Q}_0^k\mathbf{p}-\mathbf{p})\times\boldsymbol{\eta},(\mathbf{v}_0-\mathbf{v}_b)\times\boldsymbol{\eta}\rangle_{\partial T}\right|\\ &\le\left(\sum_{T\in\mathcal{T}_h}h_T\|(\mathbf{Q}_0^k\mathbf{p}-\mathbf{p})\times\boldsymbol{\eta}\|_{\partial T}^2\right)^{1/2}\left(\sum_{T\in\mathcal{T}_h}h_T\|(\mathbf{v}_0-\mathbf{v}_b))\times\boldsymbol{\eta}\|_{\partial T}^2\right)^{1/2}\\ &\le Ch^{\alpha+1}\|\mathbf{p}\|_{\alpha+1}|||\mathbf{v}_h|||.\end{aligned}$$

In a similar fashion, we obtain

$$\begin{aligned}|\mathcal{S}_2(\mathbf{L}_h\mathbf{q},\mathbf{w}_h)| &= \left|\sum_{T\in\mathcal{T}_h}h_T^3\langle\mathbf{L}_0^k\mathbf{q}-\mathbf{L}_b^k\mathbf{q},\mathbf{w}_0-\mathbf{w}_b\rangle_{\partial T}\right|\\ &\le \sum_{T\in\mathcal{T}_h}h_T^3\|\mathbf{L}_0^k\mathbf{q}-\mathbf{q}\|_{\partial T}\|\mathbf{w}_0-\mathbf{w}_b\|_{\partial T}\\ &\le Ch^{\alpha+1}\|\mathbf{q}\|_\alpha|||(\mathbf{w}_h,\mathbf{v}_h)|||.\end{aligned}$$

This completes the Lemma 7.3.2. □

Theorem 7.3.1. *Assume that* $(\mathbf{q},\mathbf{p})\in[H^\alpha(\Omega)]^{2d-3}\times[H^{\alpha+1}(\Omega)]^d$ $(\frac{1}{2}<\alpha\le k)$ *is the exact solution of the problem* (7.1.3)-(7.1.5). *Let* $(\mathbf{q}_h,\mathbf{p}_h)\in\mathbf{W}_h\times\mathbf{V}_h^0$ *be the LSWG solution of the equation* (7.2.9). *Then, we have*

$$|||(\mathbf{L}_h\mathbf{q}-\mathbf{q}_h,\mathbf{Q}_h\mathbf{p}-\mathbf{p}_h)|||\le Ch^{\alpha+1}\left(\|\mathbf{p}\|_{\alpha+1}+\|\mathbf{q}\|_\alpha\right). \qquad (7.3.4)$$

Proof. By substituting $\mathbf{v}_h = \mathbf{e}_h^{\mathbf{p}}$ and $\mathbf{w}_h = \mathbf{e}_h^{\mathbf{q}}$ in Lemma 7.3.1, we get

$$\mathcal{A}(\mathbf{e}_h^{\mathbf{q}}, \mathbf{e}_h^{\mathbf{p}}; \mathbf{e}_h^{\mathbf{q}}, \mathbf{e}_h^{\mathbf{p}}) = \mathcal{R}(\mathbf{q}, \mathbf{p}; \mathbf{e}_h^{\mathbf{q}}, \mathbf{e}_h^{\mathbf{p}}).$$

Then the desired estimate follows directly from the Lemma 7.3.2. □

Remark 7.3.1. *For* $(\mathbf{q}, \mathbf{p}) \in [H^\alpha(\Omega)]^{2d-3} \times [H^\alpha(\Omega)]^d$ $(\frac{1}{2} < \alpha \leq 1)$, *we note that*

$$|\mathcal{S}_1(\mathbf{Q}_h\mathbf{p}, \mathbf{v}_h)| + |\mathcal{S}_2(\mathbf{L}_h\mathbf{q}, \mathbf{w}_h)| \leq Ch^\alpha \left(\|\mathbf{p}\|_\alpha + \|\mathbf{q}\|_\alpha\right) |||(\mathbf{w}_h, \mathbf{v}_h)|||. \tag{7.3.5}$$

Then, from (7.3.5), *the a priori error estimate* (7.3.4) *may be recaptured as*

$$|||(\mathbf{e}_h^{\mathbf{q}}, \mathbf{e}_h^{\mathbf{p}})||| \leq Ch^\alpha \left(\|\mathbf{p}\|_\alpha + \|\mathbf{q}\|_\alpha\right). \tag{7.3.6}$$

In fact, estimate (7.3.6) generalizes Theorem 3.7 in [91] in the sense that convergence result therein required

$$\begin{aligned} (\mathbf{p}, \mathbf{q}) &\in \left[H^{m+1}(\Omega)\right]^d \times \left[H^{m+1}(\Omega)\right]^{2d-3} \quad \& \\ (\nabla \times \mathbf{p}, \nabla \times \mathbf{q}) &\in \left[H^{m+1}(\Omega)\right]^{2d-3} \times \left[H^{m+1}(\Omega)\right]^d \end{aligned}$$

in order to maintain $\mathrm{O}(h^m)$, $m \geq 1$, *convergence rate in the energy norm.*

7.4 Numerical Experiments

Below we will explore the practical performance of the proposed LSWG method through the numerical approximation of the indefinite time-harmonic problems (7.1.3)-(7.1.5) in two and three dimensions. We present a series of numerical experiments to justify the accuracy, flexibility, and efficiency of the proposed algorithm. We demonstrate the convergence and accuracy of the LSWG method on a sequence of unstructured meshes including pentagons-quadrilaterals, hexagons-pentagons-quadrilaterals, and non-uniform triangular meshes. Uniform cubic meshes with $\mathcal{P}_k$ polynomials are used for three-dimensional problems. Particular attentions will be paid on verifying its high-order convergence with high wave number and examining its robustness in dealing with low regularity solutions. In the sequel, to verify the stability of our LSWG method with large wave number, we will test the convergence rates for the relative errors in the L^2 norm which are defined by

$$\mathrm{RE}_{\mathbf{p}} := \frac{\|\mathbf{p} - \mathbf{p}_0\|}{\|\mathbf{p}\|} \quad \text{and} \quad \mathrm{RE}_{\mathbf{q}} := \frac{\|\mathbf{q} - \mathbf{q}_0\|}{\|\mathbf{q}\|}.$$

All the mesh generations and computations are conducted in the MATLAB environment.

Example 7.4.1. (**The square domain problem**) In this example, we will perform the LSWG method for a sufficiently smooth solution in a unit square $\Omega = [0,1] \times [0,1]$ with pentagons-quadrilaterals meshes. The initial mesh and its next two refinements are depicted in Figure 7.4.1(a)-7.4.1(c). We set the exact solution as [74, 91]

$$\mathbf{p} = (p_1, p_2)^t = (\sin(\gamma y), \sin(\gamma x))^t, \tag{7.4.1}$$

such that the source term and the boundary data are chosen accordingly. The numerical errors and convergence results for $k = 1, 2, 3$ with wave numbers $\gamma = 2, 8$ have been demonstrated in the Tables 7.4.1-7.4.2. Here, we observe that approximation errors $\|\mathbf{p} - \mathbf{p}_0\|$ and $\|\mathbf{q} - \mathbf{q}_0\|$ converge to zero at the optimal rate $\mathcal{O}(h^{k+1})$, for each fixed k and each γ, as h tends to zero. Further, from the numerical errors it can be seen that the convergence under triple-bar norm $|||(\mathbf{e}_h^{\mathbf{q}}, \mathbf{e}_h^{\mathbf{p}})|||$ is of order $\mathcal{O}(h^{k+1})$, which is higher than the LS-DG method presented in [91] and as predicted by Theorem 7.3.1. As the wave number γ increases, we note that the errors in the approximation to the exact solution also become larger under all error measurements. This observation is consistent with the earlier works in [74, 91, 105]. The component-wise surface plots for the exact solution and LSWG solution on the finest mesh (*i.e.*, after the fifth refinement of the initial mesh) with linear element are presented in Figures 7.4.2-7.4.3. In addition, the solution field of the LSWG solution $\mathbf{p}_h$ with quadratic element is plotted in Figure 7.4.4 for $\gamma = 1, 4$ on mesh level 4.

Example 7.4.2. (**The L-shaped domain problem with nonsmooth solution**) In this test we investigate the performance of the LSWG method for dealing with a problem that involves the singularity at the corner. Let $\Omega = (-1,1)^2 \setminus [0,1) \times (-1,0]$ be the L-shaped domain (Figure 7.4.1(d)) and we choose the analytical solution $\mathbf{p}$, in terms of the polar coordinates (r, θ), to be [74, 91, 105]

$$\mathbf{p}(x,y) = (p_1, p_2) = \nabla((\gamma r)^\alpha \sin(\alpha\theta)) + (\sin(\gamma y), \sin(\gamma x))^t, \tag{7.4.2}$$

where $\alpha = 2/3$. Hence, the exact solution $\mathbf{p}$ is nonsmooth and indeed singular at the entrant corner $(0,0)$, and $\mathbf{p} \in \mathbf{H}^{\alpha-\epsilon}(\Omega)$ for arbitrarily small $\epsilon > 0$. Here we employ non-uniform triangular mesh shown in Figure 7.4.1(d). The numerical errors and convergence results corresponding to the variables $\mathbf{p}_h$ and $\mathbf{q}_h$ on a sequence of successively finer (quasi-uniform) unstructured triangular meshes for $k = 1$ and $\gamma = 4, 6$ are presented in Tables 7.4.3-7.4.4. As in the previous example, we clearly observe that the error under triple-bar norm $|||\cdot,\cdot|||$ converges to zero at the optimal rate $\mathcal{O}(h^\alpha)$ for each fixed γ, as h tends to zero, and this convergence rate is in agreement with the rate predicted by

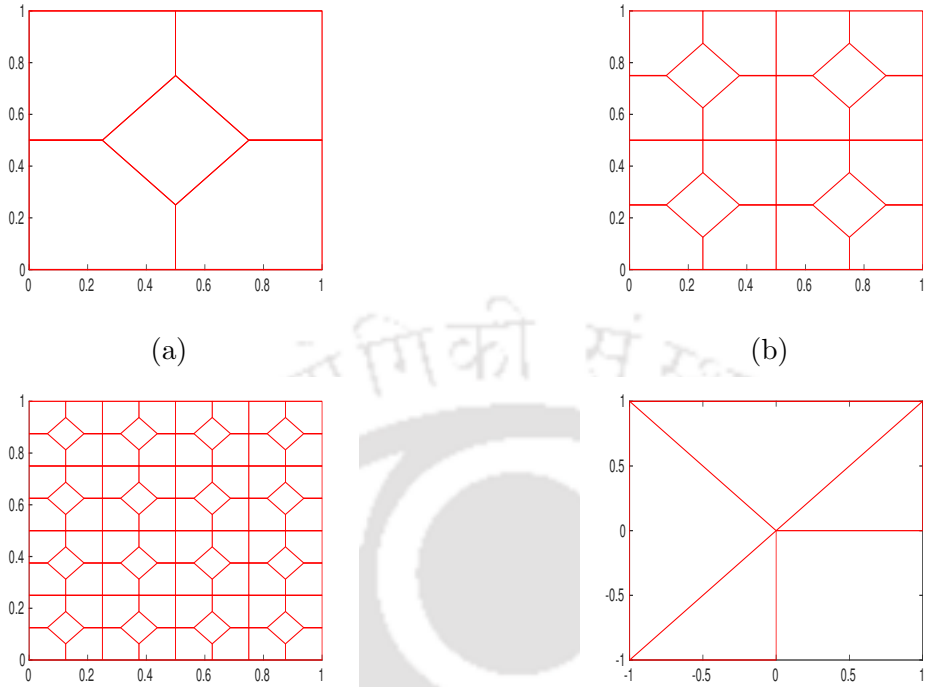

Figure 7.4.1: The first 3-mesh levels (a)-(c) for the Example 7.4.1 and initial mesh level (d) for Example 7.4.2.

estimate (7.3.6). Further, from the numerical validation we can see that the L^2 norm error $\|\mathbf{p}-\mathbf{p}_0\|$ also converges to zero at the same rate, and which is consistent with the regularity of the exact solution $\mathbf{p}$. On the other hand, for the variable $\mathbf{q}$, the numerically observed convergence rate is about $\mathcal{O}(h^{1.33})$ in terms of the L^2 norm (cf. Figure 7.4.5). This numerical phenomenon may depend on the regularity of $\mathbf{q}$ and the fact

$$\|\mathbf{q}-\mathbf{q}_0\| \approx \|\mathbf{q}-\mathbf{L}_0^k\mathbf{q}\| + \|\mathbf{L}_0^k\mathbf{q}-\mathbf{q}_0\| \approx \mathcal{O}(h^2) + \mathcal{O}(h^{.67}).$$

Such pleasant convergence phenomenon of the LS-FEM is consistent with the numerical results in [91]. In addition, the vector plots of linear LSWG solutions $\mathbf{p}_h$ for $\gamma = 6, 8$ on the mesh level 4 are depicted in the Figure 7.4.5. These numerical results show that the proposed algorithm is computationally effective for solving the time-harmonic Maxwell's equations.

Example 7.4.3. (**Smooth solution in 3D**) In this test we shall implement the algorithm in a three-dimensional domain $\Omega = (0,1)^3$ with smooth solution. We solve the test problem on a series of uniform cubic meshes for different weak Galerkin finite

Table 7.4.1: Convergence profiles for Example 7.4.1 with $\gamma = 2$

k	Level	$\|\|\|(\mathbf{e}_h^{\mathbf{q}}, \mathbf{e}_h^{\mathbf{p}})\|\|\|$	Order	$\|\mathbf{e}_0^{\mathbf{p}}\|$	Order	$\|\mathbf{e}_0^{\mathbf{q}}\|$	Order	$\|\mathbf{Q}_0^k\mathbf{p} - \mathbf{p}\|$	Order	$\|\mathbf{L}_0^k\mathbf{q} - \mathbf{q}\|$	Order
1	1	7.80e-02	—	5.28e-02	—	4.30e-02	—	5.17e-01	—	4.09e-01	—
	2	1.95e-02	1.99	1.33e-02	1.98	1.17e-02	1.87	1.26e-01	2.03	1.04e-01	1.97
	3	4.89e-03	1.99	3.34e-03	1.99	3.03e-03	1.95	3.09e-02	2.02	2.62e-02	1.99
	4	1.22e-03	1.99	8.38e-04	1.99	7.67e-04	1.98	7.67e-03	2.01	6.56e-03	1.99
	5	3.05e-04	2.00	2.09e-04	2.00	1.92e-04	2.00	1.91e-03	2.00	1.64e-03	2.00
	6	7.64e-05	2.00	5.23e-05	2.00	4.81e-05	2.00	4.78e-04	2.00	4.10e-04	2.00
2	1	4.27e-03	—	6.34e-03	—	4.77e-03	—	6.95e-02	—	5.68e-02	—
	2	5.74e-04	2.89	7.23e-04	3.13	6.38e-04	2.90	1.33e-02	2.38	6.80e-03	3.06
	3	7.40e-05	2.95	8.47e-05	3.09	8.22e-05	2.95	1.96e-03	2.76	7.76e-04	3.13
	4	9.39e-06	2.97	1.02e-05	3.05	1.04e-05	2.97	2.61e-04	2.91	9.07e-05	3.09
	5	1.18e-06	2.99	1.25e-06	3.02	1.31e-06	2.99	3.35e-05	2.96	1.09e-05	3.05
	6	1.48e-07	3.00	1.55e-07	3.01	1.64e-07	3.00	4.23e-06	2.99	1.33e-06	3.02
3	1	2.16e-04	—	6.57e-04	—	1.98e-04	—	2.48e-02	—	1.16e-02	—
	2	1.41e-05	3.93	4.03e-05	4.02	1.29e-05	3.93	2.00e-03	3.62	7.11e-04	4.03
	3	9.03e-07	3.96	2.49e-06	4.01	8.27e-07	3.97	1.36e-04	3.88	4.35e-05	4.02
	4	5.70e-08	3.98	1.55e-07	4.00	5.22e-08	3.99	8.81e-06	3.95	2.69e-06	4.01
	5	3.58e-09	3.99	9.66e-09	4.00	3.28e-09	3.99	5.59e-07	3.98	1.67e-07	4.00
	6	2.05e-10	3.99	6.03e-10	4.00	2.05e-10	4.00	3.51e-08	3.99	1.04e-08	4.00

element spaces. The exact solution is selected as [91]

$$\mathbf{p}(x, y, z) = (p_1, p_2, p_3)^t = \begin{pmatrix} \sin(\gamma y)\sin(\gamma z) \\ \sin(\gamma x)\sin(\gamma z) \\ \sin(\gamma x)\sin(\gamma y) \end{pmatrix}.$$

The initial mesh is shown in Figure 7.4.6. Then we refine each cube into eight half-sized cubes to get the next level grid. In the classical finite element method, one has to use a $\mathcal{Q}_k$ polynomial on a cubic mesh and a $\mathcal{P}_k$ polynomial on a tetrahedron mesh. For the proposed WG method, we can use $\mathcal{P}_k$ polynomials on any polyhedral mesh. To demonstrate the flexibility of the method, we use $\mathcal{P}_k$ polynomials, instead of traditional $\mathcal{Q}_k$ polynomials, on cubic meshes. The numerical errors with wave number $\gamma = 1, 10$ for the linear, quadratic and cubic LSWG methods are reported in Tables 7.4.5 and 7.4.6, respectively. It can be seen that the theoretical superconvergence (*i.e.*, $\mathcal{O}(h^{k+1})$) is achieved under triple-bar norm in this numerical test. Moreover, a convergence $\mathcal{O}(h^{k+1})$

Table 7.4.2: Convergence profiles for Example 7.4.1 with $\gamma = 8$.

k	Level	$\|\|\|(\mathbf{e}_h^{\mathbf{q}}, \mathbf{e}_h^{\mathbf{p}})\|\|\|$	Order	$\|\mathbf{e}_0^{\mathbf{p}}\|$	Order	$\|\mathbf{e}_0^{\mathbf{q}}\|$	Order	$\|\mathbf{Q}_0^k\mathbf{p} - \mathbf{p}\|$	Order	$\|\mathbf{L}_0^k\mathbf{q} - \mathbf{q}\|$	Order
1	1	1.09e+00	—	1.20e+00	—	1.05e+00	—	2.11e-01	—	3.24e+00	—
	2	3.26e-01	1.74	3.41e-01	1.81	3.13e-01	1.74	5.19e-02	2.02	8.91e-01	1.86
	3	8.53e-02	1.93	8.77e-02	1.96	8.22e-02	1.93	1.28e-02	2.02	2.36e-01	1.91
	4	2.15e-02	1.98	2.20e-02	1.99	2.08e-02	1.98	3.18e-03	2.00	6.05e-02	1.96
	5	5.41e-03	2.00	5.52e-03	1.99	5.22e-03	1.99	7.94e-04	2.00	1.52e-02	1.98
	6	1.35e-03	2.00	1.38e-03	2.00	1.30e-03	2.00	1.98e-04	2.00	3.82e-03	1.99
2	1	2.69e-01	—	4.01e-01	—	2.74e-01	—	2.21e-02	—	8.49e-01	—
	2	3.92e-02	2.77	5.32e-02	2.91	3.96e-02	2.78	2.48e-03	3.15	1.22e-01	2.79
	3	5.17e-03	2.92	6.06e-03	3.13	5.22e-03	2.92	2.71e-04	3.19	1.58e-02	2.94
	4	6.60e-04	2.97	7.07e-04	3.10	6.66e-04	2.97	3.05e-05	3.15	1.98e-03	2.99
	5	8.32e-05	2.98	8.57e-05	3.04	8.39e-05	2.98	3.55e-06	3.10	2.46e-04	3.00
	6	1.04e-05	2.99	1.05e-05	3.01	1.05e-05	2.99	4.27e-07	3.05	3.06e-05	3.00
3	1	4.87e-02	—	1.41e-01	—	4.78e-02	—	3.23e-03	—	1.83e-01	—
	2	3.30e-03	3.88	9.66e-03	3.87	3.27e-03	3.87	2.04e-04	3.98	1.39e-02	3.71
	3	2.13e-04	3.95	6.05e-04	3.99	2.11e-04	3.95	1.27e-05	4.00	9.23e-04	3.92
	4	1.34e-05	3.98	3.76e-05	4.00	1.33e-05	3.98	7.93e-07	4.00	5.81e-05	3.98
	5	8.48e-07	3.99	2.34e-06	4.00	8.40e-07	3.99	4.94e-08	4.00	3.62e-06	4.00
	6	5.31e-08	4.00	1.46e-07	4.00	5.26e-08	3.99	3.08e-09	4.00	2.26e-07	4.00

Table 7.4.3: Convergence profiles for Example 7.4.2 with $\gamma = 4$.

k	Level	$\|\|\|(\mathbf{e}_h^{\mathbf{q}}, \mathbf{e}_h^{\mathbf{p}})\|\|\|$	Order	$\|\mathbf{e}_0^{\mathbf{p}}\|$	Order	$\|\mathbf{e}_0^{\mathbf{q}}\|$	Order	$\|\mathbf{Q}_0^k\mathbf{p} - \mathbf{p}\|$	Order	$\|\mathbf{L}_0^k\mathbf{q} - \mathbf{q}\|$	Order
1	1	7.74e-01	—	4.19e-01	—	1.02e+00	—	1.44e+00	—	4.02e-03	—
	2	4.92e-01	0.65	2.66e-01	0.65	6.53e-01	0.64	9.23e-01	0.65	1.40e-03	1.52
	3	3.10e-01	0.66	1.68e-01	0.66	4.12e-01	0.66	5.85e-01	0.65	3.90e-04	1.84
	4	1.95e-01	0.66	1.05e-01	0.66	2.60e-01	0.66	3.69e-01	0.66	1.00e-04	1.95
	5	1.23e-01	0.66	6.67e-02	0.66	1.64e-01	0.66	2.32e-01	0.67	2.54e-05	1.99
	6	7.77e-02	0.67	4.20e-02	0.67	1.03e-01	0.67	1.46e-01	0.67	6.39e-06	2.00

for both $\|\mathbf{p} - \mathbf{p}_0\|$ and $\|\mathbf{q} - \mathbf{q}_0\|$ is observed for $1 \leq k \leq 3$. These numerical results are quite similar to those of the previous Example 7.4.1 with smooth solution. On the contrary, the L^2 errors for the LS-DG method presented in [91] are shown to be sub-optimal. In addition, we graph the analytic solution for $\gamma = 1$ and its linear LSWG approximation using mesh level 6 in Figures 7.4.6-7.4.7.

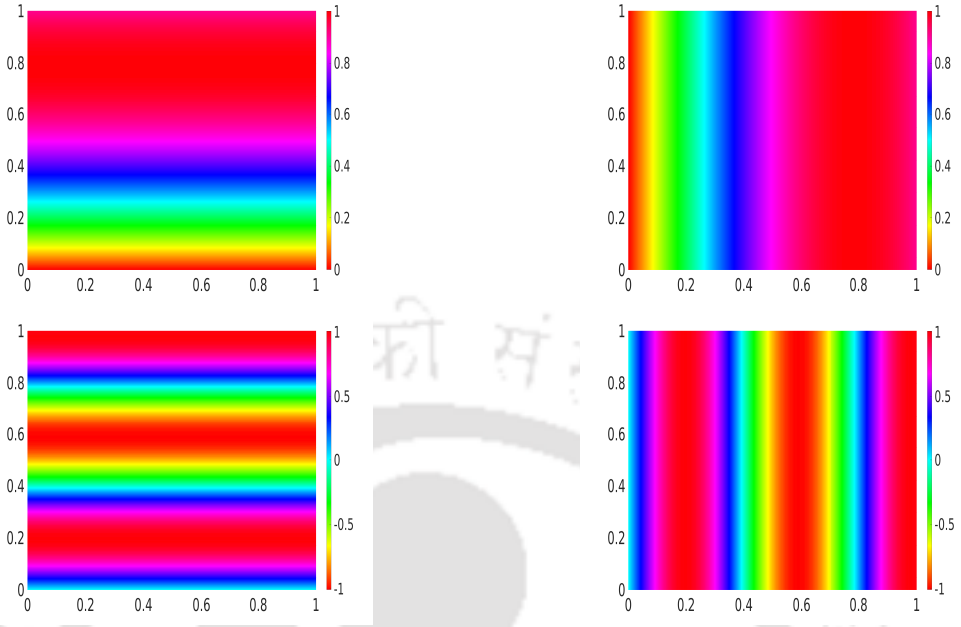

Figure 7.4.2: (Example 7.4.1) First component (left) and second component (right) of the analytical solution for $\gamma = 2$ (top) and $\gamma = 8$ (bottom).

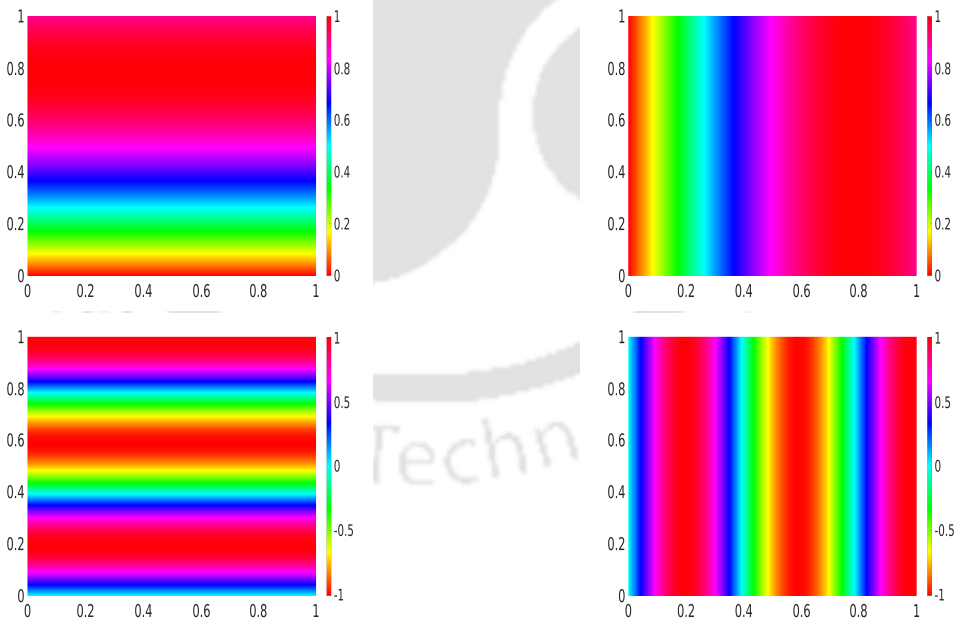

Figure 7.4.3: (Example 7.4.1) First component (left) and second component (right) of the LSWG solution for $\gamma = 2$ (top) and $\gamma = 8$ (bottom).

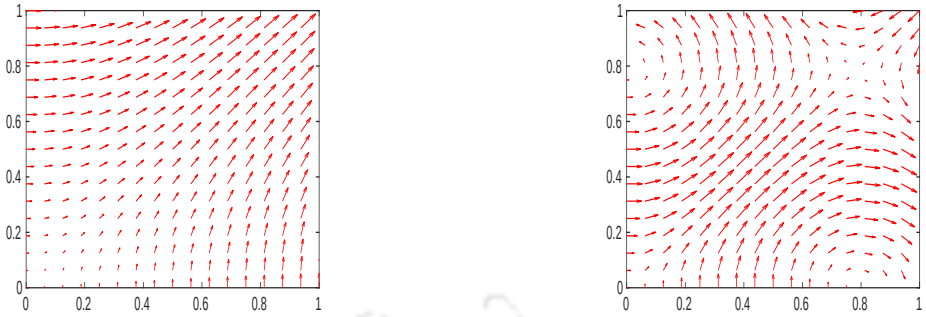

Figure 7.4.4: The LSWG solution fields for $\gamma = 1$ (left) and $\gamma = 4$ (right) of Example 7.4.1.

Table 7.4.4: Convergence profiles for Example 7.4.2 with $\gamma = 6$.

k	Level	$\|\|\|(\mathbf{e}_h^{\mathbf{q}}, \mathbf{e}_h^{\mathbf{p}})\|\|\|$	Order	$\|\|\mathbf{e}_0^{\mathbf{p}}\|\|$	Order	$\|\|\mathbf{e}_0^{\mathbf{q}}\|\|$	Order	$\|\|\mathbf{Q}_0^k\mathbf{p} - \mathbf{p}\|\|$	Order	$\|\|\mathbf{L}_0^k\mathbf{q} - \mathbf{q}\|\|$	Order
	1	3.66e+00	—	6.98e-01	—	2.58e+00	—	1.56e+00	—	6.04e-03	—
	2	1.59e+00	1.19	4.44e-01	0.65	1.41e+00	0.87	1.01e+00	0.63	2.10e-03	1.52
	3	9.00e-01	0.82	2.80e-01	0.66	8.79e-01	0.68	6.39e-01	0.65	5.86e-04	1.84
1	4	5.56e-01	0.69	1.76e-01	0.66	5.53e-01	0.66	4.03e-01	0.66	1.51e-04	1.95
	5	3.49e-01	0.67	1.11e-01	0.67	3.49e-01	0.66	2.54e-01	0.66	3.82e-05	1.98
	6	2.19e-01	0.67	7.02e-02	0.67	2.19e-01	0.66	1.60e-01	0.66	9.58e-06	2.00

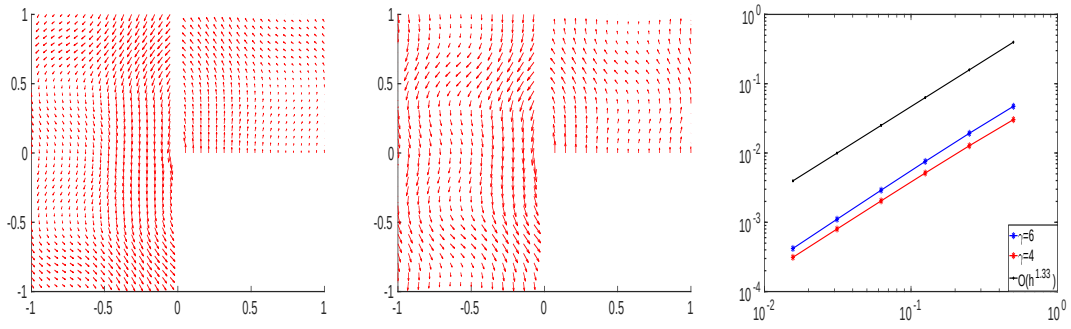

Figure 7.4.5: (Example 7.4.2) The LSWG solution fields for $\gamma = 6$ (left) and $\gamma = 8$ (middle) along with error plots (right).

Example 7.4.4. **(Nonsmooth solution in 3D)** We consider the three-dimensional domain $\Omega = (0,1)^3$ with uniform cubic partition and select the low regular exact solution $\mathbf{p}$ as (cf. [9, 90])

$$\mathbf{p}(x,y,z) = \nabla((x^2+y^2+z^2)^{\alpha/2}\sin(\alpha\theta)),$$

Table 7.4.5: Convergence profiles for Example 7.4.3 with $\gamma = 1$.

k	Level	$\|\|\|(\mathbf{e}_h^{\mathbf{q}}, \mathbf{e}_h^{\mathbf{p}})\|\|\|$	Order	$\|\mathbf{e}_0^{\mathbf{p}}\|$	Order	$\|\mathbf{e}_0^{\mathbf{q}}\|$	Order	$\|\mathbf{Q}_0^k\mathbf{p} - \mathbf{p}\|$	Order	$\|\mathbf{L}_0^k\mathbf{q} - \mathbf{q}\|$	Order
1	2	1.38e-02	—	6.95e-02	—	7.28e-02	—	2.55e-01	—	5.19e-01	—
	3	3.48e-03	1.99	1.73e-02	2.00	1.83e-02	1.98	6.33e-02	2.01	1.50e-01	1.78
	4	8.71e-04	1.99	4.34e-03	2.00	4.60e-03	1.99	1.58e-02	2.00	3.91e-02	1.94
	5	2.17e-04	1.99	1.08e-03	1.99	1.15e-03	1.99	3.96e-03	1.99	9.88e-03	1.98
	6	5.44e-05	1.99	2.71e-04	1.99	2.88e-04	1.99	9.90e-04	1.99	2.48e-03	1.99
	7	1.36e-05	2.00	6.78e-05	2.00	7.21e-05	2.00	2.47e-04	2.00	6.20e-04	2.00
2	2	1.85e-03	—	5.81e-03	—	5.22e-03	—	4.57e-02	—	1.61e-01	—
	3	2.31e-04	3.00	7.28e-04	2.99	6.53e-04	2.99	6.59e-03	2.79	2.26e-02	2.83
	4	2.89e-05	3.00	9.11e-05	2.99	8.16e-05	2.99	8.54e-04	2.94	2.91e-03	2.96
	5	3.61e-06	3.00	1.13e-05	2.99	1.021e-05	2.99	1.07e-04	2.98	3.66e-04	2.98
	6	4.52e-07	3.00	1.42e-06	2.99	1.27e-06	2.99	1.35e-05	2.99	4.58e-05	3.00
	7	5.65e-08	3.00	1.78e-07	3.00	1.59e-07	3.00	1.68e-06	3.00	5.73e-06	3.00
3	2	1.27e-04	—	3.29e-04	—	3.04e-05	—	1.19e-02	—	1.29e-02	—
	3	8.00e-06	3.99	2.09e-05	3.97	1.90e-06	3.99	8.36e-04	3.83	9.01e-04	3.84
	4	5.00e-07	3.99	1.31e-06	3.99	1.19e-07	3.99	5.36e-05	3.96	5.77e-05	3.96
	5	3.13e-08	3.99	8.23e-08	3.99	7.45e-09	4.00	3.37e-06	3.99	3.63e-06	3.99
	6	1.959e-09	4.00	5.15e-09	3.99	4.65e-10	4.00	2.11e-07	4.00	2.27e-07	4.00
	7	1.22e-10	4.00	3.22e-10	4.00	2.99e-11	4.00	1.31e-08	4.00	1.42e-08	4.00

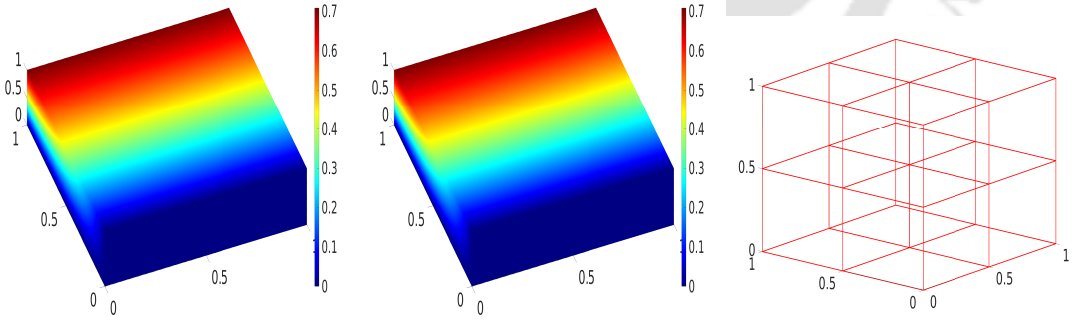

Figure 7.4.6: (Example 7.4.3) Surface plots for the first component of analytical solution (left) and its LSWG solution (middle) along with initial mesh (right).

where $\alpha \in (0, 1]$ and $\theta = \tan^{-1}(y/x)$. The solution $\mathbf{p}$ is not in $\mathbf{H}^1(\Omega)$, instead in $\mathbf{H}^{\alpha-\epsilon}(\Omega)$ for small $\epsilon > 0$. The numerical errors of the linear LSWG method for wave number $\gamma = 1, 6$ are reported in Tables 7.4.7 and 7.4.8, respectively, for different values of α. Under all error measurements, we observe that the convergence rate is $\mathcal{O}(h^\alpha)$. The

Table 7.4.6: Convergence profiles for Example 7.4.3 with $\gamma = 10$.

k	Level	$\|\|\|(\mathbf{e}_h^{\mathbf{q}}, \mathbf{e}_h^{\mathbf{p}})\|\|\|$	Order	$\|\mathbf{e}_0^{\mathbf{p}}\|$	Order	$\|\mathbf{e}_0^{\mathbf{q}}\|$	Order	$\|\mathbf{Q}_0^k\mathbf{p} - \mathbf{p}\|$	Order	$\|\mathbf{L}_0^k\mathbf{q} - \mathbf{q}\|$	Order
	2	3.04e+00	—	2.06e-01	—	2.92e-01	—	4.50e-01	—	8.78e-01	—
	3	8.09e-01	1.91	5.09e-02	2.01	7.50e-02	1.96	1.14e-01	1.98	2.34e-01	1.90
	4	2.05e-01	1.97	1.27e-02	2.00	1.90e-02	1.98	2.87e-02	1.99	5.98e-02	1.97
1	5	5.17e-02	1.99	3.17e-03	2.00	4.77e-03	1.99	7.21e-03	1.99	1.50e-02	1.99
	6	1.29e-02	1.99	7.93e-04	2.00	1.19e-03	1.99	1.80e-03	1.99	3.76e-03	1.99
	7	3.23e-03	1.99	1.98e-04	2.00	2.99e-04	2.00	4.51e-04	2.00	9.42e-04	2.00
	2	8.82e-01	—	3.91e-02	—	6.73e-02	—	7.74e-02	—	1.59e-01	—
	3	1.17e-01	2.91	5.02e-03	2.96	9.13e-03	2.88	1.03e-02	2.90	2.24e-02	2.83
	4	1.49e-02	2.97	6.31e-04	2.99	1.16e-03	2.96	1.31e-03	2.97	2.90e-03	2.95
2	5	1.87e-03	2.99	7.90e-05	2.99	1.46e-04	2.99	1.65e-04	2.99	3.66e-04	2.98
	6	2.34e-04	3.00	9.88e-06	2.99	1.83e-05	2.99	2.06e-05	2.99	4.59e-05	2.99
	7	2.93e-05	3.00	1.23e-06	3.00	2.29e-06	3.00	2.58e-06	3.00	5.75e-06	3.00
	2	1.84e-01	—	4.82e-03	—	1.16e-02	—	1.18e-02	—	1.01e-03	—
	3	1.19e-02	3.94	3.03e-04	3.99	8.25e-04	3.82	8.33e-04	3.83	6.36e-05	3.99
	4	7.60e-04	3.98	1.89e-05	3.99	5.33e-05	3.95	5.38e-05	3.95	3.98e-06	3.99
3	5	4.77e-05	3.99	1.18e-06	4.00	3.36e-06	3.98	3.39e-06	3.98	2.49e-07	4.00
	6	2.98e-06	4.00	7.41e-08	4.00	2.10e-07	3.99	2.12e-07	3.99	1.55e-08	4.00
	7	1.86e-07	4.00	4.63e-09	4.00	1.31e-08	4.00	1.32e-08	4.00	9.73e-10	4.00

solution plots of the LSWG solution $\mathbf{p}_h$ at mesh level 6 are demonstrated in the Figure 7.4.8 for $\alpha = \frac{1}{4}$ and $\alpha = \frac{2}{3}$ with $\gamma = 1$.

Example 7.4.5. (**The L-shaped domain problem with smooth solution**) In this test, we consider a bench-mark example for the time-harmonic Maxwell's equations in a L-shaped domain $\Omega = (-1,1)^2 \setminus [0,1) \times (-1,0]$, see in [2, 74, 105]. The exact solution is selected as $\mathbf{p} = \nabla \times B$, where $B = J_\beta(\gamma r)\cos(\beta\theta)$ with $r = (x^2 + y^2)^{\frac{1}{2}}$ and $\theta = \tan^{-1}(y/x)$. Here J_β is the Bessel function of the first kind of order β. We set $\beta = 0$ so that the exact solution is smooth. The hexagons-pentagons-quadrilaterals meshes have been used for the proposed algorithm, see in Figure 7.4.10. We present in Table 7.4.9 the approximation errors and corresponding convergence rates for the primal variable $\mathbf{p}_h$ and auxiliary variable $\mathbf{q}_h$ with $\gamma = 20$, from which we observe a convergence rate of $\mathcal{O}(h^{k+1})$ for both for both $\|\mathbf{p} - \mathbf{p}_0\|$ and $\|\mathbf{q} - \mathbf{q}_0\|$. Our results agree very well with the previous results reported in [105]. We also see that $(\mathbf{q}_h, \mathbf{p}_h)$ converges with order $k+1$ under triple-bar norm. These results are similar to those of smooth domain

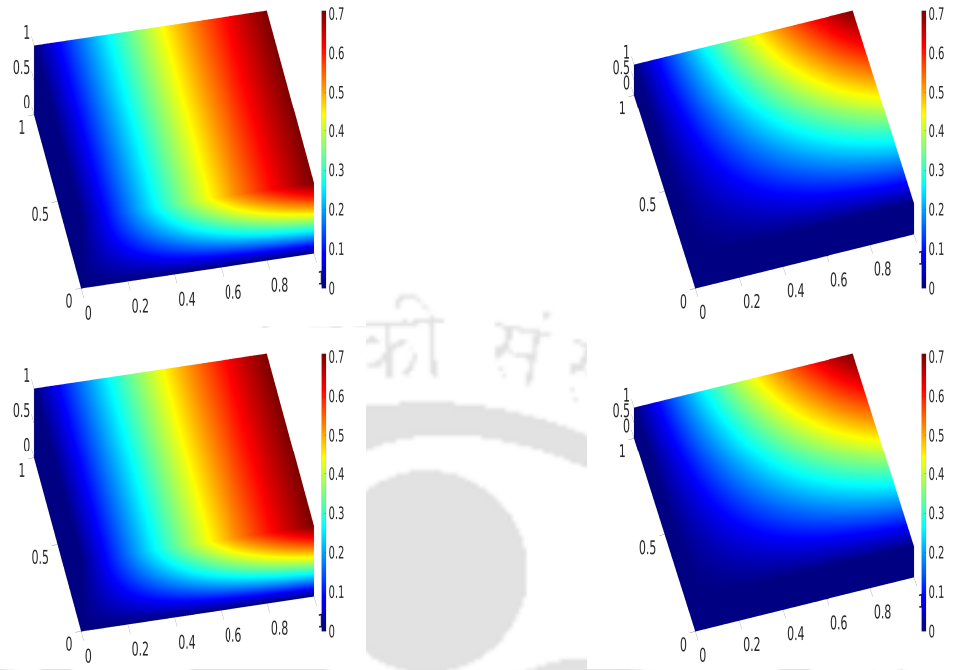

Figure 7.4.7: (Example 7.4.3) The second component (left) and the third component (right) of analytical solution (top) and its LSWG solution (bottom).

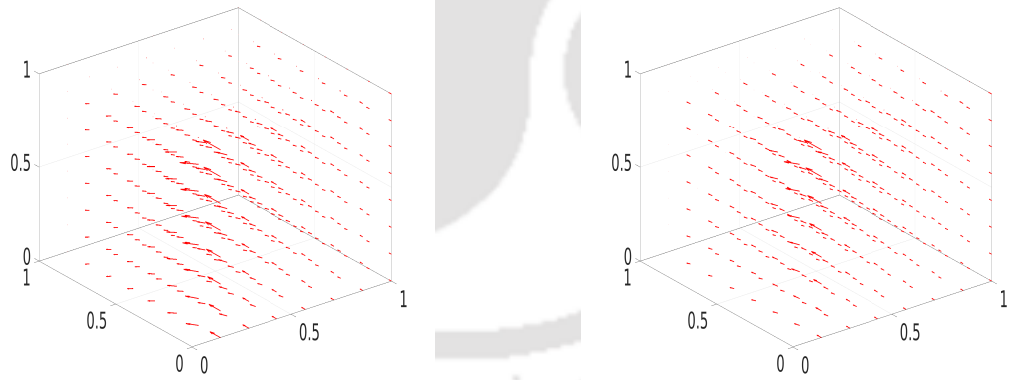

Figure 7.4.8: (Example 7.4.4) Numerical solution fields for $\alpha = \frac{1}{4}$ (left) and $\alpha = \frac{2}{3}$ (right).

problems. The robustness and effectiveness of the scheme can be visualized from the Figures 7.4.10 and 7.4.9 that illustrate the plots of $\nabla \times \mathbf{p}_h$ and component-wise surface plots of $\mathbf{p}_h$, respectively, for $\gamma = 5,\ 10$ and the same polynomial degree $k = 2$.

Example 7.4.6. (**Relative errors with non-smooth solution**) We revisit the L-shaped domain problem described in Example 7.4.5 with $\beta = 2/3$ so that the exact

Table 7.4.7: Convergence profiles for Example 7.4.4 with $\gamma = 1$.

α	Level	$\|\|\|(\mathbf{e}_h^{\mathbf{q}}, \mathbf{e}_h^{\mathbf{p}})\|\|\|$	Order	$\|\mathbf{e}_0^{\mathbf{p}}\|$	Order	$\|\mathbf{e}_0^{\mathbf{q}}\|$	Order	$\|\mathbf{Q}_0^k\mathbf{p} - \mathbf{p}\|$	Order
$\frac{1}{4}$	1	1.65e-01	—	1.33e-01	—	7.88e-02	—	3.46e-02	—
	2	1.40e-01	0.23	1.12e-01	0.24	6.63e-02	0.25	2.91e-02	0.25
	3	1.18e-01	0.24	9.46e-02	0.24	5.57e-02	0.25	2.45e-02	0.25
	4	9.94e-02	0.24	7.95e-02	0.24	4.68e-02	0.25	2.06e-02	0.25
	5	8.36e-02	0.24	6.68e-02	0.25	3.94e-02	0.25	1.73e-02	0.25
	6	7.03e-02	0.25	5.62e-02	0.25	3.31e-02	0.25	1.45e-02	0.25
$\frac{1}{2}$	1	2.65e-01	—	1.86e-01	—	1.39e-01	—	7.46e-02	0.50
	2	1.89e-01	0.48	1.32e-01	0.49	9.84e-02	0.49	5.27e-02	0.50
	3	1.34e-01	0.49	9.34e-02	0.49	6.96e-02	0.50	3.73e-02	0.50
	4	9.56e-02	0.49	6.60e-02	0.49	4.92e-02	0.50	2.63e-02	0.50
	5	6.77e-02	0.49	4.67e-02	0.49	3.48e-02	0.50	1.86e-02	0.50
	6	4.79e-02	0.49	3.30e-02	0.50	2.46e-02	0.50	1.31e-02	0.50
$\frac{3}{4}$	1	1.60e-01	—	1.08e-01	—	7.26e-02	—	8.00e-02	—
	2	9.53e-02	0.74	6.44e-02	0.74	4.31e-02	0.75	4.75e-02	0.75
	3	5.67e-02	0.74	3.83e-02	0.74	2.56e-02	0.75	2.82e-02	0.75
	4	3.37e-02	0.74	2.27e-02	0.75	1.52e-02	0.75	1.68e-02	0.75
	5	2.00e-02	0.74	1.35e-02	0.75	9.08e-03	0.75	1.00e-02	0.75
	6	1.195e-02	0.74	8.05e-03	0.75	5.39e-03	0.75	5.94e-03	0.75

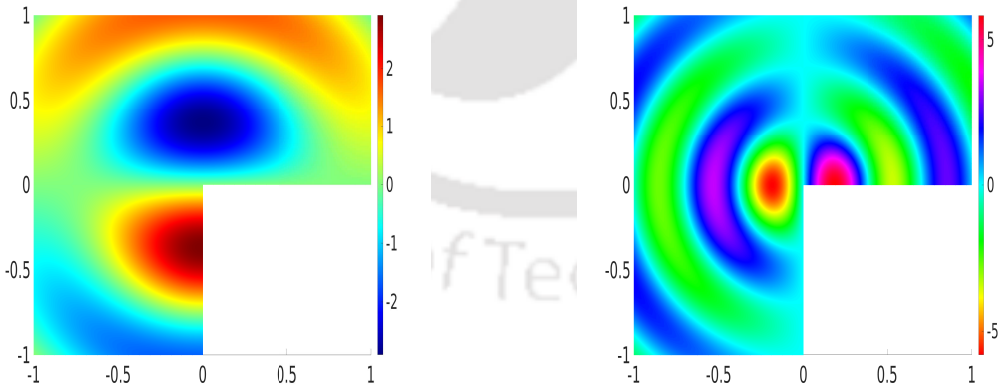

Figure 7.4.9: (Example 7.4.5) First component (left) for $\gamma = 5$ and second component (right) for $\gamma = 10$ of the LSWG solutions. These are obtained using mesh level 6 and the same polynomial degree $k = 2$.

Table 7.4.8: Convergence profiles for Example 7.4.4 with $\gamma = 6$.

α	Level	$\|\|\|(\mathbf{e}_h^{\mathbf{q}}, \mathbf{e}_h^{\mathbf{p}})\|\|\|$	Order	$\|\mathbf{e}_0^{\mathbf{p}}\|$	Order	$\|\mathbf{e}_0^{\mathbf{q}}\|$	Order	$\|\mathbf{Q}_0^k\mathbf{p} - \mathbf{p}\|$	Order
$\frac{1}{8}$	1	4.22e-02	—	4.77e-02	—	4.85e-02	—	1.20e-01	—
	2	3.87e-02	0.125	4.37e-02	0.124	4.44e-02	0.125	1.10e-01	0.125
	3	3.55e-02	0.125	4.01e-02	0.125	4.07e-02	0.125	1.01e-01	0.125
	4	3.26e-02	0.125	3.68e-02	0.125	3.74e-02	0.125	9.26e-02	0.125
	5	2.99e-02	0.125	3.37e-02	0.125	3.43e-02	0.125	8.49e-02	0.125
	6	2.74e-02	0.125	3.09e-02	0.125	3.14e-02	0.125	7.79e-02	0.125
$\frac{2}{3}$	1	8.33e-02	—	1.59e-01	—	1.73e-01	—	1.54e-02	—
	2	5.25e-02	0.66	1.00e-01	0.67	1.09e-01	0.67	9.71e-03	0.67
	3	3.30e-02	0.67	6.32e-02	0.67	6.88e-02	0.67	6.12e-03	0.67
	4	2.08e-02	0.67	3.98e-02	0.67	4.33e-02	0.67	3.85e-03	0.67
	5	1.31e-02	0.67	2.51e-02	0.67	2.73e-02	0.67	2.42e-03	0.67
	6	8.26e-03	0.67	1.58e-02	0.67	1.72e-02	0.67	1.53e-03	0.67
$\frac{4}{5}$	1	6.59e-02	—	1.43e-01	—	1.58e-01	—	2.05e-02	—
	2	3.78e-02	0.80	8.25e-02	0.79	9.12e-02	0.79	1.18e-02	0.80
	3	2.17e-02	0.80	4.74e-02	0.79	5.24e-02	0.80	6.78e-03	0.80
	4	1.25e-02	0.80	2.72e-02	0.80	3.01e-02	0.80	3.89e-03	0.80
	5	7.18e-03	0.80	1.56e-02	0.80	1.72e-02	0.80	2.23e-03	0.80
	6	4.12e-03	0.80	8.98e-03	0.80	9.93e-03	0.80	1.28e-03	0.80

solution $\mathbf{p} \in \mathbf{H}^{\frac{2}{3}-\epsilon}(\Omega)$ for $\epsilon > 0$ (cf. [105]). Hence, the exact solution is non-smooth and indeed singular at the entrant corner $(0, 0)$. In this example, we follow [97] to verify the stability of our LSWG method with large wave numbers for two different types of mesh restrictions. Figure 7.4.11 depicts the relative errors $\mathrm{RE}_{\mathbf{p}}$ and $\mathrm{RE}_{\mathbf{q}}$ for the linear LSWG algorithm with different mesh conditions. The left graph of Figure 7.4.11 displays the behavior of the relative errors with the wave number γ under the mesh condition $\gamma h = 2$. We observe that the relative errors cannot be controlled by the restriction $\gamma h = 2$ and increase with γ, which reflects the existence of the additional pollution error. Figure 7.4.11 (right) demonstrates the relative errors for the proposed algorithm with mesh condition $\gamma^3 h^2 = 2$. It displays that under this mesh restriction, the relative errors do not increase with the wave number γ. This numerical phenomenon has also been observed in Lu *et. al.* [97].

For any fixed wave number γ, we present the relative errors $\mathrm{RE}_{\mathbf{p}}$ and $\mathrm{RE}_{\mathbf{q}}$ for the linear LSWG algorithm. The left graph of Figure 7.4.12 displays the relative error of

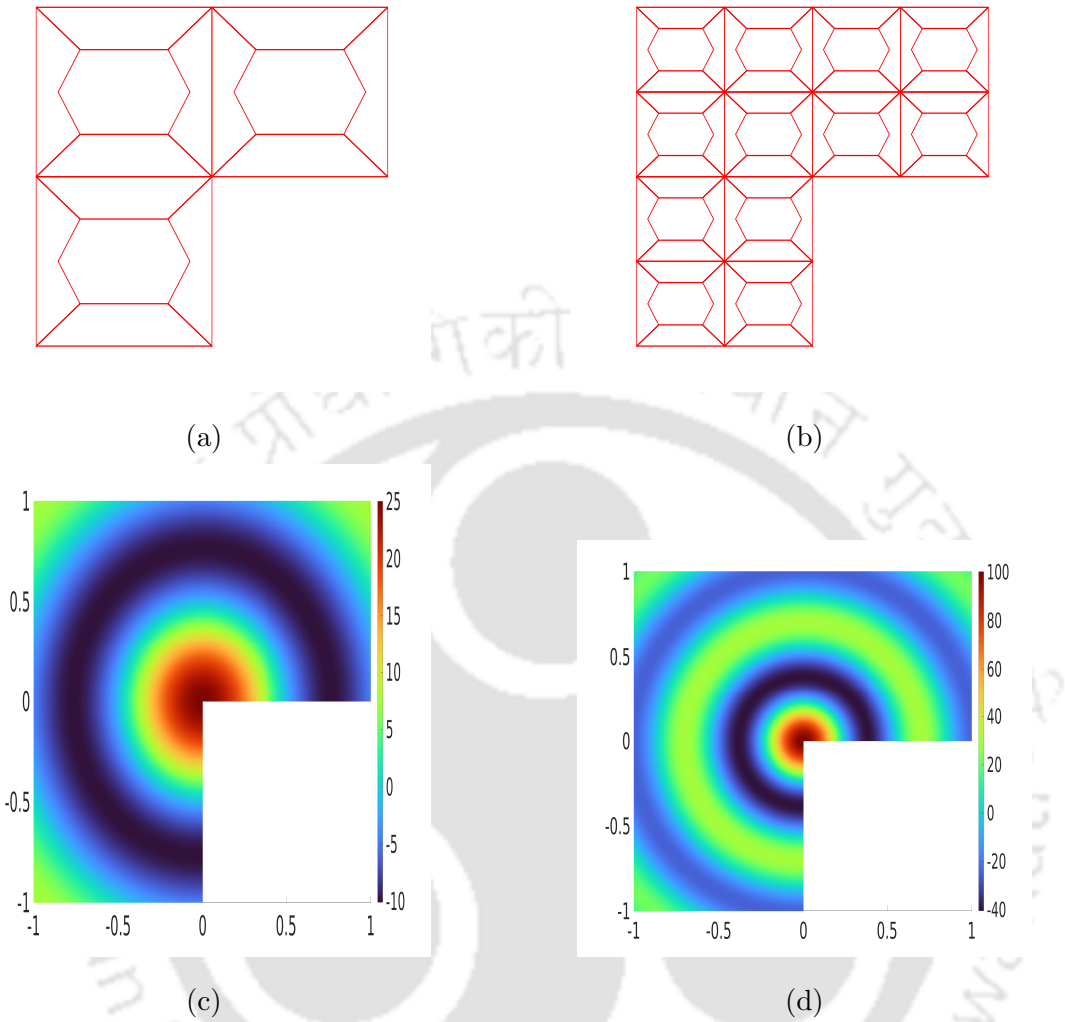

Figure 7.4.10: (Example 7.4.5) The first 2-mesh levels (a)-(b) for the proposed LSWG algorithm. The plots of $\nabla \times \mathbf{p}_h$ for $\gamma = 5$ (c) and for $\gamma = 10$ (d). These results are obtained using mesh level 6 and the same polynomial degree $k = 2$.

the LSWG solution $\mathbf{p}_0$ for $\gamma = 60, 90, 130$, while the right one shows the relative error $\text{RE}_{\mathbf{q}}$ for the same values of γ. These results predict that the LSWG methods are robust and stable for the time-harmonic Maxwell problems with high wave numbers. Figure 7.4.13-7.4.14 show that the errors $\|\mathbf{p} - \mathbf{p}_0\|$ and $\|\mathbf{q} - \mathbf{q}_0\|$ always decrease significantly for high-order polynomial approximations even in the case of low regular solution with large wave number.

Table 7.4.9: Convergence profiles for Example 7.4.5 with $\gamma = 20$.

k	Level	$\|\|\|(\mathbf{e}_h^{\mathbf{q}}, \mathbf{e}_h^{\mathbf{p}})\|\|\|$	Order	$\|\mathbf{e}_0^{\mathbf{p}}\|$	Order	$\|\mathbf{e}_0^{\mathbf{q}}\|$	Order	$\|\mathbf{Q}_0^k\mathbf{p} - \mathbf{p}\|$	Order	$\|\mathbf{L}_0^k\mathbf{q} - \mathbf{q}\|$	Order
1	2	1.44e+00	—	9.88e+00	—	7.23e-01	—	4.27e+00	—	8.43e+03	—
	3	3.83e-01	1.91	2.66e+00	1.89	1.74e-01	2.05	1.14e+00	1.90	2.40e+03	1.81
	4	9.73e-02	1.97	6.79e-01	1.97	4.31e-02	2.01	2.93e-01	1.96	6.48e+02	1.88
	5	2.44e-02	1.99	1.70e-01	1.99	1.07e-02	2.00	7.38e-02	1.98	1.67e+02	1.95
	6	6.12e-03	1.99	4.26e-02	1.99	2.68e-03	2.00	1.85e-02	2.00	4.22e+01	1.98
	7	1.53e-03	2.00	1.06e-02	2.00	6.70e-04	2.00	4.63e-03	2.00	1.05e+01	2.00
2	2	4.20e-01	—	3.54e+00	—	2.28e-01	—	1.07e+00	—	2.69e+03	—
	3	5.93e-02	2.82	4.64e-01	2.93	2.93e-02	2.96	1.41e-01	2.92	4.27e+02	2.66
	4	7.61e-03	2.96	5.90e-02	2.97	3.69e-03	2.98	1.79e-02	2.97	5.88e+01	2.86
	5	9.57e-04	2.99	7.41e-03	2.99	4.62e-04	2.99	2.25e-03	2.99	7.59e+00	2.95
	6	1.19e-04	2.99	9.27e-04	2.99	5.77e-05	3.00	2.82e-04	2.99	9.58e-01	2.98
	7	1.50e-05	3.00	1.15e-04	3.00	7.21e-06	3.00	3.53e-05	3.00	1.20e-01	3.00
3	2	1.19e-01	—	7.09e-01	—	3.28e-02	—	1.80e-01	—	7.30e+02	—
	3	7.62e-03	3.96	5.14e-02	3.78	2.59e-03	3.66	1.26e-02	3.83	6.64e+01	3.45
	4	4.82e-04	3.98	3.30e-03	3.96	1.74e-04	3.89	8.11e-04	3.95	4.82e+00	3.78
	5	3.02e-05	3.99	2.07e-04	3.99	1.10e-05	3.97	5.10e-05	3.99	3.15e-01	3.93
	6	1.89e-06	4.00	1.29e-05	3.99	6.95e-07	3.99	3.19e-06	4.00	1.99e-02	3.98
	7	1.18e-07	4.00	8.12e-07	4.00	4.35e-08	4.00	1.99e-07	4.00	1.25e-03	4.00

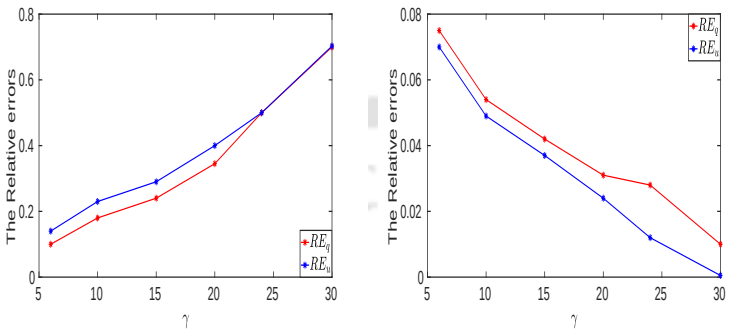

Figure 7.4.11: (Example 7.4.6) The relative errors $\|\mathbf{p} - \mathbf{p}_0\|/\|\mathbf{p}\|$ and $\|\mathbf{q} - \mathbf{q}_0\|/\|\mathbf{q}\|$ for mesh condition $\gamma h = 2$ (left) and mesh condition $\gamma^3 h^2 = 2$ (right) by the LSWG approximations.

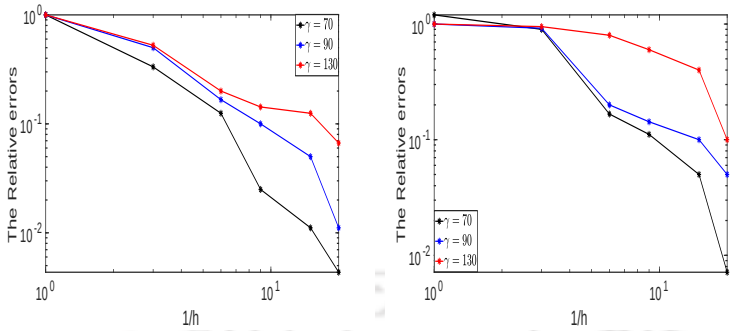

Figure 7.4.12: (Example 7.4.6) The relative errors $\|\mathbf{p}-\mathbf{p}_0\|/\|\mathbf{p}\|$ (left) and $\|\mathbf{q}-\mathbf{q}_0\|/\|\mathbf{q}\|$ (right) for $\gamma = 70, 90, 130$.

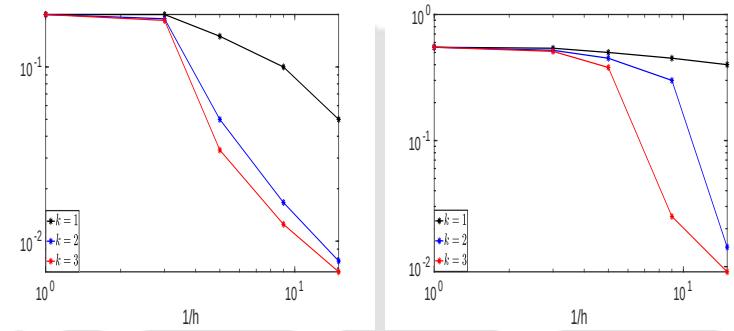

Figure 7.4.13: (Example 7.4.6) The error $\|\mathbf{p}-\mathbf{p}_0\|$ for $\gamma = 60$ (left) and $\gamma = 100$ (right).

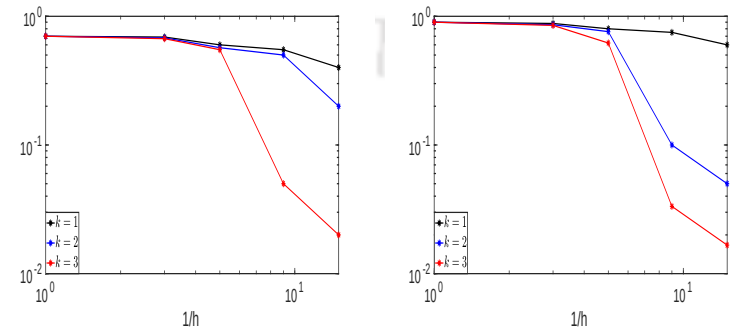

Figure 7.4.14: (Example 7.4.6) The error $\|\mathbf{q}-\mathbf{q}_0\|$ for $\gamma = 60$ (left) and $\gamma = 100$ (right).

8

Least-squares WG-FEMs for Maxwell's Equations

We present a least-squares weak Galerkin (LSWG) finite element method for the two dimensional (2D) and three dimensional (3D) Maxwell's equations. The LSWG algorithm allows the general hybrid, polygonal/polyhedral mesh partitions without compromising the desire accuracy and efficiency of the scheme. Super-convergence of order one has been derived for the energy norm, which is justified by the numerous numerical tests. Further, the optimal error estimate for L^2 norm is predicted numerically.

8.1 Introduction

We will discuss a new numerical simulations for the Maxwell's equations in this chapter. The Maxwell's equations are obtained from the coupling of Ampere's law and Faraday's law given as follows

$$\begin{cases} \nabla \cdot (\epsilon \mathbf{E}) = \rho \quad \text{and} \quad \nabla \cdot (\mu \mathbf{H}) = 0, \\ \nabla \times \mathbf{E} = -\frac{\partial(\mu \mathbf{H})}{\partial t} \quad \text{and} \quad \nabla \times \mathbf{H} = \frac{\partial(\epsilon \mathbf{E})}{\partial t} + \sigma \mathbf{E}, \end{cases} \tag{8.1.1}$$

where $\mathbf{E}$ is the electric field intensity, $\mathbf{H}$ is the magnetic field intensity, ρ is called charge density, μ is the permeability, ϵ is the permittivity and σ is known as electric conductivity.

In time-harmonic fields, the time dependent variables are assumed to be harmonic. In such cases, the Maxwell's equations (8.1.1) can be rewritten as

$$\begin{cases} \nabla \cdot (\epsilon \mathbf{E}) = \rho \quad \text{and} \quad \nabla \cdot (\mu \mathbf{H}) = 0, \\ \nabla \times \mathbf{E} = -i\omega\mu \mathbf{H} \quad \text{and} \quad \nabla \times \mathbf{H} = i\omega\epsilon \mathbf{E} + \sigma \mathbf{E}. \end{cases} \tag{8.1.2}$$

Now, testing the operator $\nabla \times \mu^{-1}$ to $\nabla \times \mathbf{E} = -i\omega\mu\mathbf{H}$, then from second equation of (8.1.2), we have

$$\nabla \times (\mu^{-1} \nabla \times \mathbf{E}) = (\omega^2 \epsilon - i\omega\sigma)\mathbf{E}. \tag{8.1.3}$$

From above equation with $\nabla \cdot (\epsilon \mathbf{E}) = \rho$, we can obtain the electric fields intensity $\mathbf{E}$ with appropriate boundary condition. The magnetic fields intensity $\mathbf{H}$ can be obtained from the (8.1.2) with suitable boundary conditions.

For our convenience, in this study we consider the models for electric field intensity $\mathbf{E}$ with $\omega = 0$ in the domain $\Omega \subset \mathbb{R}^d$ $(d = 2, 3)$. Hence, we reformulate the model problem which seeks the vector-valued function $\mathbf{p}$ and q satisfying

$$\begin{cases} \nabla \times (\beta \nabla \times \mathbf{p}) - \gamma \nabla q = \mathbf{f}_1 \ \text{ and } \ \nabla \cdot (\beta \mathbf{p}) = g \ \text{ in } \Omega, \\ \mathbf{p} \times \boldsymbol{\eta} = \mathbf{0} \ \text{ and } \ q = 0 \ \text{ on } \partial\Omega, \end{cases} \tag{8.1.4}$$

where $\beta = \mu^{-1}$ and $\gamma = \epsilon$.

Next, the vorticity vector $\boldsymbol{\psi}$ is a curl of $\mathbf{p}$:

$$\boldsymbol{\psi} = -\beta \nabla \times \mathbf{p}.$$

Then, the equivalent mixed formulation of the model (8.1.4) is given by

$$\begin{cases} \boldsymbol{\psi} + \beta \nabla \times \mathbf{p} = \mathbf{0} \ \text{ in } \Omega \ \text{ and } \ \nabla \cdot (\beta \mathbf{p}) = g \ \text{ in } \Omega, \\ \nabla \times \boldsymbol{\psi} + \gamma \nabla q = \mathbf{f}, \ \text{ in } \Omega \\ \mathbf{p} \times \boldsymbol{\eta} = \mathbf{0} \ \text{ and } \ q = 0 \ \text{ on } \partial\Omega, \end{cases} \tag{8.1.5}$$

where $\mathbf{f} = -\mathbf{f}_1$.

In this chapter, we discuss the weak Galerkin least-squares (WG-LS) finite element method for the two dimensional (2D) and three dimensional (3D) Maxwell's equations. The super-convergence of order one has been achieved for the energy norm. To justify the theoretical estimates several numerical experiments have been conducted for the 2D and 3D proposed problems. In addition, optimal convergence rate for L^2 norm has also been predicated from the numerical simulations.

The rest of the chapter is organised as follows. The WG-spaces and least-squares algorithm have been described in the Section 8.2. In Section 8.3, the error equation has been provided. We report several numerical tests to demonstrate and justify the convergence analysis in Section 8.4.

8.2 Least-squares Weak Galerkin Methodology

In this section, we are concerned with the weak Galerkin spaces, discrete operators and L^2 projections, which will be useful for our later analysis. First, we adopt the WG partitions $\mathcal{T}_h$ of the domain Ω from the Chap. 2.

Next, we define three WG spaces, namely, $\mathbf{V}_h$, $\mathbf{W}_h$, and Z_h, which are defined as follows (for more details, see in Chap. 3)

$$\begin{aligned}
\mathbf{V}_h &= \{\mathbf{v}_h = \{\mathbf{v}_0, \mathbf{v}_b = v_1\mathbf{t}_1 + (d-2)v_2\mathbf{t}_2\} : \mathbf{v}_0|_T \in [\mathcal{P}_k(T)]^d, \\
&\qquad\qquad v_1, v_2 \in \mathcal{P}_k(e), e \in \partial T, T \in \mathcal{T}_h\}, \\
\mathbf{W}_h &= \{\mathbf{w}_h = \{\mathbf{w}_0, \mathbf{w}_b\} : \mathbf{w}_0|_T \in [\mathcal{P}_k(T)]^l,\ \mathbf{w}_b|_T \in [\mathcal{P}_k(e)]^l,\ e \subset \partial T,\ T \in \mathcal{T}_h\}, \\
Z_h &= \{z_h = \{z_0, z_b\} : z_0|_T \in \mathcal{P}_k(T),\ z_b|_T \in \mathcal{P}_k(e),\ e \subset \partial T,\ T \in \mathcal{T}_h\}.
\end{aligned}$$

where, $k \geq 1$ is any non-negative integer and $l = 2d - 3$ $(d = 2, 3)$. Let $\mathbf{V}_h^0$ and Z_h^0 be two subspaces of $\mathbf{V}_h$ and Z_h respectively, given as follows

$$\begin{aligned}
\mathbf{V}_h^0 &= \{\mathbf{v}_h = \{\mathbf{v}_0, \mathbf{v}_b\} \in \mathbf{V}_h : \mathbf{v}_b \times \boldsymbol{\eta} = \mathbf{0} \text{ on } \partial\Omega\}, \\
Z_h^0 &= \{z_h = \{z_0, z_b\} \in Z_h : z_b = 0 \text{ on } \partial\Omega\}.
\end{aligned}$$

Now, for any $z_h = \{z_0, z_b\} \in Z_h$, the discrete weak gradient is a piecewise polynomial of the degree k satisfying

$$(\nabla_w z_h, \boldsymbol{\phi})_T = -(z_0, \nabla \cdot \boldsymbol{\phi})_T + \langle z_b, \boldsymbol{\phi} \cdot \boldsymbol{\eta}\rangle_{\partial T} \ \ \forall \boldsymbol{\phi} \in [\mathcal{P}_k(T)]^d. \tag{8.2.1}$$

Next, for any $\mathbf{v}_h = \{\mathbf{v}_0, \mathbf{v}_b\} \in \mathbf{V}_h$, the discrete weak divergence $\nabla_w \cdot \mathbf{v}_h \in [\mathcal{P}_k(T)]$ is defined by the equation

$$(\nabla_w \cdot \mathbf{v}_h, \phi)_T = -(\mathbf{v}_0, \nabla\phi)_T + \langle \mathbf{v}_b \cdot \boldsymbol{\eta}, \phi\rangle_{\partial T} \ \ \forall \phi \in \mathcal{P}_k(T), \tag{8.2.2}$$

and discrete weak curl of $\mathbf{v}_h$ is a unique piecewise polynomial of degree k is given by

$$(\nabla_w \times \mathbf{v}_h, \boldsymbol{\tau}_h)_T = (\mathbf{v}_0, \nabla \times \boldsymbol{\tau}_h)_T - \langle \mathbf{v}_b \times \boldsymbol{\eta}, \boldsymbol{\tau}_h\rangle_{\partial T} \ \ \forall \boldsymbol{\tau}_h \in [\mathcal{P}_k(T)]^{2d-3}. \tag{8.2.3}$$

Finally, for any $\mathbf{w}_h = \{\mathbf{w}_0, \mathbf{w}_b\} \in \mathbf{W}_h$, the discrete weak curl $\nabla_w \times \mathbf{w}_h \in [P(T)]^d$ is defined as

$$(\nabla_w \times \mathbf{w}_h, \boldsymbol{\tau}_h)_T = (\mathbf{w}_0, \nabla \times \boldsymbol{\tau}_h)_T - \langle \mathbf{w}_b \times \boldsymbol{\eta}, \boldsymbol{\tau}_h\rangle_{\partial T} \ \ \forall \boldsymbol{\tau}_h \in [\mathcal{P}_k(T)]^d. \tag{8.2.4}$$

To define the LSWG algorithm, we need the following bilinear maps given as follows:

$$\begin{aligned}
&\mathcal{A}((\mathbf{v}_h, \mathbf{w}_h, z_h); (\boldsymbol{\sigma}_h, \boldsymbol{\tau}_h, \theta_h)) \\
&= \sum_{T \in \mathcal{T}_h} \Big((\mathbf{w}_0 + \beta\nabla_w \times \mathbf{v}_h, \boldsymbol{\tau}_0 + \beta\nabla_w \times \boldsymbol{\sigma}_h) + (\nabla_w \cdot (\beta\mathbf{v}_h), \nabla_w \cdot (\beta\boldsymbol{\sigma}_h)) \\
&+ (\nabla_w \times \mathbf{w}_h + \gamma\nabla_w z_h, \nabla_w \times \boldsymbol{\tau}_h + \gamma\nabla_w\theta_h)_T \Big) + \mathcal{S}_1(\mathbf{v}_h, \boldsymbol{\sigma}_h) \\
&+ \mathcal{S}_2(\mathbf{w}_h, \boldsymbol{\tau}_h) + \mathcal{S}_3(z_h, \theta_h) \ \forall\ (\mathbf{v}_h, \mathbf{w}_h, z_h),\ (\boldsymbol{\sigma}_h, \boldsymbol{\tau}_h, \theta_h) \in \mathbf{V}_h \times \mathbf{W}_h \times Z_h,
\end{aligned}$$

where

$$\begin{aligned}\mathcal{S}_1(\mathbf{v}_h,\boldsymbol{\sigma}_h) &= \sum_{T\in\mathcal{T}_h} h_T\langle(\mathbf{v}_0-\mathbf{v}_b)\times\boldsymbol{\eta},(\boldsymbol{\sigma}_0-\boldsymbol{\sigma}_b)\times\boldsymbol{\eta}\rangle_{\partial T},\\ \mathcal{S}_2(\mathbf{w}_h,\boldsymbol{\tau}_h) &= \sum_{T\in\mathcal{T}_h} h_T^3\langle\mathbf{w}_0-\mathbf{w}_b,\boldsymbol{\tau}_0-\boldsymbol{\tau}_b\rangle_{\partial T},\\ \mathcal{S}_3(z_h,\theta_h) &= \sum_{T\in\mathcal{T}_h} h_T^3\langle z_0-z_b,\theta_0-\theta_b\rangle_{\partial T}.\end{aligned}$$

Moreover, we define the triple-bar semi-norm on $\mathbf{V}_h\times\mathbf{W}_h\times Z_h$ given by

$$|||(\mathbf{v}_h,\mathbf{w}_h,z_h)|||^2=\mathcal{A}((\mathbf{v}_h,\mathbf{w}_h,z_h);(\mathbf{v}_h,\mathbf{w}_h,z_h))\ \forall\ (\mathbf{v}_h,\mathbf{w}_h,q_h)\in\mathbf{V}_h\times\mathbf{W}_h\times Z_h.$$

For each $T\in\mathcal{T}_h$ and $e\in\mathcal{E}_h$, we define the following L^2 projections:

- $\mathbf{Q}_0^k:[L^2(T)]^d\to[\mathcal{P}_k(T)]^d,\ \ \mathbf{Q}_b^k:[L^2(T)]^d\to[\mathcal{P}_k(e)]^d,\ \ Q_b^k:L^2(e)\to\mathcal{P}_k(e).$
- $\mathbf{L}_0^k:[L^2(T)]^{2d-3}\to[\mathcal{P}_k(T)]^{2d-3},\ \ \mathbf{L}_b^k:[L^2(T)]^{2d-3}\to[\mathcal{P}_k(e)]^{2d-3}.$
- $\mathcal{R}_0^k:[L^2(e)]\to[\mathcal{P}_k(T)],\ \ \mathcal{R}_b^k:[L^2(T)]\to[\mathcal{P}_k(e)].$
- $\boldsymbol{\mathcal{Q}}_h^k:[L^2(T)]^{2d-3}\to[\mathcal{P}_k(T)]^{2d-3},\ \ \boldsymbol{\mathcal{L}}_h^k:[L^2(T)]^d\to[\mathcal{P}_k(T)]^d.$
- $\boldsymbol{\mathcal{R}}_h^k:[L^2(T)]^d\to[\mathcal{P}_k(T)]^d\ \ \&\ \ \boldsymbol{\mathcal{Q}}_{1,h}^k:L^2(T)\to\mathcal{P}_k(T).$

In addition, we define $\mathbf{Q}_h\mathbf{v}=\{\mathbf{Q}_0^k\mathbf{v},\mathbf{Q}_b^k\mathbf{v}=Q_b^k(v_1)\mathbf{t}_1+(d-2)Q_b^k(v_2)\mathbf{t}_2\}$ for all $\mathbf{v}\in[H^\beta(T)]^d$, $\mathbf{L}_h\mathbf{w}=\{\mathbf{L}_0^k\mathbf{w},\mathbf{L}_b^k\mathbf{w}\}$ for all $\mathbf{w}\in[H^\beta(T)]^{2d-3}$, and $\mathcal{R}_hq=\{\mathcal{R}_0^kq,\mathcal{R}_b^kq\}$ for all $z\in H^\beta(T)$, where $\beta>1/2$.

Lemma 8.2.1. *The functional $|||\cdot|||$ is a norm on $\mathbf{V}_h^0\times\mathbf{W}_h\times Z_h^0$.*

Proof. To prove norm, we need to justify that

$$|||(\mathbf{v}_h,\mathbf{w}_h,z_h)|||=0\ \text{ iff }\ \mathbf{v}_h=\mathbf{w}_h=\mathbf{0},\ z_h=0.$$

Since $|||(\mathbf{v}_h,\mathbf{w}_h,z_h)|||=0$ implies

$$\left\{\begin{array}{c}\nabla_w\cdot(\beta\mathbf{v}_h)=0,\ \nabla_w\times\mathbf{w}_h=-\gamma\nabla_w z_h,\ \gamma\nabla_w\times\mathbf{v}_h=-\mathbf{w}_0\ \ \forall\ T\in\mathcal{T}_h,\\ \mathbf{v}_0\times\boldsymbol{\eta}=\mathbf{v}_b\times\boldsymbol{\eta},\ \ \mathbf{w}_0=\mathbf{w}_b,\ \ \ z_0=z_b\ \ \forall\ \partial T,\ T\in\mathcal{T}_h.\end{array}\right. \tag{8.2.5}$$

We deduce from the first equation of (8.2.5) and the definition (8.2.2) that

$$\begin{aligned}0=(\nabla_w\cdot(\beta\mathbf{v}_h),z)_T &= -(\beta\mathbf{v}_0,\nabla z)_T+\langle\beta\mathbf{v}_b\cdot\boldsymbol{\eta},z\rangle_{\partial T}\\ &= (\nabla_w\cdot(\beta\mathbf{v}_0),z)_T+\langle\beta(\mathbf{v}_0-\mathbf{v}_b)\cdot\boldsymbol{\eta},z\rangle_{\partial T}\\ &= (\nabla_w\cdot(\beta\mathbf{v}_0),z)_T\ \ \forall z\in\mathcal{P}_k(T),\end{aligned}$$

where we have used the fact that $\mathbf{v}_0 \times \boldsymbol{\eta} = \mathbf{v}_b \times \boldsymbol{\eta}$ on $\forall\ \partial T,\ T \in \mathcal{T}_h$. Thus, the above equation leads to

$$\nabla \cdot (\beta \mathbf{v}_0) = 0. \tag{8.2.6}$$

Since

$$\begin{aligned}
\|\nabla_w \times \mathbf{v}_h\|^2_{T,\beta} &= \sum_{T\in\mathcal{T}_h} (\beta \nabla_w \times \mathbf{v}_h, \nabla_w \times \mathbf{v}_h)_T \\
&= \sum_{T\in\mathcal{T}_h} ((\beta \nabla_w \times \mathbf{v}_h + \mathbf{w}_0, \nabla_w \times \mathbf{v}_h)_T - (\mathbf{w}_0, \nabla_w \times \mathbf{v}_h)_T) \\
&= -\sum_{T\in\mathcal{T}_h} (\mathbf{w}_0, \nabla_w \times \mathbf{v}_h)_T \\
&= \sum_{T\in\mathcal{T}_h} (-(\mathbf{v}_0, \nabla \times \mathbf{w}_0) + \langle \mathbf{v}_b \times \boldsymbol{\eta}, \mathbf{w}_0 \rangle_{\partial T}) \\
&= \sum_{T\in\mathcal{T}_h} (-(\nabla \times \mathbf{v}_0, \mathbf{w}_0) - \langle (\mathbf{v}_0 - \mathbf{v}_b) \times \boldsymbol{\eta}, \mathbf{w}_0 \rangle_{\partial T}).
\end{aligned} \tag{8.2.7}$$

From the definition (8.2.4), we get

$$\begin{aligned}
\sum_{T\in\mathcal{T}_h} (\nabla_w \times \mathbf{w}_h, \mathbf{v}_0)_T &= \sum_{T\in\mathcal{T}_h} ((\nabla \times \mathbf{v}_0, \mathbf{w}_0)_T - \langle \mathbf{w}_b \times \boldsymbol{\eta}, \mathbf{v}_0 \rangle_{\partial T}) \\
&= \sum_{T\in\mathcal{T}_h} ((\nabla \times \mathbf{v}_0, \mathbf{w}_0)_T + \langle \mathbf{v}_b \times \boldsymbol{\eta}, \mathbf{w}_b \rangle_{\partial T}) \\
&= \sum_{T\in\mathcal{T}_h} ((\nabla \times \mathbf{v}_0, \mathbf{w}_0)_T - \langle (\mathbf{v}_0 - \mathbf{v}_b) \times \boldsymbol{\eta}, \mathbf{w}_b \rangle_{\partial T}).
\end{aligned}$$

Now, substituting the above equation into (8.2.7) and using the facts that $\mathbf{v}_0 \times \boldsymbol{\eta} = \mathbf{v}_b \times \boldsymbol{\eta}$ on each ∂T, $z_b = 0$ on $\partial\Omega$, and $\nabla_w \times \mathbf{w}_h = -\gamma \nabla_w z_h$ in each T, we get

$$\begin{aligned}
\|\nabla_w \times \mathbf{v}_h\|^2_{T,\beta} &= -\sum_{T\in\mathcal{T}_h} (\nabla_w \times \mathbf{w}_h + \gamma \nabla_w z_h, \mathbf{v}_0)_T + (\gamma \nabla_w z_h, \mathbf{v}_0)_T \\
&= (\gamma \nabla_w z_h, \mathbf{v}_0)_T \\
&= -\sum_{T\in\mathcal{T}_h} (-(\nabla \cdot (\gamma \mathbf{v}_0), z_0)_T + \langle z_b, \gamma \mathbf{v}_0 \cdot \boldsymbol{\eta} \rangle_{\partial T}) \\
&= 0.
\end{aligned} \tag{8.2.8}$$

Hence it follows from equation (8.2.8) and the definition (8.2.3) that

$$\begin{aligned}
0 = (\nabla_w \times \mathbf{v}_h, \mathbf{z})_T &= (\mathbf{v}_0, \nabla \mathbf{z})_T - \langle \mathbf{v}_b \times \boldsymbol{\eta}, \mathbf{z} \rangle_{\partial T} \\
&= (\nabla_w \times \mathbf{v}_0, \mathbf{z})_T + \langle (\mathbf{v}_0 - \mathbf{v}_b) \times \boldsymbol{\eta}, \mathbf{z} \rangle_{\partial T} \\
&= (\nabla_w \times \mathbf{v}_0, \mathbf{z})_T \quad \forall \mathbf{z} \in [\mathcal{P}_k(T)]^{2d-3}.
\end{aligned}$$

From above equation, we obtain

$$\nabla_w \times \mathbf{v}_0 = 0. \tag{8.2.9}$$

It follows from (8.2.5), (8.2.6), (8.2.9) and $\mathbf{v}_0 \times \boldsymbol{\eta} = 0$ on $\partial\Omega$ that $\mathbf{v}_0 = 0$. Hence, $\mathbf{v}_h \equiv 0$. The third equation in (8.2.5) gives us $\mathbf{w}_h \equiv 0$. Next, from the second equation in (8.2.5), we have $\nabla_w z_h = 0$.

Using the definition (8.2.1) and the fact that $z_0 = z_b$ on each ∂T, we obtain

$$\begin{aligned}
\sum_{T\in\mathcal{T}_h} (\nabla_w z_h, \mathbf{z})_T &= \sum_{T\in\mathcal{T}_h} \left(-(z_0, \nabla\cdot\mathbf{z})_T + \langle z_b, \mathbf{z}\cdot\boldsymbol{\eta}\rangle_{\partial T}\right) \\
&= \sum_{T\in\mathcal{T}_h} \left((\nabla z_0, \mathbf{z})_T - \langle (z_0 - z_b), \mathbf{z}\cdot\boldsymbol{\eta}\rangle_{\partial T}\right) \\
&= \sum_{T\in\mathcal{T}_h} (\nabla z_0, \mathbf{z})_T \quad \forall \mathbf{z} \in [\mathcal{P}_k(T)]^d.
\end{aligned}$$

From above equation, we have $\nabla z_0 = 0$ on each $T \in \mathcal{T}_h$. This implies $q_0 =$ constant. Since $z_0 = z_b = 0$ on $\partial\Omega$. Hence $z_h \equiv 0$. This completes the rest of the proof. □

Now, we are in position to derive the LSWG algorithm for the (8.1.5).

LSWG Algorithm. A LSWG approximation for (8.1.5) which seeks $(\mathbf{p}_h, \boldsymbol{\psi}_h, q_h) \in \mathbf{V}_h^0 \times W_h \times Z_h^0$

$$\begin{aligned}
\mathcal{A}((\mathbf{p}_h, \boldsymbol{\psi}_h, q_h); (\mathbf{v}_h, \mathbf{w}_h, z_h)) &= (\mathbf{f}, \nabla_w \times \mathbf{w}_h + \gamma \nabla_w z_h) \\
&+ (g, \nabla_w \cdot (\beta \mathbf{v}_h)), \qquad (8.2.10)
\end{aligned}$$

for all $(\mathbf{v}_h, \mathbf{w}_h, z_h) \in \mathbf{V}_h^0 \times W_h \times Z_h^0$.

Lemma 8.2.2. *The LSWG algorithm* (8.2.10) *has a unique solution.*

Now, we derive the commutative properties of some L^2 projections and discrete operators in the following Lemma.

Lemma 8.2.3. *For $\alpha > 1/2$, we have*

$$\begin{aligned}
\nabla_w \times \mathbf{Q}_h \mathbf{v} &= \boldsymbol{\mathcal{Q}}_h^k (\nabla \times \mathbf{v}) \quad \forall \mathbf{v} \in [H^\alpha(\Omega)]^d, \\
\nabla_w \cdot \mathbf{Q}_h \mathbf{v} &= \mathcal{Q}_{1,h}^k (\nabla \cdot \mathbf{v}) \quad \forall \mathbf{v} \in [H^\alpha(\Omega)]^d, \\
\nabla_w \times \mathbf{L}_h \mathbf{w} &= \boldsymbol{\mathcal{L}}_h^k (\nabla \times \mathbf{w}) \quad \forall \mathbf{w} \in [H^\alpha(\Omega)]^{2d-3}, \\
\nabla_w (\mathcal{R}_h z) &= \boldsymbol{\mathcal{R}}_h^k (\nabla z) \quad \forall z \in H^\alpha(\Omega).
\end{aligned}$$

8.3 Error Analysis

To derive the error equation, we introduce the following error functions

$$\mathbf{e}_h^{\mathbf{p}} = \mathbf{Q}_h\mathbf{p} - \mathbf{p}, \quad \mathbf{e}_h^{\boldsymbol{\psi}} = \mathbf{L}_h\boldsymbol{\psi} - \boldsymbol{\psi}, \quad e_h^q = \mathcal{R}_h q - q. \tag{8.3.1}$$

Moreover, the coefficients β and γ are assumed to be piecewise constants.

Lemma 8.3.1. *For each* $(\mathbf{v}_h, \mathbf{w}_h, z_h) \in \mathbf{V}_h \times W_h \times Z_h^0$, *we have*

$$\begin{aligned}\mathcal{A}((\mathbf{e}_h^{\mathbf{p}}, \mathbf{e}^{\boldsymbol{\psi}_h}, e_h^q); (\mathbf{v}_h, \mathbf{w}_h, z_h)) &= \mathcal{S}_1(\mathbf{Q}_h\mathbf{p}, \mathbf{v}_h) + \mathcal{S}_2(\mathbf{L}_h\boldsymbol{\psi}, \mathbf{w}_h) + \mathcal{S}_3(\mathcal{R}_h q, z_h)\\ &:= \mathcal{R}((\mathbf{p}, \boldsymbol{\psi}, q); (\mathbf{v}_h, \mathbf{w}_h, z_h)).\end{aligned}$$

Proof. From the equation (8.1.5), we have

$$\mathbf{L}_h\boldsymbol{\psi} + \beta\nabla_w \times \mathbf{Q}_h\mathbf{p} = \mathbf{L}_h\boldsymbol{\psi} - \boldsymbol{\psi} + \beta\nabla_w \times \mathbf{Q}_h\mathbf{p} - \beta\nabla \times \mathbf{p}.$$

Testing the above equation against $(\mathbf{v}_h, \mathbf{w}_h) \in \mathbf{V}_h^0 \times W_h$ and then using Lemma 8.2.3, we obtain

$$\begin{aligned}&\sum_{T\in\mathcal{T}_h} (\mathbf{L}_h\boldsymbol{\psi} + \beta\nabla_w \times \mathbf{Q}_h\mathbf{p}, \beta\nabla_w \times \mathbf{v}_h + \mathbf{w}_0)_T\\ &= \sum_{T\in\mathcal{T}_h} (\mathbf{L}_h\boldsymbol{\psi} - \boldsymbol{\psi} + \beta\nabla_w \times \mathbf{Q}_h\mathbf{p} - \beta\nabla \times \mathbf{p}, \beta\nabla_w \times \mathbf{v}_h + \mathbf{w}_0)_T\\ &= \sum_{T\in\mathcal{T}_h} \left(\mathbf{L}_h\boldsymbol{\psi} - \boldsymbol{\psi} + \beta\boldsymbol{\mathcal{Q}}_h^k(\nabla \times \mathbf{p}) - \beta\nabla \times \mathbf{p}, \beta\nabla_w \times \mathbf{v}_h + \mathbf{w}_0\right)_T\\ &= \mathcal{R}_1(\boldsymbol{\psi}, \mathbf{p}; \mathbf{v}_h, \mathbf{w}_h).\end{aligned} \tag{8.3.2}$$

Next, from the second equation (8.1.5), we get

$$\nabla_w \times \mathbf{L}_h\boldsymbol{\psi} + \gamma\nabla_w(\mathcal{R}_h q) = \nabla_w \times \mathbf{L}_h\boldsymbol{\psi} - \nabla \times \boldsymbol{\psi} + \gamma\nabla_w(\mathcal{R}_h q) - \gamma\nabla q + \mathbf{f}.$$

Testing the above equation with $(\boldsymbol{\psi}, q) \in W_h \times \mathbf{V}_h^0$ and using the Lemma 8.2.3, we achieve

$$\begin{aligned}&\sum_{T\in\mathcal{T}_h} (\nabla_w \times \mathbf{L}_h\boldsymbol{\psi} + \gamma\nabla_w(\mathcal{R}_h q), \nabla_w \times \mathbf{w}_h + \gamma\nabla_w z_h)_T\\ &= \sum_{T\in\mathcal{T}_h} (\nabla_w \times \mathbf{L}_h\boldsymbol{\psi} - \nabla \times \boldsymbol{\psi} + \beta\nabla_w(\mathcal{R}_h q) - \beta\nabla q + \mathbf{f}, \nabla_w \times \mathbf{w}_h + \beta\nabla_w z_h)_T\\ &= \sum_{T\in\mathcal{T}_h} (\nabla_w \times \mathbf{L}_h\boldsymbol{\psi} - \nabla \times \boldsymbol{\psi} + \beta\nabla_w(\mathcal{R}_h q - \beta\nabla q + \mathbf{f}, \nabla_w \times \mathbf{w}_h + \beta\nabla_w z_h)_T\\ &= \mathcal{R}_2\left(\boldsymbol{\psi}, q; \mathbf{w}_h, z_h\right) + \left(\mathbf{f}, \nabla_w \times \mathbf{w}_h + \beta\nabla_w z_h\right).\end{aligned} \tag{8.3.3}$$

Finally, from equation (8.1.5), we have

$$\nabla_w \cdot (\beta \mathbf{Q}_h \mathbf{p}) = \nabla_w \cdot (\beta \mathbf{Q}_h \mathbf{p}) - \nabla \cdot (\beta \mathbf{p}) + g. \tag{8.3.4}$$

Testing the equation (8.3.4) with $\mathbf{v}_h \in \mathbf{V}_h^0$ and using the Lemma 8.2.3, we arrive at

$$\begin{aligned}
&\sum_{T\in\mathcal{T}_h} (\nabla_w \cdot (\beta \mathbf{Q}_h \mathbf{p}), \nabla_w \cdot (\beta \mathbf{v}_h))_T \\
&= \sum_{T\in\mathcal{T}_h} (\nabla_w \cdot (\beta \mathbf{Q}_h \mathbf{p}) - \nabla \cdot (\beta \mathbf{p}) + g, \nabla_w \cdot (\beta \mathbf{v}_h)_T \\
&= \sum_{T\in\mathcal{T}_h} \left(\boldsymbol{\mathcal{Q}}_{1,h}^k (\nabla \cdot (\beta \mathbf{p})) - \nabla \cdot (\beta \mathbf{p}) + g, \nabla_w \cdot (\beta \mathbf{v}_h)\right)_T \\
&= \mathcal{R}_3(\mathbf{p}, \mathbf{v}_h) + (g, \nabla_w \cdot (\beta \mathbf{v}_h)) \,.
\end{aligned} \tag{8.3.5}$$

From the L^2 orthogonality of the projection operators $\mathbf{L}_h$, $\boldsymbol{\mathcal{Q}}_h^k$, $\boldsymbol{\mathcal{Q}}_{1,h}^k$, $\boldsymbol{\mathcal{L}}_h^k$ and $\boldsymbol{\mathcal{R}}_h^k$, we have $\mathcal{R}_1 \equiv 0$, $\mathcal{R}_2 \equiv 0$ and $\mathcal{R}_3 \equiv 0$. Next, by summing (8.3.2), (8.3.3), (8.3.5), and then adding $\mathcal{S}_1(\mathbf{Q}_h \mathbf{p}, \mathbf{v}_h)$, $\mathcal{S}_2(\mathbf{L}_h \boldsymbol{\psi}, \mathbf{w}_h)$ and $\mathcal{S}_3(\mathcal{R}_h q, z_h)$ to the resultant equation, we reach at

$$\begin{aligned}
\mathcal{A}((\mathbf{Q}_h \mathbf{p}, \mathbf{L}_h \boldsymbol{\psi}, \mathcal{R}_h q); (\mathbf{v}_h, \mathbf{w}_h, z_h)) &= -(\mathbf{f}, \nabla_w \times \mathbf{w}_h + \beta \nabla_w z_h) + (\mathbf{g}, \nabla_w \cdot (\beta \mathbf{v}_h)) \\
&+ \mathcal{S}_1(\mathbf{Q}_h \mathbf{p}, \mathbf{v}_h) + \mathcal{S}_2(\mathbf{L}_h \boldsymbol{\psi}, \mathbf{w}_h) + \mathcal{S}_3(\mathcal{R}_h q, z_h).
\end{aligned}$$

Subtracting the above equation from (8.2.10) completes the Lemma 8.3.1. □

Lemma 8.3.2. *Let $\mathbf{p} \in [H^{k+1}(\Omega)]^d$, $\boldsymbol{\phi} \in [H^k(\Omega)]^{2d-3}$ and $q \in H^k(\Omega)$. Then, we have the following estimates*

$$\begin{aligned}
\mathcal{S}_1(\mathbf{Q}_h \mathbf{p}, \mathbf{v}_h) &\le C h^{k+1} \|\mathbf{p}\|_{k+1} |||(\mathbf{v}_h, \mathbf{w}_h, z_h)|||, \\
\mathcal{S}_2(\mathbf{L}_h \boldsymbol{\psi}, \mathbf{w}_h) &\le C h^{k+1} \|\boldsymbol{\psi}\|_{k+1} |||(\mathbf{v}_h, \mathbf{w}_h, z_h)|||, \\
\mathcal{S}_3(\mathcal{R}_h q, \mathbf{z}_h) &\le C h^{k+1} \|q\|_{k+1} |||(\mathbf{v}_h, \mathbf{w}_h, z_h)|||.
\end{aligned}$$

for all $(\mathbf{v}_h, \mathbf{w}_h, z_h) \in \mathbf{V}_h \times \mathbf{W}_h \times Z_h$.

Proof. From the Cauchy-Schwarz inequality, trace inequality (2.2.7) and by the definitions of $\mathbf{Q}_0^k$, and $\mathbf{Q}_b^k$, we get

$$\begin{aligned}
|\mathcal{S}_1(\mathbf{Q}_h \mathbf{p}, \mathbf{v}_h)| &= \left| \sum_{T\in\mathcal{T}_h} h_T \langle (\mathbf{Q}_0^k \mathbf{p} - \mathbf{Q}_b^k \mathbf{p}) \times \boldsymbol{\eta}, (\mathbf{v}_0 - \mathbf{v}_b)) \times \boldsymbol{\eta} \rangle_{\partial T} \right| \\
&\le \sum_{T\in\mathcal{T}_h} h_T \|\mathbf{Q}_0^k \mathbf{p} - \mathbf{p}\|_{\partial T} \|(\mathbf{v}_0 - \mathbf{v}_b) \times \boldsymbol{\eta}\|_{\partial T} \\
&\le \left(\sum_{T\in\mathcal{T}_h} h_T \|\mathbf{Q}_0^k \mathbf{p} - \mathbf{p}\|_T^2 \right)^{\frac{1}{2}} \left(\sum_{T\in\mathcal{T}_h} h_T \|\mathbf{v}_0 - \mathbf{v}_b) \times \boldsymbol{\eta}\|_T^2 \right)^{\frac{1}{2}} \\
&\le C h^{k+1} \|\mathbf{p}\|_{k+1} |||(\mathbf{v}_h, \mathbf{w}_h, z_h)|||.
\end{aligned}$$

Using the definitions of $\mathbf{L}_0^k$ and $\mathbf{L}_b^k$ to obtain

$$\begin{aligned}
|\mathcal{S}_2(\mathbf{L}_h\boldsymbol{\psi}, \mathbf{w}_h)| &= \left|\sum_{T\in\mathcal{T}_h} h_T^3\langle \mathbf{L}_0^k\boldsymbol{\psi} - \mathbf{L}_b^k\boldsymbol{\psi}, \mathbf{w}_0 - \mathbf{w}_b\rangle_{\partial T}\right| \\
&\leq \sum_{T\in\mathcal{T}_h} h_T^3\|\mathbf{L}_0^k\boldsymbol{\psi} - \boldsymbol{\psi}\|_{\partial T}\|\mathbf{w}_0 - \mathbf{w}_b\|_{\partial T} \\
&\leq \left(\sum_{T\in\mathcal{T}_h} h_T^3\|\mathbf{L}_0^k\boldsymbol{\psi} - \boldsymbol{\psi}\|_T^2\right)^{\frac{1}{2}}\left(\sum_{T\in\mathcal{T}_h} h_T^3\|\mathbf{w}_0 - \mathbf{w}_b\|_T^2\right)^{\frac{1}{2}} \\
&\leq Ch^{k+1}\|\boldsymbol{\psi}\|_k|||(\mathbf{v}_h, \mathbf{w}_h, z_h)|||.
\end{aligned}$$

In similar ways, we have

$$\begin{aligned}
|\mathcal{S}_3(\mathcal{R}_h q, z_h)| &= \left|\sum_{T\in\mathcal{T}_h} h_T^3\langle \mathcal{R}_0^k q - \mathcal{R}_b^k q, z_0 - z_b\rangle_{\partial T}\right| \\
&\leq \sum_{T\in\mathcal{T}_h} h_T^3\|\mathcal{R}_0^k q - q\|_{\partial T}\|z_0 - z_b\|_{\partial T} \\
&\leq \left(\sum_{T\in\mathcal{T}_h} h_T^3\|\mathcal{R}_0^k q - q\|_T\right)^{\frac{1}{2}}\left(\sum_{T\in\mathcal{T}_h} h_T^3\|z_0 - z_b\|_T\right)^{\frac{1}{2}} \\
&\leq Ch^{k+1}\|q\|_k|||(\mathbf{v}_h, \mathbf{w}_h, z_h)|||.
\end{aligned}$$

□

Theorem 8.3.1. *Assume that* $(\mathbf{p}, \boldsymbol{\psi}, q) \in [H^{k+1}(\Omega)]^d \times [H^k(\Omega)]^{2d-3} \times H^k(\Omega)$ *is the exact solution of the problem* (8.1.5). *Let* $(\mathbf{p}_h, \boldsymbol{\psi}_h, q_h) \in \mathbf{V}_h^0 \times \mathbf{W}_h \times Z_h^0$ *be the LSWG solution of the equation* (8.2.10). *Then, we have*

$$|||(\mathbf{Q}_h\mathbf{p} - \mathbf{p}_h, \mathbf{L}_h\boldsymbol{\psi} - \boldsymbol{\psi}_h, \mathcal{R}_h q - q_h)||| \leq Ch^{k+1}\left(\|\mathbf{p}\|_{k+1} + \|\boldsymbol{\psi}\|_k + \|q\|_k\right).$$

Proof. By substituting $\mathbf{v}_h = \mathbf{e}_h^{\mathbf{p}}$, $\mathbf{w}_h = \mathbf{e}_h^{\boldsymbol{\psi}}$ and $z_h = e_h^q$ in Lemma 8.3.1, we get

$$\mathcal{A}((\mathbf{e}_h^{\mathbf{p}}, \mathbf{e}_h^{\boldsymbol{\psi}}, e_h^q); (\mathbf{e}_h^{\mathbf{p}}, \mathbf{e}_h^{\boldsymbol{\psi}}, e_h^q)) = R((\mathbf{p}, \boldsymbol{\psi}, q); (\mathbf{e}_h^{\mathbf{p}}, \mathbf{e}_h^{\boldsymbol{\psi}}, e_h^q)).$$

Now, from Lemma 8.3.2, we get

$$\left|\left|\left|(\mathbf{e}_h^{\mathbf{p}}, \mathbf{e}_h^{\boldsymbol{\psi}}, e_h^q)\right|\right|\right| \leq Ch^{k+1}\left(\|\mathbf{p}\|_{k+1} + \|\boldsymbol{\psi}\|_k + \|q\|_k\right).$$

This completes the proof of the Theorem 8.3.1. □

8.4 Numerical Experiments

In this section, we will perform some numerical experiments for the Maxwell' equations (8.1.5). The main focus is to verify the accuracy, efficiency, flexibility and robustness of the proposed LSWG algorithm. For two dimensional (2D) problems quadrilaterals, pentagons and hexagons meshes, whereas uniform cubic meshes have been used in three dimensional (3D) problems. In addition, tests have been conducted for the non-convex domains for the 2D and 3D problems.

Example 8.4.1. In this example, we first consider the 2D Maxwell's equation on the unit square domain $\Omega = (0,1)^2$. The analytical solution $(\mathbf{p}, q)$ is taken as ([101], Example 5.1.1)

$$\mathbf{p}(x,y) = (u_1, u_2)^t = \begin{pmatrix} 10x^2(x-1)^2y(y-1)(2y-1) \\ -10x(x-1)(2x-1)y^2(y-1)^2 \end{pmatrix},$$

and $q = 10(2x-1)(2y-1)$. Coefficients are chosen to be $\beta = \gamma = 1$. We have used the pentagons-quadrilateral meshes, shown in Figure 8.4.1. The surface plots for the analytical solution and least-squared WG solution with $k = 1$ and mesh-level 6 are depicted in the Figures 8.4.2-8.4.4. We listed all the computational results in Table 8.4.1, which confirms the theoretical justifications.

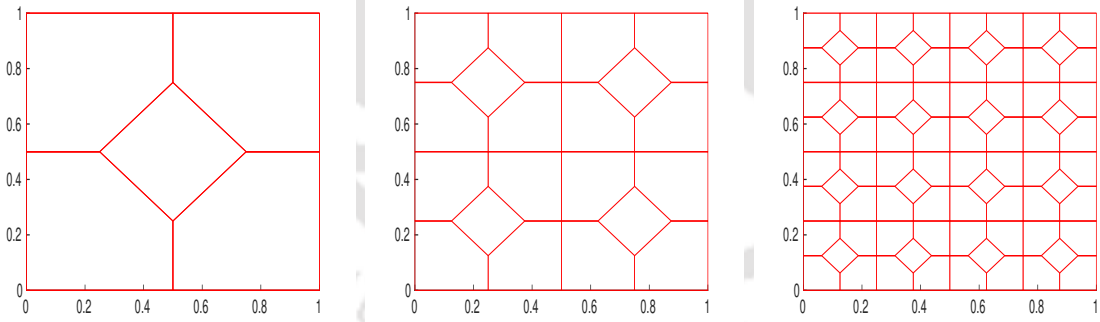

Figure 8.4.1: First 3-levels for the pentagons-quadrilateral mesh for Example 8.4.1.

Example 8.4.2. To validate the least-squares WG algorithm, we consider the 2D Maxwell' equation on the domain $\Omega = (0,1)^2$ having finite sequence of the hexagons-pentagons-quadrilaterals meshes, shown in Figure 8.4.5. The exact solution $(\mathbf{p}, q)$ is selected as ([101], Example 5.2.1)

$$\mathbf{p}(x,y) = (u_1, u_2)^t = \begin{pmatrix} -\exp(x)(y\cos(y) + \sin(y)) \\ \exp(x)y\sin(y) \end{pmatrix},$$

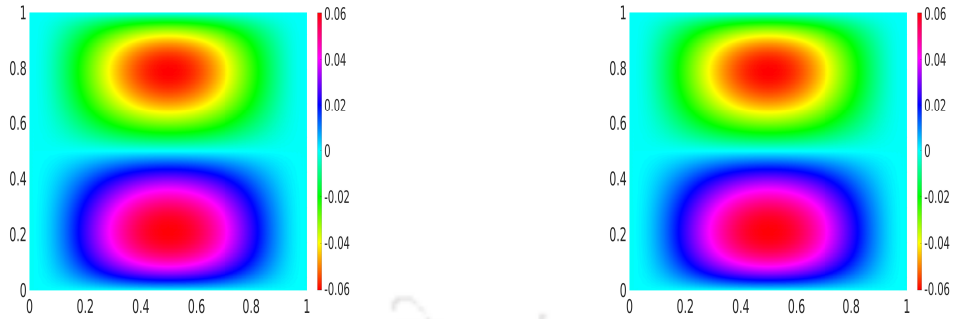

Figure 8.4.2: (Example 8.4.1) First component surface plots for the analytical solution **p** (left) and its LSWG solution (right).

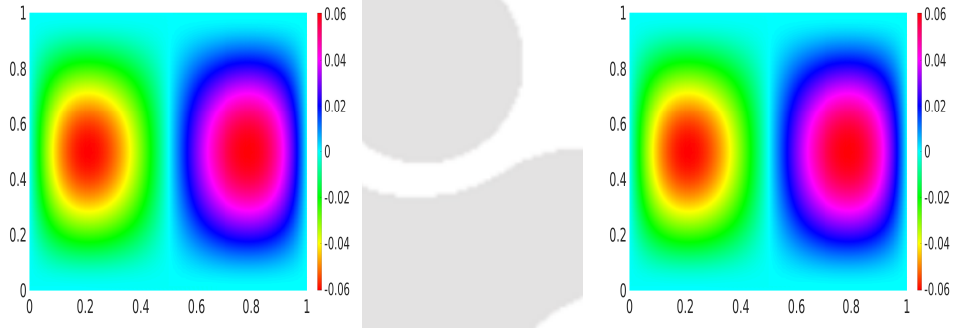

Figure 8.4.3: (Example 8.4.1) Second component surface plots for the analytical solution **p** (left) and its LSWG solution (right).

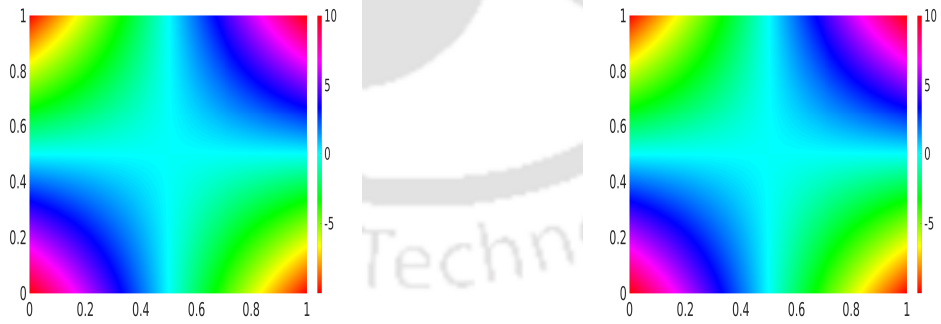

Figure 8.4.4: (Example 8.4.1) Surface plots for the analytical solution q (left) and its LSWG solution (right).

and $q(x, y) = 2\exp(x)\sin(y)$. Coefficients are assumed to be $\beta = \gamma = 1$. For $k = 2$ with mesh-level 6, the exact solution and WG solution surface plots are shown in the Figures 8.4.6-8.4.8. Table 8.4.2 validates the theoretical results of WG approximation.

Table 8.4.1: Numerical Convergence and error profiles for Example 8.4.1.

k	Level	$\|\|\|\left(\mathbf{e}_h^{\mathbf{P}}, \mathbf{e}_h^{\psi}, \mathbf{e}_h^{q}\right)\|\|\|$	Order	$\|\|\mathbf{e}_0^{\mathbf{P}}\|\|$	Order	$\|\|\mathbf{e}_0^{\psi}\|\|$	Order	$\|\|\mathbf{e}_0^{q}\|\|$	Order
1	1	5.62e-02	—	4.66e-02	—	4.45e-01	—	5.28e-02	—
	2	1.45e-02	1.95	1.25e-02	1.88	1.16e-01	1.93	1.25e-02	2.06
	3	3.68e-03	1.98	3.23e-03	1.95	2.96e-02	1.97	3.10e-03	2.02
	4	9.24e-04	1.99	8.16e-04	1.98	7.44e-03	1.99	7.72e-04	2.00
	5	2.31e-04	1.99	2.04e-04	2.00	1.86e-03	1.99	1.93e-04	2.00
	6	5.78e-05	2.00	5.11e-05	2.00	4.65e-04	2.00	4.82e-05	2.00
2	1	5.31e-03	—	6.14e-03	—	3.31e-02	—	4.23e-03	—
	2	6.52e-04	3.02	7.66e-04	3.00	4.23e-03	2.96	4.60e-04	3.19
	3	7.75e-05	3.07	9.29e-05	3.04	5.29e-04	2.99	5.13e-05	3.16
	4	9.34e-06	3.05	1.13e-05	3.03	6.60e-05	3.00	5.93e-06	3.11
	5	1.14e-06	3.02	1.40e-06	3.01	8.24e-06	3.00	7.08e-07	3.06
	6	1.41e-07	3.01	1.75e-07	3.00	1.02e-06	3.00	8.63e-08	3.03
3	1	8.76e-04	—	9.11e-04	—	3.55e-03	—	4.08e-04	—
	2	5.80e-05	3.91	6.03e-05	3.91	2.24e-04	3.98	2.57e-05	3.98
	3	3.59e-06	4.01	3.74e-06	4.00	1.39e-05	4.00	1.60e-06	3.99
	4	2.21e-07	4.02	2.31e-07	4.01	8.71e-07	4.00	1.00e-07	4.00
	5	1.36e-08	4.01	1.43e-08	4.01	5.43e-08	4.00	6.26e-09	4.00
	6	8.50e-10	4.00	8.93e-10	4.00	3.39e-09	4.00	3.91e-10	4.00

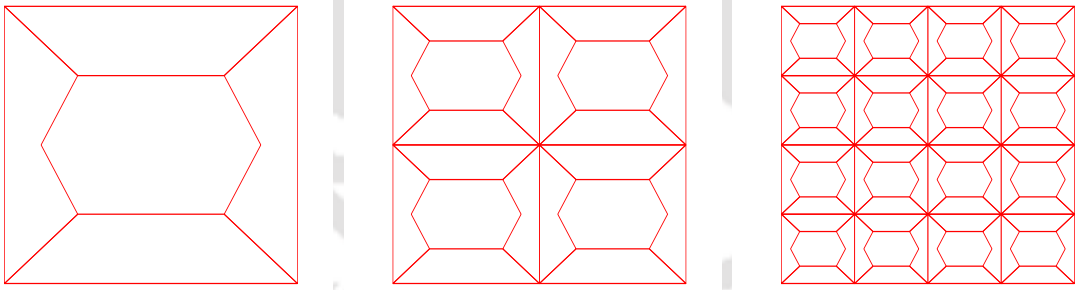

Figure 8.4.5: First 3-levels for the hexagons-pentagons-quadrilaterals mesh for Example 8.4.2.

Example 8.4.3. In this example, we have considered the 2D Maxwell's equation on non-convex L-shaped domain $\Omega = (-1,1)^2 \setminus (0,1) \times (-1,0)$. The analytical solution $(\mathbf{p}, q)$ is chosen as ([12], Example 3)

$$\mathbf{p}(x,y) = (u_1, u_2)^t = \begin{pmatrix} \exp(x)\cos(y) + \sin(y) \\ -\exp(x)\sin(y) + 1 - x^3 \end{pmatrix},$$

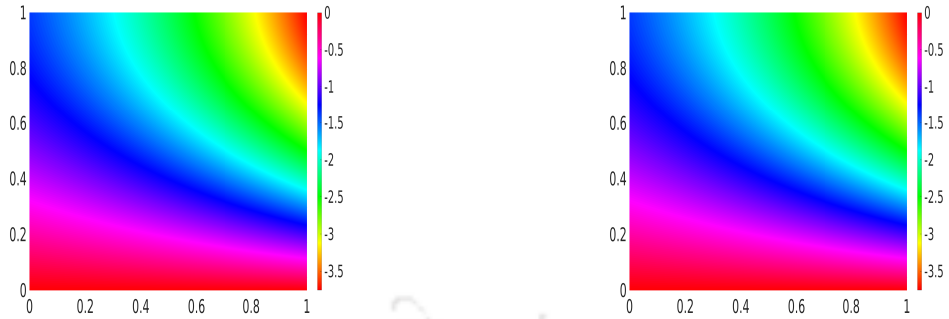

Figure 8.4.6: (Example 8.4.2) First component surface plots for the exact solution $\mathbf{p}$ (left) and its LSWG solution (right).

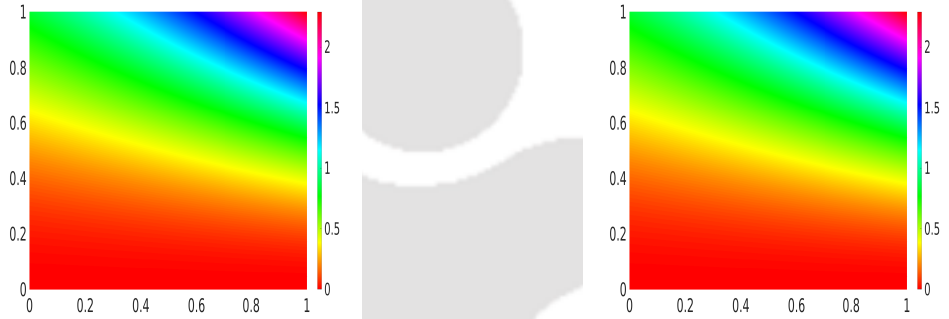

Figure 8.4.7: (Example 8.4.2) Second component surface plots for the exact solution $\mathbf{p}$ (left) and its LSWG solution (right).

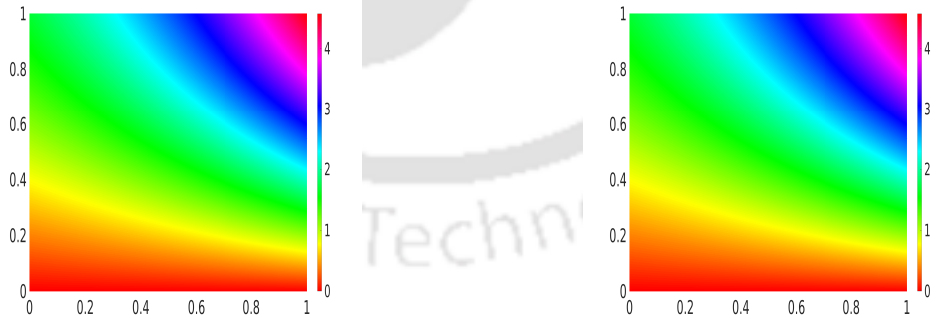

Figure 8.4.8: (Example 8.4.2) Surface plots for the exact solution q (left) and its LSWG solution (right).

and $q(x,y) = \sin(y)\cos(x) + xy^2 - \frac{1}{6} - \sin(1)(1-\cos(1))$. Note that $\beta = \gamma = 1$. A finite sequence of the hexagons-pentagons-quadrilaterals meshes (see, Figure 8.4.9) have been used for the computational purpose. For $k = 2$ with mesh-level 6, the exact solution

Table 8.4.2: Numerical Convergence and error profiles for Example 8.4.2.

k	Level	$\left\|\left\|\left\|\left(\mathbf{e}_h^{\mathbf{P}}, \mathbf{e}_h^{\psi}, \mathbf{e}_h^{q}\right)\right\|\right\|$	Order	$\|\mathbf{e}_0^{\mathbf{P}}\|$	Order	$\|\mathbf{e}_0^{\psi}\|$	Order	$\|\mathbf{e}_0^{q}\|$	Order
1	1	5.95e-02	—	3.84e-02	—	3.20e-02	—	2.47e-02	—
	2	1.60e-02	1.88	9.85e-03	1.96	8.85e-03	1.85	7.63e-03	1.69
	3	4.15e-03	1.95	2.48e-03	1.98	2.33e-03	1.92	2.07e-03	1.88
	4	1.05e-03	1.98	6.23e-04	1.99	5.97e-04	1.96	5.32e-04	1.95
	5	2.64e-04	1.99	1.56e-04	1.99	1.50e-04	1.99	1.34e-04	1.98
	6	6.61e-05	2.00	3.90e-05	2.00	3.76e-05	1.99	3.36e-05	1.99
2	1	2.96e-03	—	2.78e-03	—	6.42e-03	—	1.95e-03	—
	2	4.33e-04	2.77	3.57e-04	2.96	8.82e-04	2.86	3.14e-04	2.63
	3	5.82e-05	2.89	4.53e-05	2.97	1.15e-04	2.93	4.41e-05	2.83
	4	7.54e-06	2.94	5.71e-06	2.98	1.46e-05	2.97	5.82e-06	2.92
	5	9.59e-07	2.97	7.17e-07	2.99	1.85e-06	2.98	7.48e-07	2.96
	6	1.20e-07	2.99	8.98e-08	3.00	2.32e-07	2.99	9.48e-08	2.98
3	1	9.20e-05	—	1.61e-04	—	7.85e-04	—	5.39e-05	—
	2	6.17e-06	3.89	9.94e-06	4.02	5.33e-05	3.87	3.49e-06	3.94
	3	4.01e-07	3.94	6.14e-07	4.01	3.47e-06	3.93	2.24e-07	3.96
	4	2.55e-08	3.97	3.81e-08	4.00	2.21e-07	3.97	1.42e-08	3.97
	5	1.61e-09	3.99	2.37e-09	4.00	1.39e-08	3.99	8.98e-10	3.99
	6	1.01e-10	3.99	1.48e-10	4.00	8.77e-10	3.99	5.65e-11	3.99

and WG solution surface plots are shown in Figures 8.4.10-8.4.12 . Table 8.4.3 validates the theoretical results of WG approximation.

Figure 8.4.9: First 2-levels for the pentagons-quadrilateral mesh for Example 8.4.3.

Example 8.4.4. We consider the 3D Maxwell's equation on the unit cube domain

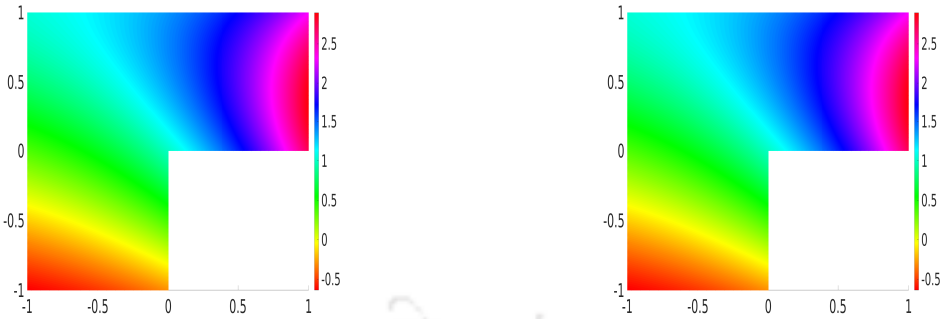

Figure 8.4.10: (Example 8.4.3) First component surface plots for the analytical solution $\mathbf{p}$ (left) and its LSWG solution (right).

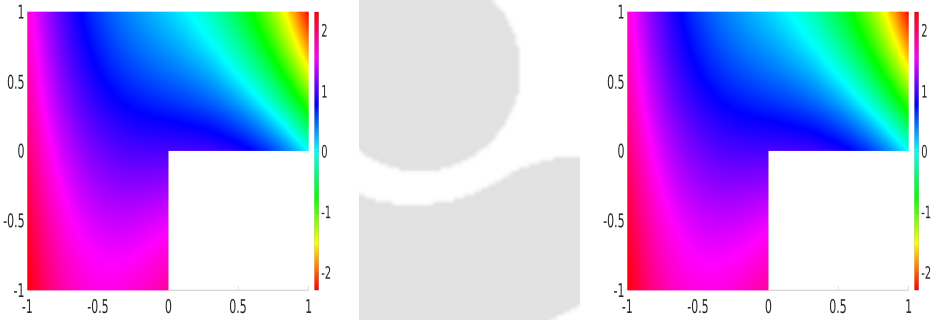

Figure 8.4.11: (Example 8.4.3) Second component surface plots for the analytical solution $\mathbf{p}$ (left) and its LSWG solution (right).

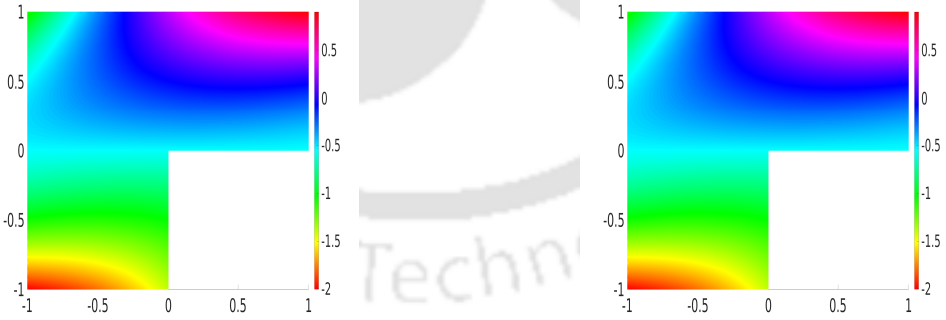

Figure 8.4.12: (Example 8.4.3) Surface plots for the analytical solution q (left) and its LSWG solution (right).

$\Omega = (0,1)^3$. The exact solution $(\mathbf{p}, q)$ is selected as ([102], Example 2)

$$\mathbf{p}(x,y,z) = (u_1,u_2,u_3)^t = \begin{pmatrix} \cos(\pi x)\sin(\pi y)\sin(\pi z) \\ \sin(\pi x)\cos(\pi y)\sin(\pi z) \\ \sin(\pi x)\sin(\pi y)\cos(\pi z) \end{pmatrix},$$

Table 8.4.3: Numerical Convergence and error profiles for Example 8.4.3.

k	Level	$\left\|\left\|\left\|\left(\mathbf{e}_h^{\mathbf{P}}, \mathbf{e}_h^{\psi}, \mathbf{e}_h^{q}\right)\right\|\right\|$	Order	$\|\mathbf{e}_0^{\mathbf{P}}\|$	Order	$\|\mathbf{e}_0^{\psi}\|$	Order	$\|\mathbf{e}_0^{q}\|$	Order
1	1	5.53e-02	—	4.82e-02	—	5.39e-01	—	5.52e-01	—
	2	1.43e-02	1.94	1.27e-02	1.92	1.35e-01	1.99	1.39e-01	1.98
	3	3.64e-03	1.97	3.26e-03	1.96	3.39e-02	1.99	3.51e-02	1.99
	4	9.17e-04	1.99	8.22e-04	1.98	8.50e-03	1.99	8.79e-03	1.99
	5	2.29e-04	1.99	2.06e-04	1.99	2.12e-03	1.99	2.20e-03	1.99
	6	5.74e-05	2.00	5.15e-05	2.00	5.31e-04	2.00	5.50e-04	2.00
2	1	2.17e-03	—	6.93e-03	—	7.36e-02	—	6.86e-02	—
	2	3.01e-04	2.84	8.88e-04	2.96	8.60e-03	3.09	7.93e-03	3.11
	3	3.94e-05	2.93	1.12e-04	2.98	1.00e-03	3.09	9.09e-04	3.12
	4	5.04e-06	2.96	1.41e-05	2.98	1.19e-04	3.07	1.06e-04	3.09
	5	6.36e-07	2.98	1.77e-06	2.99	1.44e-05	3.04	1.27e-05	3.05
	6	7.99e-08	2.99	2.22e-07	3.00	1.77e-06	3.02	1.55e-06	3.03
3	1	1.01e-04	—	5.68e-04	—	8.05e-03	—	8.83e-03	—
	2	6.46e-06	3.96	3.58e-05	3.99	5.04e-04	3.99	5.60e-04	3.97
	3	4.08e-07	3.98	2.24e-06	3.99	3.12e-05	4.01	3.46e-05	4.01
	4	2.56e-08	3.99	1.40e-07	4.00	1.93e-06	4.01	2.14e-06	4.01
	5	1.60e-09	3.99	8.74e-09	4.00	1.20e-07	4.00	1.32e-07	4.01
	6	1.00e-10	4.00	5.46e-10	4.00	7.51e-09	4.00	8.26e-09	4.00

and $q(x, y, z) = \sin(2\pi x)\sin(2\pi y)\sin(2\pi z)$. Note that $\beta = \gamma = 1$. We compute the WG solution on the uniform cubical meshes, shown in Figure 8.4.13. The surface plots for the analytical solution and least-squared WG solution with $k = 1$ and mesh-level 5 are depicted in the Figures 8.4.14-8.4.17. We listed all the computational results in Table 8.4.4, which confirms the theoretical justifications.

Figure 8.4.13: Initial mesh for the Example 8.4.4 (left) and Example 8.4.5 (right).

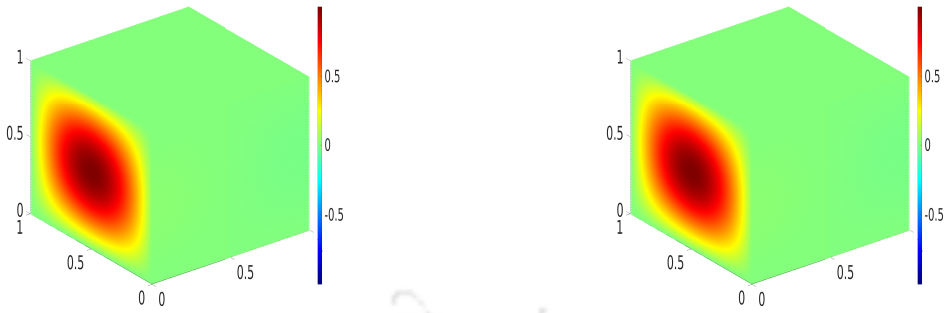

Figure 8.4.14: (Example 8.4.4) First component surface plots for the exact solution **p** (left) and its LSWG solution (right).

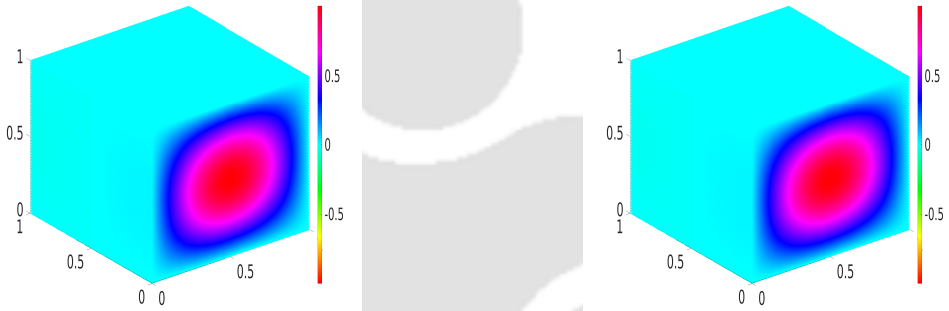

Figure 8.4.15: (Example 8.4.4) Second component surface plots for the exact solution **p** (left) and its LSWG solution (right).

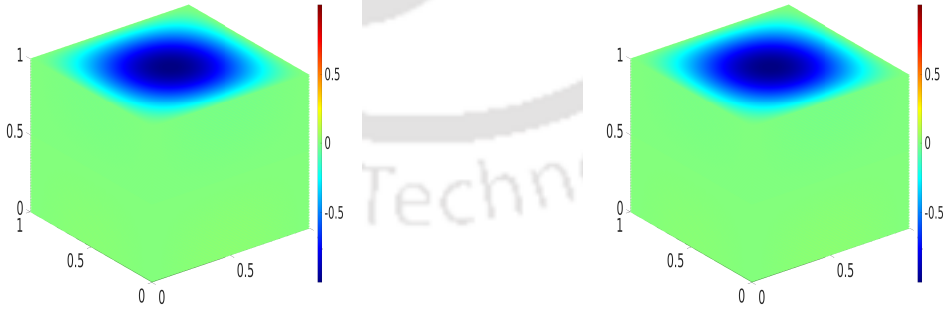

Figure 8.4.16: (Example 8.4.4) Third component surface plots for the exact solution **p** (left) and its LSWG solution (right).

Example 8.4.5. We next consider the 3D Maxwell's equation on the non-convex L-shaped domain on the $\Omega = (-1,1) \times (-1,1) \times (0,1) \setminus (0,1) \times (-1,0) \times (0,1)$ having

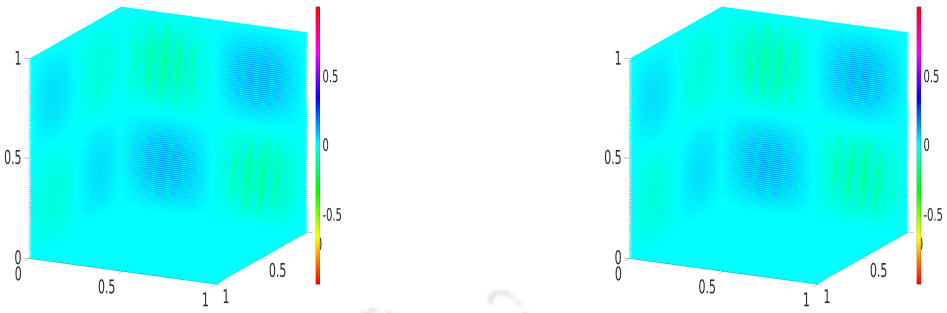

Figure 8.4.17: (Example 8.4.4) Surface plots for the exact solution q (left) and its LSWG solution (right).

Table 8.4.4: Numerical Convergence and error profiles for Example 8.4.4.

k	Level	$\left\|\left\|\left\|\left(\mathbf{e}_h^{\mathbf{P}}, \mathbf{e}_h^{\psi}, \mathbf{e}_h^{q}\right)\right\|\right\|$	Order	$\|\mathbf{e}_0^{\mathbf{P}}\|$	Order	$\|\mathbf{e}_0^{\psi}\|$	Order	$\|\mathbf{e}_0^{q}\|$	Order
1	1	1.73e-01	—	3.80e-02	—	2.52e+00	—	7.43e-01	—
	2	4.36e-02	1.98	9.77e-03	1.96	6.49e-01	1.95	1.93e-01	1.94
	3	2.73e-03	1.99	6.18e-04	1.99	1.64e-01	1.98	4.90e-02	1.97
	4	6.82e-04	1.99	1.54e-04	1.99	4.12e-02	1.99	1.23e-02	1.99
	5	1.70e-04	2.00	3.87e-05	2.00	1.03e-02	1.99	3.08e-03	1.99
2	1	1.98e-02	—	4.56e-03	—	5.72e-01	—	1.40e-01	—
	2	2.27e-03	3.12	5.46e-04	3.06	7.23e-02	2.98	1.73e-02	3.02
	3	2.67e-04	3.09	6.66e-05	3.03	8.54e-03	3.08	2.07e-03	3.06
	4	3.23e-05	3.04	8.23e-06	3.01	1.00e-03	3.08	2.48e-04	3.05
	5	3.98e-06	3.02	1.02e-06	3.00	1.19e-04	3.06	3.02e-05	3.03
	6	4.94e-07	3.01	1.27e-07	3.00	1.45e-05	3.04	3.72e-06	3.02
3	1	2.59e-03	—	3.98e-04	—	1.14e-01	—	2.04e-02	—
	2	1.61e-04	4.00	2.47e-05	4.00	7.90e-03	3.85	1.35e-03	3.91
	3	9.96e-06	4.01	1.53e-06	4.01	5.00e-04	3.98	8.49e-05	3.99
	4	6.19e-07	4.00	9.54e-08	4.00	3.09e-05	4.01	5.26e-06	4.01
	5	3.85e-08	4.00	5.95e-09	4.00	1.91e-06	4.01	3.26e-07	4.01

uniform cubic partition, shown in Figure 8.4.13 (right). The exact solution is taken as

$$\mathbf{p}(x,y,z) = (u_1,u_2,u_3)^t = \begin{pmatrix} \exp(x+y)+z^2 \\ \exp(x+y+z)+xy \\ \exp(y+z)+x^2 \end{pmatrix},$$

and $q(x,y,z) = \exp(xy)\sin(\pi z)$. The coefficients are chosen as $\beta = \gamma = 1$. Table 8.4.5 confirms the theoretical justifications.

Table 8.4.5: Numerical Convergence and error profiles for Example 8.4.5.

k	Level	$\left\|\left\|\left\|\left(\mathbf{e}_h^{\mathbf{P}}, \mathbf{e}_h^{\psi}, \mathbf{e}_h^{q}\right)\right\|\right\|$	Order	$\|\mathbf{e}_0^{\mathbf{P}}\|$	Order	$\|\mathbf{e}_0^{\psi}\|$	Order	$\|\mathbf{e}_0^{q}\|$	Order
1	1	1.07e-01	—	4.99e-02	—	1.19e-02	—	4.09e+00	—
	2	2.68e-02	1.99	1.31e-02	1.92	2.95e-03	2.01	1.09e+00	1.90
	3	6.71e-03	1.99	3.35e-03	1.96	7.42e-04	1.99	2.81e-01	1.95
	4	1.67e-03	1.99	8.44e-04	1.98	1.86e-04	1.99	7.09e-02	1.98
	5	4.19e-04	1.99	2.11e-04	1.99	4.66e-05	1.99	1.77e-02	1.99
	6	1.04e-04	2.00	5.29e-05	2.00	1.16e-05	2.00	4.45e-03	2.00
2	1	3.75e-03	—	3.01e-03	—	7.19e-04	—	2.23e-01	—
	2	4.32e-04	3.11	4.22e-04	2.83	8.02e-05	3.16	2.73e-02	3.03
	3	5.11e-05	3.07	5.59e-05	2.91	9.38e-06	3.09	3.33e-03	3.03
	4	6.18e-06	3.04	7.19e-06	2.95	1.14e-06	3.03	4.12e-04	3.01
	5	7.60e-07	3.02	9.12e-07	2.98	1.42e-07	3.00	5.12e-05	3.00
	6	9.41e-08	3.01	1.14e-07	2.99	1.78e-08	3.00	6.38e-06	3.00
3	1	1.75e-04	—	1.20e-04	—	1.00e-04	—	2.41e-02	—
	2	1.07e-05	4.02	7.90e-06	3.93	6.51e-06	3.94	1.46e-03	4.04
	3	6.63e-07	4.01	5.05e-07	3.96	4.10e-07	3.98	8.88e-05	4.04
	4	4.12e-08	4.01	3.20e-08	3.98	2.56e-08	3.99	5.43e-06	4.02
	5	2.56e-09	4.00	2.01e-09	3.99	1.60e-09	4.00	3.35e-07	4.01
	6	1.60e-10	4.00	1.26e-10	3.99	1.00e-10	4.00	2.08e-08	4.00

9

Summary and Future Scopes

In this chapter, we highlight the significance of current thesis work and the corresponding results and techniques to derive them. We also provide information for the scope of possible extensions and future investigations.

9.1 Summary of results

This thesis discussed the high-order weak Galerkin finite element methods for Maxwell's equations. The main emphasis of the thesis is to derive the optimal order error bounds in suitable Sobolev norms for the Maxwell problems. Moreover, several numerical experiments have been performed which supported the theoretical findings.

In Chapter 2, we have discussed high-order WG-FEMs for $\mathbf{H}(\mathrm{div})$-elliptic problems with variable coefficients. The divergence operator is approximated by weak form as distributions for generalized functions. The optimal order error estimates in discrete energy norm and L^2 norms are established with WG space $\Big(\big[\mathcal{P}_k(T)\big]^d,\ \big[\mathcal{P}_k(\partial T)\big]^d,\ \mathcal{P}_{k-1}(T)\Big)$, where $d = 2, 3$, $k \geq 1$ is an integer and T is an arbitrary shape polygonal/polygonal domain. Our results are intended to extend the numerical analysis of WG-FEMs for elliptic problems [121] to $\mathbf{H}(\mathrm{div})$-elliptic problems. Numerous numerical experiments have been conducted to justify the theoretical results for the both two-dimensional and three-dimensional proposed algorithms. In addition, the numerical test is also performed for the $\mathbf{H}(\mathrm{div})$-elliptic interface for the homogenous jump conditions to validate the WG algorithm.

In Chapter 3, we proceed to develop the high-order WG algorithms for $\mathbf{H}(\mathrm{curl})$-elliptic problems (1.1.8)-(1.1.9) with variable physical parameters under hybrid meshes. The error estimates of optimal order in discrete H^1 and L^2 norms are established for the approximation space $\Big(\big[\mathcal{P}_k(T)\big]^d,\ \big[\mathcal{P}_k(\partial T)\big]^d,\ [\mathcal{P}_{k-1}(T)]^{2d-3}\Big)$. More precisely, error estimates of $\mathrm{O}(h^k)$ in energy norm and $\mathrm{O}(h^{k+1})$ in L^2 norm (see, Theorem 3.3.1 and

Theorem 3.3.2) are obtained for the WG method. Numerical results are performed for the smooth/low regular exact solutions for the proposed problems to justify the theoretical results.

In Chapter 4, we are concerned with the WG-FEMs for the $\mathbf{H}(\text{curl}, \text{div})$-elliptic problems. In most of the existing literature, the well-posedness of div-curl models has been established with the help of two or more additional penalty terms, but this study justifies the uniqueness of the WG algorithm with only one stabilizer term, which reduces the computational cost significantly and simplifies the weak formulation. The optimal order convergence for energy norm and L^2 norms have been discussed with WG space $\Big(\big[\mathcal{P}_k(T)\big]^d,\ \big[\mathcal{P}_k(\partial T)\big]^d,\ [\mathcal{P}_{k-1}(T)]^{2d-3},\ \mathcal{P}_{k-1}(T)\Big)$. Moreover, numerical experiments have been carried out to justify the theoretical results.

In Chapter 5, we have extended the results derived in chapter 2 for interface problems. For this purpose, we consider $\mathbf{H}(\text{div})$-elliptic interface problems (1.1.16)-(1.1.18) with non-homogeneous jump conditions. The optimal order error estimates for discrete energy norm and L^2 norm (see, Theorem 5.4.1 and Theorem 5.4.2) are derived for the WG space $\Big(\big[\mathcal{P}_k(T)\big]^d,\ \big[\mathcal{P}_k(\partial T)\big]^d,\ \mathcal{P}_{k-1}(T)\Big)$. The numerical experiments are performed with the geometrically complicated and very irregular interfaces having sharp edges, cusps, and tips that confirmed the theoretical findings of the proposed WG algorithm.

In Chapter 6, we have studied the weak Galerkin finite element method for the $\mathbf{H}(\text{div}, \text{curl})$-elliptic problems with non-homogenous jump conditions on the general polygonal/polyhedral meshes. The error estimates of $\mathrm{O}(h^k)$ in energy and $\mathrm{O}(h^{k+1})$ in L^2 norms are obtained for the WG method with weak Galerkin space $\Big(\big[\mathcal{P}_k(T)\big]^d,\ \big[\mathcal{P}_k(\partial T)\big]^d,\ [\mathcal{P}_{k-1}(T)]^{2d-3},\ \mathcal{P}_{k-1}(T)\Big)$. The results derived in this chapter are extensions of the work described in chapter 4. In addition, numerical simulations confirm the theoretical results.

In Chapter 7, we discussed the least-squares WG-FEMs for time-harmonic Maxwell's equations on general polygonal/polyhedral meshes. The super-convergence of order one is obtained for the discrete energy norm (see, Theorem 7.3.1). The various numerical experiments are conducted for the (1.1.10)-(1.1.11) with smooth/low regular exact solutions to justify the theoretical results. These experiments confirm the proposed method's robustness, reliability, and accuracy.

In the last chapter, we designed and analyzed the LSWG-FEMs for Maxwell's equations in two-dimensional and three-dimensional settings. For the discrete energy norm, the super-convergence of order one has been derived for the proposed algorithm. An ample amount of numerical experiments are performed that are consistent with the proposed algorithm.

9.2 Future Scopes and Remarks

In this section, we have described some possible extensions of our thesis work. Here, we are briefly presented some uninvestigated models that can be demonstrated as the future scopes of our findings.

WG-FEMs for the Maxwell eigenvalue interface problems with divergence free constraint: We can extended the weak Galerkin algorithm to the following Maxwell eigenvalue interface problems with divergence free constraint (see, in Michel and Duan et al. [31]) which seeks $(\omega^2, \mathbf{p})$ such that

$$\nabla \times (\beta \nabla \times \mathbf{p}) - \omega^2 \gamma \mathbf{p} = \gamma \mathbf{f} \text{ in } \Omega, \tag{9.2.1}$$

$$\nabla \cdot \mathbf{p} = 0 \text{ in } \Omega, \tag{9.2.2}$$

subject to the boundary condition:

$$\mathbf{p} \times \boldsymbol{\eta} = 0, \quad \nabla \cdot \mathbf{p} = 0 \text{ on } \partial\Omega, \tag{9.2.3}$$

and the jump conditions at the interface Γ:

$$\begin{cases} [\mathbf{p} \times \boldsymbol{\eta}] = \mathbf{f}_1 \text{ on } \Gamma, \\ [(\beta \nabla \times \mathbf{p}) \times \boldsymbol{\eta}] = \mathbf{f}_2 \text{ on } \Gamma, \\ [\mathbf{p} \cdot \boldsymbol{\eta}] = f_3 \text{ on } \Gamma, \end{cases} \tag{9.2.4}$$

where $\Omega \subset \mathbb{R}^d$ $(d = 2, 3)$ is a bounded domain with Lipschitz continuous boundary $\partial\Omega$ and a closed smooth interface Γ which separates Ω into two non-intersecting open sub-domains Ω_1 and Ω_2 (see, Fig. 1.1.1 for an demonstration). Here, notation $\boldsymbol{\eta}$ stands for the unit outward normal vector of Γ having direction from Ω_1 to Ω_2 or unit outward normal vector of $\partial\Omega$. The coefficient function β, γ are assumed to be positive and piecewise constant across Γ. Along the interface Γ, the source function $\mathbf{f} : \Omega \to \mathbb{R}^d$ can be singular. Jump functions $\mathbf{f}_1,\ \mathbf{f}_2 : \Gamma \to \mathbb{R}^{2d-3}$ and $f_3 : \Gamma \to \mathbb{R}$ are given functions.

WG-FEMs for the generalized Maxwell eigenvalue interface problems: The present work can be extended for the following generalized Maxwell eigenvalue interface problems (see, in Roger and Ping et al. [51]) which seeks $(\omega^2, \mathbf{p})$ such that

$$-\nabla \cdot (\alpha \nabla \mathbf{p}) + \nabla \times (\beta \nabla \times \mathbf{p}) - \omega^2 \gamma \mathbf{p} = \gamma \mathbf{f} \text{ in } \Omega, \tag{9.2.5}$$

subject to the boundary conditions:

$$\mathbf{p} \times \boldsymbol{\eta} = 0, \quad \nabla \cdot \mathbf{p} = 0 \text{ on } \partial\Omega, \tag{9.2.6}$$

and the jump conditions at the interface Γ:

$$\begin{cases} [\mathbf{p} \times \boldsymbol{\eta}] &= \mathbf{f}_1 \text{ on } \Gamma, \\ [(\beta\nabla \times \mathbf{p}) \times \boldsymbol{\eta}] &= \mathbf{f}_2 \text{ on } \Gamma, \\ [\mathbf{p} \cdot \boldsymbol{\eta}] &= f_3 \text{ on } \Gamma, \\ [\alpha\nabla \cdot \mathbf{p}] &= f_4 \text{ on } \Gamma, \end{cases} \tag{9.2.7}$$

where, the coefficient function α, β, γ are assumed to be positive and piecewise constant across Γ. Jump functions $\mathbf{f}_1,\ \mathbf{f}_2 : \Gamma \to \mathbb{R}^{2d-3}$ and $f_3,\ f_4 : \Gamma \to \mathbb{R}$ are given functions.

LSWG-FEMs for the H(curl)-elliptic interface problems: It would be interesting to extend the proposed least-squares weak Galerkin schemes for the **H**(curl)-elliptic interface problems which seeks $\mathbf{p}$ such that

$$\nabla \times (\beta\nabla \times \mathbf{p}) + \gamma\mathbf{p} = \mathbf{f} \text{ in } \Omega \tag{9.2.8}$$

with Dirichlet boundary condition

$$\mathbf{p} \times \boldsymbol{\eta} = 0 \text{ on } \partial\Omega, \tag{9.2.9}$$

and the jump conditions at the interface Γ :

$$\begin{cases} [\alpha\nabla \times \mathbf{p}] &= \mathbf{f}_1 \text{ on } \Gamma, \\ [\mathbf{p} \times \boldsymbol{\eta}] &= \mathbf{f}_2 \text{ on } \Gamma, \end{cases} \tag{9.2.10}$$

where the coefficient function β, γ are assumed to be positive and piecewise constant across Γ. Jump functions $\mathbf{f}_1,\ \mathbf{f}_2 : \Gamma \to \mathbb{R}^{2d-3}$ are given.

WG-FEMs for time-dependent Maxwell's equations with discontinuous coefficients: The Maxwell's equations in a dielectric medium with permeability parameter μ and the permittivity parameter ε can be read as follows (cf. [37])

$$\begin{cases} \varepsilon\frac{\partial \mathbf{E}}{\partial t} - \nabla \times \mathbf{H} &= \mathbf{J} \text{ in } \Omega \times (0,T), \\ \mu\frac{\partial \mathbf{H}}{\partial t} + \nabla \times \mathbf{E} &= 0 \text{ in } \Omega \times (0,T), \\ \nabla \cdot (\varepsilon\mathbf{E}) &= \rho \text{ in } \Omega \times (0,T), \\ \nabla \cdot (\mu\mathbf{H}) &= 0 \text{ in } \Omega \times (0,T), \end{cases} \tag{9.2.11}$$

where $\Omega \subset \mathbb{R}^d$ $(d = 2, 3)$ is bounded polygonal (2D)/polyhedral (3D) domain with Lipschitz continuous boundary $\partial\Omega$. Further, **E** and **H** are the electric and magnetic fields, and **J** and ρ are the current density and charge density. For the recent relevant works, we refer to [91] and references therein. In most real applications, however, Maxwell's

equations are imposed in heterogonous media (see in [26, 37, 50, 70, 92]). Due to heterogeneity of the underlying medium, media parameters may have jump discontinuities across interfaces in the domain of interest and which leads to a solution in $[\mathbf{H}^r(\Omega)]^3$ for some $r < 1$. It is this very low regularity that causes enormous difficulties in the finite element solution of (9.2.11).

We assume that the permittivity parameter ε and the permeability parameter μ of the medium are discontinuous across an interface Γ, where Γ is the boundary of domain Ω_1 with $\bar{\Omega}_1 \subset \Omega$ and $\Omega_2 = \Omega \setminus \Omega_1$. Further, we assume that permittivity parameter and permeability parameter are piecewise constant in in Ω, namely,

$$\varepsilon = \begin{cases} \varepsilon_1 \text{ in } \Omega_1, \\ \varepsilon_2 \text{ in } \Omega_2, \end{cases} \qquad \varepsilon = \begin{cases} \varepsilon_1 \text{ in } \Omega_1, \\ \varepsilon_2 \text{ in } \Omega_2, \end{cases}$$

and $\varepsilon_i,\ \mu_i\ (i = 1,\ 2)$ are positive constants.
Then the system of equations (9.2.11) is completed with the following physical interface conditions across the interface Γ (cf. [37])

$$\begin{cases} [\mathbf{E} \times \mathbf{n}] = \boldsymbol{\phi}, \quad [\varepsilon \mathbf{E} \cdot \mathbf{n}] = \phi, \\ [\mathbf{H} \times \mathbf{n}] = \boldsymbol{\varphi}, \quad [\mu \mathbf{H} \cdot \mathbf{n}] = \varphi. \end{cases} \tag{9.2.12}$$

Here, $\mathbf{n}$ denotes the outward unit normal vector to Γ pointing into Ω_2; and we denote by $[\mathbf{v}] := \mathbf{v}_1 - \mathbf{v}_2$ the jump of a vector-valued quantity $\mathbf{v}$ across the interface Γ (or by $[v] := v_1 - v_2$ the jump of a scalar v) with $\mathbf{v}_i = \mathbf{v}|_{\Omega_i}$ $(v_i = v|_{\Omega_i})$, $i = 1, 2$. Further, we supplement equations (9.2.11)-(9.2.12) with the initial conditions

$$\mathbf{E}(x, 0) = \mathbf{E}_0(x), \quad \mathbf{H}(x, 0) = \mathbf{H}_0(x), \quad x \in \Omega. \tag{9.2.13}$$

Most of the continuous finite element methods either are not directly applicable or become inefficient for the interface problem (9.2.11)-(9.2.12), due to low global regularity of the true solution. There are a few finite element methods for stationary Maxwell interface problems (e.g., [26, 50, 51, 70, 92]). Surprisingly, there has been less work on the finite element methods for the time-dependent Maxwell interface problems with non-homogeneous jump conditions. In future, we propose to develop higher order WG-FEMs for the interface problem (9.2.11)-(9.2.13) along with suitable boundary conditions. At the same time, the method would be able to accommodate very irregular interfaces and low regular solutions.

Bibliography

[1] R. Adams and J. Fournier, *Sobolev Spaces, sec. ed*, Academic Press, Amsterdam, 2003.

[2] M. Ainsworth and J. Coyle, *Hierarchic hp-edge element families for Maxwell's equations on hybrid quadrilateral/triangular meshes*, Computer Methods in Applied Mechanics and Engineering, 190 (2001), pp. 6709–6733.

[3] A. Alvarado and P. Castillo, *Computational performance of LDG methods applied to time-harmonic Maxwell's equation in polyhedral domains*, Journal of Scientific Computing, 67 (2016), pp. 453–474.

[4] D. Arnold, R. Falk, and R. Winther, *Preconditioning in H(div) and applications*, Math. Comp., 66 (1997), pp. 957–984.

[5] I. Babuška, *The finite element method for elliptic equations with discontinuous coefficients*, Computing, 5 (1970), pp. 207–213.

[6] C. Bacuta, J. Jacavage, K. Qirko, and F.-J. Sayas, *Saddle point least squares iterative solvers for the time harmonic Maxwell's equations*, Computers and Mathematics with Applications, 74 (2017), pp. 2915–2928.

[7] J. W. Barrett and C. M. Elliott, *Fitted and unfitted finite-element methods for elliptic equations with smooth interfaces*, IMA J. Numer. Anal., 7 (1987), pp. 283–300.

[8] K. Bathe, C. Nitikitpaiboon, and X. Wang, *A mixed displacement-based finite element formulation for acoustic fluid-structure interaction*, Comput. & Structures, 56 (1995), pp. 225–237.

[9] R. Bensow and M. G. Larson, *Discontinuous least-squares finite element method for the div-curl problem*, Numerische Mathematik, 101 (2005), pp. 601–617.

[10] A. Bermúdez and R. Rodríguez, *Finite element computation of the vibra-*

tion modes of a fluid–solid system, Computer Methods in Applied Mechanics and Engineering, 119 (1994), pp. 355–370.

[11] P. Bochev, J. Lai, and L. Olson, *A locally conservative, discontinuous least-squares finite element method for the Stokes equations*, International journal for numerical methods in fluids, 68 (2012), pp. 782–804.

[12] P. B. Bochev, *Analysis of least-squares finite element methods for the Navier–Stokes equations*, SIAM Journal on Numerical Analysis, 34 (1997), pp. 1817–1844.

[13] P. B. Bochev and M. D. Gunzburger, *Finite element methods of least-squares type*, SIAM review, 40 (1998), pp. 789–837.

[14] A. Bossavit, *Two dual formulations of the 3D eddy-currents problem*, COMPEL, (1985).

[15] ——, *Computational electromagnetism: variational formulations, complementarity, edge elements*, Academic Press, 1998.

[16] J. H. Bramble, T. V. Kolev, and J. E. Pasciak, *A least-squares approximation method for the time-harmonic Maxwell equations*, Journal of Numerical Mathematics, 13 (2005), pp. 237–263.

[17] S. Brenner, F. Li, and L.-Y. Sung, *A locally divergence-free nonconforming finite element method for the time-harmonic Maxwell equations*, Mathematics of computation, 76 (2007), pp. 573–595.

[18] S. C. Brenner, J. Cui, F. Li, and L.-Y. Sung, *A nonconforming finite element method for a two-dimensional curl-curl and grad-div problem*, Numerische Mathematik, 109 (2008), pp. 509–533.

[19] S. C. Brenner, F. Li, and L.-Y. Sung, *A locally divergence-free interior penalty method for two-dimensional curl-curl problems*, SIAM Journal on Numerical Analysis, 46 (2008), pp. 1190–1211.

[20] F. Brezzi, J. Douglas, and L. D. Marini, *Two families of mixed finite elements for second order elliptic problems*, Numerische Mathematik, 47 (1985), pp. 217–235.

[21] F. Brezzi and M. Fortin, *Mixed and hybrid finite element methods*, vol. 15, Springer Science & Business Media, 2012.

[22] A. Buffa, H. Ammari, and J.-C. Nédélec, *A justification of eddy currents model for the Maxwell equations*, SIAM Journal on Applied Mathematics, 60 (2000), pp. 1805–1823.

[23] E. Burman, O. Duran, A. Ern, and M. Steins, *Convergence analysis of hybrid high-order methods for the wave equation*, Journal of Scientific Computing, 87 (2021), pp. 1–30.

[24] Z. Cai, R. Lazarov, T. A. Manteuffel, and S. F. McCormick, *First-*

order system least squares for second-order partial differential equations: Part I, SIAM J. Numer. Anal., 31 (1994), pp. 1785–1799.

[25] ——, *First-order system least squares for second-order partial differential equations: Part I*, SIAM J. Numer. Anal., 31 (1994), pp. 1785–1799.

[26] S. Cao, L. Chen, and R. Guo, *A virtual finite element method for two dimensional Maxwell interface problems with a background unfitted mesh*, arXiv preprint arXiv:2103.04582, (2021).

[27] ——, *Immersed virtual element methods for Maxwell interface problems in three dimensions*, arXiv preprint arXiv:2202.09987, (2022).

[28] W. Cao, C. Wang, and J. Wang, *A new primal-dual weak Galerkin method for elliptic interface problems with low regularity assumptions*, Journal of Computational Physics, 470 (2022), p. 111538.

[29] C. Carstensen, Q. Zhai, and R. Zhang, *A skeletal finite element method can compute lower eigenvalue bounds*, SIAM Journal on Numerical Analysis, 58 (2020), pp. 109–124.

[30] P. Castillo, B. Cockburn, I. Perugia, and D. Schötzau, *An a priori error analysis of the local discontinuous Galerkin method for elliptic problems*, SIAM Journal on Numerical Analysis, 38 (2000), pp. 1676–1706.

[31] M. Cessenat, *Mathematical methods in electromagnetism: linear theory and applications*, vol. 41, World scientific, 1996.

[32] C. Chang, *A least-squares finite element method for the Helmholtz equation*, Computer methods in applied mechanics and engineering, 83 (1990), pp. 1–7.

[33] H. Chen and W. Qiu, *A first order system least squares method for the Helmholtz equation*, 309 (2017), pp. 145–162.

[34] L. Chen, R. Guo, and J. Zou, *A family of immersed finite element spaces and applications to three dimensional H(curl) interface problems*, arXiv preprint arXiv:2205.14127, (2022).

[35] L. Chen, H. Wei, and M. Wen, *An interface-fitted mesh generator and virtual element methods for elliptic interface problems*, J. Comput. Phys., 334 (2017), pp. 327–348.

[36] ——, *An interface-fitted mesh generator and virtual element methods for elliptic interface problems*, Journal of Computational Physics, 334 (2017), pp. 327–348.

[37] Z. Chen, Q. Du, and J. Zou, *Finite element methods with matching and nonmatching meshes for Maxwell equations with discontinuous coefficients*, SIAM Journal on Numerical Analysis, 37 (2000), pp. 1542–1570.

[38] Z. Chen and J. Zou, *Finite element methods and their convergence for elliptic and parabolic interface problems*, Numer. Math., 79 (1998), pp. 175–202.

[39] P. G. Ciarlet, *The finite element method for elliptic problems*, SIAM, 2002.

[40] M. Cicuttin and C. Geuzaine, *Numerical investigation of a 3D hybrid high-order method for the indefinite time-harmonic Maxwell's problem*, (2022).

[41] B. Cockburn, D. A. Di Pietro, and A. Ern, *Bridging the hybrid high-order and hybridizable discontinuous Galerkin methods*, ESAIM Mathematical Modeling and Numerical Analysis, 50 (2016), pp. 635–650.

[42] ——, *Bridging the hybrid high-order and hybridizable discontinuous Galerkin methods*, ESAIM Math. Model. Numer. Anal., 50 (2016), pp. 635–650.

[43] M. Costabel, *A coercive bilinear form for Maxwell's equations*, Journal of mathematical analysis and applications, 157 (1991), pp. 527–541.

[44] M. Costabel and M. Dauge, *Weighted regularization of Maxwell equations in polyhedral domains*, Numerische Mathematik, 93 (2002), pp. 239–277.

[45] L. B. da Veiga and G. Manzini, *A virtual element method with arbitrary regularity*, IMA J. Numer. Anal., 34 (2014), pp. 759–781.

[46] B. Deka, *Finite element methods with numerical quadrature for elliptic problems with smooth interfaces*, J. Comput. Appl. Math., 234 (2010), pp. 605–612.

[47] A.-S. B.-B. Dhia, C. Hazard, and S. Lohrengel, *A singular field method for the solution of Maxwell's equations in polyhedral domains*, SIAM Journal on Applied Mathematics, 59 (1999), pp. 2028–2044.

[48] H. K. Dirks, *Quasi-stationary fields for microelectronic applications*, Electrical Engineering, 79 (1996), pp. 145–155.

[49] Z. Dong and A. Ern, *Hybrid high-order and weak Galerkin methods for the Biharmonic problem*, arXiv preprint arXiv:2103.16404, (2021).

[50] H. Duan, P. Lin, and R. C. Tan, *Analysis of a continuous finite element method for $H(curl, div; \Omega)$-elliptic interface problem*, Numerische Mathematik, 123 (2013), pp. 671–707.

[51] ——, *A finite element method for a curlcurl-graddiv eigenvalue interface problem*, SIAM Journal on Numerical Analysis, 54 (2016), pp. 1193–1228.

[52] H. Duan, J. Ma, R. C. Tan, and C. Wang, *A coercive mixed formulation for the generalized Maxwell problem*, 402 (2022), p. 113787.

[53] H.-Y. Duan, R. C. Tan, S.-Y. Yang, and C.-S. You, *Computation of Maxwell singular solution by nodal-continuous elements*, Journal of Computational Physics, 268 (2014), pp. 63–83.

[54] ——, *A mixed H^1-conforming finite element method for solving Maxwell's equations with non-H^1 solution*, SIAM Journal on Scientific Computing, 40 (2018), pp. A224–A250.

[55] H. Egger and J. Schöberl, *A hybrid mixed discontinuous Galerkin finite-*

element method for convection–diffusion problems, IMA Journal of Numerical Analysis, 30 (2010), pp. 1206–1234.

[56] A. Ern, S. Nicaise, and M. Vohralík, *An accurate H(div) flux reconstruction for discontinuous Galerkin approximations of elliptic problems*, C. R. Math. Acad. Sci. Paris, 345 (2007), pp. 709–712.

[57] H. Feng and S. Zhao, *A fourth order finite difference method for solving elliptic interface problems with the fft acceleration*, Journal of Computational Physics, 419 (2020), p. 109677.

[58] X. Feng, P. Lu, and X. Xu, *A hybridizable discontinuous Galerkin method for the time-harmonic Maxwell's equations with high wave number*, Computational Methods in Applied Mathematics, 16 (2016), pp. 429–445.

[59] X. Feng and H. Wu, *An absolutely stable discontinuous Galerkin method for the indefinite time-harmonic Maxwell equations with large wave number*, SIAM J. Numer. Anal., 52 (2014), pp. 2356–2380.

[60] V. Girault and P. RAVIART, *Finite element methods for Navier-Stokes equations: Theory and algorithms((book))*, Berlin and New York, Springer-Verlag(Springer Series in Computational Mathematics., 5 (1986).

[61] V. Girault and P.-A. Raviart, *Finite element methods for Navier-Stokes equations: theory and algorithms*, vol. 5, Springer Science & Business Media, 2012.

[62] R. D. Graglia, D. R. Wilton, and A. F. Peterson, *Higher order interpolatory vector bases for computational electromagnetics*, IEEE transactions on antennas and propagation, 45 (1997), pp. 329–342.

[63] T. Gudi, G. Mallik, and T. Pramanick, *A hybrid high-order method for quasilinear elliptic problems of nonmonotone type*, SIAM Journal on Numerical Analysis, 60 (2022), pp. 2318–2344.

[64] R. Guo, Y. Lin, and J. Zou, *Solving two dimensional H(curl)-elliptic interface systems with optimal convergence on unfitted meshes*, arXiv preprint arXiv:2011.11905, (2020).

[65] M. A. Hamdi, Y. Ousset, and G. Verchery, *A displacement method for the analysis of vibrations of coupled fluid-structure systems*, Internat. J. Numer. Methods Engrg., 13 (1978), pp. 139–150.

[66] C. Hazard and S. Lohrengel, *A singular field method for Maxwell's equations: numerical aspects for 2D magnetostatics*, SIAM Journal on Numerical Analysis, 40 (2002), pp. 1021–1040.

[67] R. Hiptmair, *Multigrid method for H(div) in three dimensions*, Electron. Trans. Numer. Anal, 6 (1997), pp. 133–152.

[68] ——, *Finite elements in computational electromagnetism*, Acta Numerica, 11

(2002), pp. 237–339.

[69] R. Hiptmair, J. Li, and J. Zou, *Convergence analysis of finite element methods for H(div)-elliptic interface problems*, J. Numer. Math., 18 (2010), pp. 187–218.

[70] R. Hiptmair, J. Li, and J. Zou, *Convergence analysis of finite element methods for H(curl)-elliptic interface problems*, Numerische Mathematik, 122 (2012), pp. 557–578.

[71] R. Hiptmair, A. Moiola, and I. Perugia, *Error analysis of Trefftz-discontinuous Galerkin methods for the time-harmonic Maxwell's equations*, Mathematics of Computation, 82 (2013), pp. 247–268.

[72] R. Hiptmair and J. Xu, *Nodal auxiliary space preconditioning in H(curl) and H(div) spaces*, SIAM J. Numer. Anal., 45 (2007), pp. 2483–2509.

[73] ——, *Nodal auxiliary space preconditioning in H(curl) and H(div) spaces*, SIAM J. Numer. Anal., 45 (2007), pp. 2483–2509.

[74] P. Houston, I. Perugia, A. Schneebeli, and D. Schötzau, *Interior penalty method for the indefinite time-harmonic Maxwell's equations*, Numerische Mathematik, 100 (2005), pp. 485–518.

[75] ——, *Mixed discontinuous Galerkin approximation of the Maxwell's operator: the indefinite case*, ESAIM: Mathematical Modelling and Numerical Analysis, 39 (2005), pp. 727–753.

[76] P. Houston, I. Perugia, and D. Schötzau, *An a posteriori error indicator for discontinuous Galerkin discretizations of H(curl)-elliptic partial differential equations*, IMA J. Numer. Anal., 27 (2007), pp. 122–150.

[77] Q. Hu and R. Song, *A variant of the plane wave least squares method for the time-harmonic Maxwell's equations*, ESAIM: Mathematical Modelling and Numerical Analysis, 53 (2019), pp. 85–103.

[78] J. Huang and J. Zou, *Some new a priori estimates for second-order elliptic and parabolic interface problems*, Journal of Differential Equations, 184 (2002), pp. 570–586.

[79] P. Huang, H. Wu, and Y. Xiao, *An unfitted interface penalty finite element method for elliptic interface problems*, Computer Methods in Applied Mechanics and Engineering, 323 (2017), pp. 439–460.

[80] T. J. Hughes, A. Masud, and J. Wan, *A stabilized mixed discontinuous Galerkin method for Darcy flow*, Computer Methods in Applied Mechanics and Engineering, 195 (2006), pp. 3347–3381.

[81] L. Huynh, N. Nguyen, J. Peraire, and B. Khoo, *A high-order hybridizable discontinuous Galerkin method for elliptic interface problems*, Int. J. Numer. Methods Engrg., 93 (2013), pp. 183–200.

[82] J.-M. Jin, *The finite element method in electromagnetics*, John Wiley & Sons, 2015.

[83] G. Kanschat and Y. Mao, *Multigrid methods for H(div)-conforming discontinuous Galerkin methods for the Stokes equations*, J. Numer. Math., 23 (2015), pp. 51–66.

[84] A. Khan, C. S. Upadhyay, and M. Gerritsma, *Spectral element method for parabolic interface problems*, Computer Methods in Applied Mechanics and Engineering, 337 (2018), pp. 66–94.

[85] R. Kumar and B. Deka, *Weak Galerkin finite element methods for H(curl) and H(curl,div)-elliptic problems*, revised version submitted to Computers and Mathematics with Applications.

[86] ——, *Weak Galerkin finite element methods with and without stabilizers for H(div)-elliptic problems*, accepted in ZAMM, https://doi.org/10.1002/zamm.202200207.

[87] ——, *High-order weak galerkin scheme for h (div)-elliptic interface problems*, Journal of Computational and Applied Mathematics, 432 (2023), p. 115269.

[88] C. Lehrenfeld and A. Reusken, *Analysis of a high-order unfitted finite element method for elliptic interface problems*, IMA Journal of Numerical Analysis, 38 (2018), pp. 1351–1387.

[89] J. Li, J. M. Melenk, B. Wohlmuth, and J. Zou, *Optimal a priori estimates for higher order finite elements for elliptic interface problems*, Appl. Numer. Math., 60 (2010), pp. 19–37.

[90] J. Li, X. Ye, and S. Zhang, *A weak Galerkin least-squares finite element method for div-curl systems*, Journal of Computational Physics, 363 (2018), pp. 79–86.

[91] R. Li, Q. Liu, and F. Yang, *A discontinuous least squares finite element method for time-harmonic Maxwell equations*, IMA Journal of Numerical Analysis, 42 (2022), pp. 817–839.

[92] ——, *A reconstructed discontinuous approximation on unfitted meshes to H(curl) and H(div) interface problems*, Computer Methods in Applied Mechanics and Engineering, 403 (2023), p. 115723.

[93] R. Li and F. Yang, *A sequential least squares method for Poisson equation using a patch reconstructed space*, SIAM Journal on Numerical Analysis, 58 (2020), pp. 353–374.

[94] P. Lin, *A sequential regularization method for time-dependent incompressible Navier–Stokes equations*, SIAM J. Numer. Anal., 34 (1997), pp. 1051–1071.

[95] ——, *A sequential regularization method for time-dependent incompressible*

Navier-Stokes equations, SIAM J. Numer. Anal., 34 (1997), pp. 1051–1071.

[96] H. Liu, L. Zhang, X. Zhang, and W. Zheng, *Interface-penalty finite element methods for interface problems in H^1, H(curl), and H(div)*, Computer Methods in Applied Mechanics and Engineering, 367 (2020), p. 113137.

[97] P. Lu, H. Chen, and W. Qiu, *An absolutely stable hp-HDG method for the time-harmonic Maxwell's equations with high wave number*, Mathematics of Computation, 86 (2017), pp. 1553–1577.

[98] P. Monk, *A finite element method for approximating the time-harmonic Maxwell's equations*, Numerische mathematik, 63 (1992), pp. 243–261.

[99] ——, *Finite element methods for Maxwell's equations*, Oxford University Press, 2003.

[100] H. J.-P. Morand and R. Ohayon, *Interactions fluides-structures*, vol. 154, Masson Paris, 1992.

[101] L. Mu, *Pressure robust weak Galerkin finite element methods for Stokes problems*, SIAM Journal on Scientific Computing, 42 (2020), pp. B608–B629.

[102] L. Mu, J. Wang, X. Ye, and S. Zhang, *A weak Galerkin finite element method for the Maxwell equations*, Journal of Scientific Computing, 65 (2015), pp. 363–386.

[103] L. Mu, J. Wang, X. Ye, and S. Zhao, *A new weak Galerkin finite element method for elliptic interface problems*, Journal of Computational Physics, 325 (2016), pp. 157–173.

[104] J.-C. Nédélec, *A new family of mixed finite elements in $\mathbb{R}^3$*, Numerische Mathematik, 50 (1986), pp. 57–81.

[105] N. C. Nguyen, J. Peraire, and B. Cockburn, *Hybridizable discontinuous Galerkin methods for the time-harmonic Maxwell's equations*, Journal of Computational Physics, 230 (2011), pp. 7151–7175.

[106] B. F. Nielsen, *Finite element discretizations of elliptic problems in the presence of arbitrarily small ellipticity: An error analysis*, SIAM J. Numer. Anal., 36 (1999), pp. 368–392.

[107] L. G. Olson and K.-J. Bathe, *A study of displacement-based fluid finite elements for calculating frequencies of fluid and fluid-structure systems*, Nucl. Eng. Des., 76 (1983), pp. 137–151.

[108] P.-A. Raviart and J.-M. Thomas, *A mixed finite element method for 2nd order elliptic problems*, (1977), pp. 292–315.

[109] J. Saranen, *On generalized harmonic fields in domains with anisotropic nonhomogeneous media*, Journal of Mathematical Analysis and Applications, 88 (1982), pp. 104–115.

[110] ——, *On electric and magnetic problems for vector fields in anisotropic nonhomogeneous media*, Journal of Mathematical Analysis and Applications, 91 (1983), pp. 254–275.

[111] J. Schöberl and S. Zaglmayr, *High order Nédélec elements with local complete sequence properties*, COMPEL, 24 (2005), pp. 374–384.

[112] S. Shields, J. Li, and E. A. Machorro, *Weak Galerkin methods for time-dependent Maxwell's equations*, Computers & Mathematics with Applications, 74 (2017), pp. 2106–2124. Advances in Mathematics of Finite Elements, honoring 90th birthday of Ivo Babuška.

[113] S.-C. Soon, B. Cockburn, and H. K. Stolarski, *A hybridizable discontinuous Galerkin method for linear elasticity*, Internat. J. Numer. Methods Engrg., 80 (2009), pp. 1058–1092.

[114] M. Tang, L. Zhong, and Y. Xie, *A modified weak Galerkin method for H (curl)-elliptic problem*, Computers and Mathematics with Applications, 139.

[115] P. S. Vassilevski and R. D. Lazarov, *Preconditioning mixed finite element saddle-point elliptic problems*, Numerical linear algebra with applications, 3 (1996), pp. 1–20.

[116] C. Wang, *New discretization schemes for time-harmonic Maxwell's equations by weak Galerkin finite element methods*, Journal of Computational and Applied Mathematics, 341 (2018), pp. 127–143.

[117] C. Wang and J. Wang, *Discretization of div-curl systems by weak Galerkin finite element methods on polyhedral partitions*, J. Sci. Comput., 68 (2016), pp. 1144–1171.

[118] H. Wang, J. Chen, P. Sun, and F. Qin, *A conforming enriched finite element method for elliptic interface problems*, Applied Numerical Mathematics, 127 (2018), pp. 1–17.

[119] J. Wang, R. Wang, Q. Zhai, and R. Zhang, *A systematic study on weak Galerkin finite element methods for second order elliptic problems*, J. Sci. Comput., 74 (2018), pp. 1369–1396.

[120] J. Wang and X. Ye, *A weak Galerkin finite element method for second-order elliptic problems*, Journal of Computational and Applied Mathematics, 241 (2013), pp. 103–115.

[121] ——, *A weak Galerkin mixed finite element method for second order elliptic problems*, Mathematics of Computation, 83 (2014), pp. 2101–2126.

[122] ——, *A weak Galerkin finite element method for the Stokes equations*, Adv. Comput. Math., 42 (2016), pp. 155–174.

[123] N. Wang and J. Chen, *Convergence analysis of nitsche extended finite element*

methods for H(curl)-elliptic interface problems, International Journal of Numerical Analysis & Modeling, 19, pp. 487–510.

[124] X. Wang, X. Ye, and S. Zhang, *Weak Galerkin finite element methods with or without stabilizers*, Numer. Algorithms, 88 (2021), pp. 1361–1381.

[125] Y. Xie, M. Tang, and C. Tang, *A weak Galerkin finite element method for indefinite time-harmonic Maxwell equations*, Applied Mathematics and Computation, 435 (2022), p. 127471.

[126] Y. Zeng and J. Chen, *A priori and a posteriori error estimates for H(div)-elliptic problem with interior penalty method*, Commun. Comput. Phys., 14 (2013), pp. 753–779.

[127] L. Zhu, T.-Z. Huang, and L. Li, *A hybrid-mesh hybridizable discontinuous Galerkin method for solving the time-harmonic Maxwell's equations*, Applied Mathematics Letters, 68 (2017), pp. 109–116.